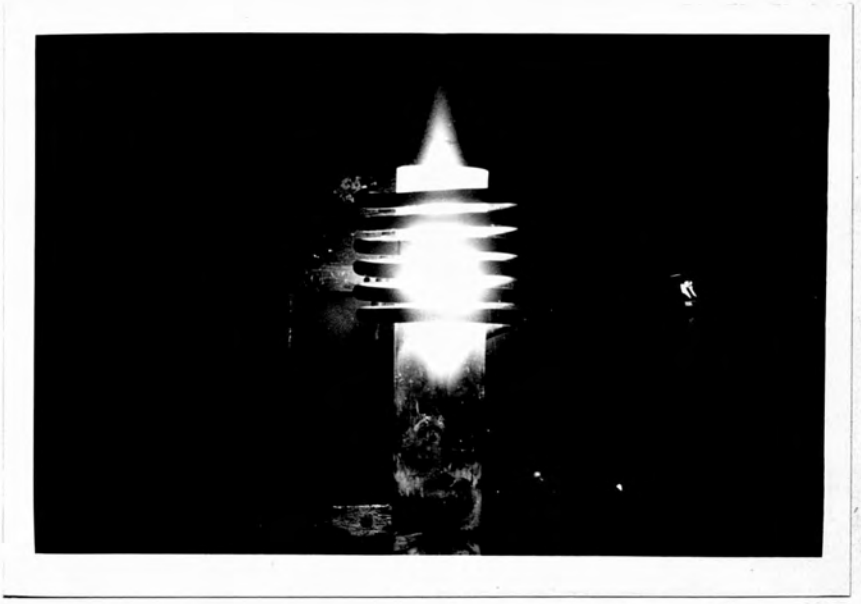

THE R.F INDUCTION PLASMA TORCH

HIGH PRESSURE RADIO FREQUENCY PLASMA IN A PULSED MAGNETIC FIELD

by

Ahmed Shamim

Thesis submitted for the

Degree of Doctor of Philosophy

to

the University of London

R.M.C. LIBRARY
CLASS No. T BPP Sha
ACC No. 132,978
DATE ACC Oct. 76

Royal Holloway College

March 1976

ProQuest Number: 10097851

All rights reserved

INFORMATION TO ALL USERS
The quality of this reproduction is dependent upon the quality of the copy submitted.

In the unlikely event that the author did not send a complete manuscript
and there are missing pages, these will be noted. Also, if material had to be removed,
a note will indicate the deletion.

ProQuest 10097851

Published by ProQuest LLC(2016). Copyright of the Dissertation is held by the Author.

All rights reserved.
This work is protected against unauthorized copying under Title 17, United States Code.
Microform Edition © ProQuest LLC.

ProQuest LLC
789 East Eisenhower Parkway
P.O. Box 1346
Ann Arbor, MI 48106-1346

ACKNOWLEDGEMENTS

I wish to express my gratitude to Dr E.R. Wooding for providing the research facilities in the Physics Department of Royal Holloway College, University of London. I also thank him for constant interest, advice and encouragement during the course of this work. Thanks are also due to Mr D. Brown and Dr D.W. Hughes for lively and useful discussion. I also thank the Department of Education, Government of Pakistan for personal financial support during the first three years.

The members of the technical staff, Messrs J. Henley, R. Mason, L.P. Ellison, W. Howell and J. Taylor are thanked for their help and co-operation with the construction of apparatus.

ABSTRACT

The high pressure plasma produced by an r.f. induction plasma torch has been investigated in a pulsed magnetic field using spectroscopy, high speed photography, inductive probes and a diamagnetic loop. Radiation and temperature of the plasma have been measured under various conditions of the torch and various intensities of the pulsed field. In most cases Joule-heating has been found the main mechanism of energy transfer to the plasma. From the decay of temperature in the plasma after glow a value of radiative recombination in a dense argon plasma has been found. Various properties of the torch in the absence of a pulsed magnetic field have also been investigated. These investigations cover gas breakdown at the torch initiation, measurements of the r.f. magnetic field in the plasma and the plasma instabilities. The measurements of the r.f. magnetic field provide information leading to estimates of plasma conductivity, electrical parameters and efficiency of the torch. The study of plasma instabilities reveals their sources and helps to suppress the acoustic noise from the torch.

To

My Mother and Sister

CONTENTS

CHAPTER 1

INTRODUCTION

An r.f. induction torch is a convenient source of high pressure plasma for spectroscopy [1-11] and the study of ionic reactions. [12] The torch consists of a quartz tube through which a steady stream of a gas flows and r.f. power is inductively coupled into the plasma by means of a water cooled coil, energised by an r.f. generator. The plasma is vortically stabilised by feeding the gas tangentially at one end of the quartz tube and is allowed to exhaust to the atmosphere at the other end.

The temperature of the plasma increases up to about 10,000 ^{o}K with power but further increase in power produces a larger plasma with little increase in temperature. If the volume of the plasma could be restricted and energy injected very rapidly the temperature could be expected to increase. To examine the possibilities a pulsed magnetic was applied to the steadily burning plasma torch in such a way that adiabatic heating occurred. In this thesis the method of applying the magnetic field and its effect on the plasma temperature are studied.

An increase in temperature would be expected to increase the radiation. In order to find suitable conditions for temperature measurements a study of the emitted radiation is made under various operating conditions of the torch. This study, as will be seen later, also helps to understand the behaviour of radiation from an induction plasma torch in a pulsed magnetic field. The temperature is measured spectroscopically and the instabilities are studied with the aid of high speed photography.

The present work is also extended to a study of various properties of the induction plasma torch in the absence of a pulsed magnetic field.

These investigations cover gas breakdown at torch initiation, measurements of the r.f. magnetic field in the plasma and plasma instabilities.

The gas breakdown is studied with high speed photography. In addition initial changes in the plasma temperature and current in the r.f. indicator are also investigated.

To understand the torch operation values of the r.f. magnetic field through the plasma are required. Already the techniques of measuring magnetic fields in a plasma are well established. They have been mainly restricted to low density transient plasmas. To measure the field distribution in a high density continuously burning plasma torch a water-cooled probe has been designed. In addition, techniques have been developed for making estimates of plasma conductivity, temperature, torch efficiency, plasma impedence and coupling factor. It will be seen that a few measurements, which are relatively simple to make, can provide valuable information to achieve efficient operation of the torch .

An induction plasma torch, even at a low power, is accompanied by high levels of acoustic noise, which may be traced back to instabilities in the plasma. These instabilities have been studied in acoustic noise and radiation. Their spectrum-analysis provides information about the causes of their generation and helps to suppress the low frequency instabilities which produce acoustic noise.

The basic properties of a plasma and the related processes, which are essential to understand the torch and explain various phenomena outlined above, are presented in the next chapter.

A word about the units. In the body of this thesis S.I. units are used but to facilitate reference to literature quantities in the second, third and fourth chapters are left in the original form

CHAPTER 2

PROPERTIES OF A PLASMA

In this chapter some of the properties and equations of a plasma are described to aid the explanation of the behaviour of an induction plasma torch.

2.1. Definition of a Plasma

Langmuir used the word 'plasma' to describe the material of the positive column of a discharge. A gas in this state consists of electrons, atoms and molecular ions, neutral atoms and molecules. Generally different plasma constituents have different temperatures. Although electrically conducting, a plasma has nearly equal positive and negative charges. This quasi neutrality of the plasma is preserved only over dimensions greater than the Debye-length, which is defined by

$$\lambda_D = (kT/4\ n_e\ e^2)^{\frac{1}{2}} = 740\ (kT/n_e)^{\frac{1}{2}}\ \text{cm} \qquad (2.1)$$

where kT is the energy of thermal motion in electron volts (kT = 1 at T = 11,600 ^{o}K) and n_e is measured in cm^{-3}. In dimensions less than λ_D the number density of particles would be too low to secure quasi-neutrality.

2.2 Basic Plasma Equations

The plasma tends to behave as a homogeneous conducting fluid and obeys the magnetohydrodynamic equation

$$\rho_m \frac{d\bar{v}}{dt} = \bar{J} \times \bar{B} - \text{grad } p \qquad (2.2)$$

where the total pressure p is the sum of electron pressure p_e and the ion pressure p_i. At each point, the state of the plasma is characterised by the current density J, mass density ρ and the velocity v, which are given by

$$J = (n_e v_e - n_i v_i) e \qquad (2.3)$$

$$\rho_m = (n_e m_e + n_i m_i) = (\rho_e + \rho_i) \qquad (2.4)$$

$$v = \frac{1}{\rho_m} (\rho_e v_e + \rho_i v_i) \qquad (2.5)$$

In such a case the plasma must move as a whole and to a first approximation $v = v_i = v_e$. For continuity of matter

$$\frac{d\rho}{dt} + \text{div } (\rho_m v) = 0 \qquad (2.6)$$

and for continuity of charge

$$\frac{d\rho_q}{dt} + \text{div } J = 0 \qquad (2.7)$$

The relation of current density J with electric and magnetic fields and with pressure gradient is given by generalised Ohm's law [13]

$$\bar{J} + \frac{1}{\nu_e} \frac{dJ}{dt} = \sigma(\bar{E} + \bar{v} \times \bar{B}) + \frac{1}{n_e e} \text{grad } P_e - \frac{\bar{J} \times \bar{H}}{n_e e} \qquad (2.8)$$

If the current does not appreciably change during the collision time $1/\nu_e$, the second term on the left hand side can be neglected. The above equation differs from simple Ohm's law because of the presence of the last two terms

on the right hand side. The first of these terms shows that the current density is produced not only by the electric field, but also by the difference of electron pressure at different points in the plasma. The last term ($\bar{J}X\bar{B}$) expresses the effect of the magnetic field on the motion of electrons. A plasma also satisfies Maxwell's equations.

$$\text{div } \bar{B} = 0 \tag{2.9}$$

$$\text{Div } \bar{E} = (\rho_e - \rho_i) \tag{2.10}$$

$$\text{curl } \bar{B} = \bar{J} + \frac{\delta \bar{E}}{\delta t} \tag{2.11}$$

$$\text{curl } \bar{E} = -\frac{\delta \bar{B}}{\delta t} \tag{2.12}$$

2.3 Ionization and the Distribution Function

In a collisional plasma electrons continuously gain energy from an electric field. This directed energy is randomised during elastic collisions with heavy plasma particles, leading to a distribution function which is very often Maxwellian. A small number of electrons at the tail of the distribution function have more energy. These electrons by virtue of their large initial energy are accelerated to much higher velocities by the electric field. They are mainly responsible for excitation and ionization of the gas. The distribution function is a result of the dynamic equilibrium among all processes occurring in the plasma, and is an important plasma parameter. A small change in the distribution function can bring about a significant change in the tail and consequently in excitation and ionization phenomena.

2.4 Local Thermodynamic Equilibrium (L.T.E.)

A plasma, in which collisions dominate, can be described by the same laws which govern a plasma in complete thermodynamic equilibrium with the exception of the emitted radiation. Thus in a L.T.E. plasma each process is balanced by its reverse, but the radiation emitted is not equal to the radiation absorbed. All plasmas at atmospheric and higher pressure are in L.T.E.

In an actual electric discharge, the electrons are continuously gaining energy from the electric field and are handing over a part of it to heavy plasma particles. Consequently a total transfer of the surplus electron energy to atoms, molecules or ions will never be realised. The temperature of the electrons always remains somewhat higher than that of the gas. Equilibrium is reached when the energy transfer is equal to the energy gain from the field. The relative difference in temperature is given by

$$\frac{\Delta T}{T} = \frac{T_e - T}{T_e} = \frac{(\lambda_e \, e \, E)^2 \, m_o}{(3/2 \, k \, T_e)^2 \, 4 m_e} \tag{2.13}$$

(14)

According to Griem, the number density of electrons necessary to obtain L.T.E. is given by

$$n_e \geqslant 9 \times 10^{17} \, (E_2 / \chi_H)^3 \, (kT/\chi_H)^{\frac{1}{2}} \ \text{cm}^{-3} \tag{2.14}$$

2.5 Boltzmann's Distribution Law

In thermodynamic equilibrium or L.T.E., energy of every type is distributed over all particles of the plasma-gas according to Boltzmann's law

$$\frac{n_n}{n_m} = \frac{g_n \exp(-E_n/kT)}{g_m \exp(-E_m/kT)} \qquad (2.15)$$

2.6 Saha-Eggert Equation

The degree of ionisation of an equilibrium plasma is given by Saha equation

$$\frac{n_e\, n_z}{n_{z-1}} = \frac{2U_i\, (2\pi m\, kT)^{3/2}}{u_o\, h^3} \exp(-\chi_i/kT) \qquad (2.16)$$

The number Z gives the number of positive charges seen by the outer electron. Z = 1 for neutrals and Z = 2 for singly ionized atom. The degree of ionization for an atmospheric pressure argon plasma is shown in Fig. 2.1. as a function of temperature, according to Saha equation.

2.7 Time for Establishment of Kinetic Equilibrium Between Electrons and Heavy Particles

According to Griem, [14] the time to obtain L.T.E. between electrons and atoms or ions is given by

$$\tau_{kin} = \left[7.5 \times 10^{-7} (\chi_H/kT)^{3/2} n_e\right]^{-1} \frac{n_o\, m_o}{n_i\, m_e} \qquad (2.17)$$

where n is the total number density of particles of the same kind. The factor 3×10^{-7} given by Griem has been changed after recalculation. [15]

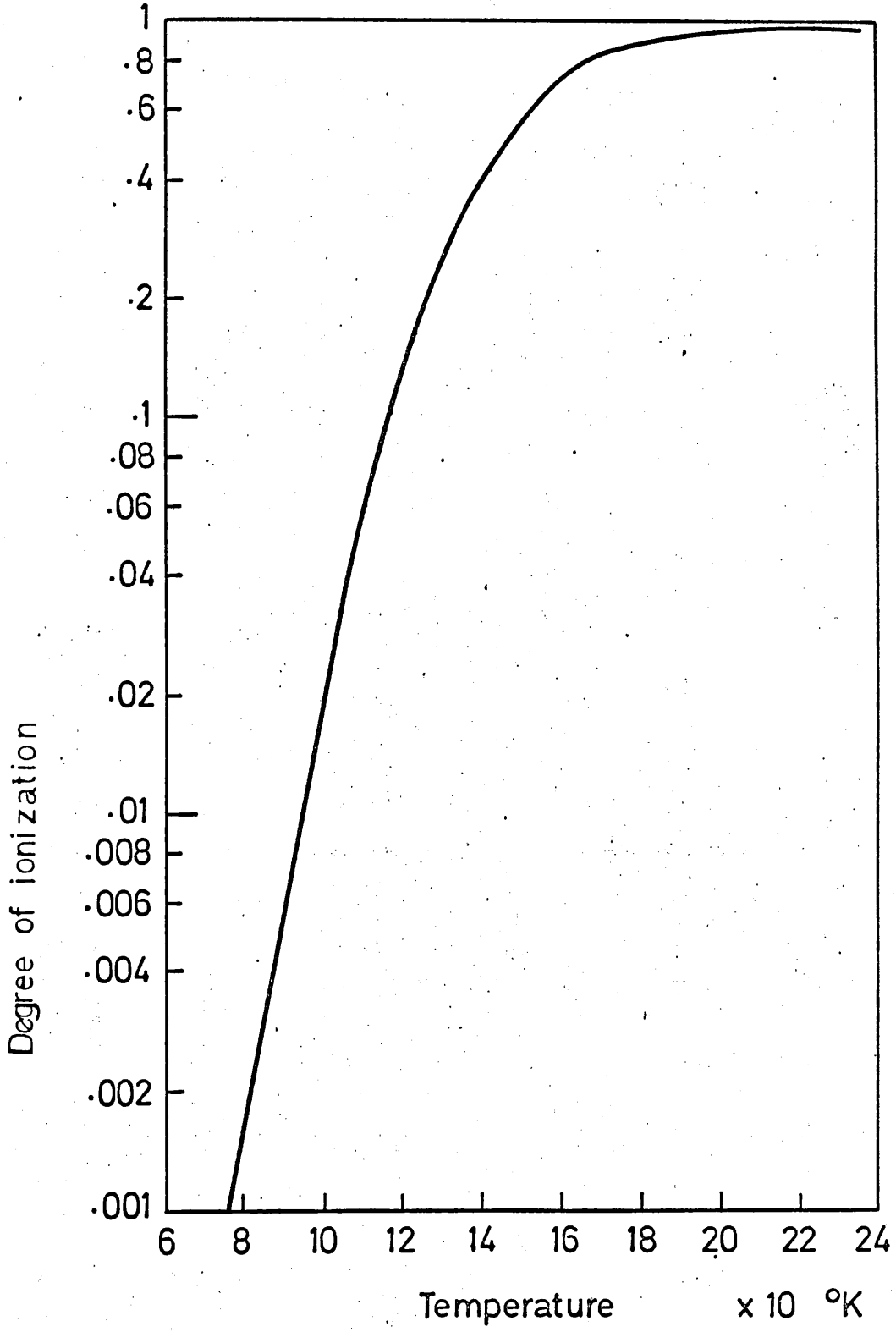

FIG. 2·1 Degree of ionization of argon as a function of temperature.

2.8 Time for Distribution of Energy over the Discrete Terms of Heavy Particles According to Boltzmann's Law

The kinetic equilibrium discussed above leads to a distribution of energy over the excited states of the atoms according to Boltzmann's law after a certain time. This time for thermal population of the upper level of the resonance line for complete L.T.E. down to the ground level E_1 is given by

$$\tau_1(\text{sec}) = 1.1 \times 10^7 \cdot \frac{Z^3}{f_{1,2}\, n_e} \cdot \frac{n_Z}{n_Z + n_{Z-1}} \cdot \frac{E_{Z-1,2}}{Z^2\, \chi_H} \left(\frac{kT}{Z^2\, \chi_H}\right)^{\frac{1}{2}} \exp\left(\frac{E_{Z-1,2}}{kT}\right) \tag{2.18}$$

The time of establishment of L.T.E. depends upon n_e. If n_e is initially small the time for establishment of L.T.E. is increased by the time to produce sufficiently high value of n_e.

2.9 Reduction of the Ionization Potential in the Plasma

Although a plasma is quasi neutral as a whole i.e. it has nearly equal numbers of positive and negative charges, the neutrality of the plasma is not preserved in small volumes i.e. for distances less than the Debye length. As a result the plasma is polarised and consequently the energy of ionization is somewhat reduced. The lowering of the ionization potential, according to Griem,[14] is given by

$$\Delta\chi_i = 2.9 \times 10^{-8} \left(\frac{n_e}{T}\right)^{\frac{1}{2}} \tag{2.19}$$

2.10 The Electrical Conductivity of a Plasma

The electrical conductivity 'σ' of a plasma is directly proportional to the mobility of electrons. In a very slightly ionised gas close encounters between the electrons and the neutral particles govern the electron mobility. In a completely ionised gas, on the other hand, the distant encounters due to long range coulomb force between ions and electrons dominate the mobility. For an intermediate degree of ionization the conductivity σ may be approximated by

$$(1/\sigma) = (1/\sigma_c) + (1/\sigma_d) \qquad (2.20)$$

where $(1/\sigma_c)$ denotes the resistivity due to close encounters and $(1/\sigma_d)$ the resistivity due to distant encounters. Lin et al [16] combined the expression for σ of a slightly ionized gas of rigid elastic spherical molecules, due to Chapman and Cowling [17] with the Spitzer and Harm's [18] formula for the conductivity of a fully ionized gas. For a moderately ionized gas they obtained

$$\sigma = \left[1.88 \frac{(m_e\, kT)^{\frac{1}{2}}\, Q_{oe}}{\alpha' e^2} + 1.69 \frac{m_e^{\frac{1}{2}} e^2}{(kT)^{\frac{1}{2}}} \ln (\lambda_D/b_o)\right]^{-1} \qquad (2.21)$$

where the impact parameter $b_o = e/3kT$. The values of $\ln(\lambda_D/b_o)$ were computed for an atmospheric pressure Ar plasmas. The results of this computation are presented in Table 2.1. The values Q_{oe}, the momentum transfer collision cross-section for electrons in argon, at various plasma temperatures, were taken from S.C. Brown's work.[19] It may be recalled that the first and second terms within the brackets on the right hand side are respectively $(1/\sigma_c)$ and $(1/\sigma_d)$. Values of σ were computed at various temperatures with the aid of Equation (2.21) and the results are presented in Fig. 2.2.

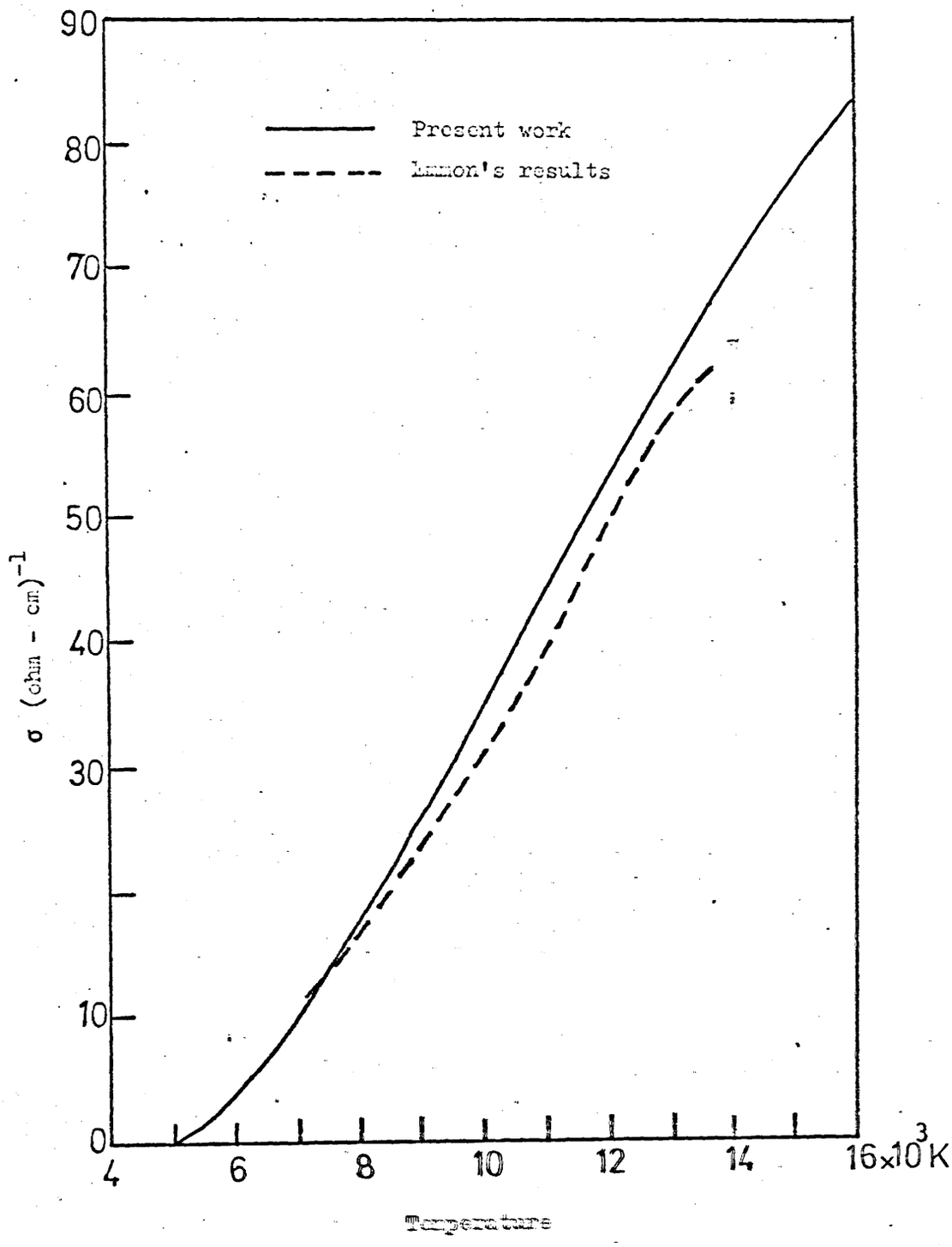

Fig.2.2. Variation of the electrical conductivity of Ar with temperature at 1 atm.

TABLE 2.1. Variation of the Coulomb's Logarithm '$\ln \lambda_D/b_o$' with Temperature for an Argon Plasma at 1 atm.

Temp	$\ln \lambda_D/b_o$
5,000 °K	7.90
6,000 °K	6.62
7,000 °K	5.74
8,000 °K	5.10
9,000 °K	4.63
10,000 °K	4.26
12,000 °K	3.77
14,000 °K	3.63
16,000 °K	3.69
18,000 °K	3.86
20,000 °K	4.17

2.11 Losses from a Plasma

A plasma loses mass through particle diffusion and energy through thermal conduction and radiation. In order to assess these losses the relevent coefficients are described below.

2.11.1 Electron Diffusion

Electron diffusion from the plasma is governed by Fick's law[20]

$$\frac{\delta n_e}{\delta t} = -\nabla^2 (D_e n_e) \qquad (2.22)$$

where the diffusion coefficient is given by

$$D_e = 1/3\ \lambda_e \langle v_e \rangle = \langle v_e \rangle / 3 n_o Q_{oe} \qquad (2.23)$$

Here the degree of ionization is assumed low so that electron-ion collisions can be neglected.

2.11.2 Ambipolar Diffusion

Because of their large velocity electrons tend to diffuse much faster than the ions thereby giving rise to an electric field, which, in turn, slows down the electrons and accelerates the positive ions. The resulting ambipolar diffusion coefficient is given by

$$D_a = \frac{\mu_i D_e + \mu_e D_i}{\mu_i + \mu_e} \qquad (2.24)$$

For a plasma, generally, $\mu_e = \mu_i$ and $\mu_i D_e = \mu_e D_i$, therefore,

$$D_a = 2 D_i \qquad (2.25)$$

The determination of D_i involves ion to ion and ion to atom collision cross-sections.

2.11.3 Thermal Conduction

The thermal conductivity of a plasma depends on electrons, ions and neutral particles. The ordinary or 'contact' thermal conductivity due to simple diffusion, should be distinguished from the 'reaction'

thermal conductivity due to ionization-recombination.[21] The total thermal conductivity is the sum of both. Devoto [22] computed the conductivity for a 1 atm argon plasma at various temperatures above 5000 ^{o}K. His results, which are based on the formula given by Spitzer and Harm,[18] are compared with Emmon's [23] experimental results on a d.c. arc in argon, burning at 1 atm, in Fig. 2.3. Values of 'k' below 5000 ^{o}K shown by the dotted line are taken from the 'Tables of Thermodynamic and Transport Properties!'[24]

2.11.4 Radiation

A high temperature plasma emits both continuum and line radiation, the continuum radiation consisting of Bremsstrahlung and recombination radiation, But at temperature below 40,000 ^{o}K Bremsstrahlung is negligible.[25] In the following pages power losses from an argon plasma due to each mechanism, will be described.

2.11.4.1 Recombination Radiation

A free electron may be captured by an ion, resulting in a free-bound or recombination radiation. As the captured electrons have a continuous spectrum of energy the recombination is continuous.

The capture of an electron may leave the atom in an excited state in which case continuous recombination radiation is accompanied by the line emission. The electrons capture in any energy level produces a recombination continuum peculiar to that level. Overlapping of all such continua forms the resultant recombination radiation.

The theory of recombination radiation was formulated by Unsold [26] and later developed by Biberman and Norman [27] and Schluter.[28] According to Lochte-Holtgreven[29] the emission coefficient for recombination radiation is given by

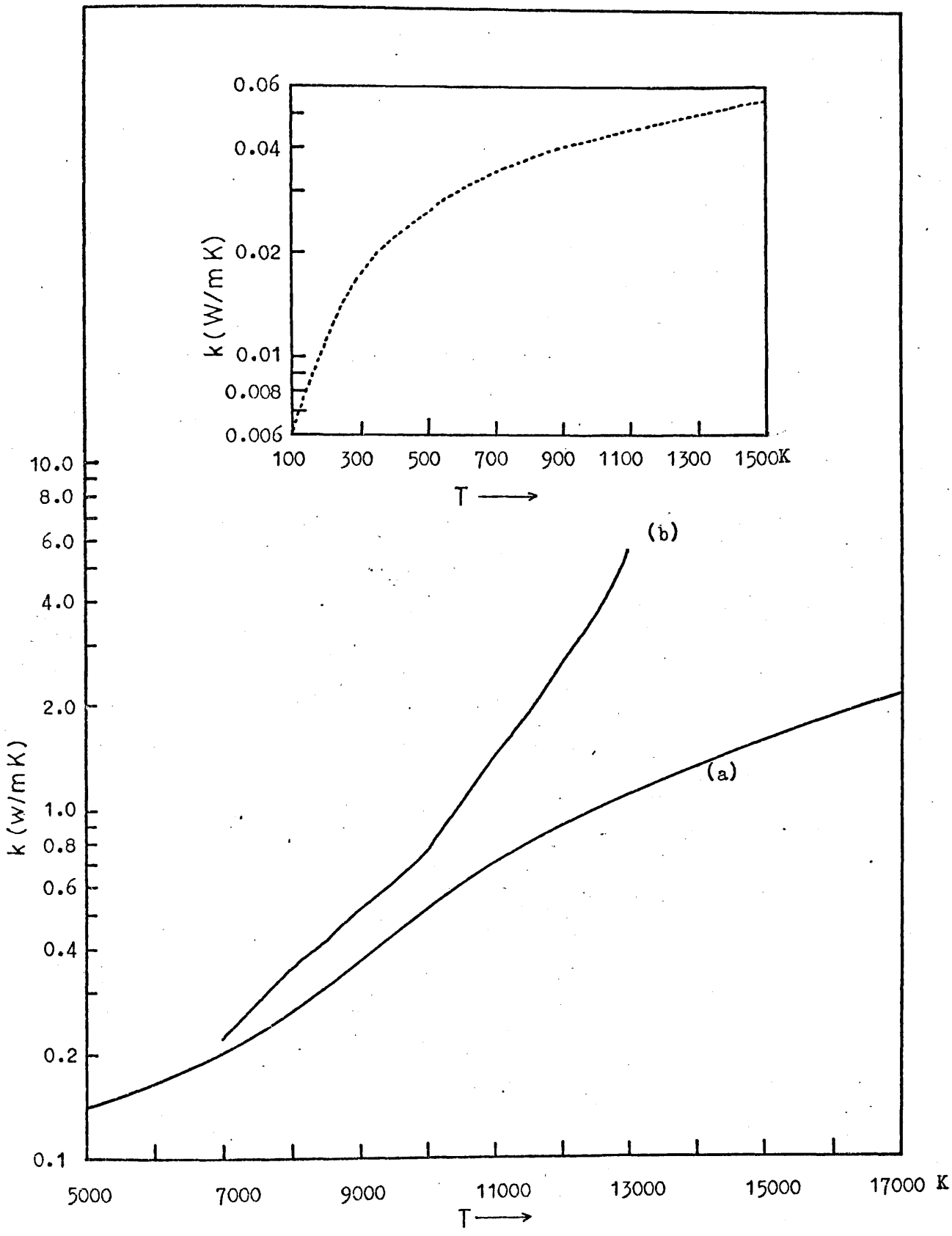

Fig.2.3 Thermal conductivity of argon plasma at one atmos as a fuction of temperature. (a) Devoto's results (b) Emmons results.

$$\varepsilon = C_1 Z^2 \frac{n_i n_e}{T^{\frac{1}{2}}} \left([1 - \exp(-h\nu/kT)] \frac{\tilde{\gamma} \bar{g}_{bf}}{U_Z} \xi(\nu,T) \right) \qquad (2.26)$$

where $C_1 = \frac{16 \pi e^6}{3c^3 (6 \pi m_e^3 k)^{\frac{1}{2}}}$

$\tilde{\gamma}$ is a parameter which takes account of the different statistical weight of the ground term of the parent ion as compared to that of hydrogen and $\xi(\nu,T)$ a parameter which accounts for the penetration of the combining electron into the electron cloud surrounding the nucleus. For the plasma considered here the Gaunt factor is taken to be unity. The quantity $\tilde{\gamma}/U_Z$ may be put equal to 5.5 [25] in Equation (2.26). For Ar at wavelengths greater than 825 nm. $\xi(\nu,T)$ is almost equal to unity at all temperatures, but below 825 nm $\xi(\nu,T)$ changes considerably with wavelength and temperature as shown in Fig. 2.4.

2.11.4.2 Spectral Lines

In view of the large number of spectral lines from an argon-plasma they are divided into several groups. Each group is investigated separately. For the optically thick lines the light intensity coming out of the plasma depends on the geometrical depth along the line of observation. A simplified model of the plasma, having a cylindrical shape of diameter 'd' is adopted in this work. It may be assumed that the light energy flux leaves the plasma cylinder normally. Such a gross simplification is justified by the comparatively small contribution made by optically thick lines to the total radiated energy from an argon plasma, as will be shown later.

Two spectral lines of 4s - 3p array are broadened mainly by the Stark effect. They are strongly absorbed so that for each one of them the power loss is [30]

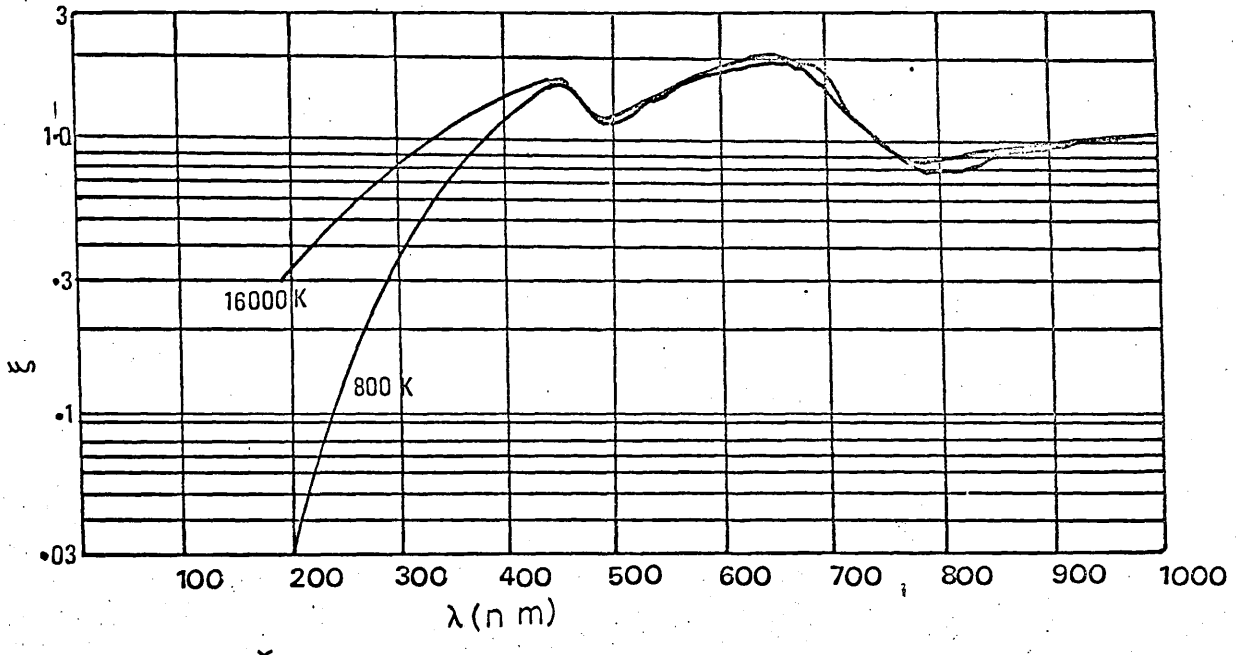

FIG. 2.4. ξ - FACTOR FOR ARGON

$$P_2 = \pi B_\nu \tilde{S} \left(\frac{2\pi e^2}{m_e C} n_k f_{i,2} d\delta\nu \right)^{\frac{1}{2}} \qquad (2.27)$$

30 lines of 4p - 4s array are also broadened by the Stark effect and considerably absorbed. Their frequencies are near enough for their contribution to be written as

$$P_3 = \pi B_\nu \tilde{S} \left(\frac{2\pi e^2}{m_e C} n_o \exp\left(\frac{-E_i}{kT}\right) \delta\nu \, d \right)^{\frac{1}{2}} \sum_{i=1}^{30} (g_i f_i)^{\frac{1}{2}} \qquad (2.28)$$

All the other lines show little or no absorption at all. For them the power loss can be written as

$$P_4 = \upsilon \sum \frac{h\nu \; A_{ki} \; n_o}{U_o} \exp\left(-\frac{E_k}{kT}\right) \qquad (2.29)$$

The spectral lines considered correspond to transitions 5p - 4s, 6p - 4s and the transitions from 3d, 5s, 4d, 6s, 5d, 7s to 4p level. The remaining lines which arise from transitions between excited states may be assumed hydrogenic. Such an approximation is possible because of their comparatively small contribution to the total radiation as will be seen later. Their contribution to the power loss is [31]

$$P_5 = \frac{2C_2}{\beta} \frac{\gamma\upsilon}{U_o} n_o \exp\left(-\frac{\chi_i}{kT}\right) \left\{ \frac{1}{\sqrt{3}} \left(\exp(\beta/n^2) - \exp(\beta/\tilde{n}^2) \right) - \exp(\beta/\tilde{n}^2) \left(\frac{1}{n^2} - \frac{1}{\tilde{n}^2} \right) \right\} \qquad (2.30)$$

where $\beta = h R_y/kT$; R_y is the Rydberg Constant in frequency units, χ_i the effective ionization potential and

$$c_2 = \frac{6\ 4\pi e^2\ h\ R_y^{\ 3}}{3\sqrt{3}\ m_e\ c^3} = 0.0858 \qquad (2.31)$$

The total radiation power is

$$P = \varepsilon\, \upsilon + P_2 + P_3 + P_4 + P_5 \qquad (2.32)$$

In the succeeding chapters the plasma properties described above will be used as the basis of measurement on the plasma and in developing a theory of the r.f. induction torch.

CHAPTER 3

REVIEW OF PLASMA TORCHES

INTRODUCTION

The atmospheric pressure plasma torch in which radiofrequency power is coupled inductively produces a high temperature plasma free from electrode contamination. Such a torch is called an r.f. induction plasma torch.

Plasma torches and jets were developed from early investigations on arcs in gases at atmospheric pressure. It was found that the discharge could be constricted mechanically or by magnetic fields to provide higher temperatures.

Work on radio-frequency discharges provided two modes of coupling electrical power to a gas discharge; E-mode coupling or capacitive-coupling through the electric field and the H-mode coupling or the inductive-coupling through the magnetic field. E-mode coupling resulted in the development of the high frequency monopole torches and the H-mode coupling gave rise to the development of the induction plasma torches.

These developments are discussed in detail in this chapter with a final section on the effect of a pulsed magnetic field on a high pressure induction plasma confined in a sealed vessel.

3.1. THE d.c. ARCS

The history of the high pressure plasma devices can be traced back to the late 19th century when carbon arcs were commonly used for illumination. The first patent of an arc device in which the anode slowly vapourised to form a plasma tail flame* was made by Beck (32) in 1910 in Germany. In

* The word 'flame' is used here to describe the appearance of the discharge and should not be confused with a chemical flame.

1922, Gerdien [33] reported the effect of mechanically constricting the arc. The 3cm long and 3mm wide arc, struck between carbon electodes, and consuming 50kW d.c. power, was constricted by two annular ceramic nozzles whose inner surfaces were water cooled. The cooling of the outer layers of the arc confined the current to a smaller cross-section. The increased current density resulted in a hotter plasma and an extension in the tail flame. Rapid consumption of electrodes and presence of water in the plasma ruled out its most potential applications. However, Gerdien's arc demonstrated the advantage of arc constriction in stabilising and concentrating the plasma.

The original Gerdien's arc was modified by McGinn [34] to produce a plasma jet at right angles to the cathode axis. With power input up to 200kW, temperature of about 10^4 ^oK were obtained in the tail flame. This device has found an important application in high temperature supersonic wind tunnels.

Olsen [35] made detailed investigations on an argon arc with tungsten cathode and a water cooled flat copper anode. The ½cm long bell shaped arc, consuming 25.6kW, was highly stable. Olsen assumed thermal equilibrium in the arc and spectroscopically measured the arc temperature. His results, presented in Fig. 3.1, show a maximum temperature of about 27,000 ^oK at the axis.

3.1.2. STREAMING IN d.c. ARCS

In a cylindrical d.c. discharge the Lorentz force is always perpendicular and directed towards the axis. But in the bell-shaped d.c. arc mentioned above, the Lorentz force has an axial component due to current divergence from the cathode which pushes the plasma towards the anode and allows the surrounding gas to flow inwards. This process is called streaming or magnetohydrodynamic pumping and plays an important role in the arc mechanism, with plasma velocities as high as 6×10^4 cm/sec.

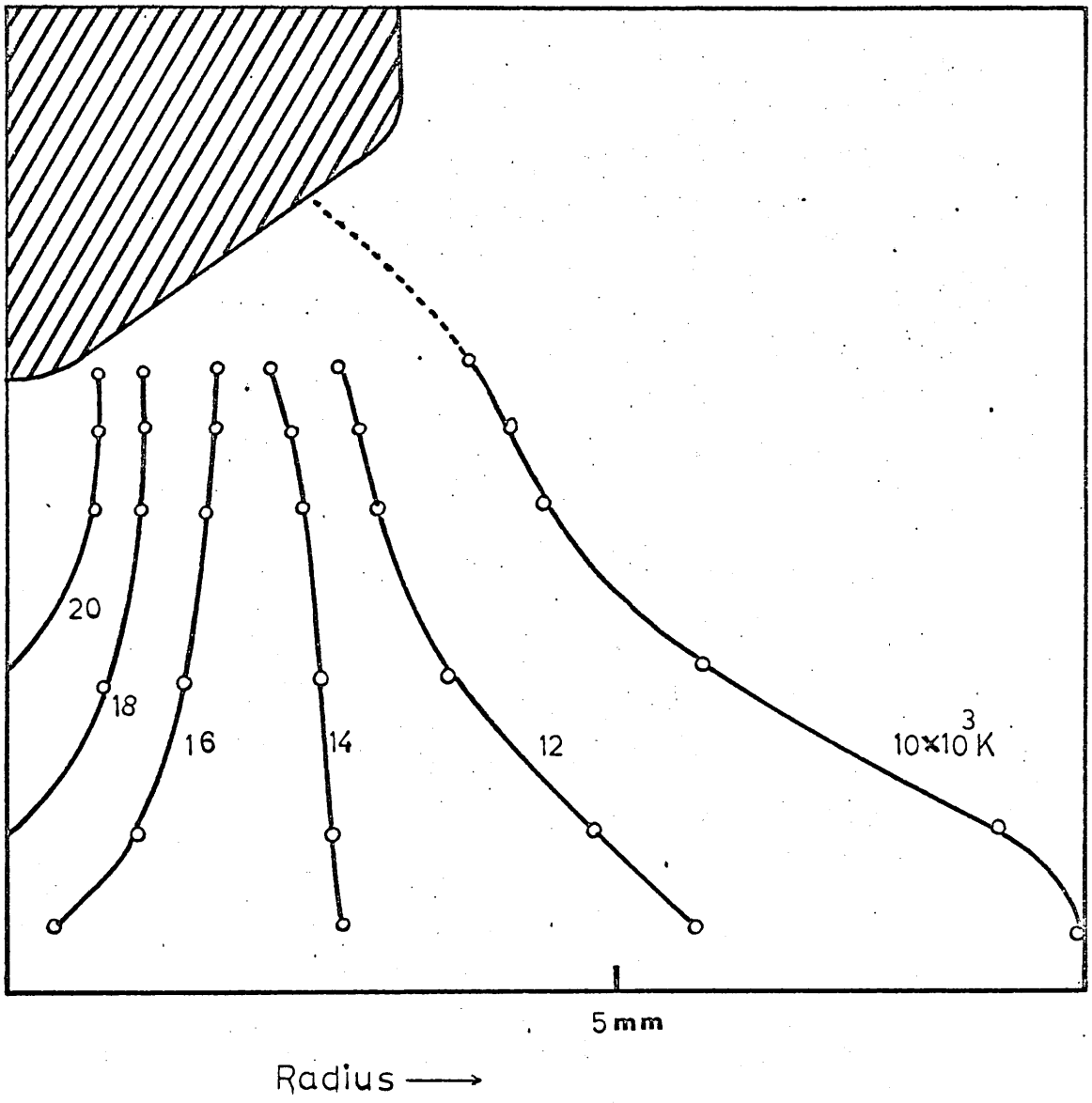

Fig 3.1. Temperature-distribution in a 400-amp, 5-mm long atmospheric argon arc, after Olsen.

Streaming led to the development of the d.c. torch which will be described below.

3.2. DEVELOPMENT OF THE d.c. PLASMA TORCH

If a hole is made in the flat anode of an arc discharge, streaming carries the plasma beyond the anode in the form of a laminar flame. In a d.c. plasma torch the anode forms an enclosure around the cathode which is provided with a copper nozzle to control the plasma flow. The development of the d.c. plasma torch from a d.c. arc is traced in Fig. 3.2. In the torch both the cathode and the anode must be water cooled to prevent erosion. Also, hydrostatic rather than hydromagnetic pressure is used to accelerate the plasma. The gas is introduced under pressure through a side arm to increase the plasma velocity, but the flame then becomes turbulent. Decreasing the gas velocity, however, increases the laminar length of the flame. Jordan [36] reported a 45cm long laminar flame at a 4.6×10^4 cm/sec gas velocity in nitrogen but the end of the flame was turbulent. The turbulent end of the flame was found to be further away from the burner outlet as the Reynolds number decreased. The turbulent region is thought to be due to friction in the boundary layer between the plasma and air, causing changes in the viscosity and density of the flame.

A variety of d.c. plasma torches have been developed depending on the type of stabilisation. Vortex stabilised, gas sheath stabilised, wall stabilised and magnetically stabilised torches have been developed.[37] Only the transfered arc plasma torch, because of its extensive use; will be described here. In this design, the current between the electrodes is limited to between 20 to 100 amps by a resistance as shown in Fig. 3.3. The weak plasma jet so produced provides a conducting path through which an intense arc strikes to the metal work piece which acts as the anode. Resistance heating of the arc provides heat for melting while the high velocity hot plasma blows out the molten metal.

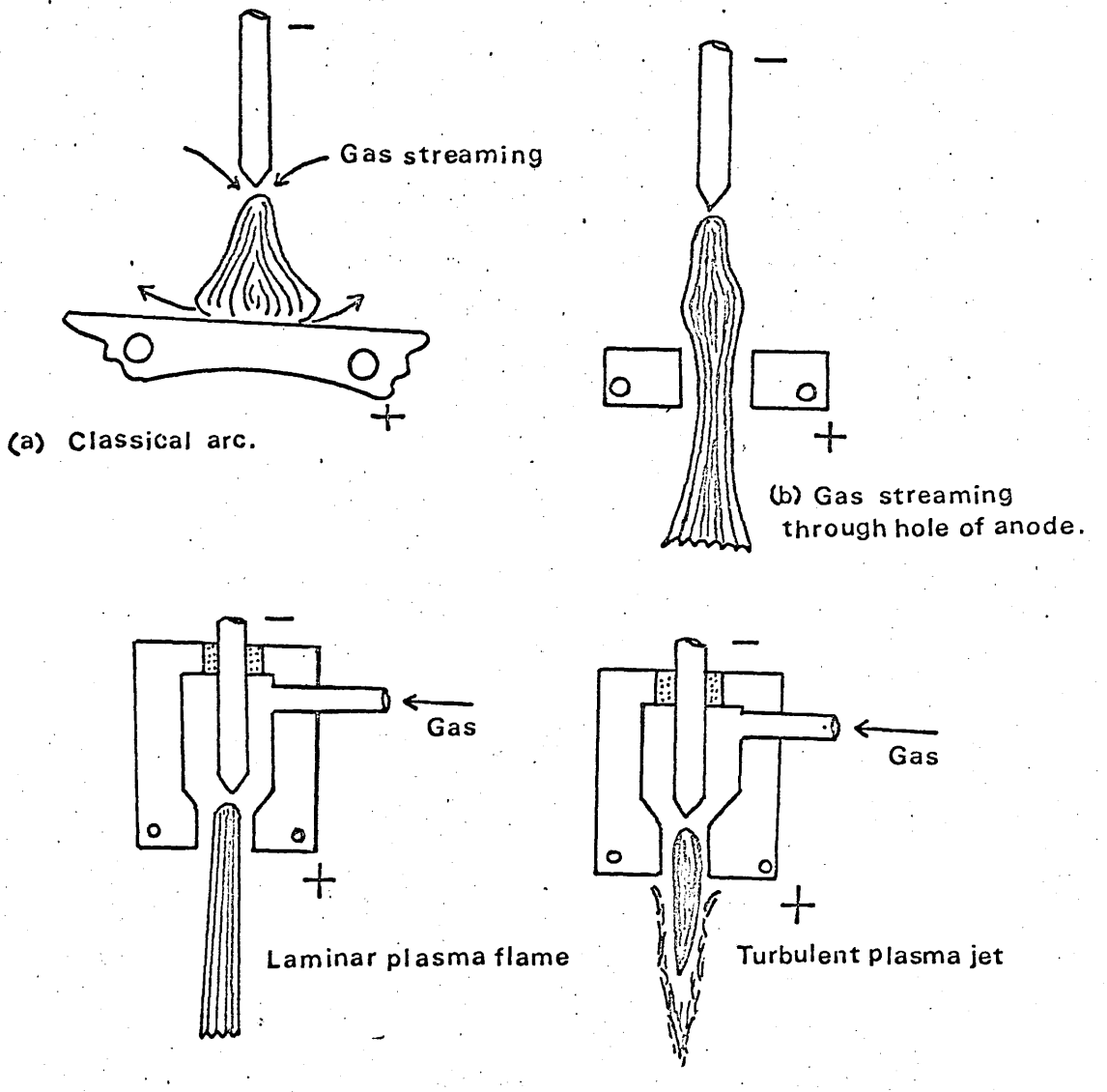

(a) Classical arc.

(b) Gas streaming through hole of anode.

(c) High enthalpy, low velocity plasma jet.

(d) Plasma jet

Fig.3.2 Evolution of the plasma torch from the d.c. arc, after Reed.

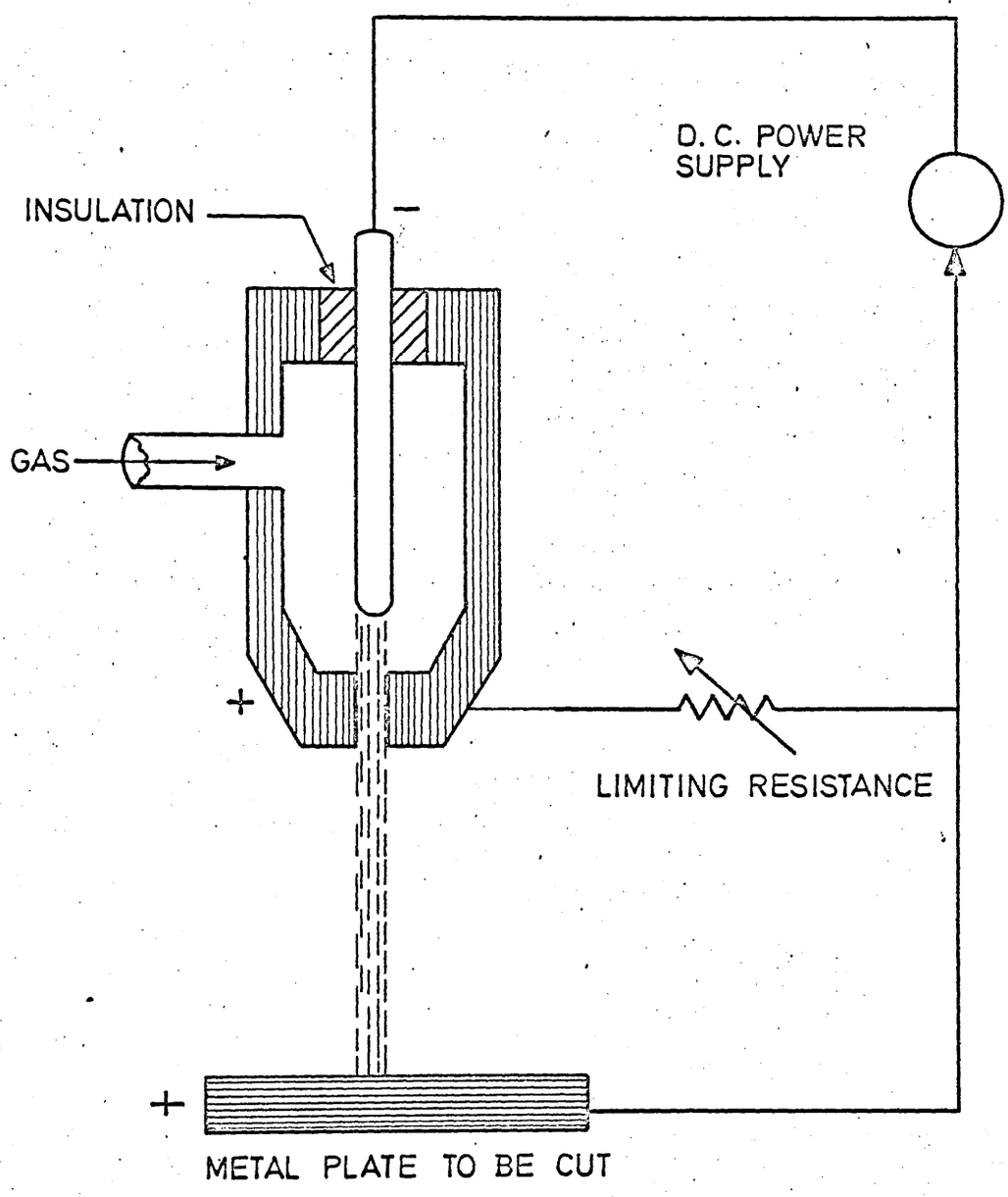

FIG. 3.3 Transferred arc plasma jet

3.2.1. BASIC PROPERTIES OF THE d.c. PLASMA TORCH

Temperature and electron density distribution are the most important characteristics of a plasma torch. Depending on the power input, and gas flow velocity, the maximum temperature in the torch may vary from less than 3500 ^{o}K to well over 15000 ^{o}K. Reinzi and Gaydon [38] reported a maximum temperature of 8030 ^{o}K 2mm above the torch head with a power input of 4.35kW and the argon flow rate of 34 litres/min. The discharge current was 150 amps.

Measurements on various processes occuring in the torch have been made. Watson et al [39] report a value for the ambipolar coefficient to be of the order of 10^{4} cm^{2} sec^{-1} and a value for the radiative recombination coefficient to be approximately 6×10^{-9} cm^{3} sec^{-1}.

3.2.2. EFFICIENCY OF THE d.c. PLASMA TORCH

If the total input power to the torch is 'W_t' and the power 'We' is consumed at electrodes and 'Wg' is supplied to the gas, then

$$W_t = We + Wg = (Ve + Vg)i \qquad (3.1)$$

where 'Ve' is the total electrode voltage drop and 'Vg' is the voltage drop across the arc and 'i' is the current.

$$\text{Therefore, efficiency} = Vg / (Ve + Vg) \qquad (3.2)$$

With increasing working voltage 'Vg' increases more rapidly than (Ve + Vg) so that the torch has higher efficiency at higher working voltage. Typically torch efficiencies range from a few per cent to 90 per cent for modern high power designs.

3.2.3. OSCILLATIONS IN THE d.c. PLASMA TORCH

The gas flowing through the throat of a d.c. plasma torch extends the arc column in the form of a very narrow flame. This extension continues until the voltage drop across the column exceeds the breakdown voltage between the column and the throat. The column then short circuits to the throat. The gas flow, however, removes the short circuiting plasma and the process is repeated over and over again, producing oscillations. The amplitude and frequency of the oscillations so generated, depend on the current and the gas flow rate. These oscillations appear as a saw-tooth component of the arc voltage. In a 100 ampere jet, Jordan [40] and King observed oscillations having an amplitude of 22V and a frequency of 23kHz in a turbulent torch, while at the same current in a laminar flame the oscillations had an amplitude of 75V and a frequency of 12kHz.

R.F. instead of d.c. power may be used to produce ionization in a plasma torch. The development of such a torch, which is called the r.f. plasma torch, is traced in the following articles.

3.3. HIGH FREQUENCY DISCHARGE IN A GAS AT A HIGH PRESSURE

An air discharge at one end of a high frequency line was reported by Rohde and Scharz [41] in 1933. Later, the spectrum of this air discharge was found to contain OH and O_2 lines.[42] This observation led to the conclusion that the air discharge was similar to that of the d.c. arc. These early observations laid the foundation of monopole plasma torches.

An important development took place in 1947 when Babat [43] published his work on the high pressure electrodeless thermal plasmas. But before an account of his work can be given, an understanding of the ways in which r.f. power can be coupled into the electrodeless discharge is essential. So these are described first.

Two types of radio-frequency electrodeless discharges, namely,

capacitive or E-type discharge and inductive or H-type discharge, are possible.[43, 44, 45] These are described separately below.

3.3.1. E-TYPE DISCHARGE

In an E-type discharge excitation of the gas is caused by an oscillating electric field between two conductors which are symmetrically placed around the discharge tube as shown in Fig. 3.4(a). An oscillating axial conduction current flows through the plasma, and outside the plasma a displacement current flows through a nonconducting region to the external rings. Consequently the coupling increases with the frequency and varies inversely with the distance between the rings.

3.3.2. H-TYPE DISCHARGE

In this type of discharge a solenoid, carrying a radio-frequency current, surrounds the discharge tube, as shown in Fig. 3.4(b). This arrangement produces an oscillating axial magnetic field which induces an azimuthal closed current and causes joule heating of the plasma. An H-type discharge is, thus, characterised by induced azimuthal closed currents and high power consumption. The discharge may be considered as a current transformer in which the plasma presents a short circuited secondary [34] with the r.f. solenoid as the primary.

At frequncies generally employed in an induction plasma torch, the electric field between turns of an r.f. solenoid is much stronger[46] than that induced by the oscillating axial magnetic field. Therefore, at low pressures, the discharge is mainly produced by the former field so that a low pressure discharge has always an E-mode coupling. As the pressure is increased to a high value (10^5 N/m^2) the induced electric field begins to dominate the excitation mechanism, and the weak E-type discharge changes to an intense H-type discharge. At intermediate pressures a hybrid discharge

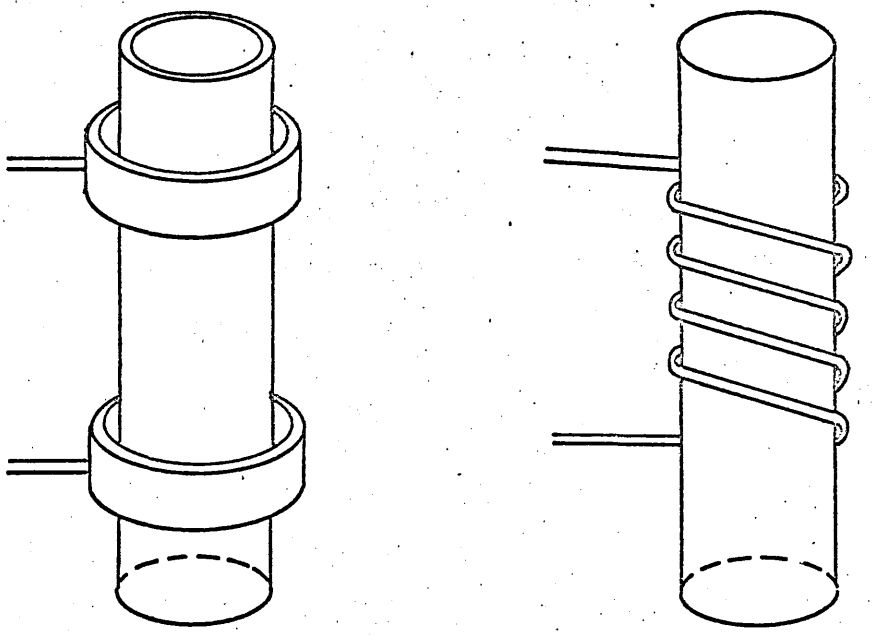

FIG. 3.4 (a) E and (b) H discharge

may be obtained.

3.3.3 BABAT's WORK

Babat [43] produced and studied both E and H-type electrodeless high pressure thermal plasmas. Both types of discharges can be easily ignited by lowering the pressure in a discharge tube and subsequently the pressure may be gradually increased. At pressures below 5 torr, the discharge is a hollow cylinder adhering to the wall of the diacharge tube. As the pressure is increased, the discharge contracts and separates from the wall. Between 20 - 100 torr the increased particle collision frequency produces a small spherical discharge in thermal equilibrium. With further increase, the discharge spreads out along the tube until at one atmospheric pressure it is spindle shaped with a bright middle and faintly glowing outer layer.

To produce E-type high pressure thermal plasma frequencies about 10^7 Hz are required. The general physical appearance of an E-type discharge is similar to that of an H-type discharge. No temperature measurements of the discharge were made by Babat.

Babat's work was of fundamental importance to the development of the r.f. induction plasma torch. With the problem of producing and stabilising a high pressure plasma in the atmosphere still unresolved, Babat's work was followed by an increasing interest in the development of monopole radio-frequency torches, using more and more powerful electronic valves.

3.4. DEVELOPMENT OF THE HIGH-FREQUENCY MONOPOLE TORCH

Cobine and Wilbur [47] made significant contributions in this field. They reported, in detail, their work on a 1000 MHz microwave plasma torch. In this torch magnetrons of 1kW and 5kW were successively coupled to a cavity resonator which in turn was coupled to a coaxial line. The coaxial

line was terminated into the torch head as shown in Fig. 3.5. The magnetron was tuned and matched to the discharge load by means of a slug in the cavity resonator and the adjustable length of telescopic section of the coaxial line. They obtained discharges in air, carbon dioxide, nitrogen, helium and argon. The flame showed a central core, with a comparatively dark space around it. The dark space, in turn, was surrounded by a luminous glow of lower intensity. Monoatomic-gas-flames drew very little power and would not burn even a piece of paper held perpendicular to the flame. On the other hand diatomic gas flames were very hot and would melt a quartz rod. The difference in temperature was attributed to the large dissociation energy released during the recombination of atoms to form molecules. The measurements obtained with an air cooled nickle-tube-probe revealed a d.c. voltage gradient of the order of 20V/cm.[47] This is the same as obtained for a nitrogen arc of 10 amps at one atmospheric pressure. The mass transport of ions by the gas flow tends to produce charge separation which would then produce a d.c. potential gradient in the plasma.

The maximum electron temperature was of the order of 13.4×10^3 decreasing to 7.85×10^3 ^{o}K at the tip. The reactive component of the torch impedence was capacitive and was found to increase with the gas velocity. A change of gas velocity affected both real and imaginary components of the torch impedence.

In a 600 MHz, 100 watts air discharge Mollwo [48] obtained a gas temperature of 4000 ^{o}K, an electron temperature of 130,000 ^{o}K and an electron density of 10^{14} cm^{-3}.

Grigorovici and Cristescu [49, 50] made temperature measurements on a 60 - 80 MHz discharge in air. Using rotational temperature and the sodium line reversal method, they obtained temperature 3600 - 3800 ^{o}K in the core of the discharge and 3000 ^{o}K in the outer sheath.

Grigorovici and Cristescu [50] developed a theory based on radial conduction losses to explain the results of previous workers. Assuming the radiation and ambipolar diffusion losses to be negligible below 7000 ^{o}K,

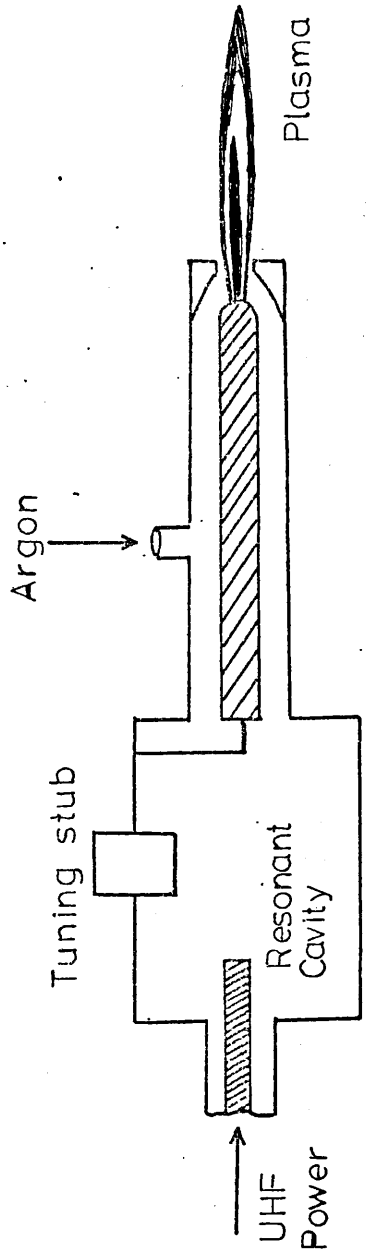

Fig. 3.5 Microwave Plasma Torch.

the maximum temperature obtained in h.f. torches, and the thermal sources to be concentrated in the core of the discharge, they solved the Elenbass-Heller differential equation and derived a temperature dependent function $F(T_m)$. They correlated this function to the power density and the channel radii and, as a result, showed that the mean discharge temperature was independent of the power input. Only the radial heat conduction loss was allowed in the above analysis. They also showed that in the range 10^7 - 10^8 Hz the maximum temperature of the channel could be approximately given by the empirical formula

$$T_{max} = 1150 \ln f + 5050 \qquad (3.3)$$

This theory does not apply to forced gas-flow and so cannot explain the results of Cobine and Wilbur. (47)

Swift (51) designed and examined the operating characteristics of a microwave plasma torch, working at 2.4 GHz. Up to 2.5 kW were applied from a magnetron to a slotted line output. As in experiments of Cobine and Wilbur (47) monoatomic gases produced cool flames whereas flames of diatomic gases were very hot. Swift also studied the effect of the gas flow rate on flame stability. With very low gas flows the flame became short. It was extinguished if the gas flow velocity was too great. A value of 1.2 cm/min was found satisfactory.

Talsky (52) attempted to show an analogy between a monopole torch discharge and a low pressure d.c. glow discharge. From the change in the resonance frequency and the Q-factor of the resonant circuit when the torch ignited, Talsky was able to determine the equivalent parallel resistance and capacity of the plasma. From the impedence of the torch discharge and the h.f. voltage on the electrode, he constructed volt-ampere characteristics of the torch discharge in which three regions may be identified. The first region is equivalent to a d.c. glow, the second an abnormal glow and the third corresponds to an arc as shown in Fig. 3.6.

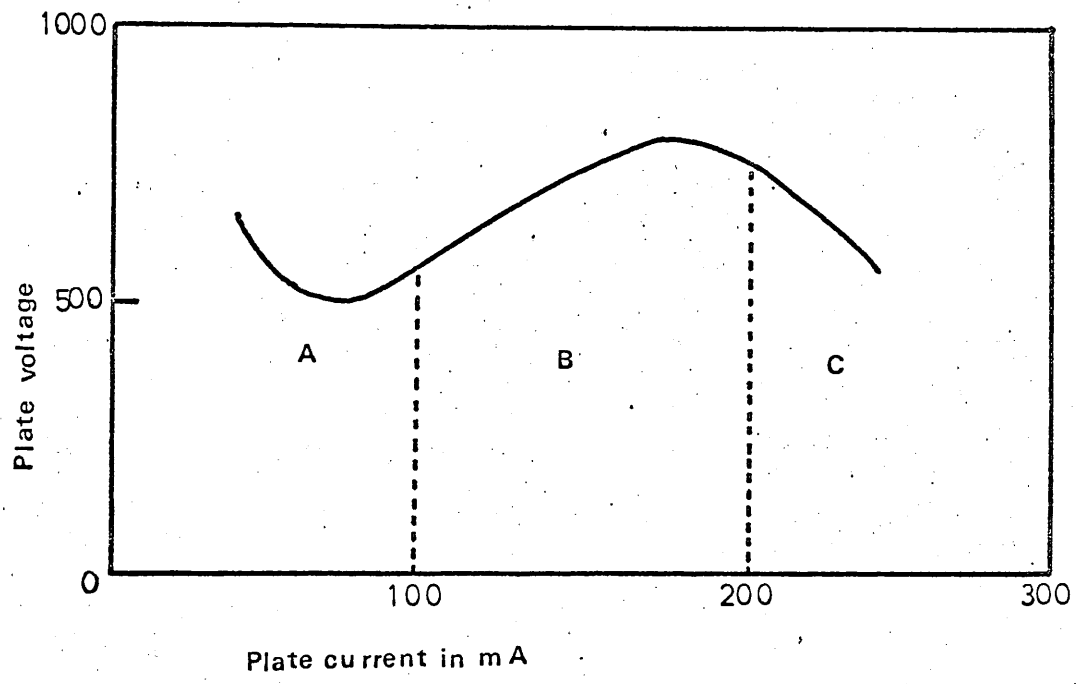

Fig.3.6 Volt-ampere characteristics of the monopole torch discharge.
(A) Normal torch discharge analogous to the normal glow discharge.
(B) Abnormal glow discharge.
(C) Torch arc, after Talsky.

It is evident from this division that most of the work on h.f. torches is confined to the d.c. abnormal glow discharge.

3.5. DEVELOPMENT OF THE r.f. INDUCTION PLASMA TORCH

Reed [53] produced the first induction torch with a plasma flowing into the atmosphere. In the original design the torch consisted of a quartz tube open at one end with gas supplied at the other end, the gas flowing spirally downward. A 5-turn r.f. solenoid made of water cooled copper tubing, surrounded the quartz tube and coupled up to 10 kW of r.f. power at 4 MHz to the plasma. The complete torch is shown in Fig. 3.7. It was found later that a flat pancake type of coil would also produce a stable plasma.

3.5.1 STARTING PROCEDURE

In earlier experiments Reed [53] used a conventional 60 - cycle/sec a.c. arc to provide initial ionisation to start the torch, but the torch may also be started by heating a graphite rod or a refactory wire in the r.f. field within the quartz tube with gas flowing in the tube. Initiating ionisation is produced by an intense r.f. field at the tip of the rod as well as by heating. The r.f. power from the inductor is then readily coupled to the pilot plasma, immediately enlarging it into a main plasma. As soon as the main plasma is formed the wire is withdrawn from the tube.

Alternatively the torch may be started with a Tesla coil [54] held outside against the quartz tube some distance away from the r.f. inductor.

3.5.2. TORCH STABILISATION

After the plasma has been formed, some ionisation process must continue in the region of r.f. field otherwise the plasma is swept out of

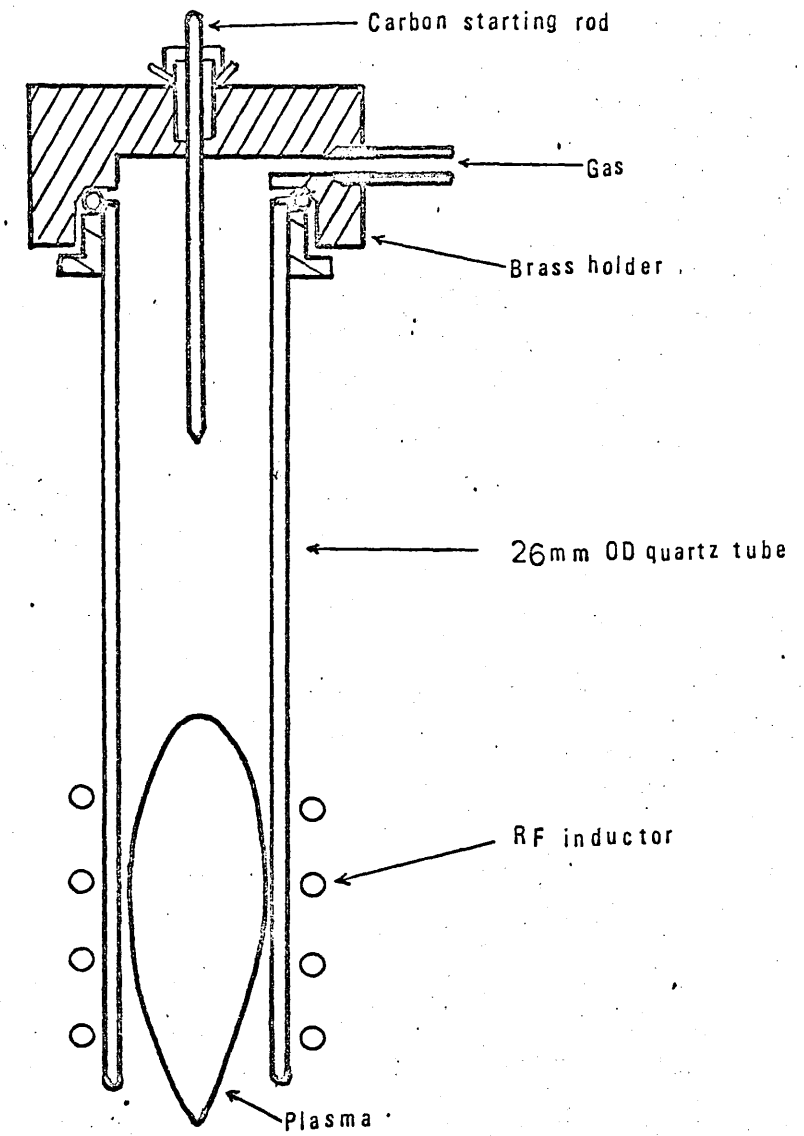

Fig.3.7 Reed's plasma torch

the field by the gas flow. At low gas velocities heat conduction is sufficient to maintain thermal ionisation in the mid power-absorbing region. At higher gas velocities thermal conduction is not enough and vortex stabilisation is often used. The gas is fed tangentially in the quartz tube and spirals down the tube producing a low pressure zone at the axis of the quartz tube. This pressure gradient causes plasma to flow up counter current to the main gas stream. With this type of stabilisation, the plasma flame extends further up stream with increasing gas flows and the gas flow along the wall drives the plasma towards the axis, cooling the quartz tube.

In another type of plasma stabilisation the gas is injected from a small diameter tube below the plasma region. The aspiration of gas into the jet causes a recirculation of the gas which results in good stabilisation.[53]

3.5.3. COOLING OF THE DISCHARGE TUBE

Heating of the discharge tube due to its proximity to the plasma offers no problem at power inputs below 3 or 4 kW, but becomes a serious problem at powers of 7 kW or more. The problem is reduced with diatomic gases as heat, conducted away from the plasma, is spent in dissociating the gas rather than heating the wall.

With a monoatomic gas cooling of the discharge tube becomes essential. Eckert et al [55] kept the plasma away from the wall of the discharge tune by increasing the diameter of the discharge tube, but too much increase in the diameter of the discharge tube makes the plasma unstable.[55]

In some of the commercially available induction plasma torches, the discharge tube is surrounded by a quartz tube jacket through which a cooling gas is fed radially. At the open end of the jacket cooling gas escapes along with the plasma gas. It is a common practice to use the same gas for cooling and plasma formation. Water instead of gas can be circulated

through the jacket which is now sealed to the discharge tube.

In another type of cooling arrangement plasma is generated in a water cooled hollow metallic cylinder[56] which contains eight to ten narrow slots less than 1mm wide parallel to the cylinder axis to allow the electromagnetic field to penetrate inside. The discharge inside the chamber carries annular eddy currents. Efficient cooling of the chamber promotes intensive recombination of the charged particles in the slots, and prevents a shunting current from forming. The metallic discharge chamber is surrounded by a quartz tube to prevent plasma gas from coming in contact with r.f. coil. The maximum temperature of the quartz tube was reported to be less than 100 ^{o}C by Donskoi et al [56] in this type of cooling.

3.5.4. PLASMA GASES

Argon was found to be one of the easiest gases in which plasma can be struck. This is due to [57] its low heat capacity and low thermal conductivity at ionising temperatures. Once the torch is started and the plasma is formed, argon may be replaced partially and in some cases completely by other gases such as helium, hydrogen and oxygen. When argon is replaced by a diatomic gas, the discharge contracts and power consumption increases because the gas requires additional energy for dissociation. Also the discharge temperature is lower [55] in a diatomic gas than in argon. To maintain the discharge, the replacement of argon by a diatomic gas should be gradual and should be accompanied by a corresponding increase in the power input. Too fast an increase in the concentration of a diatomic gas extinguishes the torch, while too fast an increase in power input can destroy an uncooled discharge tube. It has been found that the transition from argon to a diatomic gas is easier in a large diameter tube.

3.5.5. THE LOW FREQUENCY INDUCTION PLASMA TORCH

Earlier efforts by Reed [53] to initiate the r.f. induction plasma torch at 400 kHz failed. However, Floyd et al [58] in 1966, reported successful running of an induction plasma torch at 280 kHz. They used a 5cm (outside) diameter quartz discharge tube in which argon flowed downward at the rate of 60l/min. A pilot plasma was produced at 3.8 MHz by an r.f. solenoid placed around the upper part of the discharge tube. A second r.f. solenoid, which could be energised by a separate r.f. generator at 280 kHz, was placed 4 or 5 cm below the first one. When the second r.f. solenoid was energised, the plasma extended into the region of the lower solenoid and became brighter. It was found possible to maintain the plasma at the lower frequency but the length and the diameter of the plasma, then, decreased. Temperature measurements so vital for plasma description, were not made during these experiments. Attempts to initiate the torch at 280 kHz were unsuccessful.

3.5.6. TEMPERATURE IN THE INDUCTION PLASMA TORCH

Reed [53] determined the temperature distribution across the plasma torch spectroscopically. Using the Fowler Milne method [59] he obtained a maximum temperature of 16000 ^{o}K on the discharge axis. However, Johnston [60] obtained an off-axis peak temperature of 9000 ^{o}K with line intensity ratio mehtod.[61, 62] He showed that the Fowler Milne method could not be used to measure temperature in an induction plasma torch. The off-axis peak in the radial distribution of 763.5 nm line observed by Reed [53] was due to an off-axis peak temperature produced by the skin effect and not due to the norm-temperature.

Donskoi et al [56] employed a modified version of the induction plasma torch, mentioned previously in Art. 3 5.3. at a power of 4.5 kW. They used the absolute intensity recombination continuum in the region 430 - 470 nm

to measure the plasma temperature. The temperature distribution showed an off-axis peak at 9500 ^{o}K and a sharp decline towards the plasma periphery.

Goldfarb et al [63] measured the temperature distribution in a 20kW induction plasma torch, using the absolute intensity of argon recombination continuum. They obtained an off-axis peak temperature of 10,200 ^{o}K with a sharp decline near the periphery as before.

3.5.7. INDUCTION PLASMA TORCH IN AIR

Eckert et al [55] succeeded, in 1968, in completely replacing argon with air in a 100mm wide discharge tube of an r.f. induction plasma torch. The atmospheric pressure discharge in air consumed 20kW power. The diatomic gases in the air caused extensive cooling of the plasma during molecular dissociation and lowered the discharge temperature. A maximum temperature of 6300 ^{o}K was recorded in this air discharge.

3.5.8. THERMAL EQUILIBRIUM IN AN INDUCTION PLASMA TORCH

In an atmospheric pressure plasma at a temperature of about 10^{4} ^{o}K the mean free path is of the order of 3×10^{-4} cm [63] and consequently the collision frequency is very high ($\sim 10^{11}$ Hz). Under these conditions it is unlikely that electrons acquire energies much in excess of those of atoms and ions. An estimate of the field strength provides an approximate test for the difference of temperature between electrons and other heavy particles. For thermal equilibrium [53, 64]

$$\frac{Te - T}{T} = \frac{m_o}{4m_e} \left(\frac{\lambda e E}{3/2\ kT} \right)^2 << 1 \qquad (3.4)$$

From the knowledge of the power Q supplied to the plasma, electrical conductivity σ and the plasma volume $\mathcal{V}$, E can be estimated from [63]

$$E^2 \simeq Q \Sigma (1/\sigma v) \qquad (3.5)$$

For an induction plasma torch, running at 25 MHz and consuming 8kW, Gol'dfarb et al [63] found that

$$0.07 < (Te - T)/T < 0.25$$

The above estimate was made in the inductor zone. In the tail, the electric field is much smaller, consequently (Te - T) is also much smaller. Conditions are, therefore, more favourable for the thermal equilibrium.

3.5.9. FLOW VELOCITY OF THE PLASMA

Gol'dfarb et al [63] measured the radial velocity distribution in the plasma by moving water cooled pilot tube in a perpendicular plane 3mm from the discharge tube open end. To work out the velocity, radial density distribution was subsequently determined from radial temperature distribution.

The flow velocity was also estimated from photographs of the length of tracks of carbon particles, originating from a carbon rod introduced in the inductor region. With an exposure of 1/1000 sec tracks were found to be 1 - 2cm long. Flow velocities of 10-20 m sec^{-1} were estimated. Also mass flow was found to drop towards the periphery. [63]

3.5.10. ELECTRON DENSITY AND ELECTRICAL CONDUCTIVITY OF THE TORCH

Once the temperature is known, electron number density can be easily determined, using Saha's equation. Hughes and Wooding [65] obtained a value of 1.1×10^{16} cm^{-3} for the electron density and 24.5 $(ohm\ cm)^{-1}$ for the electrical conductivity of the plasma at a torch temperature of 9000 ^{o}K in argon. [66] They also determined electrical conductivity independently by

observing the change in the oscillator frequency when plasma is formed in the r.f. solenoid. The change in frequency was previously calibrated against conductivity by inserting different metals and salt solutions of different but known conductivities and of the same dimensions as the plasma. The value of electrical conductivity of 30(ohm - cm)$^{-1}$ so found was in agreement with the previously computed value of 24.5 (ohm - cm)$^{-1}$.

In general electron density and electrical conductivity are different in different parts of the plasma for the same power input. Both electron density and conductivity increase with temperature. Electrical conductivity plays a very important role not only in the power transfer mechanism, but also at the initial breakdown stage of the gas discharge.

3.5.11. ENERGY BALANCE IN THE TORCH

The total electrical power consumed in the plasma is dissipated by the hot gases flowing away from the plasma, thermal conduction to the wall of the discharge tube and by radiation. Reed [53] measured the amount of heat carried away by hot gases calorimetrically, using a hollow calorimeter with a successively decreasing hole, sealed to the open end of the quartz tube. The gas left this heat exchanger at room temperature. Heat lost to the wall of the discharge tube was measured by water flowing along the outside of the quartz tube. Radiation losses were measured by the rate of temperature rise in a brass hemisphere around the quartz tube. His results are tabulated below.

TABLE 3.1.

Plasma	Argon flow (l/mm)	Power to gas (W)	Power to radiation (W)	Power to Walls (W)	Total power to plasma (W)
1	9.4	350	540	740	1630
2	14.2	660	300	640	1600
3	18.9	700	290	560	1550
4	18.9	1000	550	980	2350

Reed, [53] as mentioned above, obtained these results by independent experiments. Therefore, these were not affected by his wrong estimate of the plasma temperature. No detailed determination of these losses appear elsewhere in the available literature. However, the radiation losses mentioned in Table 3.1 agree well with the results obtained by Rovinskii et al [67] in argon and by Grusdev et al [68] in Xenon one-atmospheric pressure r.f. induction plasmas in closed vessels.

3.6. MAGNETIC PINCH EFFECT IN AN INDUCTION PLASMA TORCH

In an r.f. induction plasma torch energy is coupled to the discharge through eddy currents induced in the plasma by the axial magnetic field of the r.f. solenoid. The resulting Lorentz force compresses or pinches the plasma. In addition the eddy currents in the plasma induce a magnetic field which opposes the applied magnetic field at the axis and assists it near the discharge periphery. The induced field thus makes an additional contribution to the Lorentz force. However, the applied magnetic field is small. Consequently the Lorentz force is also small. [57]

In a paper, which is mainly theoretical, Chase [69] developed a method of calculating the magnetic pressure across the closed ring discharge path. of an r.f. induction plasma torch. This method he applied to calculate the magnetic pressure at the axis of a 2.5 kW torch running at 4.7 MHz.

In an r.f. induction plasma torch, due to the low degree of ionisation ($\sim 10^{-2}$), [68] the applied magnetic field penetrates into the plasma so that the magnetic pressure cannot be determined from the relevent term in the global momentum equation which is based on complete ionisation. Chase considered the distribution of J and B within the plasma to determine the total magnetic pressure at the discharge axis.

3.6.1. TEMPERATURE AND ELECTRICAL CONDUCTIVITY DISTRIBUTION IN THE PLASMA

An atmospheric pressure induction plasma torch is near thermal equilibrium so that the electron density of the plasma can be calculated from Saha's equation, if the plasma temperature is known. The knowledge of electron density enables the electrical conductivity to be determined through equation (2.21). J can, then, be determined if the electric field in the plasma is known. To determine J, knowledge of the temperature distribution in the plasma is necessary. Chase, however, made no temperature measurements of the plasma. Instead he adapted the results of Dresvin et al [70] on a 25 MHz induction torch, running at the same power as his own, to his torch. To justify this he quotes several authors [25, 65] who have shown that the change in operating frequency has negligible effect on the peak plasma temperature, but has a noticeable effect in reducing the discharge diameter by a small amount. To account for the latter effect, Chase applied a correction factor which consisted in multiplying the plasma diameter of his torch by 0.93. After determining the temperature profile of the plasma, Chase directly determined the electrical conductivity of the discharge as a function of temperature from the data reported by Dresvin et al. [70]

Chase showed that the absolute value of the pressure gradient due to the Lorentz force is given by

$$\frac{\delta P}{\delta r} = -JB \qquad (3.6)$$

The negative sign means that the pressure is maximum at the axis. Both J and B change sign simultaneously so that the Lorentz force always acts inward.

3.6.2. MAGNETIC AND ELECTRIC FIELDS IN THE PLASMA

Chase assumed the plasma to be a cylinder of uniform diameter and of constant electrical conductivity. He applied the theory of inductive heating of a metallic cylinder placed along the axis of a solenoid, carrying an r.f. current, and calculated the electric and magnetic fields. The current density was calculated by

$$J = \sigma E \tag{3.7}$$

The determination of both E and H requires a knowledge of the magnetic field produced by the r.f. solenoid, which is given by

$$H_o = \gamma \frac{N i}{l} \tag{3.8}$$

where γ is the coupling factor which takes into account the deviation of the actual solenoid from the ideal case of an infinitely long and closely wound solenoid. From the work of Vermeulen et al [71] on the measurement of the magnetic field in the presence of an r.f. plasma, Chase used a value of 0.25 for γ in his calculations. He obtained the flux density from

$$B_o = \mu_o H_o \tag{3.9}$$

where μ_o is the permeability of free space and has a numerical value of $4\pi \times 10^{-7}$.

3.6.3. ESTIMATE OF EXCESS PRESSURE AND ITS EXPERIMENTAL VERIFICATION

In order to estimate the total magnetic pressure at the axis of the discharge, Chase divided the plasma into twelve homogenous coaxial

cylinders each 1mm thick. He determined J and B within each section to get the total magnetic pressure at the axis. His results show a steep pressure gradient at the discharge periphery. He further argued that the inductive plasma was compressed in two directions but not in the third. Under these conditions streaming or plasma flow would occur at the open ends of the plasma cylinder and the pressure energy of a volume element at the centre would be converted into kinetic energy. An axial cooled pressure probe at the centre of the discharge would measure static pressure whereas a probe near the axis-boundary of the plasma would measure the stagnation pressure, resulting from the outward flow against the probe tip.

Chase further suggested that to make up the axial outward gas flow, some gas might flow inward from the sides twice in each cycle when both J and B became zero. He took pressure measurements at the centre of the plasma and obtained a value of 71.5 dynes/cm^2 which was close to the calculated value of 64.5 dynes/cm^2.

3.6.4. EFFECT OF BUOYANCY

Assuming 9000 ^oK as the plasma temperature and 500 ^oK as the temperature of the surrounding gas, the buoyancy force was calculated by Chase to be 4.9 dynes/cm^2 which was less than 5% of the magnetic pressure and hence did not interfere with the measurements.

3.6.5. EFFECT OF GAS FLOW AND VORTEX STABILISATION

In the above discussion the effect of gas flow was ignored. This was justified by Chase by the fact that the flow velocity of the plasma was generally small, only of the order of 0.3 cm/sec. This would hardly influence the pinch effect.

During experiments on the measurements of the magnetic pressure, Chase introduced the gas into the plasma torch as a curtain flow through

1/16 inch holes around the inside periphery of the quartz confining tube at a rate of 16 litres/min S.T.P. so that there was no tangential component of the gas flow. Later, when he tried vortex stabilisation, he observed a low pressure area in the middle of the discharge. In fact he observed negative pressures on the axis of magnitude larger than those measured with no tangential flow. It was for this reason that he did not introduce the gas tangentially in his work.

The outward axial flow of the gas explains the existance of the apparent barrier of the plasma to axial flow of the feed powder directed through it when refractory crystals are grown. [72, 73] This was mentioned by Chase in support of his work.

3.7. EFFECT OF A PULSED MAGNETIC FIELD ON A HIGH PRESSURE INDUCTION PLASMA

Mitin and Pryadkin [74] studied the effect of a pulsed magnetic field on a static high pressure spherical induction plasma 5.0 cm across, produced in a closed vessel. The pulsed magnetic field was produced by discharging a capacitor through a single turn coil around the discharge tube in the immediate vicinity of the r.f. inductor. The pulsed magnetic field had a half period of 4.0 micro-secs. The field intensity was not measured but only estimated at 1.0 T by Mitin and Pryafkin. As a result of the pulsed magnetic field light intensity increased by 50 - 100 times and a prolonged after-glow was observed. The light intensity was found to reach a maximum when the magnetic field had almost fallen to zero. Mitin and Pryadkin made no temperature measurements. However, from the slope of straight time plot of $(I)^{-\frac{1}{2}}$ versus t, they obtained a radiative recombination of $\alpha = 2.7 \times 10^{-14}$ cm^3 sec^{-1}, assuming $n_e \propto \sqrt{I}$. This value is in fair agreement with their theoretical value [74] of 3.4×10^{-14} cm^3 sec^{-1} at 10^4 ^oK. Their work was, however, of an elementary nature and no further progress was reported in this field by these authors.

After reviewing the development and some of the properties of an r.f.

induction plasma torch it is desirable to review the related theoretical work on the torch. This is done in the next chapter.

CHAPTER 4

THEORY OF AN INDUCTION PLASMA TORCH

4.1 Introduction

The radio-frequency induction discharge at a high pressure has been known since 1947, when Babat [43] gave a detailed account of his experiments. However, its mechanism was not well understood at that time and little work was undertaken until 1961 when Reed [53] invented the induction plasma torch. His invention stimulated great interest in both experimental and theoretical work all over the world. Theoretical papers since 1961 have dealt with the high pressure r.f. induction discharges with flowing and static plasmas.

A theoretical study of a static induction plasma makes it possible to explain the important features of a flowing plasma in an induction torch. Most papers have neglected the small flow velocity of the plasma and have reduced the theoretical consideration to that of a high pressure static induction discharge. A comprehensive theory embracing all physical phenomena taking place in the induction plasma torch, has not so far been established, but the theories covering various aspects of the physical state of the torch are traced in this chapter. The transformer-theory, dealing with the mechanism of power transfer is dealt with first. This is followed by 'the metallic cylinder model'. The theory presented in Section 4.4 attempts to base the discharge analysis on the distribution of temperature and electrical conductivity in the discharge rather than assuming them constant and uniform over the plasma cross-section as is done in the metallic

cylinder model. Finally, in a theory put forward by Raizer.[77], the induction torch is compared with an ordinary chemical flame.

4.2 Transformer Theory

The discharge may be regarded as the short-circuited single turn secondary of a transformer [69] whose primary is the radio-frequency inductor of the oscillator tank circuit. Fig. 4.1 shows, schematically, the inductor current i_1 (r.m.s. value), flowing in the N-turn primary of inductance L_1. The plasma, assumed as a purely resistive load, is shown connected across the single turn secondary which has an inductance L_2. If γ is the coupling coefficient, the mutual inductance is given by

$$M = \gamma \sqrt{L_1 L_2} \quad \text{(S.I. Units)} \tag{4.1}$$

When the discharge is running

$$V_2 = i_2 R_2 = j\, i_1 \omega M - j\, i_2 \omega L_2 \tag{4.2}$$

Let a_1 and l_1 be the cross-sectional area and the length of the r.f. inductor and let a_2, l_2 be the corresponding quantities for the plasma. Then,

$$L_1 = \mu N^2 a_1 / l_1 \tag{4.3}$$

$$L_2 = \mu a_2 / l_2 \tag{4.4}$$

$$M = \mu N a_2 / l_1 \tag{4.5}$$

The magnetic field produced by the inductor is given by

$$H_o = \gamma N i_1 / l_1 \tag{4.6}$$

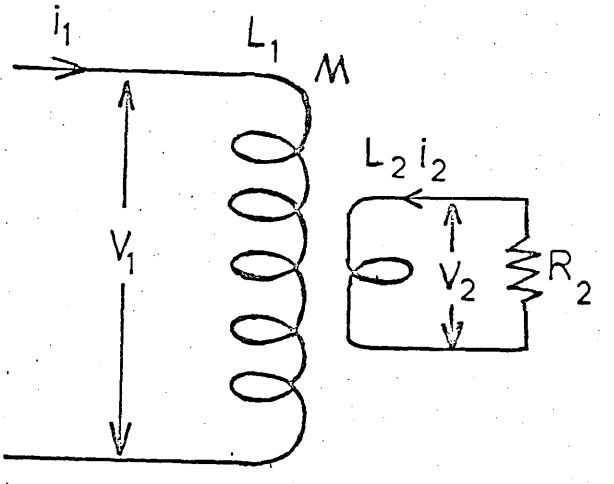

Fig.4.1 Induction plasma torch represented by a transformer with a short circuited single turn secondary winding.

Constant γ (<1) is introduced to take into account the leakage of the flux. From equations (4.2) to (4.6) it can be shown that [78]

$$V_2 = \frac{R_2 l_2}{\gamma} H_o (1 + j R_2 l_2/\mu_o \omega a_2)/(1 + R_2^2 l_2^2/\mu^2 \omega^2 a_2^2) \qquad (4.7)$$

If R_2 is much bigger than $\mu\omega a_2$, Equation (4.7) reduces to

$$V_2 = j\omega H_o \mu\omega/\gamma \qquad (4.8)$$

The knowledge of V_2 is helpful for an understanding of the torch mechanism and combined with the discharge diameter it gives the value of the electric field E, which may be used to estimate the degree of thermal equilibrium in the torch from equation (3. 4).

This theory assumes the current paths in the discharge to be well defined and does not consider the limited skin-depth which exists at the frquencies employed in the induction plasma torches. Moreover, an energy balance consideration cannot be obtained from this simple theory.

A better picture of the discharge is presented by a model described below, in which the discharge is regarded as equivalent to a metallic cylinder placed coaxially in an r.f. inductor.

4.3 Metallic Cylinder Model

In this model the discharge is treated as a metallic cylinder with constant uniform electrical conductivity and a constant radius R in a discharge tube of radius R_o [77] as shown in Fig. 4.2. The small axial velocity of the plasma is neglected and the plasma is assumed stationary. The only energy loss included in the model is the thermal conduction loss along the radius whilst convection loss along the axis and the radiation

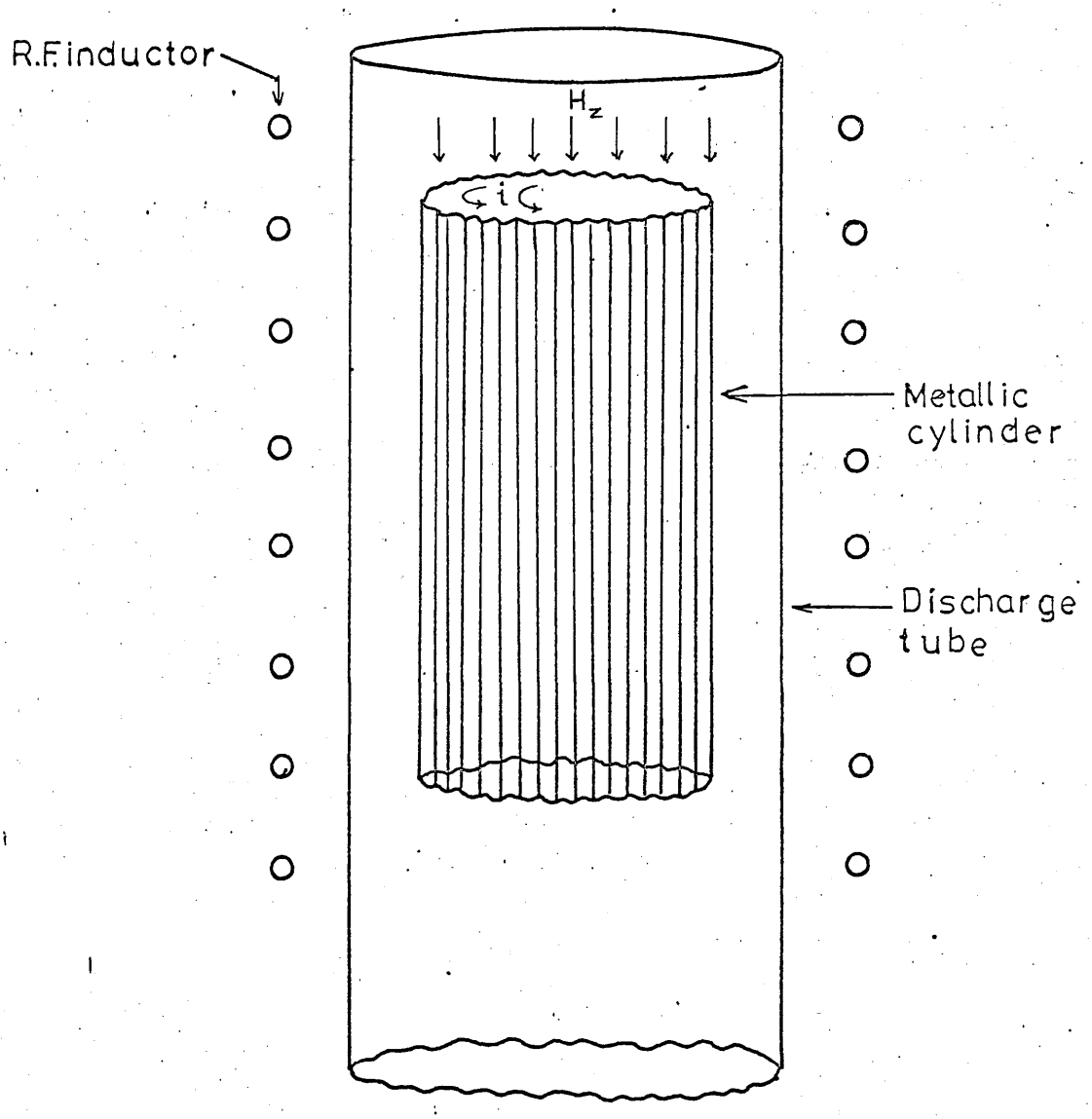

Fig.4.2 Metallic cylinder model of an r.f. induction plasma torch

losses are neglected. This simple model describes the torch mechanism fairly well. The r.f. solenoid is considered to be long so that the process is assumed to be one dimensional. The cold gas between the discharge and the tube only serves to push the plasma away from the tube wall and plays no part in power dissipation. Estimates for low pressure induction discharge based on this model were first made by Thomson [79] in 1926.

If both E and H fields are proportional to expt ($j\omega t$), the Maxwell's equations in cylindrical co-ordinates become, with the z-axis along the axis of the discharge tube

$$-\frac{\delta H}{\delta r} = \sigma E \qquad (4.9)$$

$$\frac{1}{r}\frac{\delta}{\delta r}(rE) = j\omega H\mu \qquad (4.10)$$

The amplitude of the magnetic field is not a function of position in the non-conducting region between the discharge and the r.f. inductor and is given by

$$H_o = N i_1 \qquad (4.11)$$

Eliminating E from Equations (4.9) and (4.10) leads to

$$\frac{\delta^2 H}{\delta^2 r} + \frac{1}{r}\frac{\delta H}{\delta r} - j\omega\mu\sigma H = 0 \qquad (4.12)$$

This differential equation has the solution

$$H = H_o\left[\frac{(\mathrm{ber}(\sqrt{2}r/\delta))^2 + (\mathrm{bei}(\sqrt{2}r/\delta))^2}{(\mathrm{ber}(\sqrt{2}R/\delta))^2 + (\mathrm{bei}(\sqrt{2}R/\delta))^2}\right]^{1/2} \qquad (4.13)$$

Where ber and bei are Kelvin's functions. The skin depth δ is given by

$$\delta = (\pi\mu\sigma f)^{-\frac{1}{2}} \tag{4.14}$$

Similarly E can be shown to be given by

$$E = (\sqrt{2}\, H_o/\sigma\delta)\left[\frac{(\text{ber}'(\sqrt{2}r/\delta))^2 + (\text{bei}'(\sqrt{2}r/\delta))^2}{(\text{ber}(\sqrt{2}R/\delta))^2 + (\text{bei}(\sqrt{2}R/\delta))^2}\right]^{1/2} \tag{4.15}$$

where ber' and bei' are first derivatives of ber and bei respectively.

The power dissipated per unit length of the discharge W/l_2 is given by

$$W/l_2 = \int_o^{R_o} 2\pi r E^2 \sigma \, dr$$

or,

$$W/l_2 = (\delta\pi H_o^2 R/\sigma\delta) \times F \tag{4.16}$$

where,

$$F = \sqrt{2}\, \frac{\text{ber}(\sqrt{2}R/\delta)\,\text{ber}'(\sqrt{2}R/\delta) + \text{bei}(\sqrt{2}R/\delta)\,\text{bei}'(\sqrt{2}R/\delta)}{(\text{ber}(\sqrt{2}R/\delta))^2 + (\text{bei}(\sqrt{2}R/\delta))^2} \tag{4.17}$$

Alternatively W/l_2 may be expressed in terms of Poynting's vector $\bar{P}_R$ which is given by

$$|\bar{P}_R| = |\bar{E}\Lambda\bar{H}| = 3.16 \times 10^{-2} \cdot (Ni_l \text{ (amp-turn/cm)} \cdot f(\text{M Hz})/\sigma(\text{ohm-cm})^{-1}) \tag{4.18}$$

i.e. $$W/l_2 = 2\pi R \bar{P}_R F \tag{4.19}$$

The plasma temperature is determined by the energy balance equation

$$\bar{\tau} + \bar{P} = 0 \tag{4.20}$$

where

$$\tilde{\tau} = -k \frac{dT}{dr} \tag{4.21}$$

and $\bar{P}$ is the Poynting-vector at a radial position 'r'. The flux of electromagnetic energy from the solenoid to the axis ($\bar{P} < 0$) is cancelled out by the heat flux going in the direction of the wall ($\tau > 0$). Eliminating E from equation (4.18) and (4.9), one obtains,

$$\bar{P} = -\frac{1}{2\sigma} \frac{d(H^2)}{dr} \tag{4.22}$$

Substituting the values of $\bar{P}$ and $\tilde{\tau}$ from equations (4.21) and (4.22) in (4.20), multiplying throughout by σ and finally integrating the resultant equation with the boundary conditions that at $r = R_o$, $T = 0$ and $H = H_o$ one obtains,

$$\int_0^{T_o} \sigma k dT = H_o (1 - H^2(r)/H_o^2) = H_o \left[1 - \frac{(\mathrm{ber}(\sqrt{2}r/\delta))^2 + (\mathrm{bei}(\sqrt{2}r/\delta))^2}{(\mathrm{ber}(\sqrt{2}R/\delta))^2 + (\mathrm{bei}(\sqrt{2}R/\delta))^2} \right] \tag{4.23}$$

Where H_o is the magnetic field on the plasma-surface. At the axis where the temperature has its maximum value T_m the above equation becomes,

$$\int_0^{T_m} \sigma k dT = \left(\frac{Ni}{2}\right)^2 \left[1 - \frac{H^2(o)}{H_o^2} \right] = \left(\frac{Ni}{2}\right)^2 \left[1 - \frac{1}{(\mathrm{ber}(\sqrt{2}R/\delta))^2 + (\mathrm{bei}(\sqrt{2}R/\delta))^2} \right] \tag{4.24}$$

Where H(o) is the magnetic field on the plasma axis. At high temperatures ($\sim 10{,}000\ ^{o}K$) and high frequencies $\delta < R$, equation (4.24) becomes,

$$\int_0^{T_m} \sigma k dT = \left(\frac{Ni_l}{2}\right)^2 \qquad (4.25)$$

Then, the discharge temperature depends only on the ampere turns per centimetre of the coil and on the gas properties but is independent of the frequency and the tube radius.

At atmospheric pressure the plasma is nearly in thermal equilibrium, therefore, both σ and k become functions of temperature only. Fig. 4.3 shows a plot of $\int \sigma k dT$ against T. After calculating T_m, the maximum temperature, $\sigma(T_m)$, the conductivity, may be determined with the aid of Fig. 4.4 given by Raizer,[77] and then the skin-depth δ may be evaluated from equation (4.14). Finally the power dissipation may be calculated with the aid of equation (4.16) or equation (4.19).

Metallic cylinder model neglects the effect of the electrical conductivity variation caused by a temperature distribution across the discharge. Eckert[80] developed a theory for the induction torch, which took the radial distribution of temperature and electrical conductivity of the plasma into account. This is presented in the following pages.

4.4 Analysis of an Induction Plasma Torch Dominated by Radial Conduction Losses - (Due to Eckert)

For a long cylindrical plasma column which loses heat by radial conduction and which is maintained by the dissipation of electric power, the energy balance equation can be written as

$$\frac{d^2s}{dr^2} + \frac{1}{r}\frac{ds}{dr} + \sigma E^2 = 0 \qquad (4.26)$$

where the heat conduction potential is defined by

$$S = \int_0^T k dT \qquad (4.27)$$

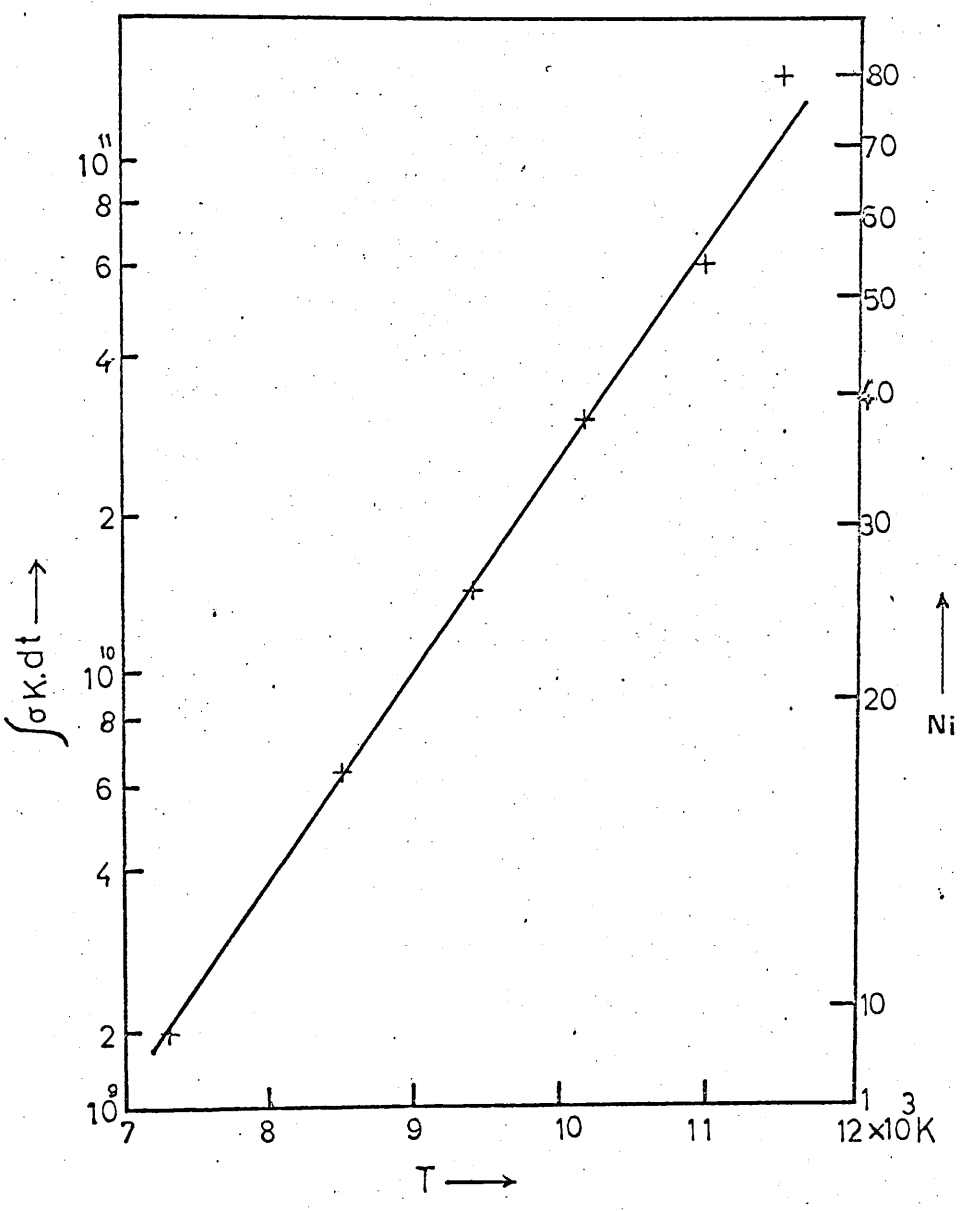

Fig.4.3 Variation of $\int \sigma k dT$ with 'T' and Ni

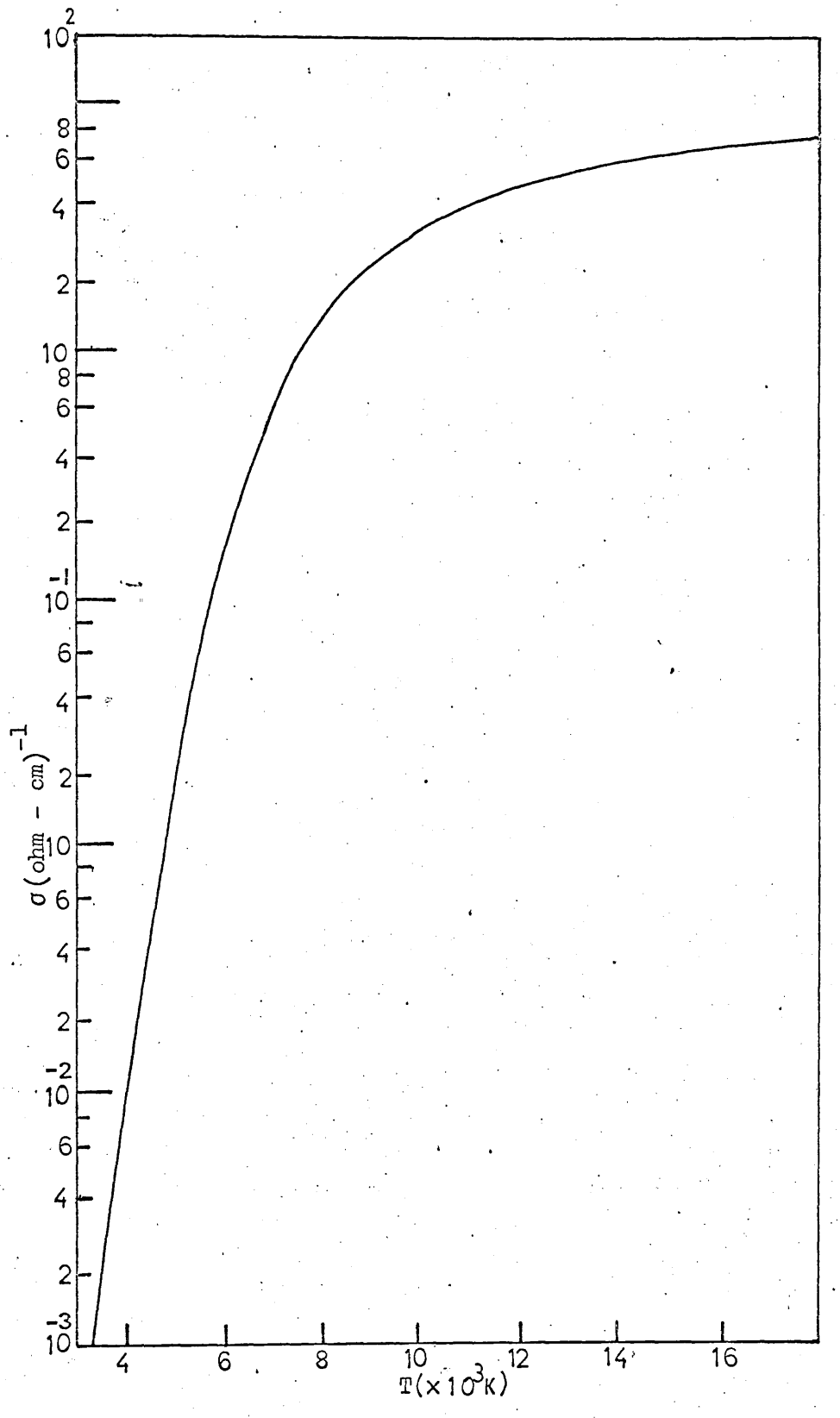

Fig.4.4 Electrical conductivity of argon at one atm, after Raizor.

The variation of s with T for argon at a pressure of 1 atm, according to Emmon's [23] experimental results on a d.c. arc, is plotted in Fig. 4.5. The dependence of σ on s may be approximated by the linear relationship

$$\sigma = C_K^2 S \tag{4.28}$$

where C_K is a constant depending on the gas. For argon $C_K = 1.6\ V^{-2}$. The variation of σ with s predicted by equation (4.28), is compared with Emmon's experimental results in Fig. 4.6. Substituting the value of σ in equation (4.26) from equation (4.28) yields

$$\frac{d^2S}{dr^2} + \frac{1}{r}\frac{dS}{dr} + (C_K^2 E^2)S = 0 \tag{4.29}$$

To solve the above equation for S the value of E, given by the following equation, must be known.

$$\frac{d^2E}{dr^2} + \frac{1}{r}\frac{dE}{dr} - (j\omega\mu\sigma + 1/r^2)E = 0 \tag{4.30}$$

Now, equation (4.29) may be integrated if the distribution of E is approximated by a power law, which follows as a solution of equation (4.30) provided the conductivity varies according to

$$\sigma = \sigma_R \rho^{-2} \tag{4.31}$$

where $\rho = (r/R)$. When combined with equation (4.31), equation (4.30) has the solution

$$E = E_R \rho^{\tilde{p}} \tag{4.32}$$

where $\tilde{p}$ is a complex number with its real part

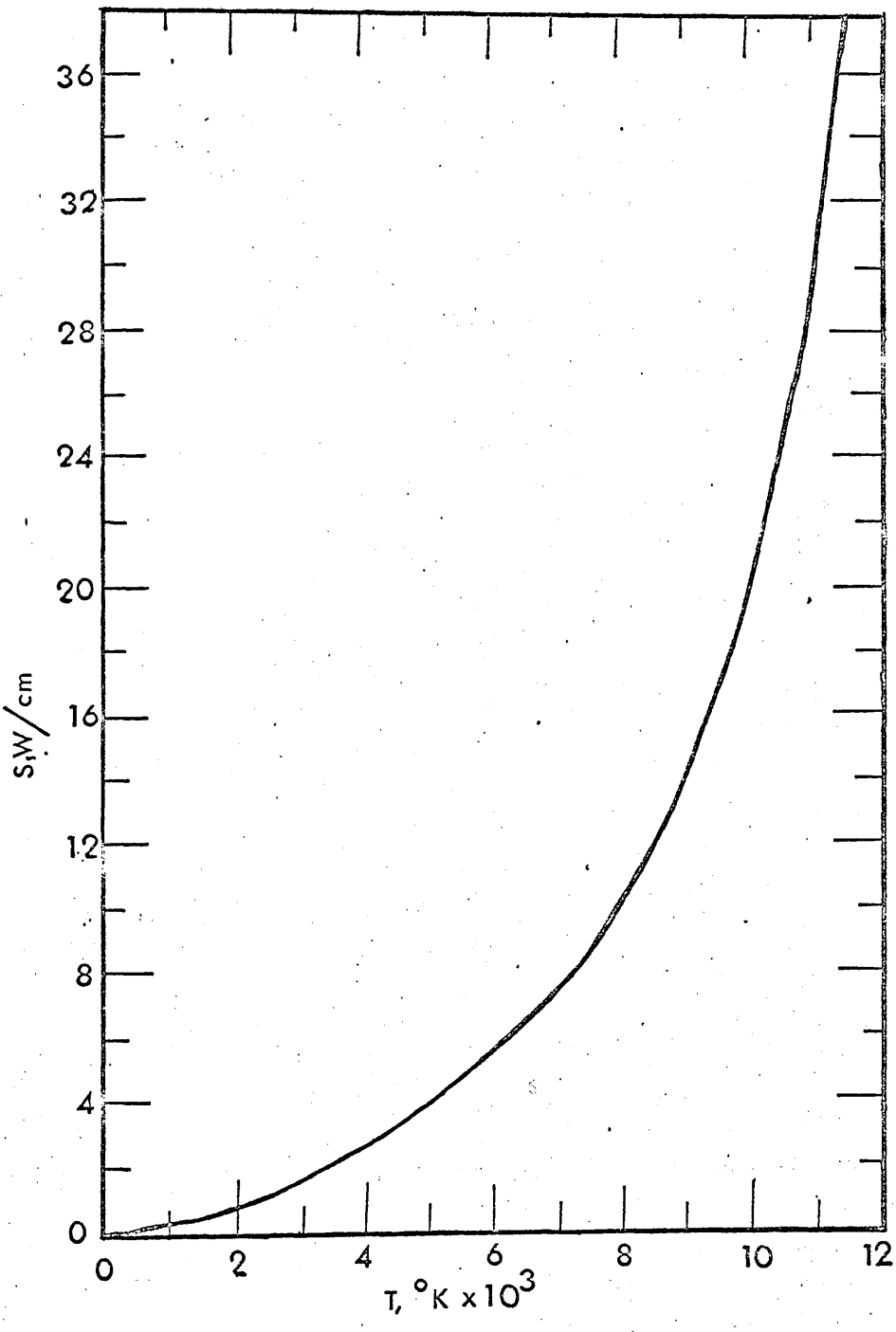

Fig4.5 Variation of 'S' with 'T'.

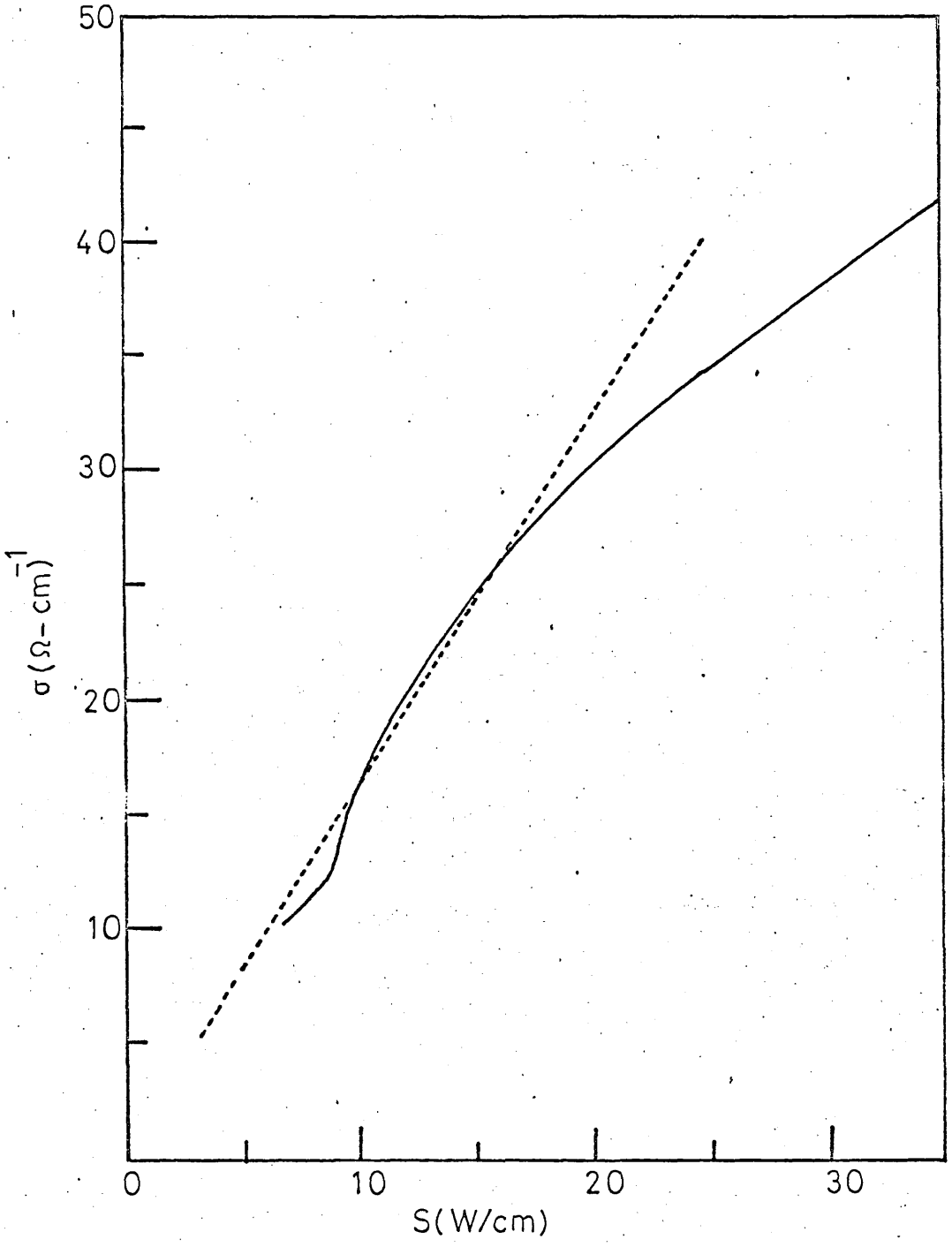

Fig 4.6 Variation of σ with s (i) solid line - Emmon's experimental curve (ii) dotted line-according to Eq 4.28

$$q = \left(\tfrac{1}{2}\left\{1 + \left[1 + 4\,(R/\delta)^4\right]^{\frac{1}{2}}\right\}\right)^{\frac{1}{2}} \tag{4.33}$$

where the skin depth δ is given by

$$\delta = (2/\omega\mu\,\sigma_R)^{\frac{1}{2}} \tag{4.34}$$

Fig. 4.7 shows the variation of q with R/δ. It is seen that for $R/\delta > 2$, q is practically equal to R/δ. Considering only the real component of E

$$E = E_R\,\rho^q \tag{4.35}$$

Equation (4.31) gives an infinite peak for σ at the axis, which presents a very poor approximation of the actual σ distribution. However, this equation is to be used only in the combination σE^2, which is well-behaved.

Introducing equation (4.35) in equation (4.29) and solving gives,

$$S = S_o\,J_o\left(K'^{\frac{1}{2}}/(q+1)\;\rho^{q+1}\right) \tag{4.36}$$

where J_o is the Bessel function of zero order and $K' = (C_K\,E_R\,R)^2$

At the plasma boundary $\rho = 1$ and $S = 0$. Therefore,

$$K'^{\frac{1}{2}}/(q+1) = \pm\lambda_n \tag{4.37}$$

Where λ_n are the zeroes of J_o. In the steady state only the first mode with $\lambda = 2.405$ can exist. This gives

$$S = S_o\,J_o\,(2.405\,\rho^{q+1}) \tag{4.38}$$

Because of equation (4.28) the same distribution exists for σ i.e.

$$\sigma = \sigma_o\,J_o\,(2.405\,\rho^{q+1}) \tag{4.39}$$

σ_o is the electrical conductivity at the axis.

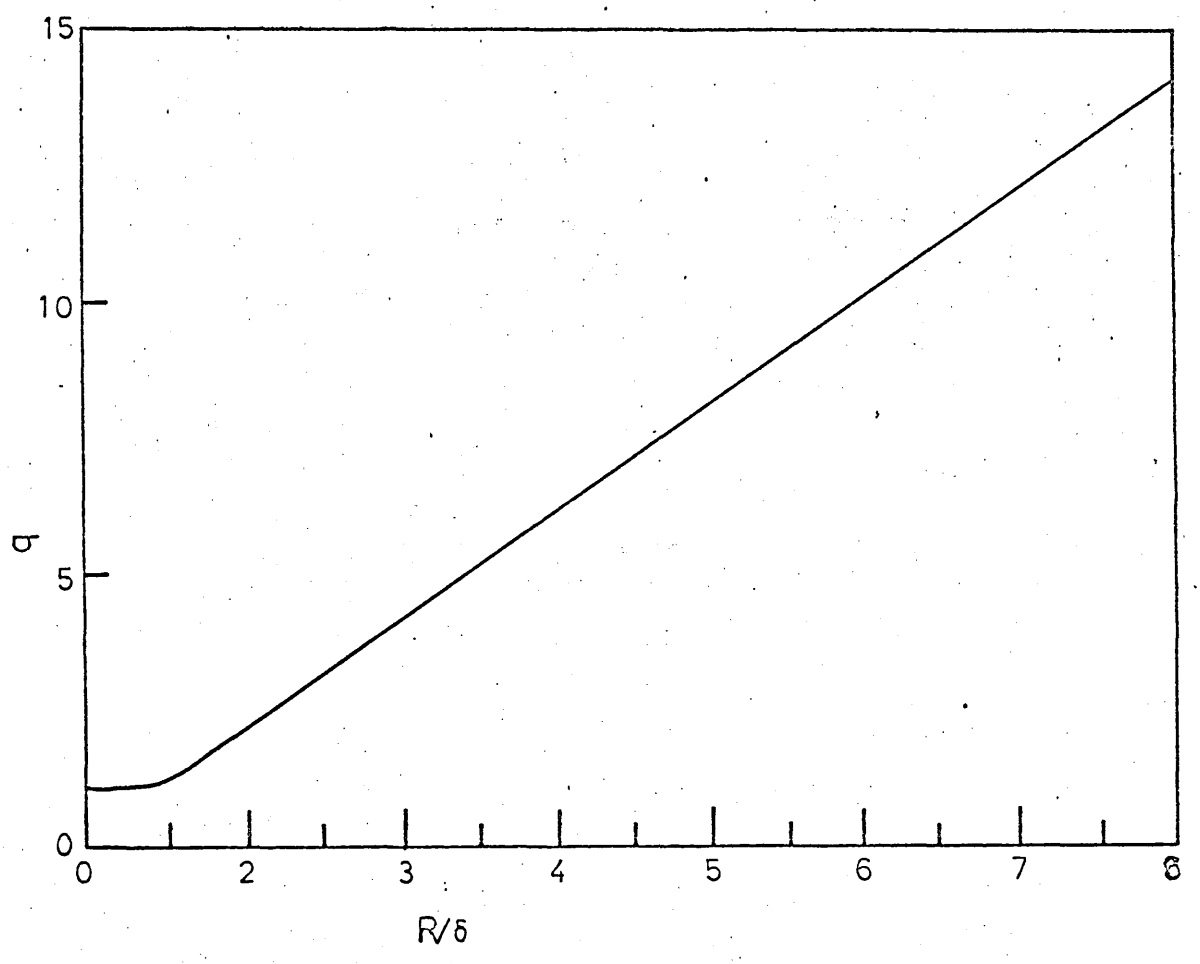

Fig 4.7 Exponent in power law describing electric field distribution vs plasma (radio/skin depth) ratio, after Eckert.

4.4.1 Relationship Between σ_R and σ_o

It is important to see how σ_o which determines the amplitude of the conductivity profile, is related to σ_R, which through R/δ and q determines its shape. This relation can be obtained from consideration of the power dissipated per unit discharge length.

$$W/l_2 = 2\pi R^2 \int_0^1 \sigma E^2 \rho \, d\rho \tag{4.40}$$

Combining the above with Eqs. (4.31) and (4.35) yields

$$W/l_2 = 2\pi R^2 E_R^2 (\sigma_R/2q) \tag{4.41}$$

While equations (4.35) and (4.39) combined with equation (4.40) yield

$$W/l_2 = 2\pi R^2 E_R^2 [\sigma_o/(q+1)] J_1(\lambda)/\lambda \tag{4.42}$$

where J_1 is the Bessel function of the first order. Combining equations (4.41) and (4.42) gives

$$\sigma_o = 2.31 [(q+1)/q] \sigma_R \tag{4.43}$$

For the vanishing conductivity q = 1 and (σ_o/σ_R) has the maximum value of 4.62. For $q \to \infty$ $(\sigma_o/\sigma_R) \to 2.31$.

4.42 Determination of σ_o, S_o and T_o

In order to determine the S and σ distributions σ_o and S_o must first be determined from the external parameters, which are,

(i) the external magnetic field H_o which is determined by the turn-spacing and the r.f. current.

(ii) the excitation frequency.

(iii) the plasma radius R.

The above variables can be replaced by a single variable the time rate of change of the magnetic flux ϕ'_o. The link between the internal and external conditions can be established in the following way.

Equation (4.37) yields

$$E_R = \lambda(q + 1)/C_K R \tag{4.44}$$

From the law of electromagnetic induction

$$\rho^{-1} \frac{d}{d\rho} (\rho E) = - jR\mu\omega H \tag{4.45}$$

With $E \propto e^{j\theta}$ and the E-distribution of equation (4.35) the above equation yields

$$E_R = - R\omega\mu H_o/(q + 1) \text{ Sin } \theta_R \tag{4.46}$$

From Poynting's theorem

$$W/l_2 = -2\pi R E_R H_o \text{ Cos } \theta_R \tag{4.47}$$

where θ_R is the phase angle between E_R and H_o. Eliminating W/l and θ_R from equations (4.41), (4.46) and (4.47) one gets

$$(E_R R \sigma_R/2q H_o)^2 = 1 - [E_R(q + 1)/R\mu\omega H_o]^2 \tag{4.48}$$

Introducing the time rate of change of the magnetic flux

$$\phi'_o = \pi R^2 \mu\omega H_o \tag{4.49}$$

and using equations (4.34), (4.44), (4.48) and (4.49) one gets

$$\phi_o' = [\pi\lambda(q+1)/C_K]\,[(1/q^2)\,(R/\delta)^4 + (q+1)^2]^{\frac{1}{2}} \qquad (4.50)$$

Since q is related to (R/δ) by equation (4.33), the above equation gives an explicit relation between ϕ_o' and (R/δ). For weak screening i.e. for $R/\delta \to 0$ and, therefore, $q \to 1$

$$\phi'_{omin} = 4\pi\lambda/C_K \approx 24V \qquad (4.51)$$

This means that the discharge cannot be ignited if the voltage induced at the circumference is less than 24V. For $R/\delta \to \infty$, where $q \approx R/\delta$ equation (4.50) reduces to

$$\phi_o' = (\sqrt{2}\,\pi\lambda/C_K)\,(R/\delta)^2$$

or

$$(R/\delta) = 0.34(\phi_o')^{\frac{1}{2}} \qquad (4.52)$$

The variation of R/δ with ϕ_o' expressed by equation (4.50) is plotted in Fig. 4.8 along with the asymptotic expressions from equations (4.51) and (4.52). Knowing R/δ, the terms $\sigma_o\mu\omega R^2$ can be found from equations (4.34) and (4.43). For the limiting case $\phi_o' \to \infty$. Combination of these equations with equation (4.52) yields,

$$\sigma_o = 1.7\,H_o \qquad (4.53)$$

Thus at a high rate of flux change the plasma conductivity changes in proportion to the applied magnetic field. The variation of $\sigma_o\mu\omega R_o^2$ with ϕ_o' along with the equations (4.51) and (4.53) are plotted in Fig. 4.9. S_o

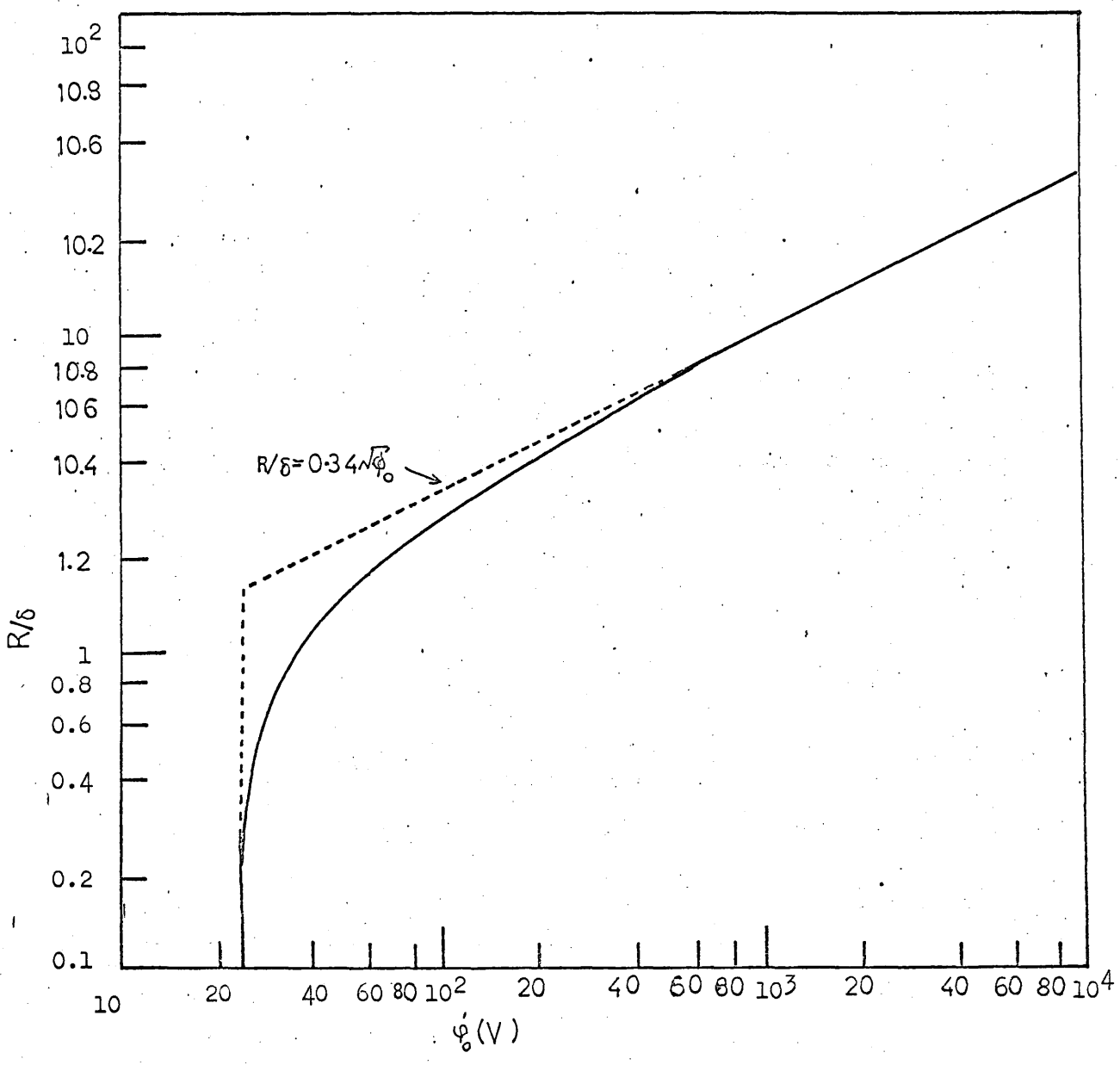

Fig.4.8 Variation of plasma (radius/skin depth) ratio with rate of change of applied magnetic flux. Argon, 1 atm, After Eckert.

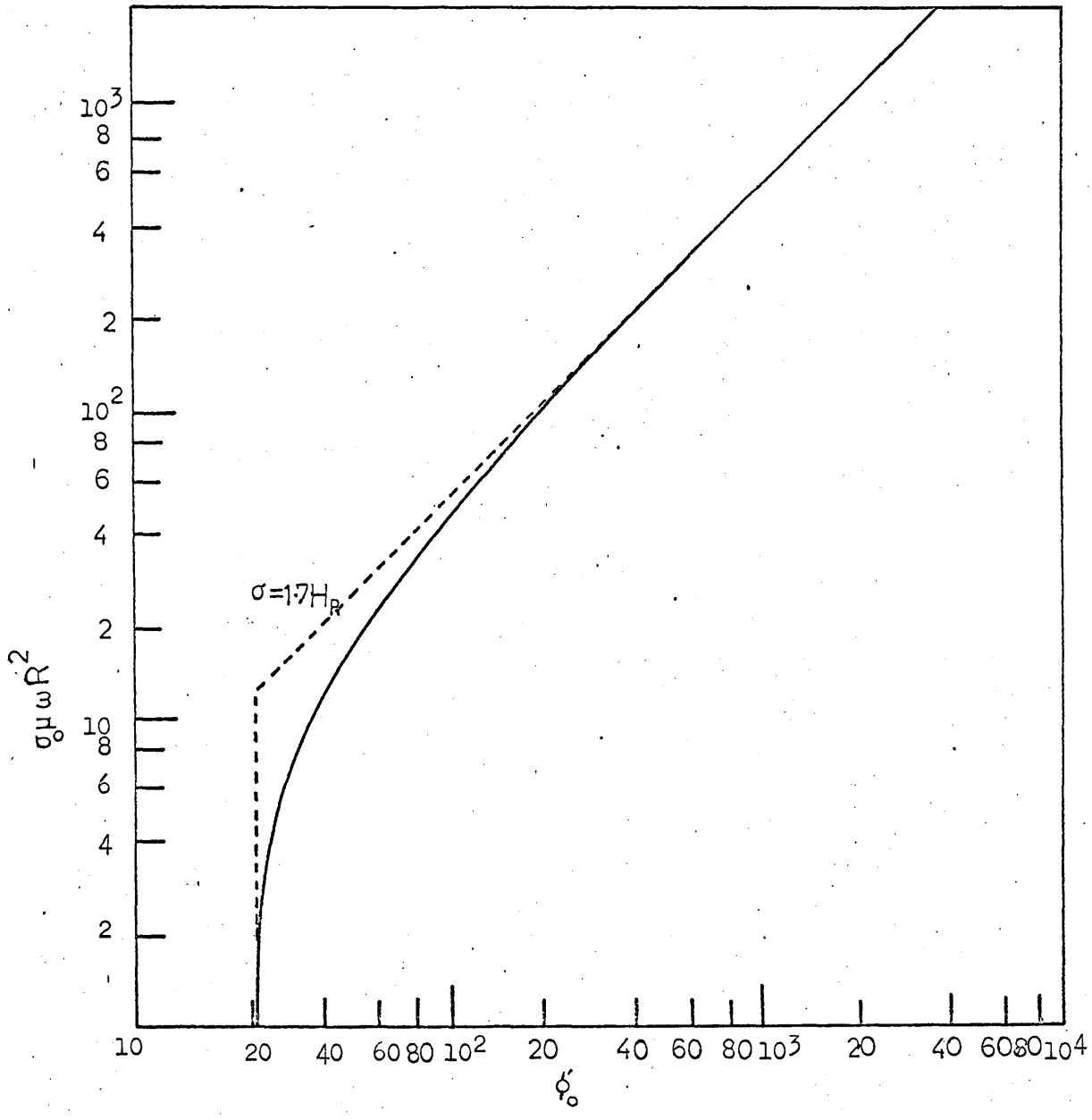

Fig.4.9 Scaling law for electrical conductivity at axis of plasma column in argon at 1 atm. After Eckert.

and q can be obtained from Figs. 4.6 and 4.7, respectively, once σ_o and (R/δ) have been determined for a particular value of ϕ'_o. Absolute distributions of S and σ can then be obtained from equations (4.38) and (4.39). From the S-distribtuion, T-distribution can be obtained from Fig. 4.4.

4.4.3 Power Dissipation

Combining equations (4.47), (4.41), (4.34) and (4.49) yields

$$(W/l_2)\ \mu\omega R^2 = 2q\phi_o'^2/\pi(R/\delta)^2\ \cos^2\theta_R \qquad (4.54)$$

from which ϕ'_o may be eliminated using equations (4.44) and (4.46). This gives

$$(W/l_2)\ \mu\omega R^2 = \frac{2q}{\pi(R/\delta)^2}\left[\phi_o'^2 - \left(\frac{\pi\lambda(q+1)^2}{C_K}\right)^2\right] \qquad (4.55)$$

Equation (4.55) has been plotted in Fig. 4.10, where the curve starts with an infinite slope at ϕ'_{min} and for large values of ϕ'_o becomes proportional to $(\phi'_o)^{3/2}$. In the same figure the broken line represents the equation

$$(W_o/l_2)\mu\omega R^2 = \pi^{-1}\ \phi_o'^2 \qquad (4.56)$$

where $W_o = \pi R^2 l_2 \mu\omega H_o^2$ is the magnetic power available in the discharge volume. Dividing equation (4.55) by equation (4.56) gives the rate at which the discharge converts magnetic energy into heat. This is

$$W/W_o = \frac{2q}{(R/\delta)^2}\left[1 - \left\{\frac{\pi\lambda(q+1)^2}{C_K\ \phi'_o}\right\}^2\right] \qquad (4.57)$$

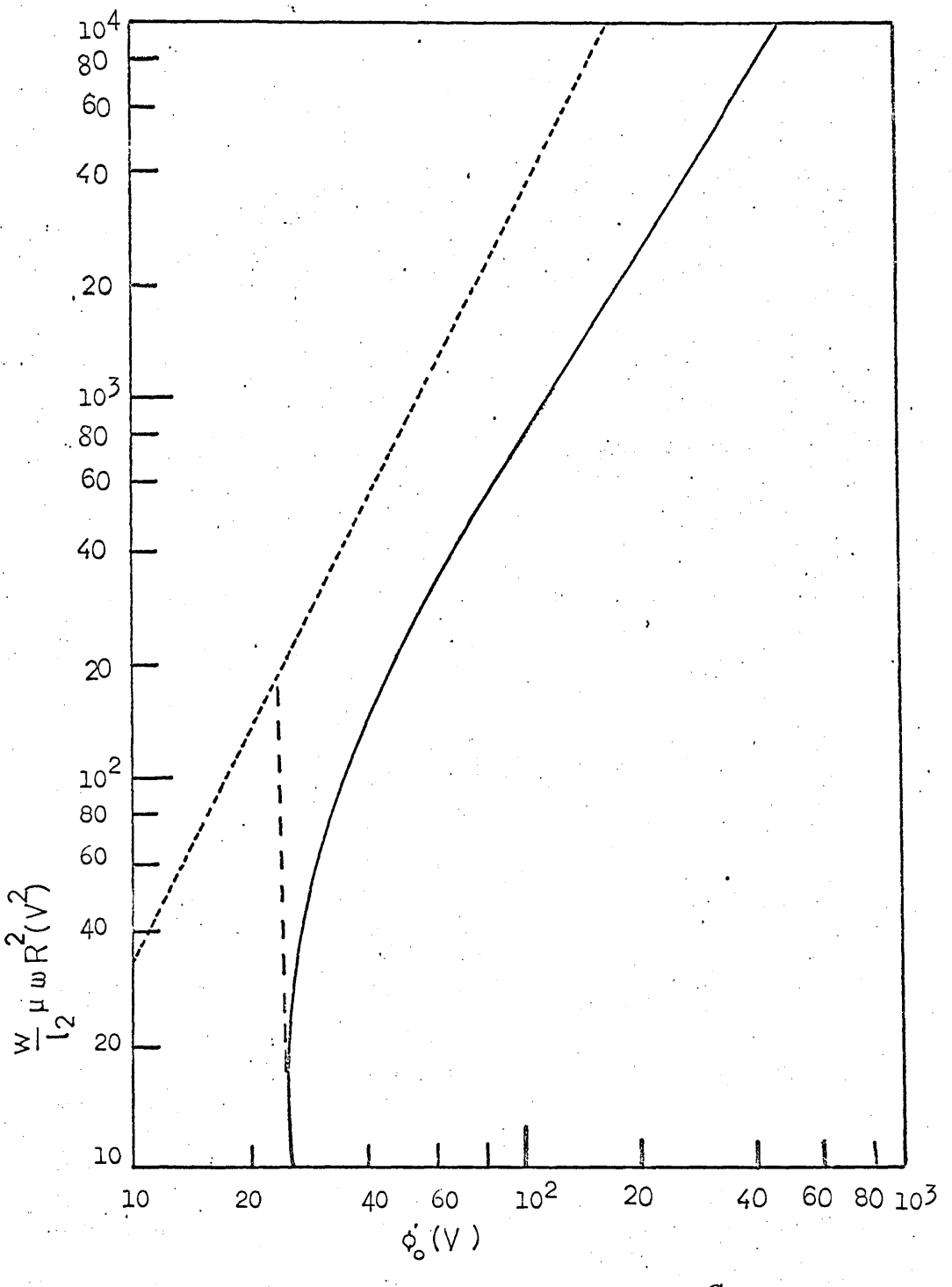

Fig.4.10 Scaling law for power per cm plasma column.
(i) ------ available magnetic power
(ii) —— dissipated power.
After Eckert

This result is compared with that of solid conductor model described in section 4.3, having a fixed conductivity, in Fig. 4.11 where W/W_o has been plotted against R/δ for each case. In the case of a solid conductor the conversion rate reaches a maximum of about 37% at $R/\delta = 1.7$ whereas the results of the present analysis give a maximum energy conversion rate of about 30% at $R/\delta = 1.5$. For the optimum condition $R/\delta = 1.5$. Fig. 4.8 then gives

$$\phi_o' = 48V \tag{4.58}$$

which is twice the minimum value. The effective flux maintaining the discharge is reduced by the secondary current and is not an independent variable. Since

$$\phi' = 2\pi R E_R = 2\pi\lambda(q + 1)/C_K \tag{4.59}$$

For the optimum condition $q = 1.68$ and therefore

$$\phi' \approx 32V \tag{4.60}$$

that is the flux is reduced to two thirds of the applied value.

The above analysis disregards the radiation losses and therefore gives a flat plateau at the axis rather than a small dip in the temperature profile generally observed in the experimental results.[24, 63, 66, 81] With $R = 1.5$ cm; $f = \omega/2\pi = 26$ M Hz and $H_o = 20$ to 30A/cm, Eckert compares the results of th present analysis with those obtained numerically. This analysis over estimates the plateau temperature by about 15% but gives the correct temperature profile.

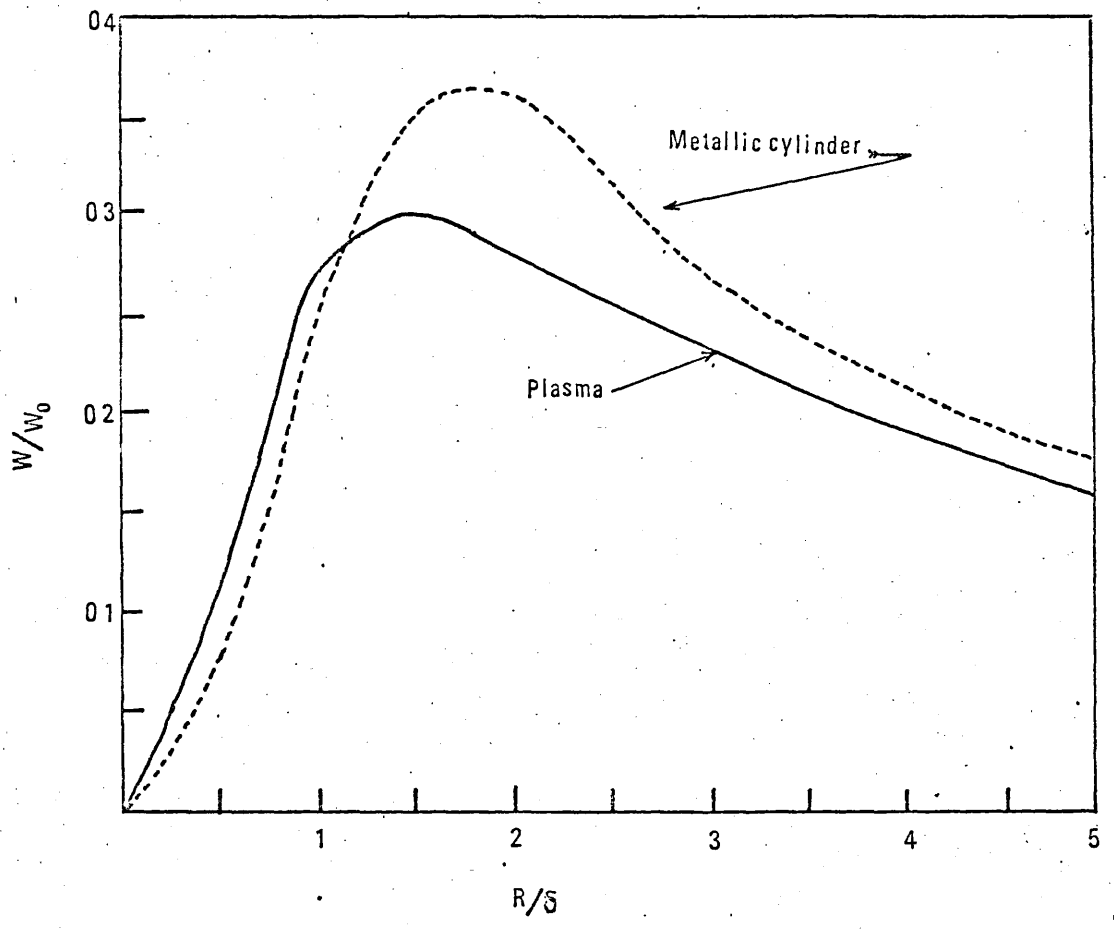

Fig. 4.11 Dissipation rate of magnetic power vs plasma (radius/skin) depth ratio. After Eckert.

4.5. Analogy of an Induction Plasma Torch with a Chemical Flame

A different approach is that of Raizer [77] in which the r.f. induction plasma torch is compared with an ordinary flame.

4.5.1. Qualitative Analysis

According to Raizer the electrical conductivity of a gas increases with temperature (shown in Fig.4.4) in a similar manner as the rate of the chemical reaction in a flame. As in a chemical flame it is appropriate to define an ignition temperature T_o for the discharge such that for $T < T_o$, the gas is practically nonconducting and for $T > T_o$, the Joule heating of the induction current is released and the r.f. field is attenuated. The surface at which the temperature is T_o may be called the 'discharge front'.

The energy release occurs in an annular ring inside the discharge. The effective width of the discharge ring 'a' which is equal to one half of the skin depth δ, is rather small compared to the radius in most cases. The thickness 'Δ' of the heated air in front of the discharge is several times larger than 'a'. The zones of the discharge which consist of 'a' and 'Δ' and form the flame are shown doubly cross hatched in Fig. 4.12. The figure also shows the streamline or the projections of the helical lines on the plane of the diametrical cross-section. The streamlines are refracted in the flame due to gas expansion and its subsequent acceleration principally in a direction perpendicular to the surface. The internal cavity of the discharge is filled with gas equivalent to combustion products in a flame, heated to the final temperature T_m & leading to an increase of pressure in the axial region. It is possisble that the heated gas is drawn from this region into the low pressure vertical zone to produce the hot-gas recirculation noticed by Reed [53].

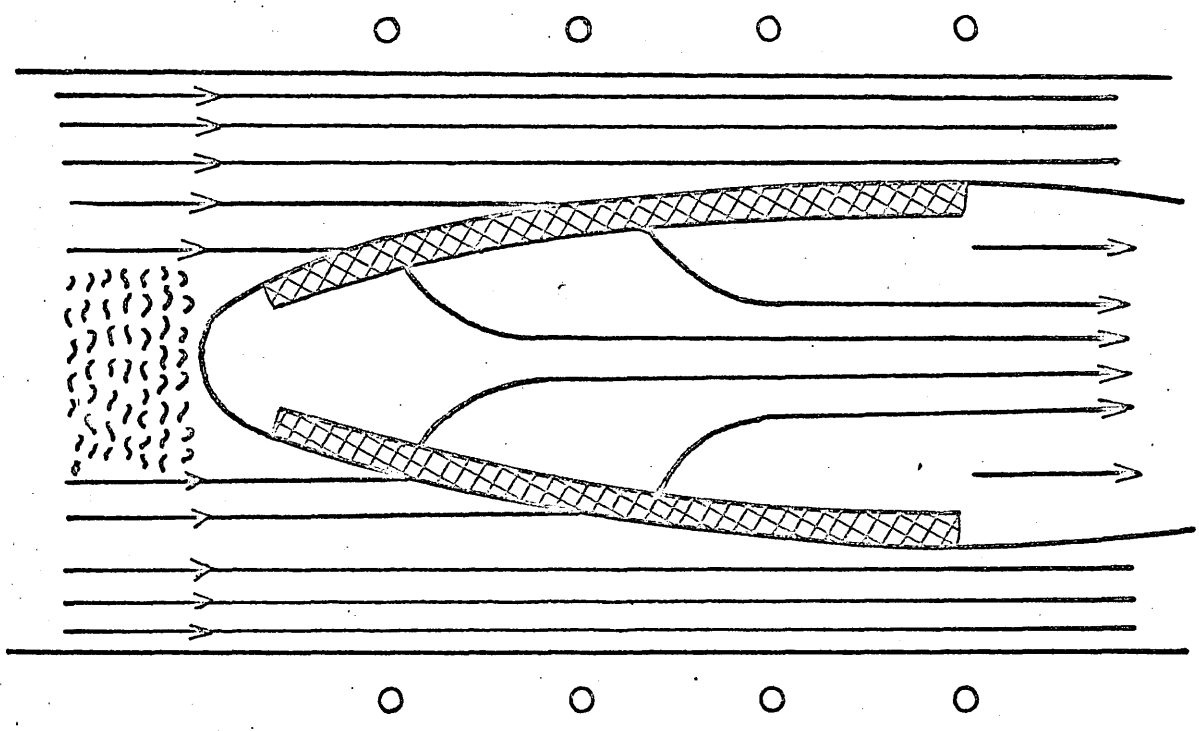

Fig.4.12 The zones of the discharge, showing the discharge doubly cross-hatched.

The most important feature of the discharge is that its lateral front is inclined to the incoming gas in such a way that the gas enters the plasma in a normal direction with a well defined velocity 'V_{x1}'. The fact that the lateral front can never become parallel to the gas stream can be seen quite easily. Suppose that the lateral part is parallel to the gas stream or in other words parallel to the tube wall. Confining one's attention to a small part of this parallel front at the rear of the discharge, one finds that due to radial heat conduction the next layer would be heated up. And when it attains the ionisation temperature T_o, the discharge front moves to the new position away from the axis. At the same time the stream is moving up so that this small portion of the front moves farther away from the axis as it moves up along the stream. The front becomes inclined to the gas stream, at the same time resulting in an increasing temperature gradient between the plasma and the tube wall due to the decreasing width of the non-conducting annular gas region between the plasma and the wall. The stationary state is established when the heat loss is exactly balanced by the heat supply. This occurs when the velocity of the gas flux attains the normal velocity 'V_{x1}'.

4.5.2 Mathematical Analysis

To facilitate calculations the problem is idealised by neglecting the radiation losses and by assuming that (i) the discharge is almost parallel to the inductor axis so that E and H fields become tangent to the discharge surface, (ii) the solenoid is infinitely long. Also the heat loss to those cold gas layers which only push the plasma away from the tube wall and the radiation losses are neglected. The heat diversion from the heat release zone to those cold layer which subsequently fall into the discharge is not a loss, since the heat still remains in the plasma. For a thin skin layer a small section of the discharge can be considered plane as shown in Fig. 4.13. In the same figure the x-axis is

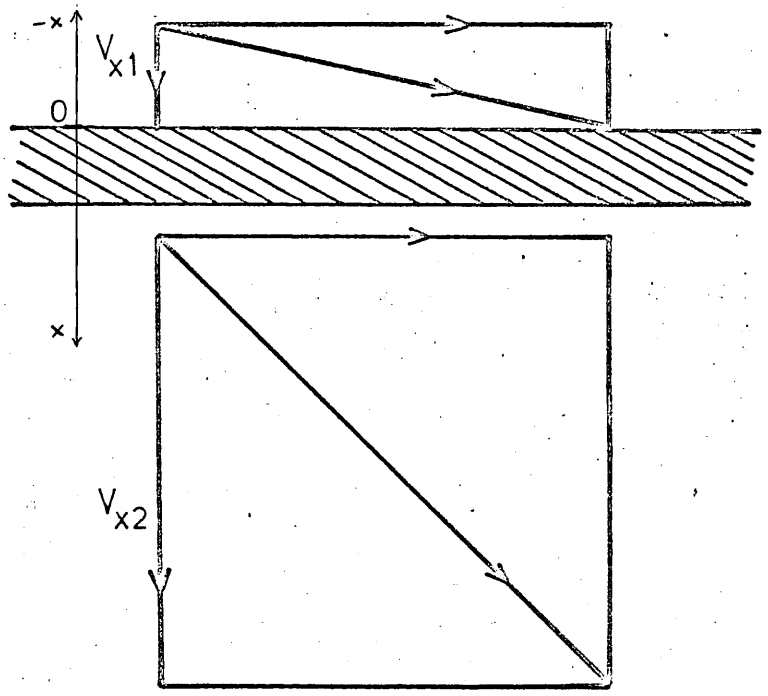

Fig.4.13 Change of normal component of velocity of the gas as it enters the discharge.

shown perpendicular and directed into the discharge with the origin fixed on the discharge surface. The tangential component of the velocity of the obliquely incoming gas stream remains unchanged, but the normal component changes from V_{x1} to V_{x2} according to the continuity equation

$$\rho_o V_{x1} = \rho V_{x2} \tag{4.61}$$

The energy balance equation for the layer can be written as

$$\rho_o C_p \frac{dT}{dt} = \rho_o C_p V_{x1} \frac{dT}{dx} = - \frac{d\bar{\tau}}{dx} + \sigma E^2 \tag{4.62}$$

where

$$\bar{\tau} = - k \frac{dT}{dx} \tag{4.63}$$

Maxwell's equations in the planar case can be written as

$$- \frac{dH}{dx} = \sigma E \tag{4.64}$$

$$\frac{dE}{dx} = j\omega\mu H \tag{4.65}$$

The above four equations containing H, E, T and $\bar{\tau}$ must satisfy the following boundary conditions

$$\begin{aligned} &\text{At} \quad x = + \infty; \quad \bar{\tau} = 0 \text{ and } H = 0 \\ &\text{At} \quad x = - \infty \quad \bar{\tau} = 0 ; \quad T \neq 0 \text{ and } H = H_o = N i \end{aligned} \tag{4.66}$$

This is possible only for a specific value of the propagation velocity V_{x1}, which enters the system as an unknown parameter and must be determined by solving the above equations.

The set of equations (4.62) - (4.65) has an integral which reflects the conservation of total energy flux. Integrating equation (4.62)

between $-\infty$ and x one obtains

$$\rho_o V_{x1} Q_H + \tilde{\tau} + \tilde{P} = \tilde{P}_o \tag{4.67}$$

where the specific enthalpy of the gas $Q_H = \int_o^T Cp\, dT$

and

$$\tilde{P} = |\bar{E}\bar{X}\bar{H}| = -\frac{1}{2\sigma}\frac{d\,H^2}{dx} \tag{4.68}$$

Referring equation (4.67) to the point $x = -\infty$ one gets

$$\rho_o V_{x1} Q_f = \tilde{P}_o \tag{4.69}$$

where $Q_f = Q_H(T_f)$. Substituting the value of $\tilde{P}_o$ in equation (4.67) one gets

$$\tilde{\tau} = \rho_o V_{x1} (Q_f - Q_H) - \tilde{P} \tag{4.70}$$

The power 'W' delivered to the plasma and the gas 'G', flowing into the discharge and being heated, are determined respectively by

$$W = \int \tilde{P}_o\, dF \tag{4.71}$$

$$G = \int V_{x1} dF \tag{4.72}$$

where the integration is carried over the outer surface of the discharge.

It is possible to obtain an approximate solution of the set of equations (4.62) - (4.65) if the true distribution of conductivity $\sigma(x)$ and of the temperature $T(x)$ are replaced by step functions, which are shown by dotted lines in Fig. 4.14. This is equivalent to introducing an effective ionization temperature T_o which serves as a profiling parameter. One then obtains the solutions

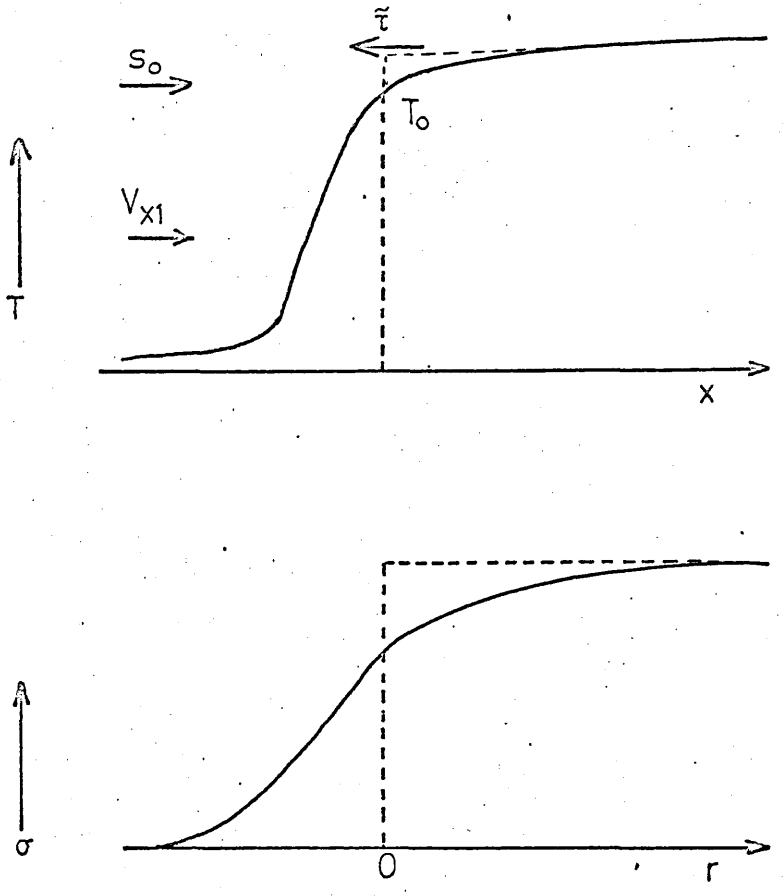

Fig.4.14 Real distributions of T and σ replaced by step functions.

$$H = H_o \exp(-x/\delta) \tag{4.73}$$

$$E = E_o \exp(-x/\delta) \tag{4.74}$$

$$\tilde{P} = \tilde{P}_o \exp(-x/a) \tag{4.75}$$

where $a = \delta/2$. In front of the discharge i.e. at $x < 0$, $H = H_o$ and $\tilde{P} = \tilde{P}_o$.

For an approximate determination of T_m one may use the integral equation

$$\int_o^{T_m} \sigma(T)\, k(T) \left[1 - \frac{\rho V_{x1} (Q_f - Q_H)}{\tilde{\tau}}\right] dT = \left(\frac{N i}{2}\right)^2 \tag{4.76}$$

which may be readily derived by multiplying equation (4.70) by $\sigma(T)$ replacing $\tilde{\tau}$ by $-k \frac{dT}{dx}$ (equation 4.63) and by $-\frac{1}{2\sigma}\frac{dH^2}{dx}$ (equation 4.68) and integrating the resultant equation from $-\infty$ to $+\infty$. In the static case $V_{x1} = 0$ and equation (4.76) changes to equation (4.25). Unlike the stationary case, however, equation (4.76) does not enable one to determine T_m exactly, since V_{x1} is not known. However, it is possible to find an approximate solution. [77, 82] Approximating the energy flux distribution to $\tilde{P} = \tilde{P}_o \exp(-x/a)$ one obtains from equation (4.67) the temperature distribution $T(x)$ in the first approximation. One then also obtains the function $\tilde{\tau}(T) = -k \frac{dT}{dx}$, in the same approximation, and by substituting it in equation (4.76), one obtains an equation which contains T_m and T_o. A second equation for T_o can be obtained by referring $T(x)$ to the point $x = 0$. Simultaneous solution of these equations gives $T_m(H_o)$.

The fact that the profiling temperature T_o differs little from the final temperature T_m in most cases, renders further support to the analogy of the induction torch with a chemical flame, where due to strong dependence of the rate of chemical reaction, the ignition temperature does

not differ much from the final temperature. Almost the whole heat generated in the reaction zone of a chemical flame is conducted away to the initial mixture where it raises the temperature of the mixture to the ignition temperature. A similar situation in the discharge causes the energy balance equation (4.76) to differ little from equation (4.25). For the same reason the maximum temperature at the axis in this case is not much different from the maximum temperature in a static discharge for the same ampère turns per centimetre.

The analysis leads to the conclusion that (i) the plasma temperature depends little on whether the discharge is produced in a static or in a flowing gas, (ii) the maximum temperature is determined by the electric and thermal conductivities of the gas and by the ampere turns per unit length of the r.f. inductor, (iii) the actual distribution of temperature in the central region of the discharge and, in particular, the small decrease of temperature at the axis is caused by radiation losses. Thermal conductivity plays no part in it.

4.6 Conclusion

The transformer theory provides the preliminary basis for a theory of an induction plasma torch. It satisfactorily explains the mechanism of energy transfer from an r.f. inductor into the plasma. However, it is much limited in its scope and provides no information either about the plasma temperature or the power going into the discharge. It disregards the skin depth effect and assumes the current paths to be well defined.

Eckert's theroy makes an attempt to include the distribution of the electrical conductivity into the torch analysis. However, the assumption that the conductivity varies inversely as the radius does not reflect the actual situation. This assumption seems to be made simply to facilitate mathematical calculations. The fact that this theory predicts steep temperature gradients near the discharge surface and that the variation

of power efficiency with the ratio of the discharge radius to the skin depth is nearly the same as in a metallic cylinder model brings the two theories nearer.

Raizer's theory based on the analogy of an induction plasma torch with a chemical flame approximates to the metallic cylinder model in its final analysis, especially when it replaces the actual electrical conductivity and the temperature distribution near the plasma boundary by step functions.

The metallic cylinder model, despite its limitations, provides satisfactory basis for solving problems related to an induction plasma torch.

CHAPTER 5

APPARATUS

5.1. Introduction

The plasma torch used in this study was inductively coupled to an r.f. power supply by means of a helical coil; gas flowed vortically upward through a quartz tube coaxial with the helix and the resulting plasma emerged into the atmosphere. To study the effect of a pulsed magnetic field applied to a dense plasma, a large current pulse was passed through a single turn coil (Theta coil) co-axial with the induction plasma torch. The effect of the pulsed field was studied by spectroscopic measurement of the increased plasma temperature and high speed photography, the pulsed field being measured with an inductive probe (type I) and the r.f. magnetic field in the plasma with a water cooled inductive probe (type II).

5.2. The r.f. induction plasma torch

The torch, shown in Fig. 5.1, consists of a vertical quartz tube mounted on a head through which gas flowed tangentially to achieve vortex stabilisation of the resultant plasma. The upper end of the quartz tube was open to permit hot gases to exhaust to the atmosphere. A water cooled copper helical inductor coil energised by an r.f. generator, surrounded the quartz discharge tube near its upper end. The length of the tube protruding above the r.f. inductor was sufficient (about 1cm) to prevent the plasma shorting to the copper helix.

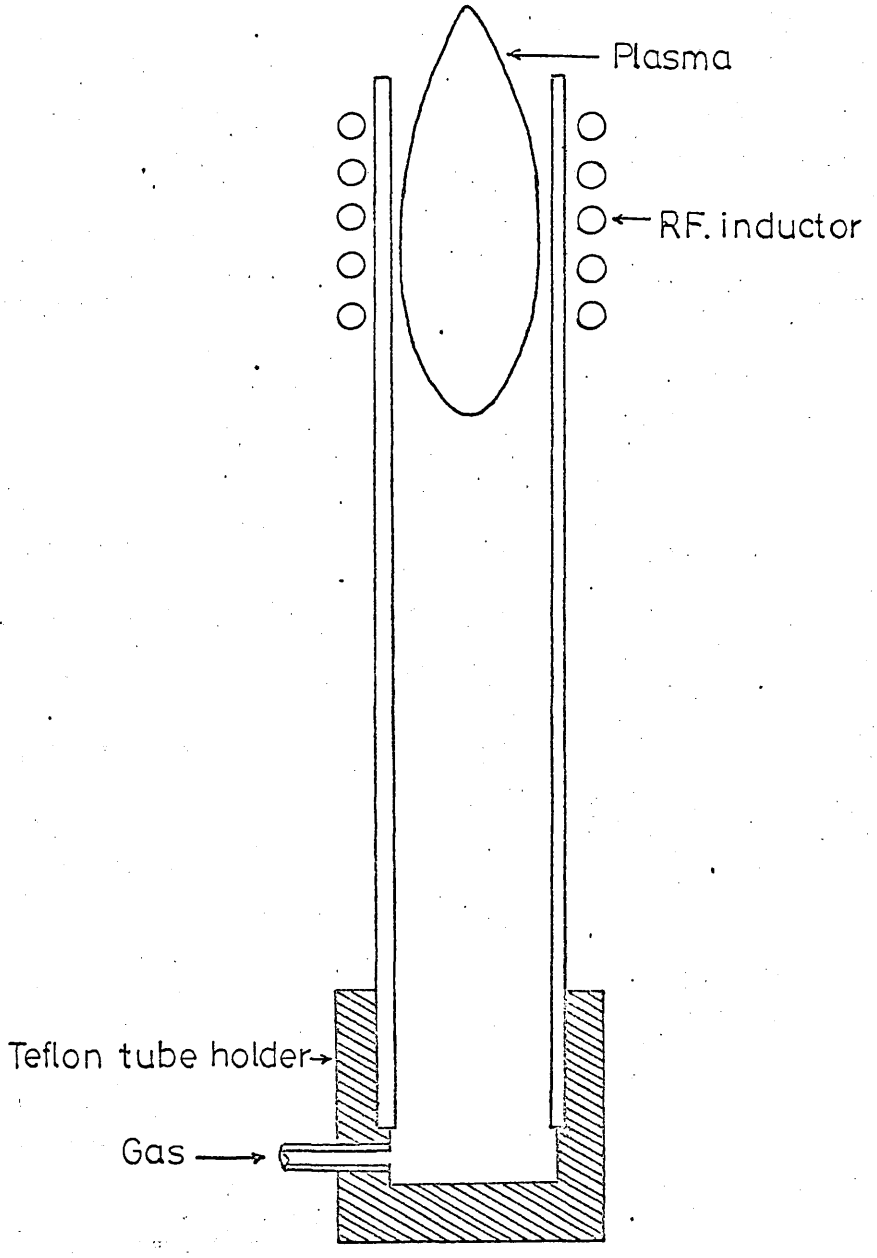

Fig 5.1 Plasma torch used in this work.

5.2.1 The discharge tube and the torch head

The discharge tube guides the gas through the plasma region to exhaust to the atmosphere. The torch head serves to hold the discharge tube and provide a means of introducing the gas into the discharge tube. Its design depends on the torch to be used [83]. In the original design the torch-head was made of brass and accommodated two co-axial quartz tubes of different diameters as shown in Fig. 5.2. The gas, supplied tangentially into the inner tube, formed the main plasma whereas the linear gas flow through the outer tube served to cool the discharge tube. The inner tube lay a little below the r.f. inductor or helix so that the gas in the outer tube not only served to cool the discharge tube, but also took part in plasma formation. This introduced uncertainties in the measurement of gas flow-rate. Therefore, the two-tube system was replaced by a single tube. In the present work two sizes of discharge tube tabulated below were used for studying the effect of the pulsed magnetic field on the induction plasma torch.

TABLE 1 Dimensions of the discharge tubes

Type of Discharge tube	Length	Inner diameter	Outer diameter
DT-1	25.0 cms	3.5 cms	3.9 cms
DT-2	25.0 cms	5.14 cms	5.4 cms

The torch heads for these discharge tubes were made of Tufnol. Due to the large diameter of the discharge tube DT-2 it was found necessary to use two tangential gas inlet tubes to produce a stable discharge. At a power of about 2.0 kW the torch was run for over an hour without damage to the Tufnol torch head, but the torch could only be run for about ½ a minute at a power of 13.0 kW without damage. In the absence of any cooling arrangement the flame was found to destroy the discharge tube rather than

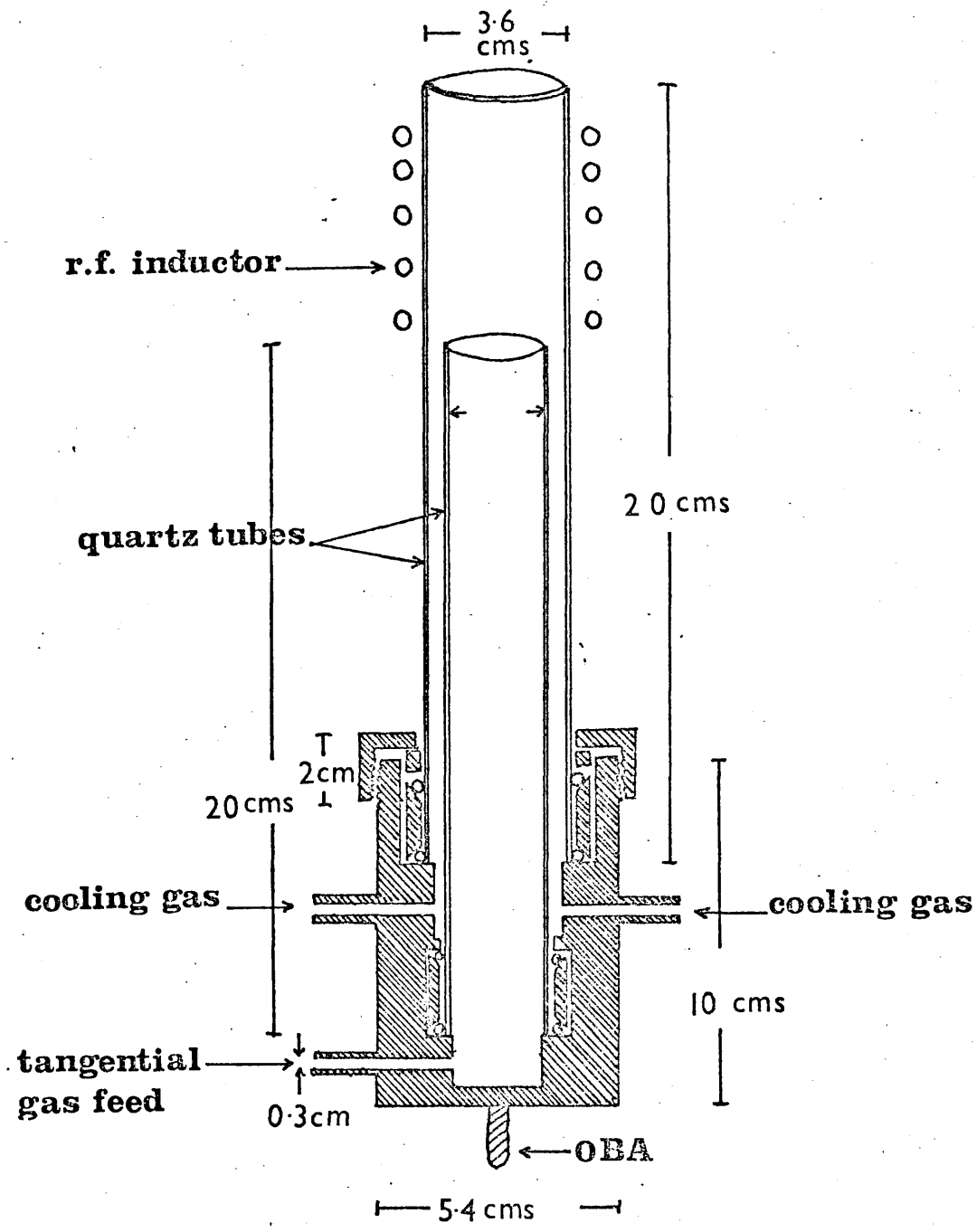

Fig.5.2 Plasma torch

the torch head. With the large diameter tube DT-2 it was essential to use an insulating torch head since the plasma shorted to the metallic head.

5.2.2. The r.f. inductors

Two water cooled inductors made of copper tube, one for each discharge tube, were used in this work. Their specifications, along with the discharge tubes they were used with, are tabulated below.

TABLE 5.1 Specifications of the r.f. inductors

Type of the discharge tube	I	II
Type of the r.f. inductor	I	II
Length	5.1 cms	6.0 cms
Diameter	6.6 cms	7.8 cms
Number of turns	5.75	5.75
Inductance	1.55×10^{-6} H	2.7×10^{-6} H

5.2.3. Gas-flow control

Technical quality argon was used in these experiments. The gas was fed into the discharge tube through a calibrated Rotameter flow guage, type 10P, the gas flow rate being controlled by means of a diaphragm valve.

5.2.4. The r.f. generator

The Radyne r.f. generator model C170/H used in this work, could supply up to 15 kW of power at frequencies between 4 and 7 MHz. The r.f. power could be controlled remotely by a saturable reactor. Safety devices were incorporated in the generator for protection against excessive current or excessive voltage on the oscillator anode.

5.2.5. Matching the oscillator to the plasma load

Unless the oscillator was matched electrically to the load offered by the helical coil containing the discharge, the plasma is found to be unstable or small. In case of extreme mismatch the plasma is either extinguished after a short time or it is not ignited at all. In such a case it is advantageous to increase the frequency [83] of the oscillator. If the plasma column is narrow, the operating frequency should be decreased, as a higher frequency decreases the plasma [69] diameter.

5.2.6 Plasma torches used for temperature measurement

Three induction plasma torches were used for temperature measurement in this work. These are designated by their power input: their specifications being tabulated below.

TABLE 5.2 Specification of plasma torches

Type of torch	2.0 kW	13.0 kW	11.6 kW
Gas flow	4.5 l/m	10.5 l/m	7.3 l/m
Discharge tube	Type I	Type I	Type II
R.F. inductor	Type I	Type I	Type II

The 13.0 kW and the 2.0 kW torches were quite stable. Theformer extended only a little below the r.f. inductor, the latter was confined to the upper part of the inductor. In the 11.6 kW torch a bigger discharge, which extended deep below the r.f. inductor (about a few cms), was produced. The lower part of the discharge was fairly stable but the upper part was unstable and moved from side to side in the discharge tube.

5.3. Production of the pulsed magnetic field

The apparatus used to produce the pulsed magnetic field is shown in a block diagram in Fig.5.3. The main capacitor 'C' was connected to the theta coil THC (Described in Section 5.4) through a strip transmission line and a low inductance spark gap [84]. The capacitor 'C' was charged by means of a Brandenburg stabilised EHT power supply. The 40 kV pulse to fire the spark gap was obtained from a Marx generator MxG, which was triggered by the pulse generator PG. The pulse generator PG was provided with a remote push-button-trigger. A low voltage pulse in phase with the main pulse was also obtained from the pulse generator to trigger the oscilloscope which was used to record the photomultiplier signal during measurements of the spectral line intensities when the magnetic field was pulsed on the torch. A calibrated Rogowskii Coil RGC was included in the transmission line to measure current in the theta coil.

In the r.f. generator the high voltage d.c. anode power supply was not filtered and had a 300 Hz ripple. Since the pulsed magnetic field duration was considerably less than one period of the ripple an interlocking circuit was used in the triggering circuit of the pulse generator PG, to discharge capacitor 'C' at the same phase position of the ripple.

A safety interlocking circuit was incorporated in the discharging system to allow the capacitor to charge when the dumping swith 'DS', connected across the capacitor 'C' through a one kilo ohm carbon tube resistor, was open. Charging could only be started after the voltage control of the EHT supply was set to zero and was stopped when the theta coil was fired. This prevented any high current pulse to the discharged capacitor and consequent damage to the EHT supply.

5.3.1 The theta coil

Two theta coils, THC-1 and THC-2 were used in this work. Both coils

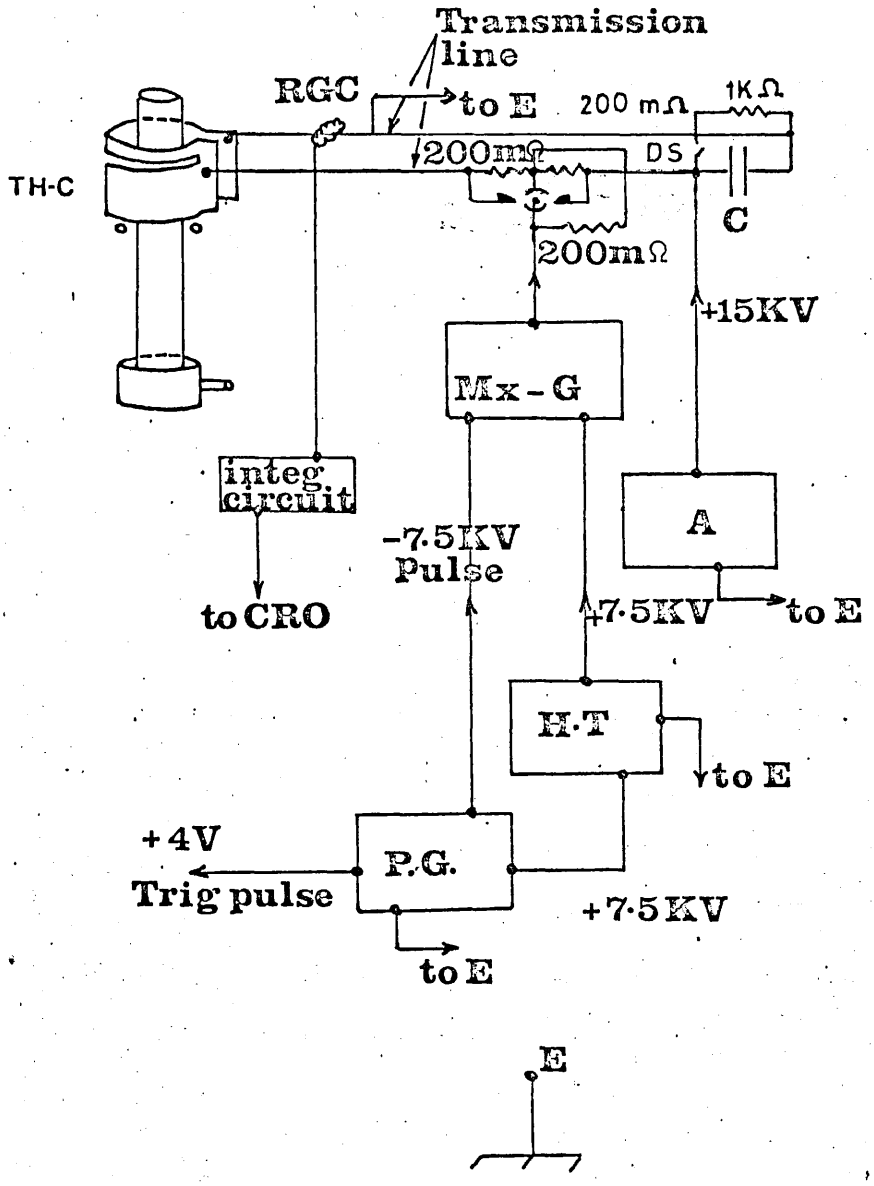

A	High Voltage Supply (Brandenburg)
HT	+7.5Kv Power Supply
PG	Pulse Generator
MxG	Marx Generator
SpG	Spark Gap
RGC	Rogowski Coil
C_1	5mfd 20Kv Capacitor
E	Earth
TH-C	Theta Coil
DS	Dumping switch

Fig.5.3 Apparatus for producing a pulsed magnetic field

had a length 10.7 cms and a diameter 8.0 cms. The THC-1 coil was made of copper sheet and had a 2.0 mm wide slit along its circumference, as shown in Fig. 5.4. This coil was used for measurements of radial temperature distributions in the plasma. The theta coil, THC-2 was made of expanded copper sheet which allowed the plasma to be viewed through the coil. This coil was used during high speed photography and some of the temperature measurements. Both coils had an inductance of 81 nH and were connected to the capacitor 'C' through the strip transmission line, having an inductance of 36 nH.

5.4. Plasma diagnostics

The r.f. and the pulsed magnetic fields were measured with inductive probes. To study the effect of the pulsed magnetic field on the plasma, the radiation from the torch was measured with a photomultiplier. Plasma temperature was measured by a spectroscopic technique [85,86]. The instabilities were studied with high speed photography. The acoustic noise was studied with a microphone in conjunction with a spectrum analyser and a Tektronix oscilloscope.

5.4.1. Measurement of the r.f. and the pulsed magnetic fields

The r.f. magnetic field was measured with the magnetic probe type II which is described in Section 5.6. The probe was cooled by circulating deionized water at the rate of 500 cc per minute. The probe was calibrated with the aid of the calibrating circuit type II, described in Section 5.6.1. at the frequency of the r.f. generator.

The inductive probe type I was used to determine the distribution of the pulsed field in air because of its overall small size. But the probe type II was used to measure the pulsed field in plasma because of the cooling facility. Both probes, in this case, were calibrated with the aid

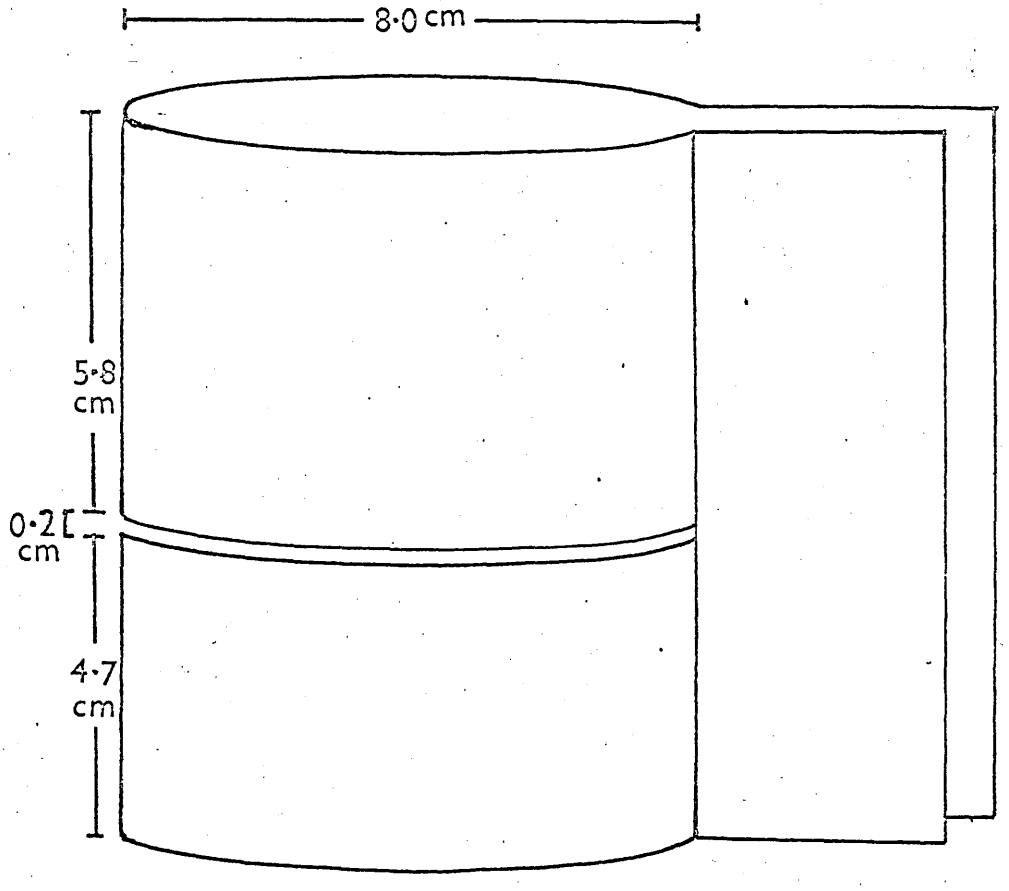

Fig 5.4 Theta coil typeI

of calibrating circuit type I described in Section 5.6.1. During measurements of the pulsed magnetic field in air the theta coil was held in the same position, but the r.f. inductor (helix) was removed. Later on the r.f. inductor was replaced and was found to make no detectable screening effect on the pulsed field at the axis.

The pulsed magnetic field was also investigated in the absence and then in the presence of the plasma with a diamagnetic loop, consisting of a shielded wire and placed 4.0 cms below the r.f. inductor so as to minimise the r.f. pick up from the inductor. The loop signal was integrated by the circuit shown in Fig. 5.5 and finally displayed on a Tektronix oscilloscope. The integrating circuit not only integrated the loop signal but also shorted any r.f. pick up.

5.4.2. Measurement of current in the r.f. inductor

The current in the r.f. inductor was measured with a Tektronix high current transformer type CT5 in conjunction with a Tektronix current probe type P 6021 and a Tektronix oscilloscope.

5.4.3. Measurement of current in the theta coil

The current in the theta coil was measured with a Rogowskii coil, which had a mean major diameter of 12.5 cms and a mean minor diameter of 5.0 cms. The Rogowskii coil was calibrated with its integrating circuit with the aid of the circuit used for calibrating the inductive probe type I, at the frequency of the pulsed magnetic field.

5.4.4. Light intensity measurement

The application of a pulsed magnetic field had a pronounced effect on the light intensity. So it was chosen as a useful parameter for the

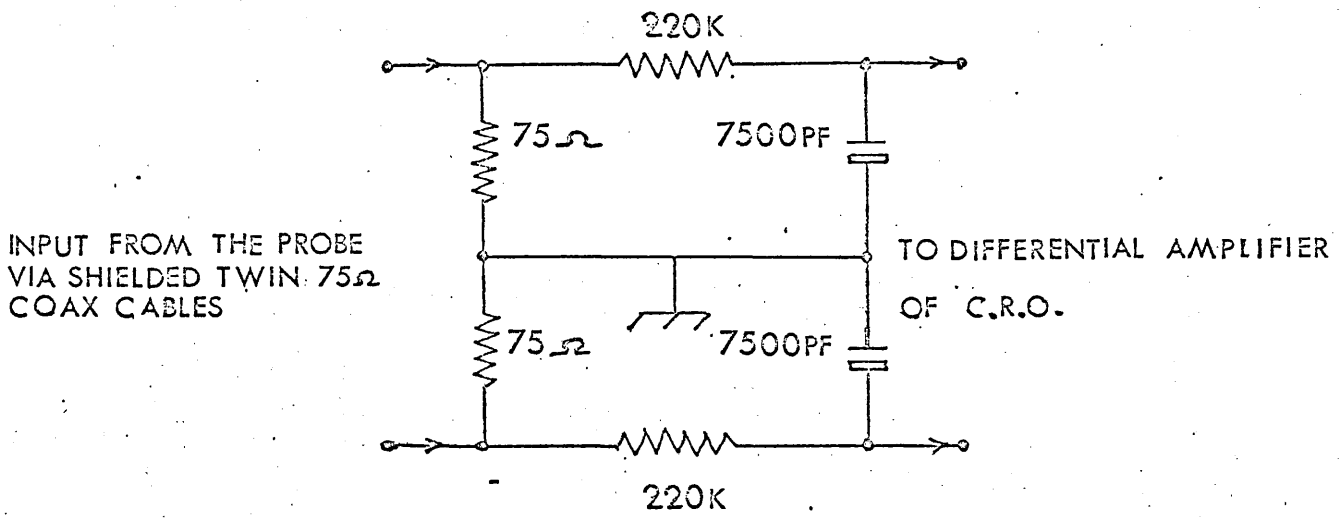

Fig. 5.5 Integrating circuit.

plasma torch diagnostic. The light intensity was measured with the aid of an E.M.I. photomultiplier type 9592B. Because of the high intensity of the incident light a number of neutral filters were placed in front of the photomultiplier. A glass-lens was used to form a diminished image on photocathode of the photomultiplier. This arrangment enabled the photomultiplier to detect the integrated effect of the incoming radiation from different parts of the torch.

The r.f. generator was subject to a 300 Hz ripple due to the absence of a smoothing filter in the high voltage supply of the oscillator. This caused the torch light to be modulated at the same frequency. But consistant results were obtained by firing the theta coil at the same phase position in the ripple in each experiment as described before in Section 5.3.

5.4.5. Measurement of the plasma temperature

Temperature as high as encountered in a plasma can only be measured spectroscopically. In the following sections methods of determining the plasma temperature and the necessary experimental arrangement are described.

5.4.5.1. Relative line intensity method

When self absorption is negligible the measured integrated line intensity of an atomic emission line is given by [87]

$$I = \frac{K'' A h\nu g_k}{U_o} n_o \exp(-E_k/kT) \qquad (5.1)$$

where K'' is the instrumental constant and g_k the statistical weight of the upper level 'K'. Taking logs on both sides of the above equation

$$\log (I\lambda/g_k A) = - (\log_{10} e/kT)\, E_K + \log (K'' h n_o/U_o) \qquad (5.2)$$

$$\text{Here, } (\log_{10} e)/k = 0.62487 \text{ cm } k^{-1} \qquad (5.3)$$

If $\log(I\lambda/gA)$ is plotted against E_K, a straight line, the so called Boltzmann plot, of slope $(- .62487/T)$ is obtained. From this slope plasma temperature can be easily determined. Essentially the above method gives the electron temperature, but for a plasma in thermal equilibrium, this gives the common plasma temperature.

5.4.5.2. Fowler-Milne method

A quicker method of determining the temperature distribution or time variation of temperature in the plasma is to follow the intensity variation of a spectral line. The variation in the intensity can be easily converted to temperature variation with the aid of Eq. (5.1), if the intensity is normalised at a known plasma temperature. Generally, one plots I (in arbitrary units) against T. One then normalises the intensity at the known plasma temperature to the appropriate value of intensity on the graph. All the observed intensities are changed in the appropriate ratio to lie on the I versus T curve. Temperatures corresponding to various intensities can then be easily read off from the graph . Fig. 5.6. shows such an I-T plot for the 425.9 nm line of Ar I at 1 atm. Care should be taken in applying Fowler-Milne method to determine temperature in r.f. plasmas, where the skin effect causes an off-axis peak in the radial temperature distribution. This should not be confused with the norm-temperature, T_{norm} [35] which is the temperature at the maximum intensity in the I-T plot such as shown in Fig. 5.6. At temperatures below T_{norm}, the intensity decreases due to decrease in temperature and at temperature above T_{norm} the intensity decreases with an increase in temperature due to a

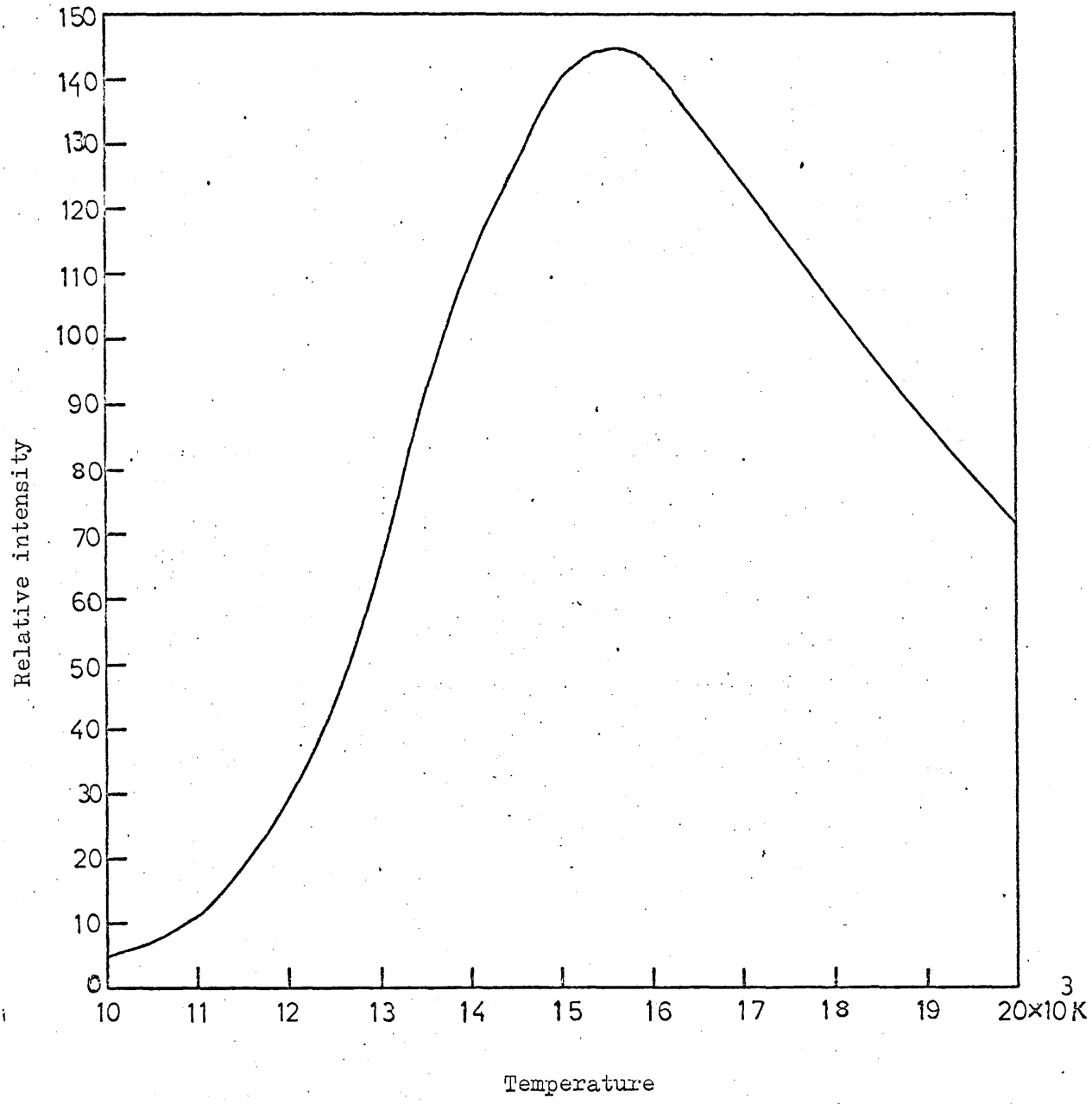

Fig.5.6 Variation of the intensity of 425.9 n.m. ArI - line with temperature

decrease in n_o. If the plasma dimensions do not change, Fowler-Milne method can be used to determine time variation of the plasma temperature. If they do change an allowance should be nade for that. In such cases relative line intensity method is preferable.

5.4.5.3. Measurement of the rotational temperature

In a comparatively cold plasma (temp $< 10^4$ K) in thermal equilibrium, the temperature can be determined from the relative line intensities in an emission band. In the absence of self absorption the intensity of a line in the band is given by [88]

$$I_m = \frac{\nu^4((J+1)^2 - 1/4)}{(J+1)} \exp\left[- \frac{h^2}{8\pi^2 \Theta kT} J(J+1) \right] \qquad (5.4)$$

Plotting $(\ln I_m - \ln [\nu^4((J+1)^2 - 1/4)/(J+1)])$ against $J(J+1)$ yields a straight line of slope $-h^2/(8\pi^2 \Theta kT)$ from which T can be determined. At higher temperatures molecules of the gas are completely dissociated and one gets atomic line spectra.

5.4.5.4. Radial distribution of intensity of a spectral line

In order to determine the radial temperature distribution in a cylindrically symmetric plasma column the radial intensity distribution must be determined from the measured lateral intensity, which is integrated across the plasma. It is seen from Fig. 5.7. that for an optically thin plasma the lateral intensity measured at any cross-section x is given by

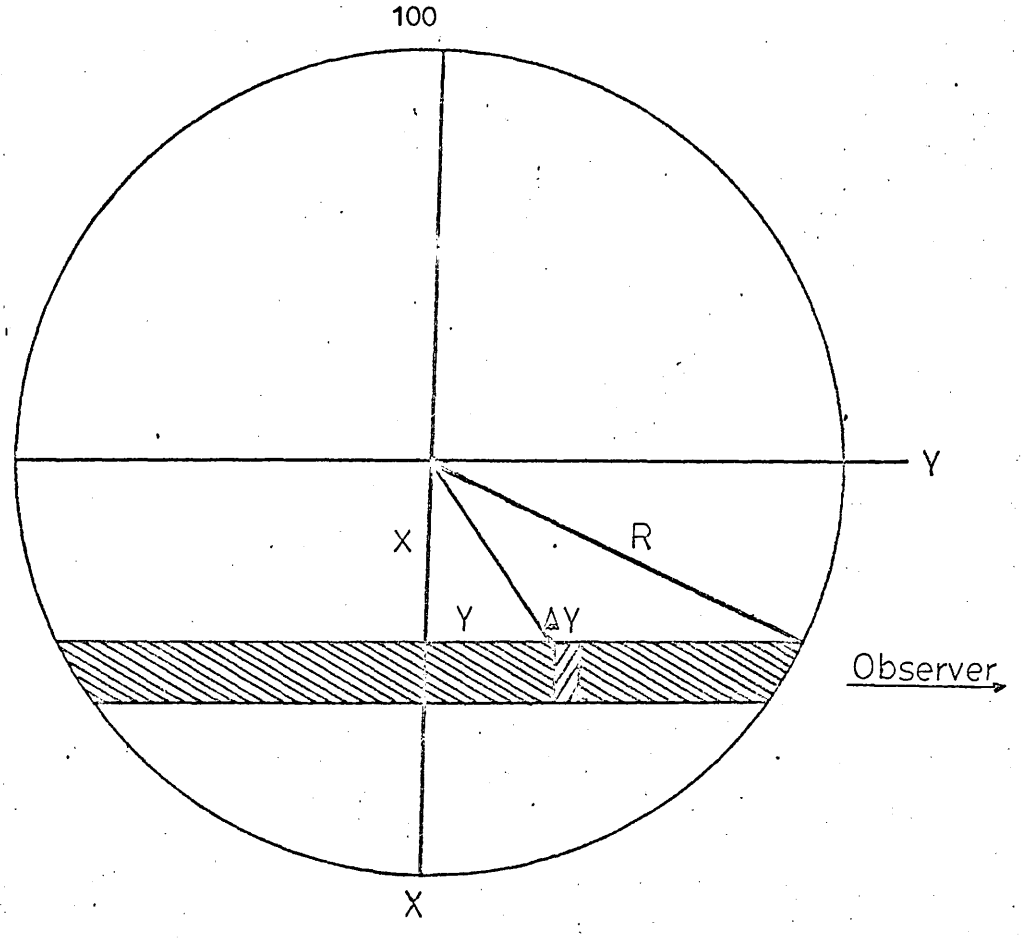

(a) Geometry of analytical expression,

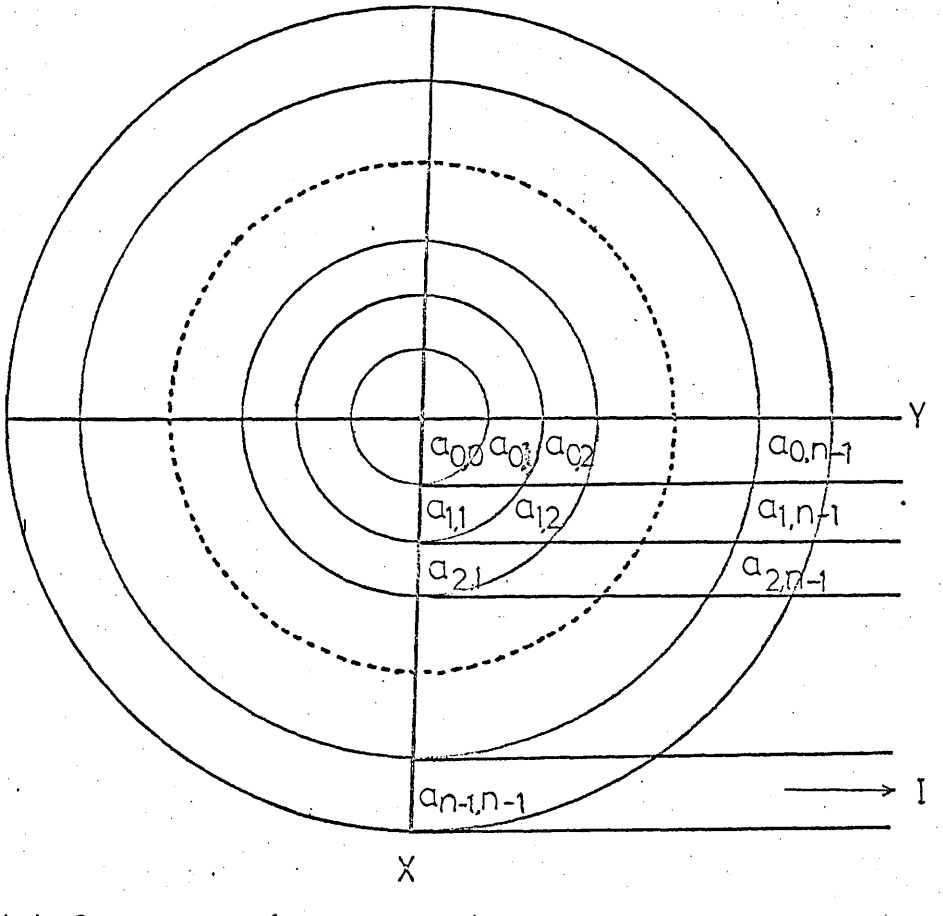

(b) Gemetry of numerical expressin.

Fig 5.7 The Abel Inversiam Geometry

$$I(x) = 2 \int_0^{(R^2 - y^2)^{\frac{1}{2}}} I(r)\,dy$$

$$= 2 \int_0^R \frac{I(r)\,dr}{(R^2 - x^2)^{\frac{1}{2}}} \qquad (5.5)$$

which may be inverted by an Abel transformation to give the radial intensity

$$I(r) = -\frac{1}{\pi} \int_r^R \frac{I(x)\,dx}{(x^2 - r^2)^{\frac{1}{2}}} \qquad (5.6)$$

The boundary radius R is defined by the condition $I = 0$ for $x \geqslant R$. This inversion is best performed by a numerical method. In practice the plasma is divided into N co-axial regions of equal thickness as shown in Fig. 5.6(b). The thickness is taken small enough for the temperature in it to be regarded constant. The measured lateral intensity I(x) can be introduced in the calculations as a sequence of readings $I(x)_k$ for equidistant x_k values, $x_k = kR/n$ $(k = 0, 1, 2 \ldots n - 1)$ to give [89]

$$I(r)_j = \frac{1}{R} \sum_k a_{jk}\, I(x)_k \qquad (5.7)$$

Corresponding to $r_j = jR/n$ $(j = 0, 1, 2 \ldots n - 1)$ where a_{jk} are certain coefficients. The above equation is solved with the help of a computer.

5.4.5.5. Selection of spectral lines and the spectroscopic data

Spectral lines of wavelength 415.9, 418.2, 425.9, 426.6 and 427.2 nm, lying in the blue part of the spectrum, are not self absorbed [90] They are also fairly strong and easily identified, therefore, these were

chosen for the measurement of plasma temperature. Transition probabilities and other spectroscopic data used in this work were taken from ref (87). They are presented in Table 5.3.

Table 5.3. Spectroscopic data for temperature measurement

λ	E_n (cm^{-1})	$A_{nm} \times 10^{-5}$	$\frac{dA}{A}$ %	log (λ/gA)
415.9 nm	117,183.7	11.0	15	1.8786
418.2 nm	118,459.7	4.58		2.4834
425.9 nm	118,871.0	36.0		2.0730
426.6 nm	117,183.6	2.8	15	2.4839
427.2 nm	117,151.4	7.1	15	2.3022

5.4.5.6. Experimental technique to measure the plasma temperature

The apparatus, used to measure the temperature distribution across the torch, consisted of an optical system to scan the plasma and focus the emitted radiation on to the entrance slit of the monochromator. The output of the monochromator was received by a photomultiplier and displayed on a Tektronix oscilloscope.

5.4.5.6.1. The optical system

The optical system used to scan the torch and form a spectrum, is shown in fig. 5.8. A lens, L_1, formed a real image of the plasma median plane, magnified 1.4 times in the vertical plane of a 0.1 cm wide and 0.5 cm long slit 'S'. To keep the final image always at the monochromator slit as the plasma was scanned, light from the slit was rendered parallel by a lens, L_2 and deflected at right angles by a front silvered mirror M, the

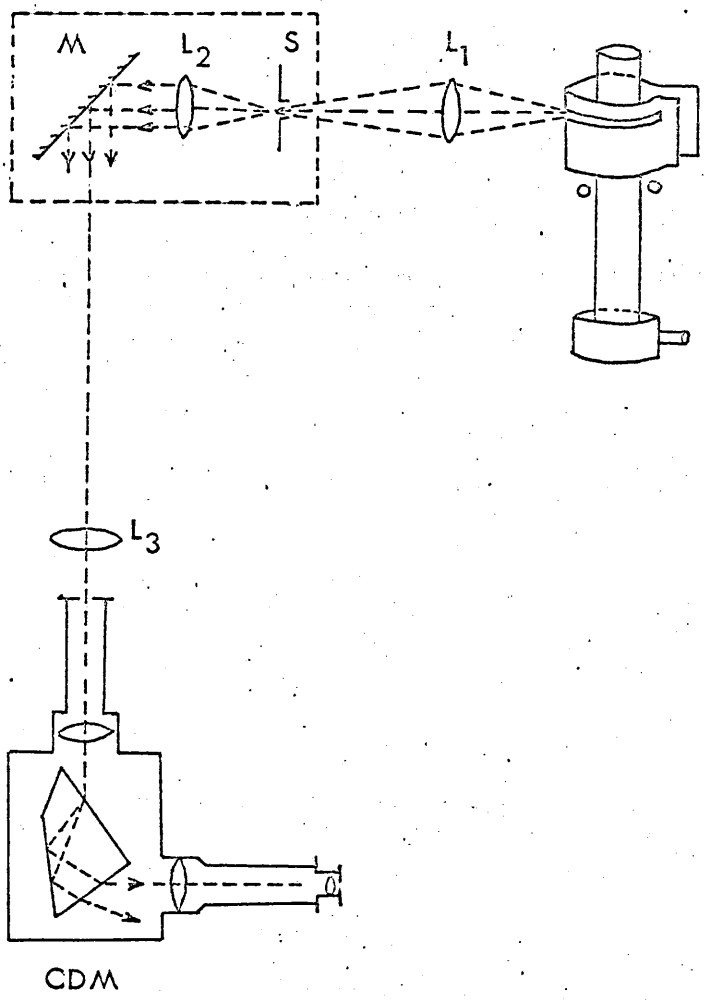

CDM Constant Deviation Spectrograph
$L_1L_2L_3$ Converging Lenses
M------Plane Mirror
S------Scanning Slit

Fig.5.8 Optical arrangement to scan the torch

slit S, and the lens L_2 and the mirror M being fixed on a metal block which could be moved by a micrometer. The parallel rays were brought to a focus by a lens L_3 forming a diminished image of 'S' on the first slit of a constant deviation Hilger and Watts spectrograph.

5.4.5.6.2. Setting the optical system

The spectrum of the torch radiation was observed visually through the telescope of the spectrograph. The outlet slit in the telescope was then narrowed so as to contain only a single spectral line. The final setting of the spectrometer was, however, achieved by observing the line through the photomultiplier for maximum signal. During this setting the entrance slit of the spectrometer was illuminated by the torch burning at a low power. A high power torch would destroy the quartz tube in a few minutes. In order to suppress noise and the 300 Hz mains ripple the signal from the photomultiplier was passed through the smoothing filter SF-1 shown in Fig. 5.9. before its display on the oscilloscope. The presence of the smoothing circuit would drastically reduce any time varying signal, it was, therefore, removed while measuring time varying light intensities. The continuum radiation in the vicinity of the spectral line was also measured and subtracted from the observed line intensity. The lateral line intensities so obtained were converted to radial intensities as described in Section 5.4.5.4. The numerical coefficients used in the transformation were computed from a formula given by Bohn et al [91]. The computer programme for this conversion is given in Appendix I.

The values of the radial intiensities obtained from the computer were smoothed and $\log(I\lambda/Ag)$ was plotted against the upper excitation energy level for each spectral line. Figs. 5.10 and 5.11 show some typical Boltzmann plots, used for temperature determination in Section 6.4.2.2. and 6.4.2.1.2.1. respectively. The procedure of determining temperature was repeated at each radial point to obtain the radial temperature

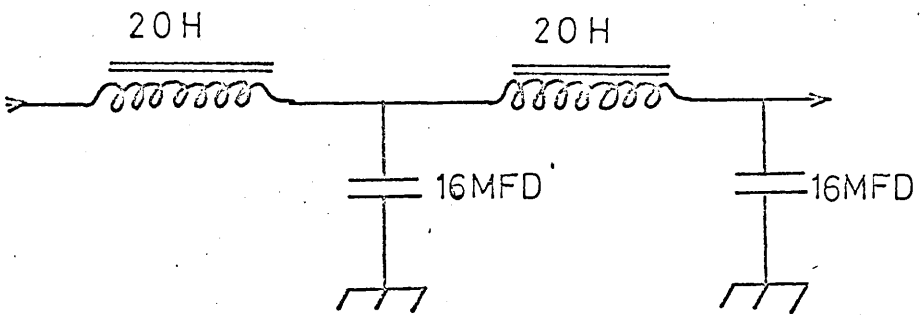

Fig 5.9 Filter to suppress various frequencies in the photomultiplier output.

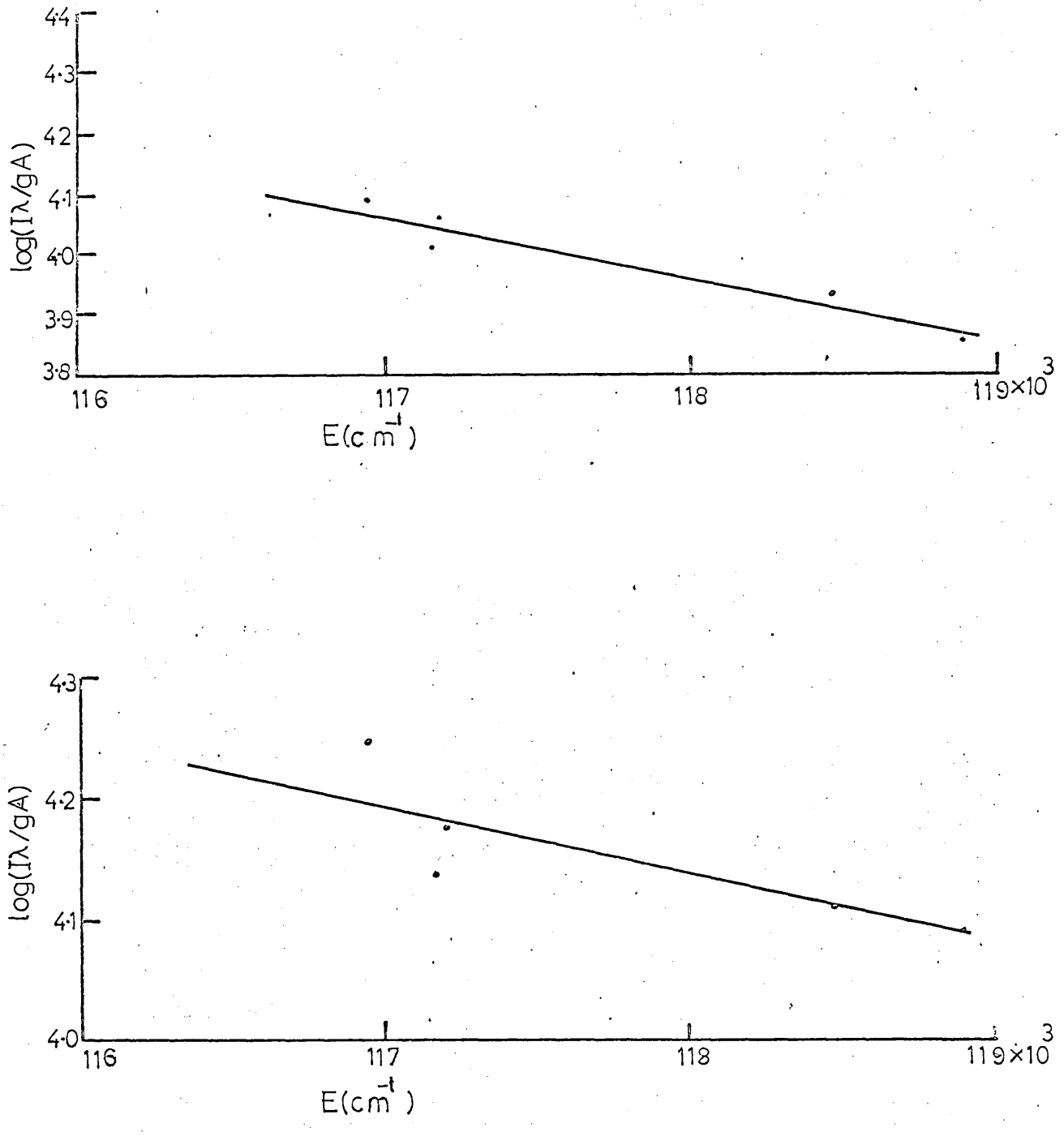

Fig.5.10 Boltzmann plots for steady and peak temperature determination for a 2.0 K.W. torch at Z = 0.3 cms (a) No pulsed magnetic field, position r = 7 mm (b) when pulsed magnetic field is at peak value 1.25T, position r = 10 mm.

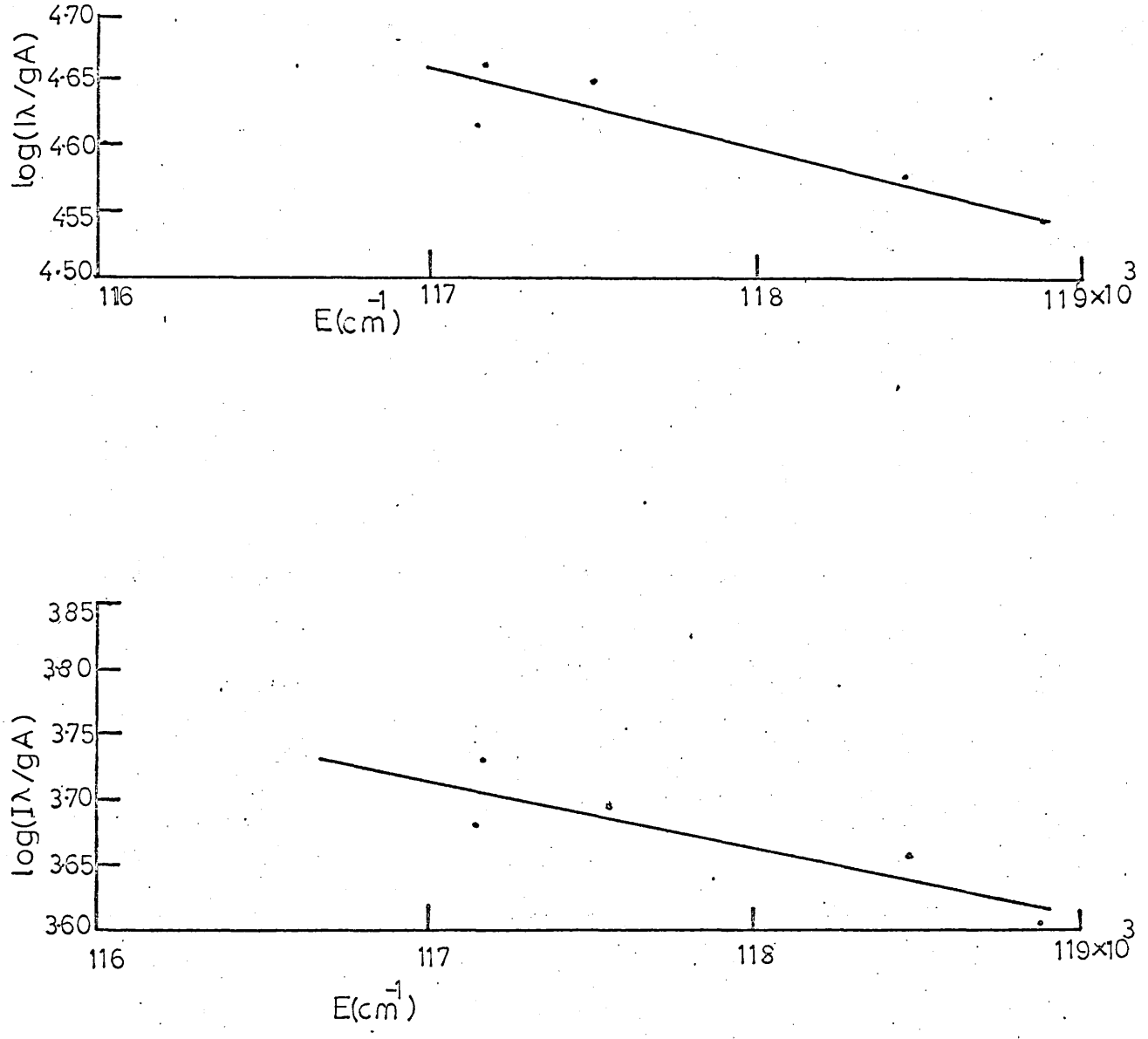

Fig.5.11 Boltzmann plots for steady and peak temperature - determination for a 13 K.W. torch at Z = 0.3 cm (a) no pulsed magnetic field, position r = 6 mm (b) when pulsed magnetic field is at peak value 1.25T positionr= 2 mm.

distribution in the plasma.

5.5. The photomultipliers

Fig. 5.12 shows the wavelength response of the E.M.I. photomultiplier type 9592B, used to measure the total radiation from the torch. The cut-off on the lower wavelength side was, however, shifted to 300 nm, as shown by the dotted line, to account for the use of a glass lens in this work in accordance to the manufacturers data [92] on the effect of the window materials on the photomultiplier's wavelength response.

The E.M.I. photomultiplier type 9524B used to measure the plasma temperature was claibrated during this work. First the wavelength calibration of the spectrometer was corrected by observing several isolated spectral lines of ArI. The torch was then replaced by a tungston ribbon lamp operated at a known temperature and the photomultipler calibrated for wavelength response with the optical system by comparing the intensities observed and theoretically calculated for the lamp. Fig. 5.13 presents both the experimental and the theoretical black body curves, which are normalised at 415.0 nm. The lamp temperature was quoted as 3040 ^{o}K at an input power of 108 watts by an NPL calibration.

5.6. The inductive probes

The inductive probe type I consisted of 60 turns of 32 S.W.G. insulated copper wire in a double layered coil, 0.85 mm in diameter. This coil was sealed with Araldite into a 1.6 mm diameter stainless steel tube of 0.025 mm wall thickness. The probe (shown in Fig. 5.14) with the shielded integrating circuit (shown in Fig. 5.5) was calibrated with the aid of a circuit which is described in the next section.

The magnetic probe type II was developed during the present work to measure the magnetic field of the r.f. inductor in the plasma. To reduce

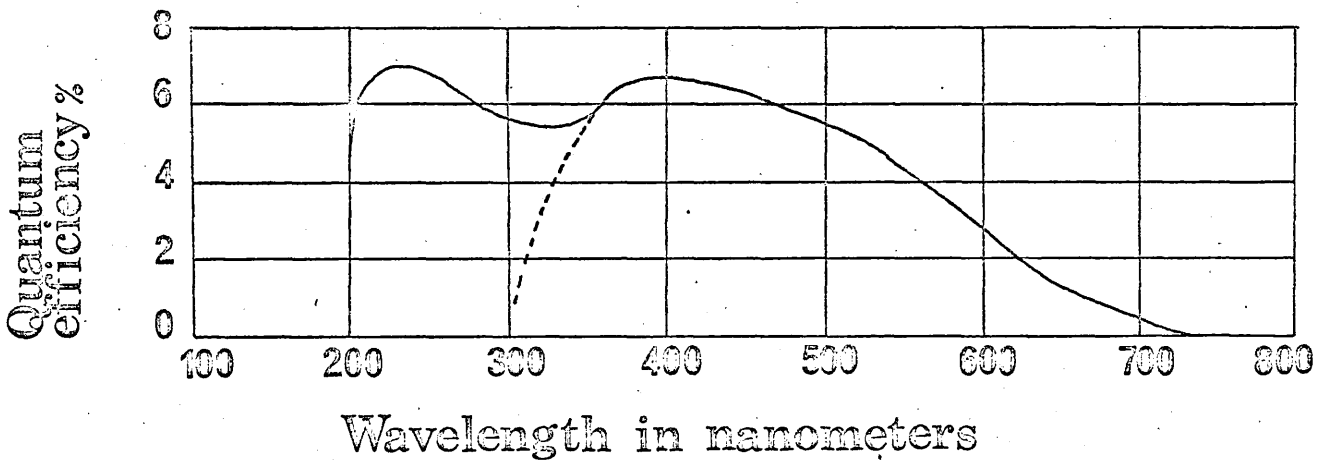

Fig5.12 Spectral response of photomultiplier type 9592B after e.m.i.

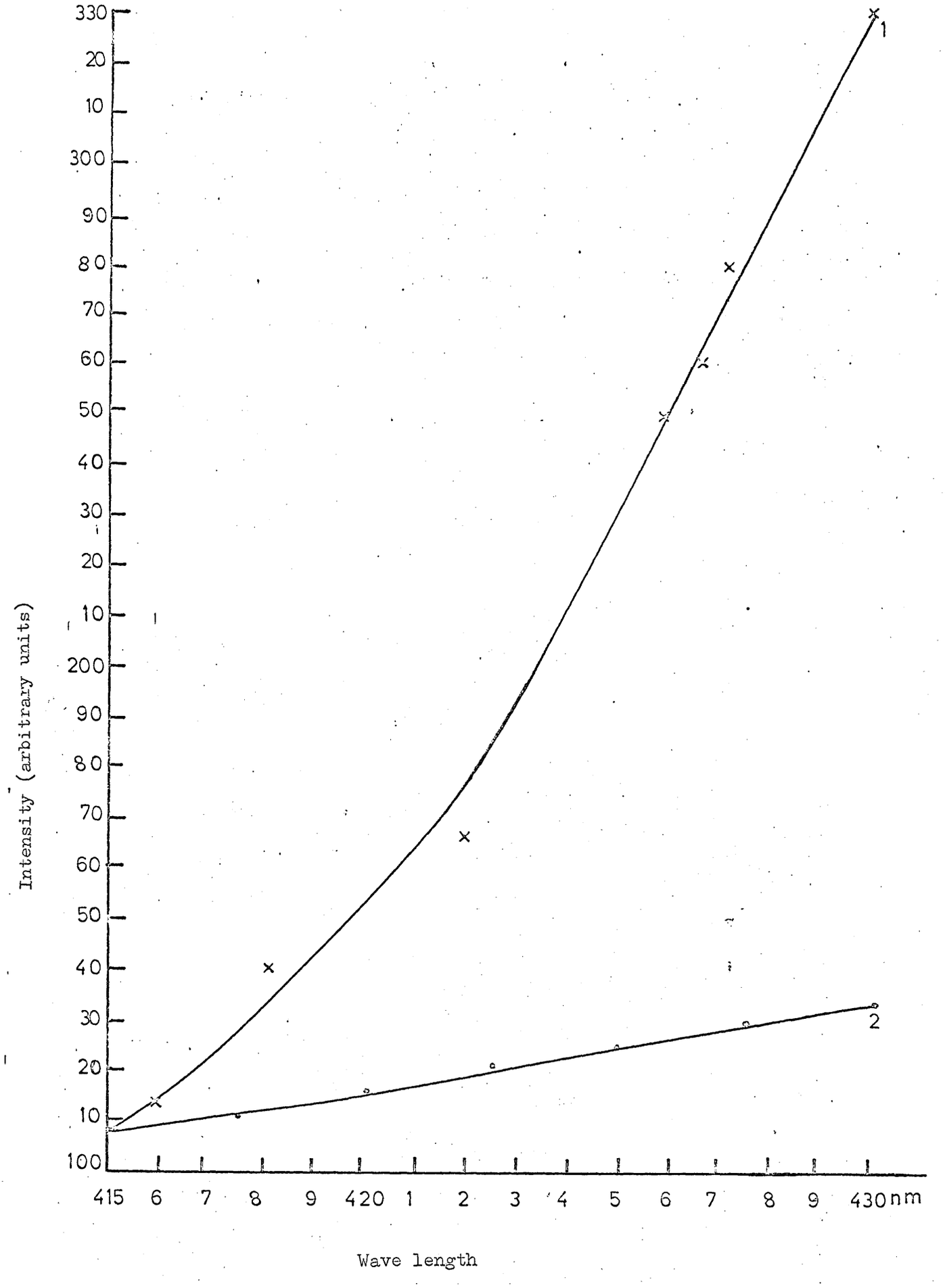

Fig.5.13 Spectral response of photomultiplier type 9524B with the optical system (1) Experimental curve (2) Theoretical black body curve for 3040°K.

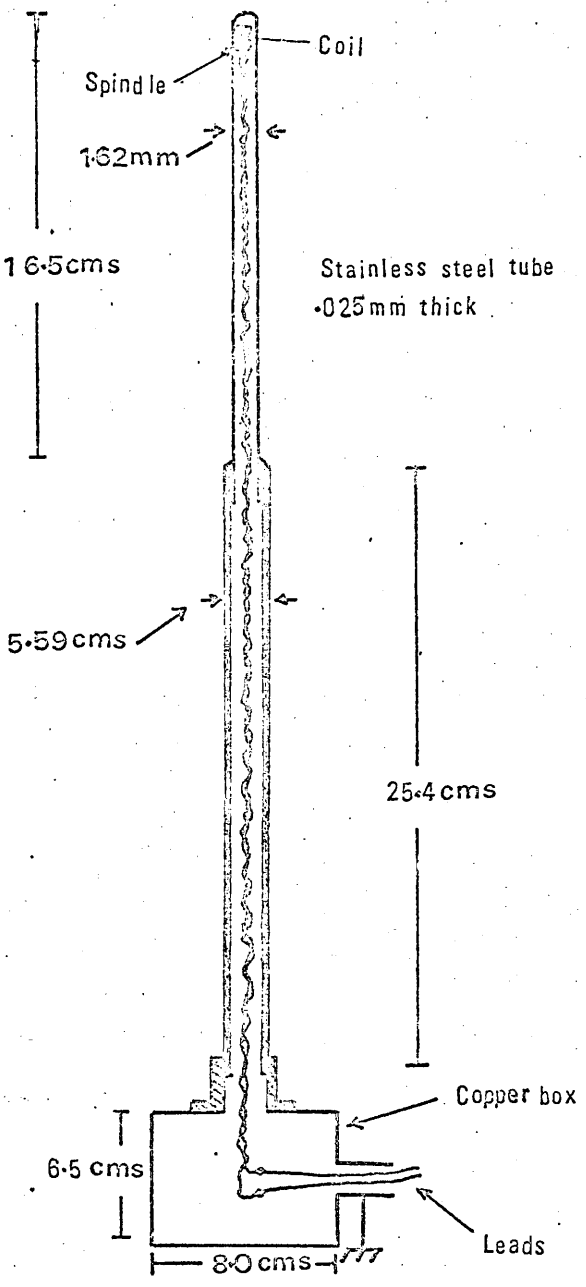

Fig. 5.14 Magnetic probe type I

capacitive coupling between the plasma and the probe-coil a balanced inductive design was chosen. Six turns of 0.025 mm thick insulated copper wire were wound near the end of a pyrex tube. A layer of epoxy resin about 0.3 mm thick held the turns in position and provided electrical insulation. The epoxy resin layer was coated with silver Dag, leaving four slits each about a millimetre wide and parallel to the axis of the coil to minimise circulating currents, the silver being thin enough (0.15 mm) to allow the magnetic field to penetrate whilst reducing the capacitive coupling. The central tap of the coil was connected to the silver coating and grounded through the metallic body of the probe holder. The probe was enclosed in a quartz tube closed at one end. Both tubes were fixed in a metallic holder with epoxy resin as shown in Fig. 5.15.

5.6.1. Calibration of the inductive probes

To calibrate the inductive probe type I, the calibrating circuit shown in Fig. 5.16 was used. A Helmholtz coil was connected to a 0.05 M.F.D. high voltage capacitor through a modified spark gap, the capacitor being fired by pulling the Melinex insulator from the spark gap. The current in the Helmholtz coil was measured with a Tektronix current probe type P6021 and the uniform pulsed field produced by the coils was computed [93] from

$$B = \mu_o \frac{0.715}{R} N i \qquad (5.8)$$

Each Helmholtz coil consisted of 4 turns of 18 S.W.G. insulated copper wire and had a mean diameter of 10.0 cms so that the damped oscillations had the same frequency as that of the pulsed field in the main experiment.

The inductive probe type II was calibrated at the frequency of r.f. generator with the aid of the circuit shown in Fig. 5.17. The pick up coil was placed near the r.f. inductor of the torch and the circuit tuned. The intensity of the uniform field between the Helmholtz coils was determined

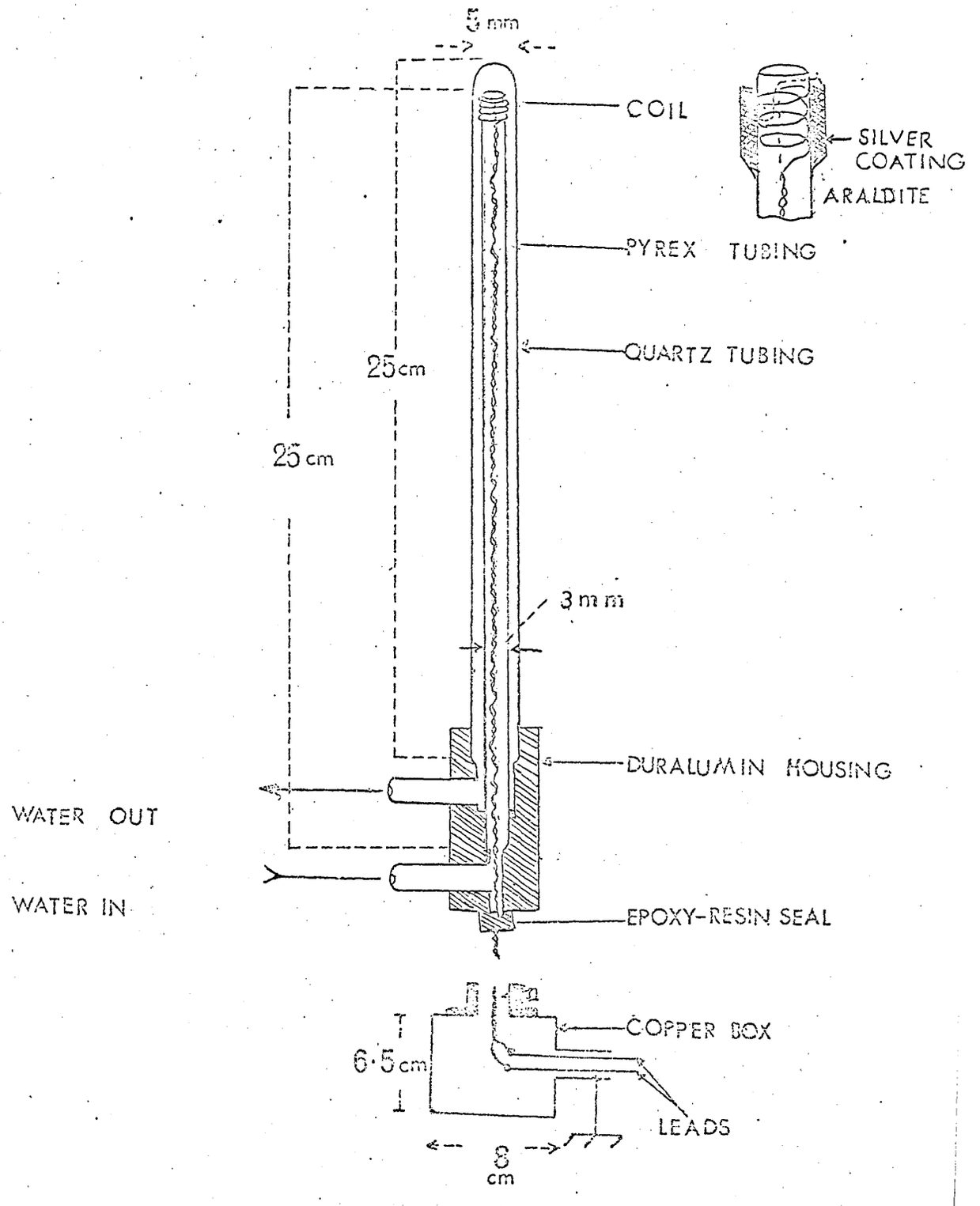

Fig 5.15 Inductive probe type II

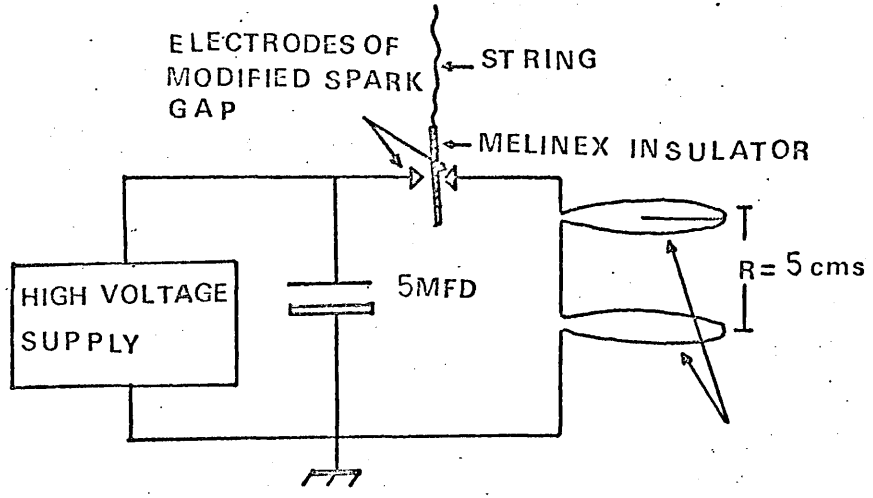

Fig. 5.16 Calibrating circuit type I.

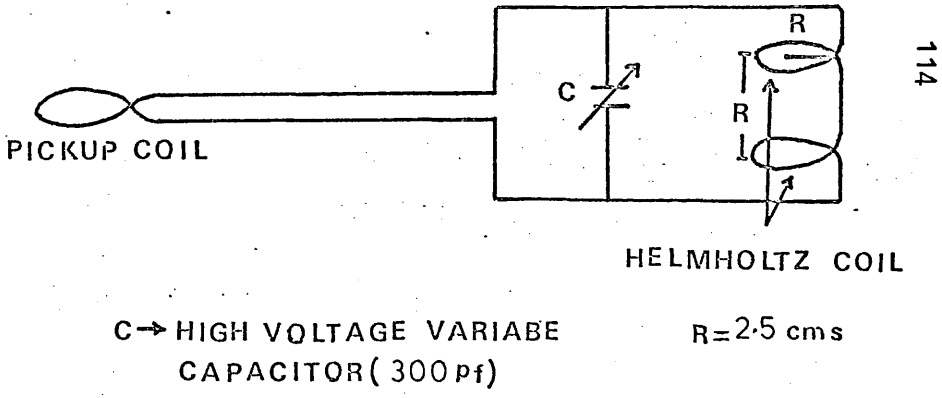

Fig. 5.17 Calibrating circuit type II.

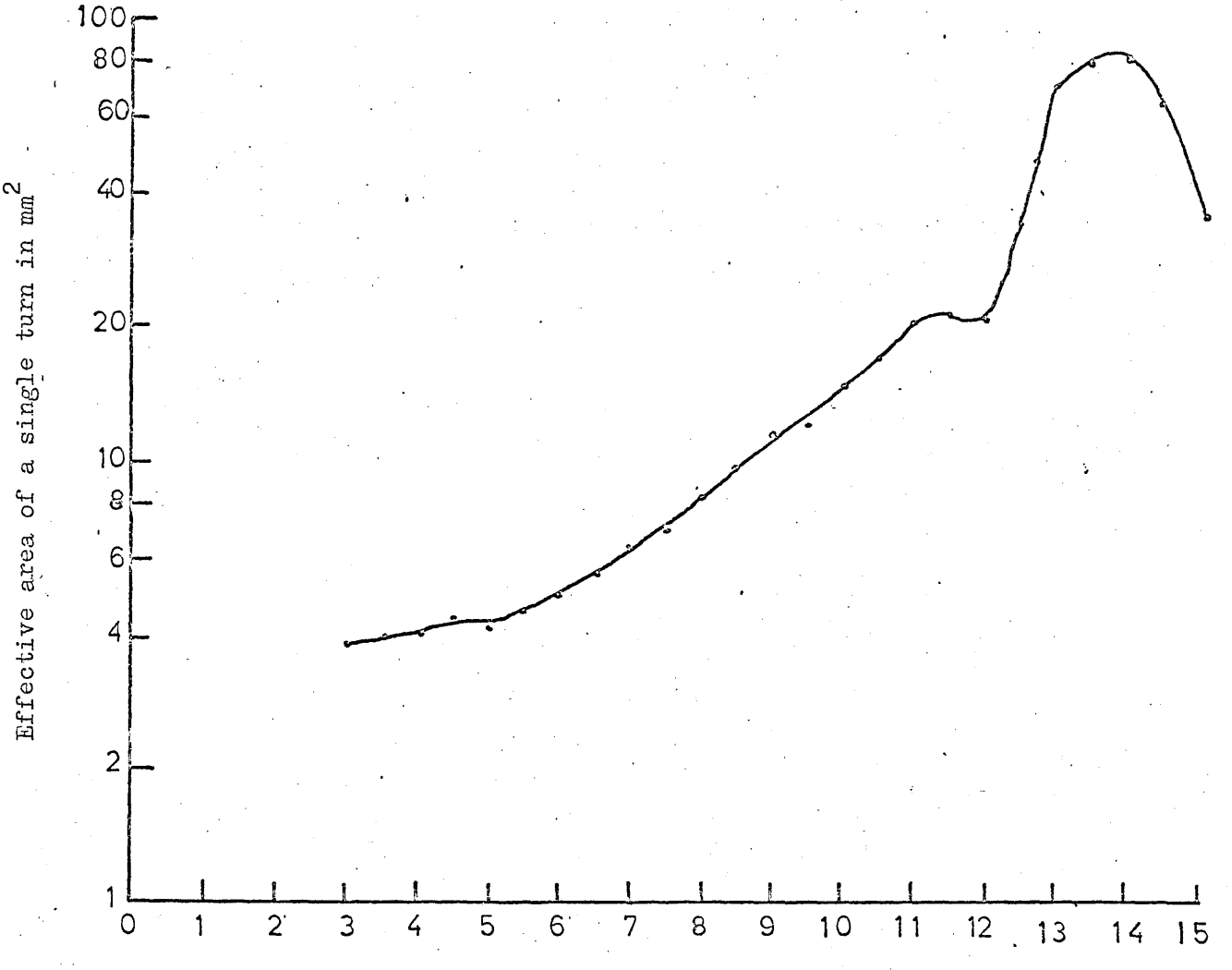

Fig.5.18 Frequency response of the magnetic probe type II

as before. To obtain the frequency response of the probe the calibrating circuit was excited by an Airmech oscillator type 304A by removing the pick up coil and connecting the leads to the output terminals of the oscillator. At every selected frequency of the Airmech oscillator the calibrating circuit was tuned for maximum magnetic field, the uniform field being determined as before. The frequency response curve of the probe, shown in Fig. 5.18, gives the actual cross sectional area of a single probe turn at 6 MHz. The figure shows a weak resonance at 11.25 MHz and a fairly strong resonance at 14.0 MHz.

5.7. High speed photography of the torch

During the high speed photography of the torch a Beckman and Whitelay Model 501 electronic biplanar image converter camera and a Fastax cine camera were used. The 501 camera could take pictures with exposure times between 5 and 1000 nano-seconds and delays of 10 nano-seconds upward. To minimise break through, the aperture of the camera was kept at F22. The Fastax camera had a rotating mirror and could scan 16000 frames per second.

5.8. Conclusion

The optical system to scan the plasma, developed during this work, was found quite satisfactory. The laborious experimental work of measuring the plasma temperature in a pulsed magnetic field could be simplified if it were possible to measure the intensities of more than one spectral lines with their background continuum simultaneously.

The water cooled magnetic probe type II, also developed during this work, was found very useful. Measurements obtained with this probe provided vast amount of information [94] about the induction torch and led to the development of a new and simple technique [95] to measure the temperature of an induction plasma torch.

CHAPTER 6

EXPERIMENTAL RESULTS AND THEIR DISCUSSION PART I

(The plasma-torch in a pulsed magnetic field)

6.1. Introduction

Pulsed magnetic fields of various intensities were applied to a steadily running torch and their effect on the plasma temperature and stability was studied. The temperature and instabilities were found to be much larger in a wider plasma, which was produced in a discharge tube of a large diameter. Whenever appropriate, the maximum temperature attained by the plasma in a pulsed magnetic field is compared with that of the steadily running torch.

In order to find suitable conditions for temperature and other measurements, the radiation from the torch was studied under various operating conditions.

As the study of the radiation changes with the gas flow rate and the oscillator power in a steady torch helps to understand the behaviour of radiation from a torch in a pulsed field, therefore, it is described first. This is followed by the measurements of the pulsed magnetic field. The measurements of radiation, temperature and instabilities in a torch in a pulsed magnetic field are, then, presented in their chronological order. Each type of measurement is followed by its appropriate interpretation and discussion. At the end of the chapter, the factors which control the overall behaviour of the torch in a pulsed field are discussed.

6.2. Radiation from a steady torch

The variation of the light intensity with the oscillator power and the argon flow rate was investigated in a torch burning in the discharge tube DT.1. A constant scale of arbitrary units was used to measure the light intensities throughout this work. The variation of the light intensity as a function of the oscillator power and the argon flow rate is presented in Fig. 6.1. It is seen that at 4.0 kW the light intensity decreases from a comparativley high value at 1.9 l/m to a low value at 7.3 l/m. At 7.0, 10.5 and 13.0 kW, the light intensity remains constant between 4.5 and 10.5 l/m. However, it decreases on both sides of this region. The maximum intensity increases with the oscillator power.

An increase in the gas flow above 10.5 l/m causes excessive cooling of the plasma and a consequent decrease in the radiated power. An important point is that at higher gas flows, the discharge size is increased by the deeper upstream penetration of the plasma which flows counter current to the main (77) gas stream near the axis in a vortex stabilisation. This causes an increase in the radiated power, but this effect is masked by the reduced plasma temperature, and a net decrease in the radiated power results.

These opposing phenomena may be traced back into the region of constant intensity where they balance each other. They are more pronounced at a high oscillator power as seen by a bigger drop in light intensity for 13.8 l/m argon flow with the increasing oscillator power. Below 4.5 l/m there is a less gas available for plasma formation. A smaller plasma emitting less light is thus produced. In a 4.0 kW torch the available power is small so that plasma cooling becomes effective as soon as the argon flow is increased above 4.5 l/m. It is interesting to observe that the plateau or maximum intensity is proportional to the oscillator power as shown in Table 6.1.

A study of the pulsed magnetic field, viz. its variation in time and

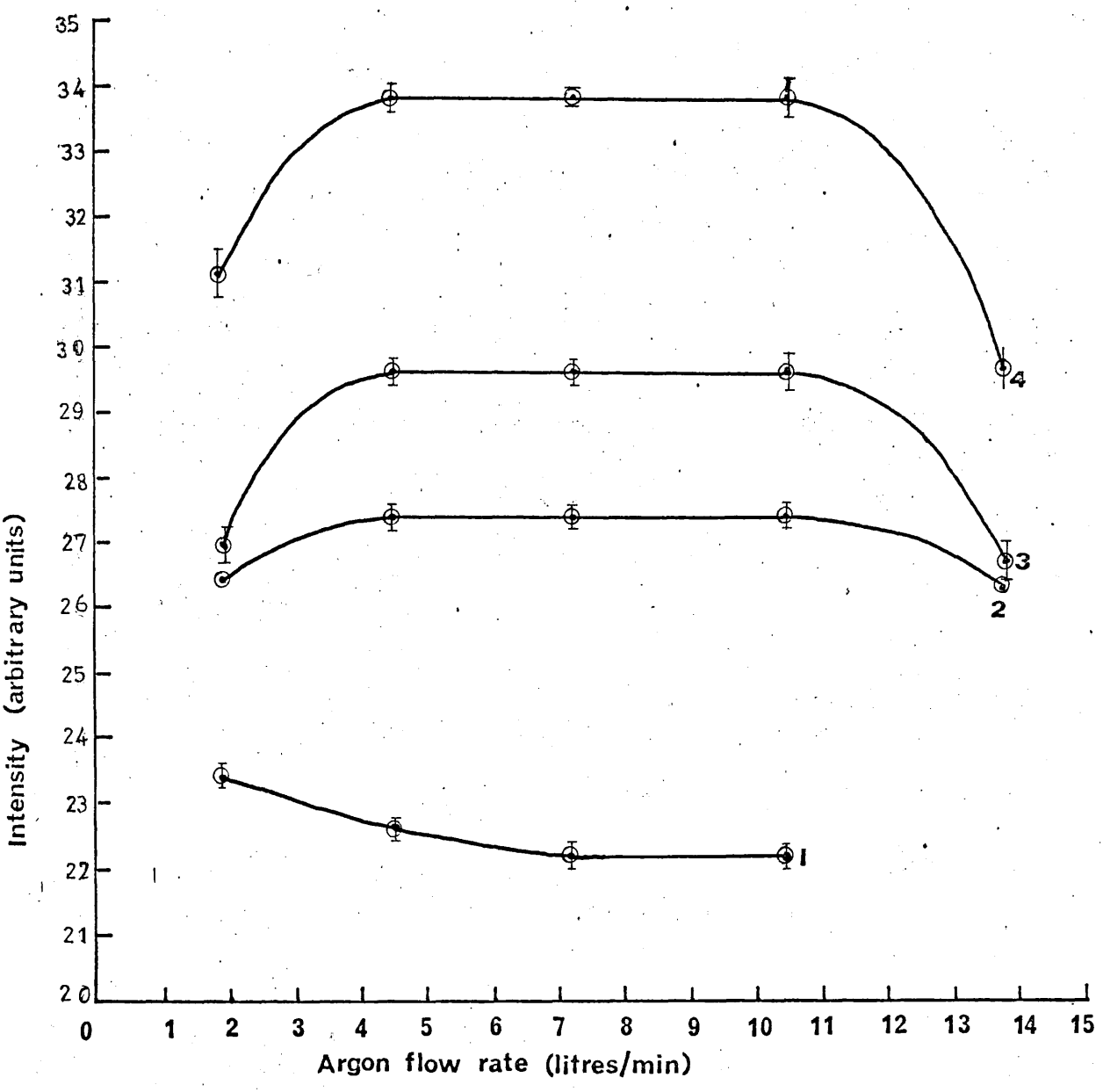

Fig. 6.1 Variation of the light intensity from the torch with argon flow rate at d.c. oscillator power inputs of 1) 4.0 kW 2) 7.0 kW 3) 10.5 kW 4) 13.0 kW.

Table 6.1

Oscillator power (A)	Maximum intensity (B)	B/A
13.0 KW	13.8 units	1.06
10.5 "	9.7 "	0.92
7.0 "	7.4 "	1.05

space, will be desirable before studying its effect on the torch radiation.

6.3. The pulsed magnetic field

The variation of current in time is shown in Fig. 6.2. The magnetic field was found to follow the variation of the current. Henceforth the maximum value of the pulsed field will be denoted by H_m. Variation of H_m with the charging voltage on the main capacitor 'C' (Fig. 5.3.) is shown in Fig. 6.3. H_m is also plotted as a function of the axial position in Fig. 6.4. and as a function of radial position in Fig. 6.5. for the same voltage on capacitor 'C'. Measurements of the radial distribution of the pulsed field were made along a diameter perpendicular to that part of the transmission line which was adjacent to the theta coil. It is seen that the pulsed field changes considerably along the axis, but only a little along the radius for a voltage of 15 kV on the capacitor 'C'.

The pulsed magnetic field was also investigated in the presence of the plasma by the method described in Section 5.4.1. With the 13.0 kW torch burning in the discharge tube DT-1, identical diamagnetic loop signals were obtained with and without the plasma. However, the pulsed magnetic field measured with the water cooled magnetic pulse type II was found to be negligibly small in the middle of the r.f. inductor in the presence of the 13.0 kW torch. With the 11.6 kW torch, burning in the discharge tube DT-2 diamagnetic loop signal, presented in Fig. 6.6, shows a trapped field and plasma instabilities. For comparison a signal without plasma is also presented in the same figure.

6.4. The plasma torch in a pulsed magnetic field

6.4.1. Plasma radiation

On pulsing the magnetic field on the torch, burning in the discharge

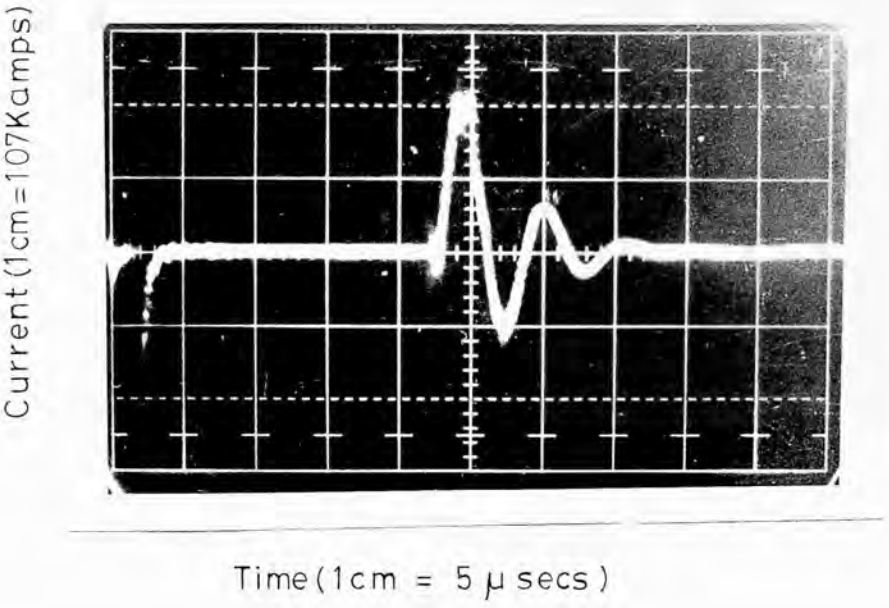

Fig.6.2. Variation of the current in the Theta coil with time, forapulsed magnetic field H_m = 1.25T.

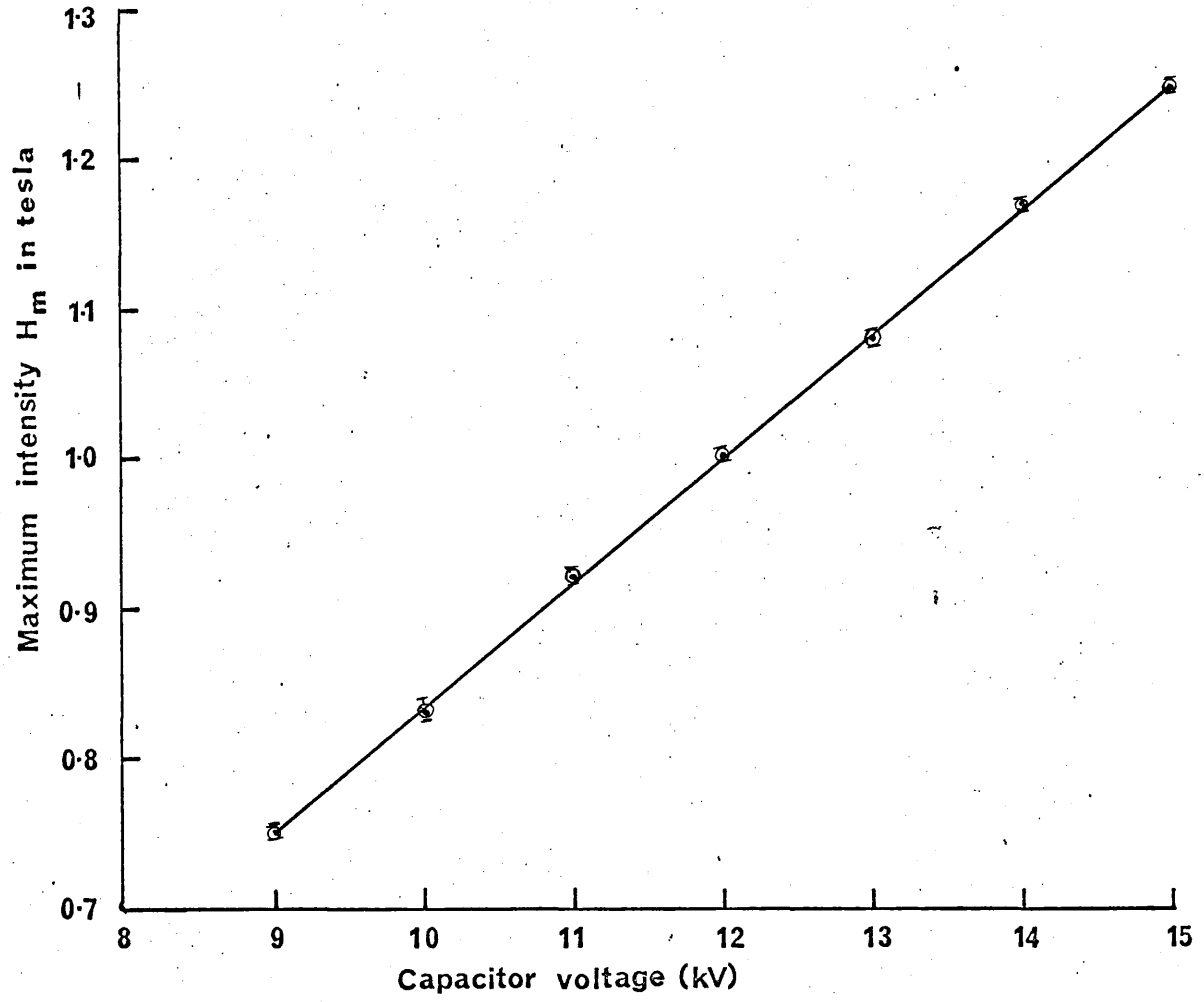

Fig. 6.3 Variation of the maximum intensity of the pulsed magnetic field with the capacitor voltage.

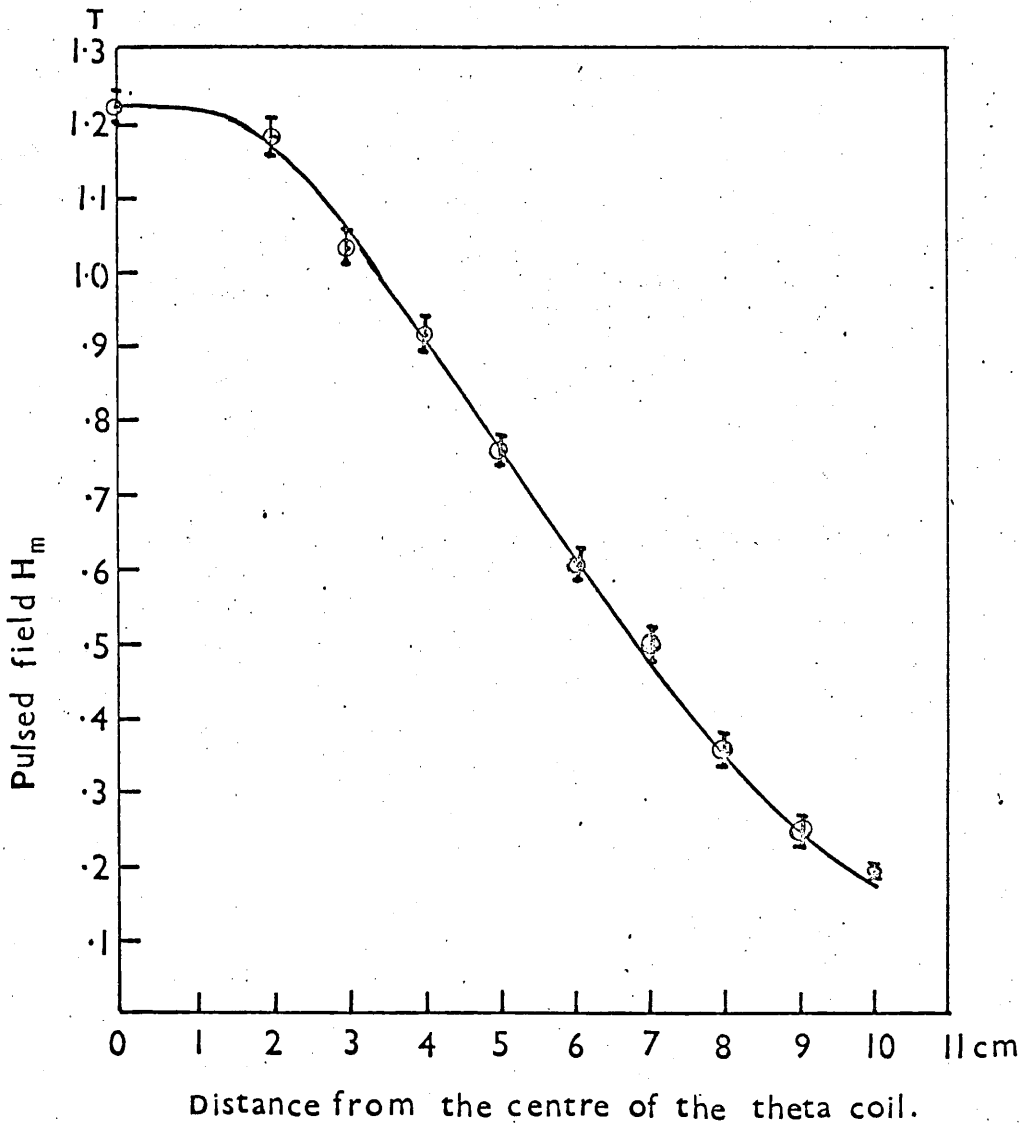

Fig. 6.4 Axial distribution of the pulsed magnetic field Hm for a capacitor voltage of 15 KV.

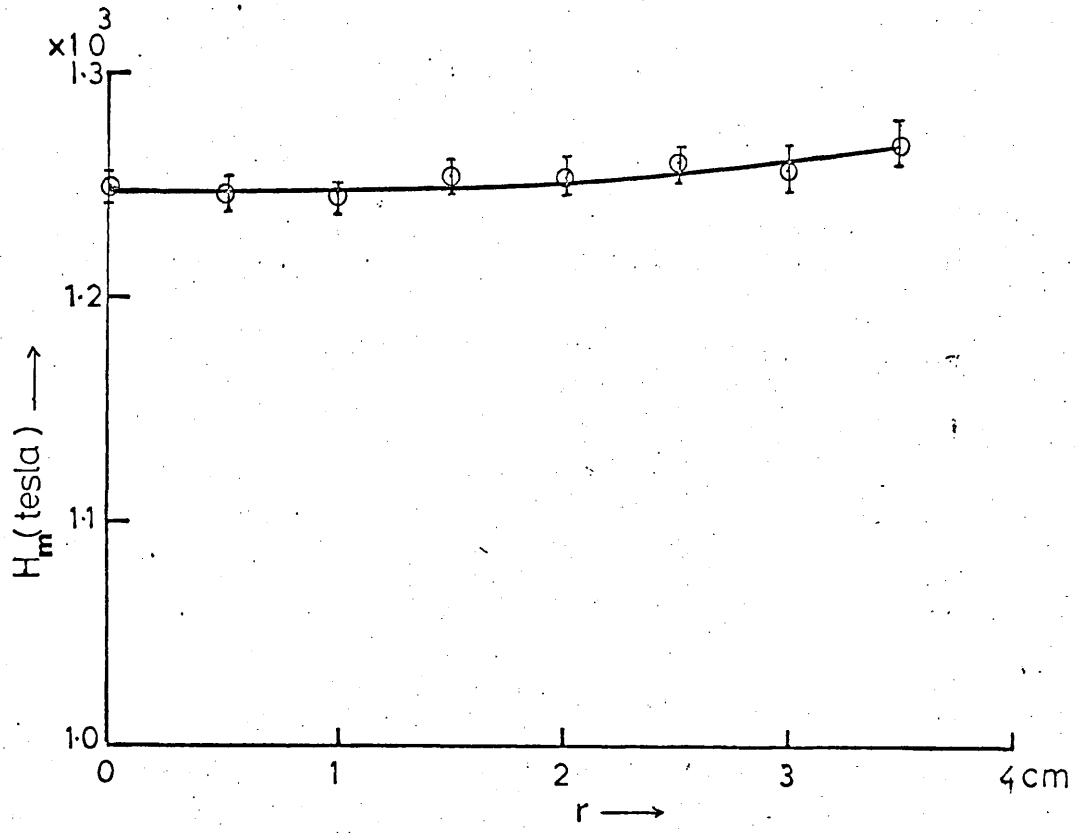

Fig 6.5 Radial distribution of H_m in the mid plane of theta coil for a capacitor voltage of 15KV.

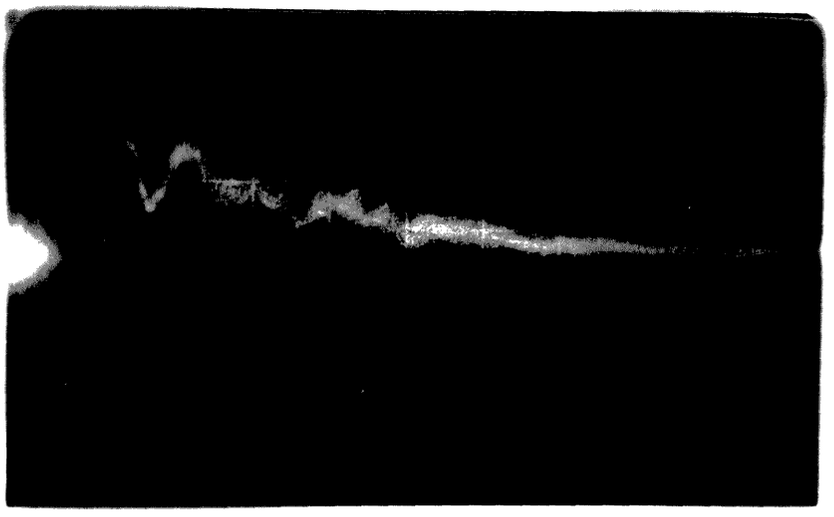

a

b

1 cm = 5 micro seconds

Fig.6.6 Diamagnetic loop signal showing trapped magnetic field in a11.6 KW torch(a)with plasma (b)without plasma

tube DT-1, the light intensity rose to a maximum in less than 10 micro-secs and then decreased slowly to its original value over hundreds of micro-secs. The torch remained burning after the magnetic pulse.

The maximum intensity of light I_m, as a function of the maximum magnetic field H_m and the gas flow rate is plotted in Figs. 6.7, 6.8, 6.9 and 6.10 at d.c. oscillator power inputs (henceforth called the oscillator powers) of 13.0, 10.5, 7.5 and 4.0 kW respectively with curves numbered 1, 2, 3, 4 and 5 belonging to argon flows of 1.9, 4.5, 7.3, 10.5 and 13.8 l/m respectively. In all cases I_m increases with H_m. Also the slope of I_m - H_m curve increases with H_m, showing that the radiation efficiency of the pulsed field increases with its magnitude. I_m has the largest value for an argon flow of 10.5 l/m and the smallest value for an argon flow of 1.9 l/m within the working range of the magnetic field. Curves belonging to 4.5 and 7.3 l/m of argon fall between these limits with the latter lying above the former. All these curves lie separate from each other at 13.0 kW (Fig. 6.7). Curves 2, 3 and 4 come closer together with the decreasing oscillator power and the pulsed field. At 10.5 kW they overlap (Fig. 6.8.) up to 1.0T, where curve 2 separates out, but the separation of curves 3 and 4 occurs at a higher value of H_m. At an oscillator power of 7.5 kW (Fig. 6.9) curves 3 and 4 remain overlapping even at the highest available magnetic field. At 4.0 kW (Fig. 6.10) curves 2, 3 and 4 overlap each other even at the highest available field.

Curve 5, corresponding to an argon flow of 13.8 l/m, behaves in a peculiar way. For lower values of the magnetic field it lies closer to curve 1 and, for higher field values, it tends to approach curve 4. Curve 5 has not been plotted at 4.0 kW as the torch became unstable and finally went out at an argon flow of 13.8 l/m.

The effect of the pulsed magnetic fields on the radiation from a 11.6kW torch, burning in the discharge tube DT-2, was also studied. The torch was extinguished with a hissing sound after the application of the pulsed field. The light intensity I_m plotted against H_m for different gas flows, all

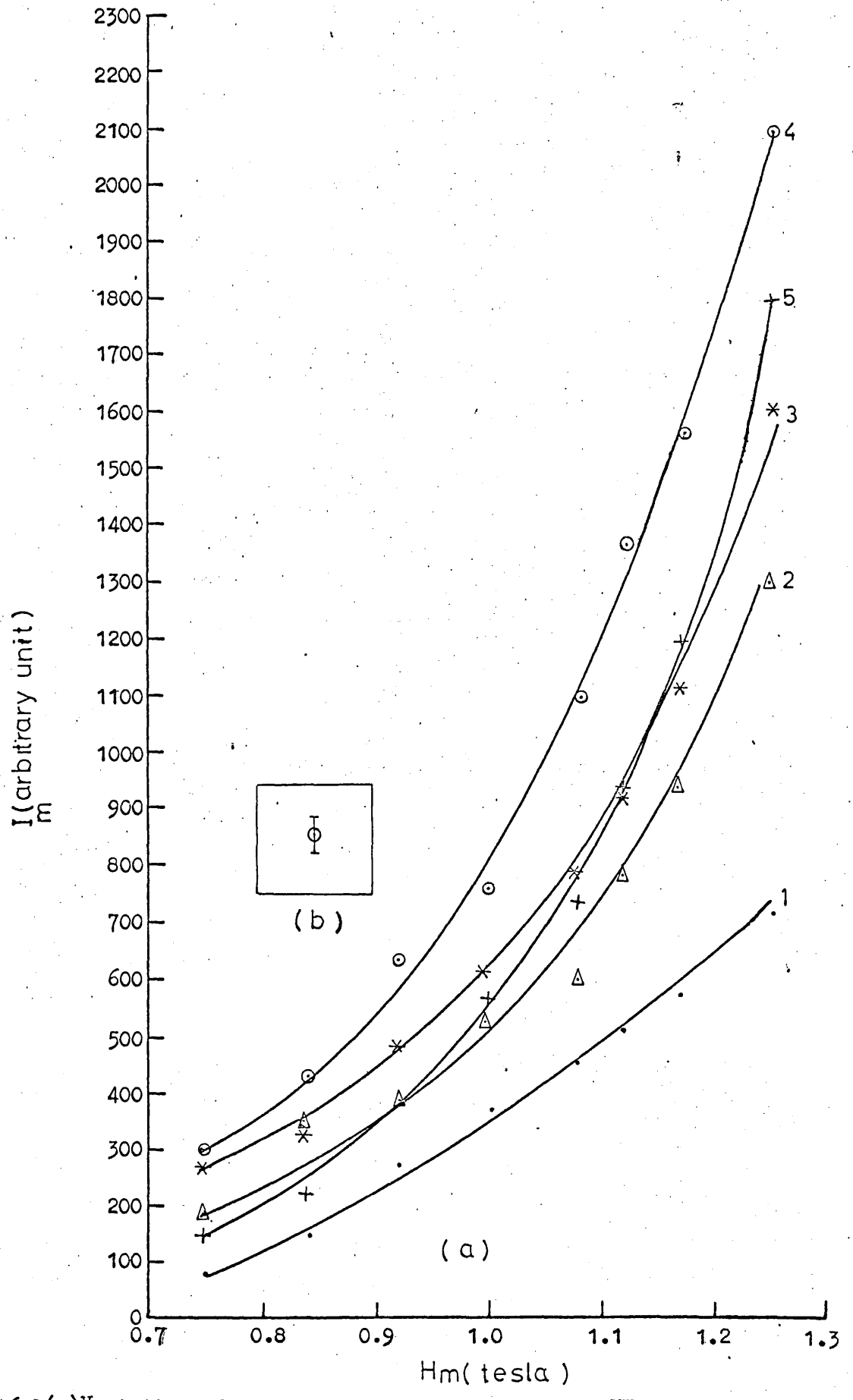

Fig.6.7(a)Variation of the light intensity from a 13.0KW torch with pulsed magnetic field for argon flows 1) 1.8 l/m 2) 4.2 l/m 3) 7.3 l/m 4) 10.5 l/m 5) 13.8 l/m (b) Standard deviation at 10.5 l/m Argonflow for H_m=7.5T.

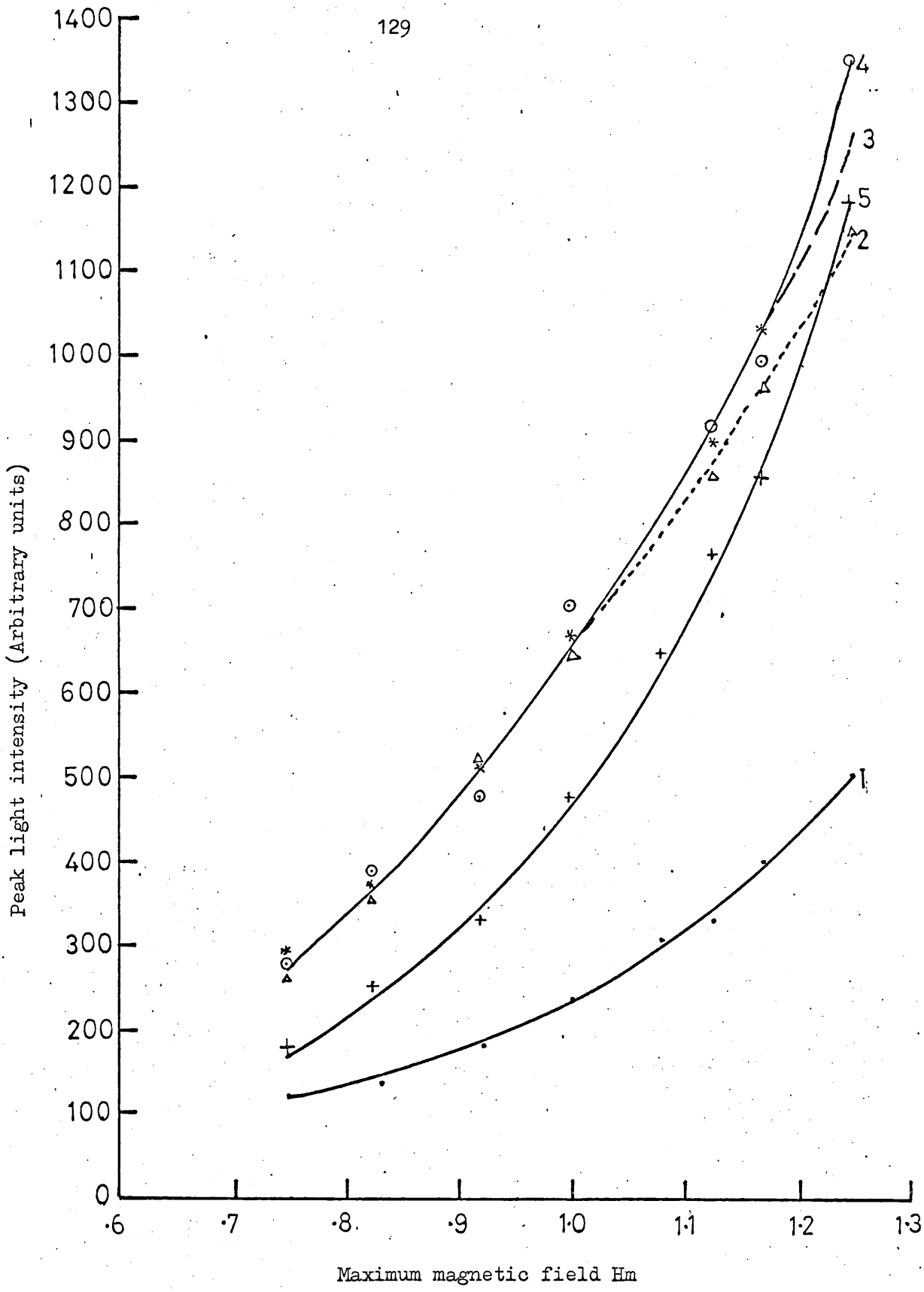

Fig.6.8 A Variation of the light intensity from a 10.5 K.W torch with the pulsed magnetic field for argon flow rates of 1) 1.8 l/m, 2) 4.2 l/m, 3) 7.3 l/m, 4) 10.5 l/m, 5) 13.8 l/m.

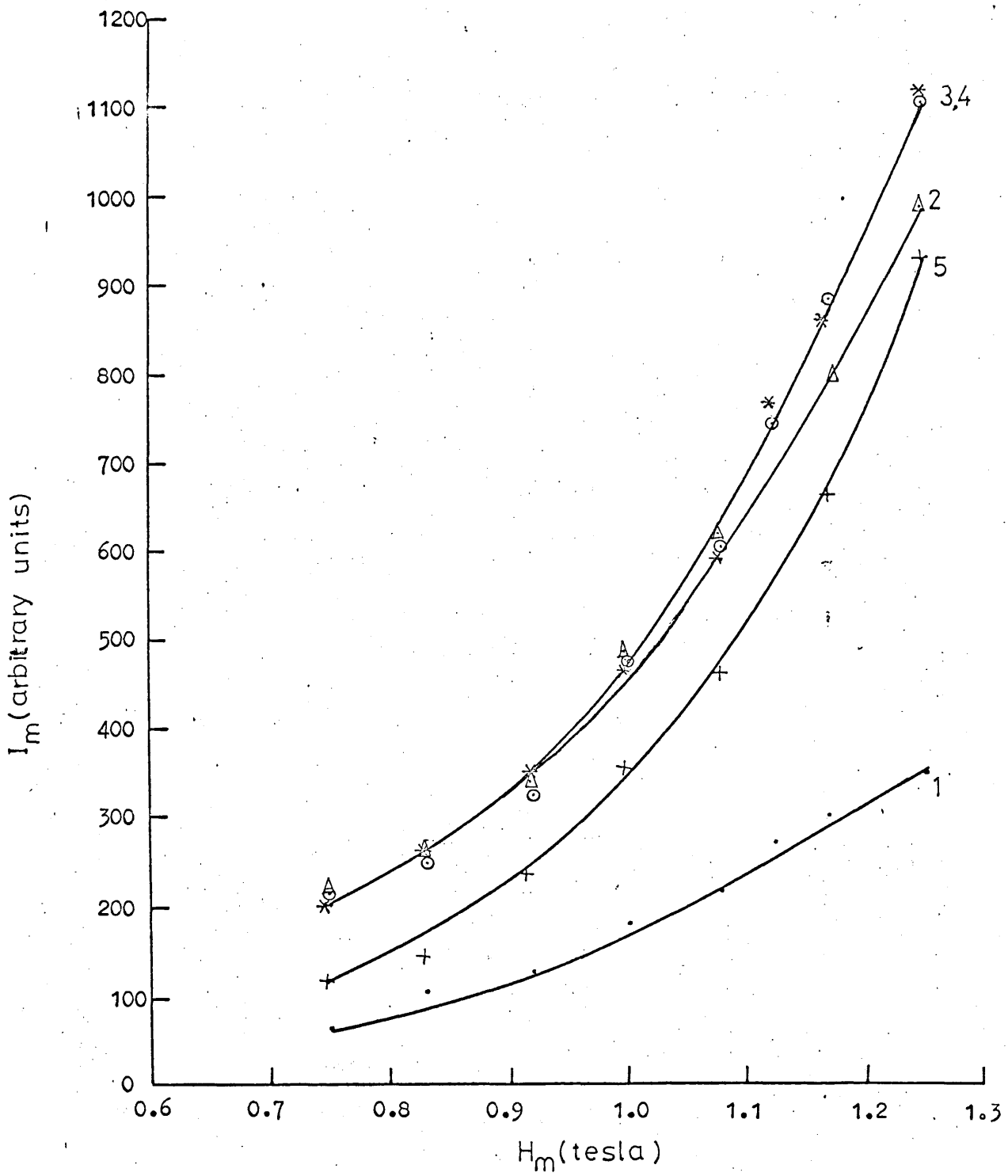

Fig.6.9 Variation of light intensity from a 7.5KW torch with pulsed magnetic field for Argon flow rates 1)1.8 l/m 2)4.2 l/m 3)7.3 l/m 4)10.5 l/m 5)13.8 l/m.

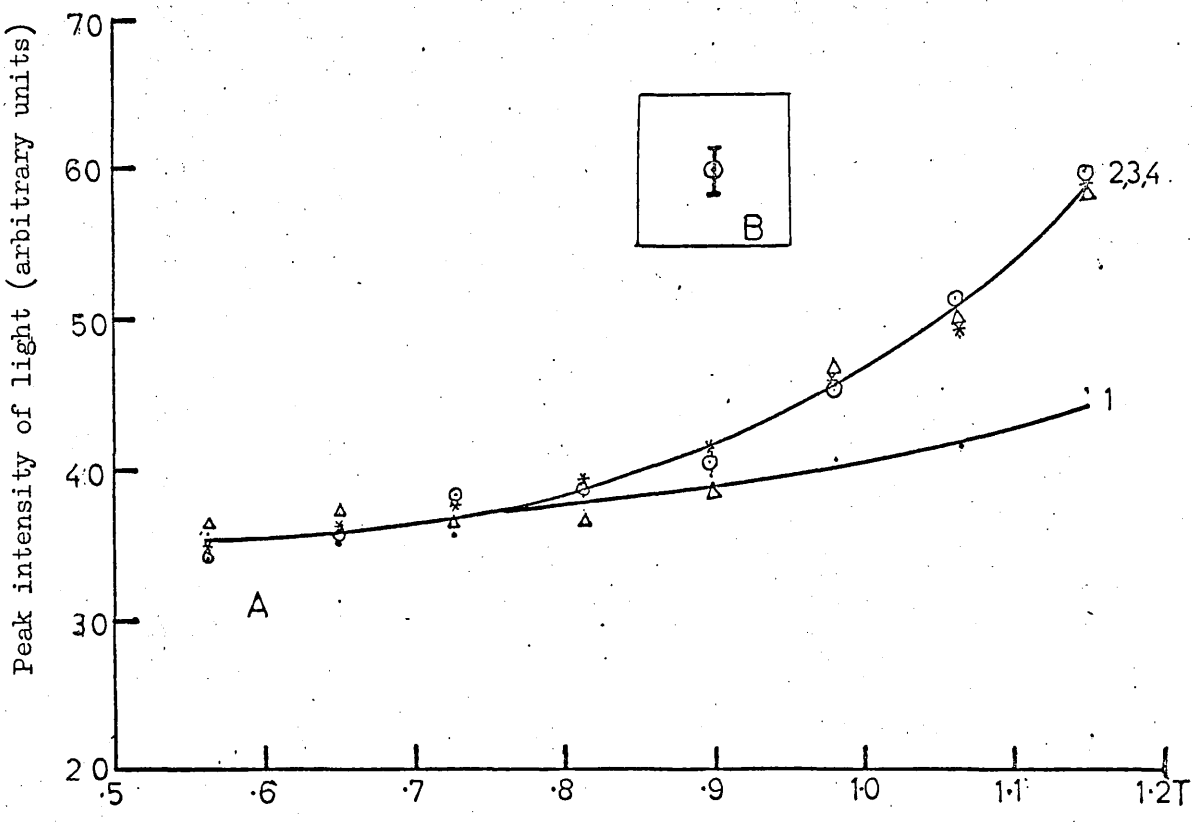

Fig.6.10 A Variation of the light intensity from a 4 K.W plasma torch with the pulsed magnetic field for argon flow rates of 1) 1.8 l/m, 2) 4.2 l/m, 3) 7.3 l/m, 4) 10.5 l/m.

B Typical standard deviation at an intensity of 35 units.

coincide with one another as shown in Fig. 6.11.

6.4.1.1 Interpretation and discussion

It is shown in Appendix II that the photomultiplier calibration factor is 412.8 watts/unit light intensity. Variation of the radiated power in a pulsed magnetic field may be explained by making the following assumptions.

(i) The pulsed energy is coupled only into the plasma already available. The formation of the new plasma by virtue of an increase in the plasma size is small* (this is shown by the high speed photography) because of the short duration of the magnetic pulse ($\sim$10 micro-seconds).

(ii) As the plasma is heated by the magnetic pulse it heats up the adjoining layer of the cooler gas which eventually becomes a part of the plasma, The thickness of this layer 'Δr', though essentially small, increases with the temperature.

(iii) The contribution of this layer to the radiated power depends on the number density 'n_o' of the particles, which is high, before the magnetic pulse. The loss of particles due to diffusion from the layer is negligible during the short pulse length.

For a given gas flow the size of the plasma (and so also its radius) increases with oscillator power. This fact combined with (i) explains why all curves belonging to high oscillator powers generally lie higher up (except curve 5) in Fig. 6.7 to 6.10. In a vortex stabilisation the gas density near the tube wall is high. Because the heavy particle density in

* A small increase in the plasma radius was observed during scanning of the discharge as shown by the radial temperature distribution in Fig.6.12

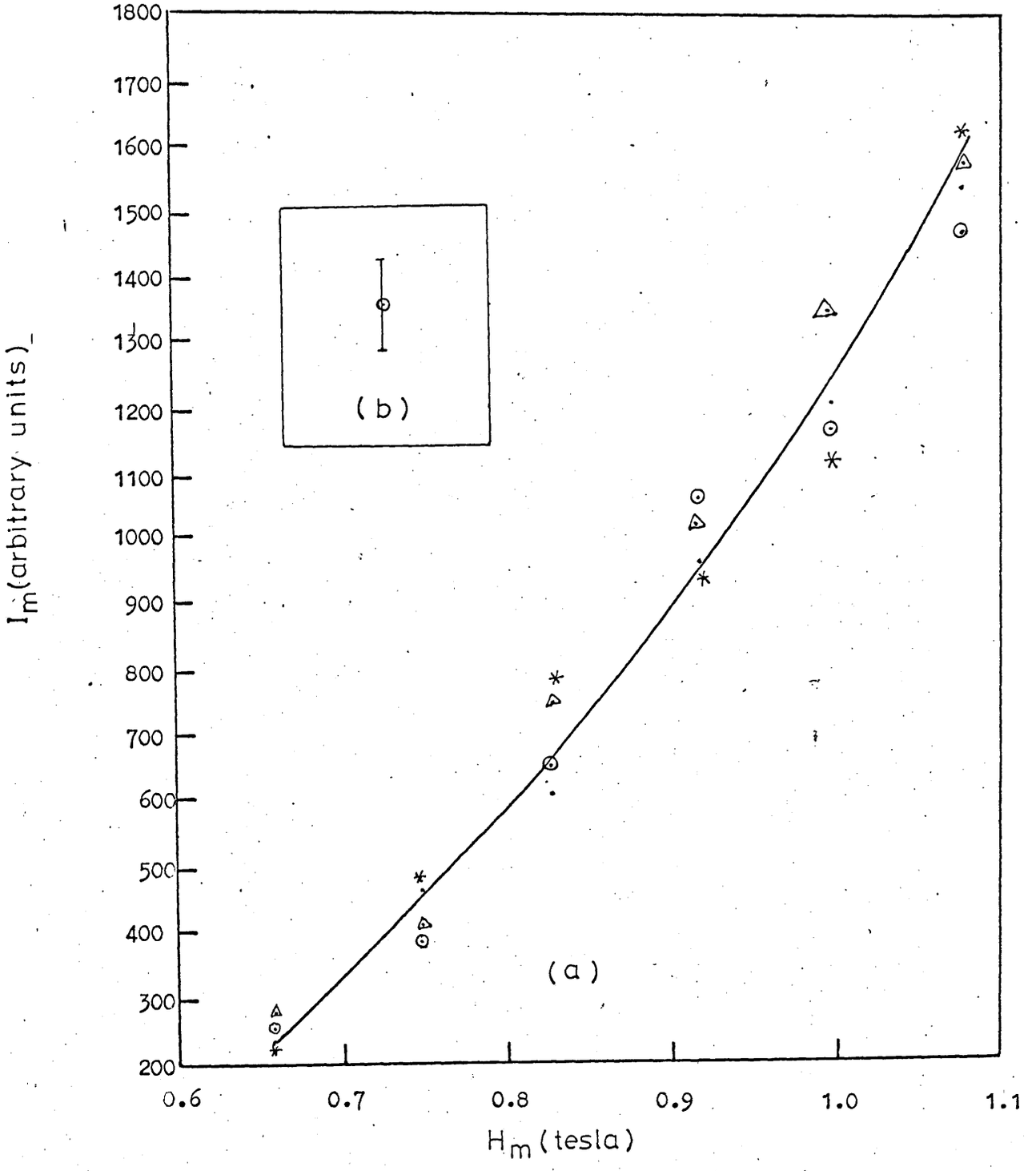

Fig.6.11 (a) Variation of light intensity from a 11.5 KW torch with pulsed magnetic field , various Argon flows being indicated by different type of points (.)---1.8 l/m (△)---4.2 l/m (*)---7.3 l/m (⊙)---10.5 l/m
(b)Standard deviation at Argon flow=10.5 l/m and H = 1.0 T.

the plasma is low due to high temperature and because a part of the plasma flows counter current to the main gas stream, the main gas flow takes place through the narrow annular space between the plasma and the discharge tube. The density of the gas in the annular region depends on (a) the width of the annular space i.e. on the effective plasma diameter. (b) on the gas flow rate. At a high oscillator power (narrow annular space) an increase in the gas flow rate produces a more pronounced increase in the gas density. In the absence of diffusion, 'n_o' and 'Δr' determine the intensity of radiation from the layer. This explains why the curves are separate in Fig. 6.7. and why in general the separation between the curves increases with the increasing H_m. At lower oscillator powers the annular space is wider and therefore, n_o is nearly the same for various gas flows. As a result various curves coincide with each other as they do in Fig. 6.10 for lower values of H_m. To magnify the effect of small changes in n_o larger Δr and therefore higher H_m is required. The separation of curves at higher values of H_m is thus explained.

The effect of various factors mentioned above (gas flow, oscillator power etc.) on the radiation emitted from the main plasma, whose radius remains unchanged during the magnetic pulse, must also be included in the analysis. It was shown in Section 6.2. that an increase in the gas flow increased the plasma volume. The only necessary thing is to examine how this increase in plasma volume is further affected by the oscillator power. It can be shown by a simple reasoning that at a high oscillator power more pronounced changes in plasma volume would be produced by a given change in the gas flow. This means the radiation from the main plasma responds to changes in gas flow and oscillator power in the same way as does the radiation from the heated layer when the pulsed field is applied. The two affects are complementary.

The peculiar behaviour of the curve[5] in Fig. 6.7. may now be explained. It was shown in Section 6.2. that, in the absence of H_m a low intensity of light would be emitted by a large plasma at a low temperature (for 13.0 kW

torch with 13.8 l/m gas flow). This is also true at lower values of H_m, when plasma heating by H_m is small. As a result curve 4 lies near smaller values of I_m for low H_m. As H_m increases so does the plasma temperature. And as the energy absorbed, and therefore, the energy radiated depends on the plasma volume, the light intensity increases more rapidly with the magnetic field in this case than with a smaller plasma.

A natural conclusion of the above theory is that all curves, corresponding to different gas flows, should coincide for a sufficiently wide annular space. A 11.6 kW torch, burning in a 5.4 cm wide discharge tube (type II) had a wide annular space. Experiments were performed using this torch to check the above conclusion and their results presented in the last article confirm it.

6.4.2. Plasma temperature.

When energy is fed into the plasma by a pulsed magnetic field its temperature rises to a maximum decreasing afterwards. In this work the maximum or the peak value of the time varying temperature at a radial position 'r' in the cylindrical plasma will be denoted by T(m,r). This value for r = 0 will be denoted simply by T(m). The peak value of the time varying temperature averaged over a plasma diameter will, however, be denoted by T(a).

As regards the choice of various parameters for measuring the plasma temperature, it was shown in section 6.4.1. that the light intensity was greater for an oscillator of 13.0 kW, and a magnetic field of 1.25T and an argon flow of 10.5 l/m than for any other combination of these parameters. The light intensity increased with the magnetic field. As the oscillator power of 13.0 kW and the magnetic field of 1.25T could not be much exceeded with the available equipment these values were chosen for the temperature measurement of the plasma in the discharge tube DT-1. For comparison the the lowest oscillator power of 2.0 kW, which became available with the improvement

in the power control system of the r.f. generator at this stage, was also chosen for the measurement of plasma temperature at an argon flow of 4.5 l/m and a pulsed field H_m = 1.25T.

In the 11.6 kW torch burning in the discharge tube DT-2, the gas flow of 7.3 l/m was arbitrarily chosen for measuring the plasma temperature. Pulsed magnetic fields of H_m = 1.08T and H_m = 1.25T were chosen for these measurements.

6.4.2.1. The 13.0 kW torch

6.4.2.1.1 Average temperature along a plasma diameter

As a preliminary step, the average temperature along a plasma diameter T(a) in the middle of the r.f. inductor was measured in a 13.0 kW torch for various values of H_m. The results are presented in Table 6.2. As expected a higher temperature was obtained at a higher field intensity. The temperature rise in this case is mainly due to Joule heating of the plasma as will be shown in Section 6.4.5.3.

TABLE 6.2. Average plasma temperature at various pulsed magnetic fields

The pulsed magnetic field H_m	Temperature T(a)
1.25T	12.5×10^3 °K
1.17T	12.2×10^3 °K
1.13T	11.95×10^3 °K
1.08T	11.8×10^3 °K
1.00T	11.4×10^3 °K
0.92T	11.1×10^3 °K

6.4.2.1.2. Radial distribution of temperature

Fixing the origin at the upper end of the r.f. inductor and the Z axis along the axis of the discharge tube, two positions at Z = 0.3 cm and Z = 1.2 cm were chosen to determine the radial distribution of temperature in a 13.0 kW torch

6.4.2.1.2.1. Temperature at Z = 0.3 cm

Radial distributions of temperature with and without the application of a pulsed field of various intensities were determined. The results are presented in Fig. 6.12 where experimental points for the temperature distribution at H_m = 1.25 are also shown. The distribution of the steady temperature agrees well with the previous work.[25,63,66,94] Both distributions show off-axis peaks. The off axis peak in the temperature distribution of the steady torch is well documented and is attributed to the skin[77] effect combined with the power loss through radiation in the axial region. The off-axis peak at about 0.7 cm for H_m = 1.25T may similarly be attributed to the skin effect. This point will be discussed in detail in Section 6.4.5.1.1.

To see the effect of (i) the pulsed field H_m (ii) the total power, which consists of c.w.r.f. power and the pulsed power, averaged over the pulse length (11 micro-seconds), on the plasma temperature, the latter is plotted against (i) and (ii) in Figs. 6.13 and 6.14 respectively. In each case the temperature T_m shows a little tendency towards saturation, which is probably due to a marked increase in the radiation losses and an increased amount of energy required to produce enhanced ionization at higher temperatures. A closer examination made in Section 6.4.5.1.4. however reveals that the ionization effect dominates.

Measurements on the decay of the plasma temperature, after the application of the pulsed magnetic field H_m = 1.25T, were also made at 50

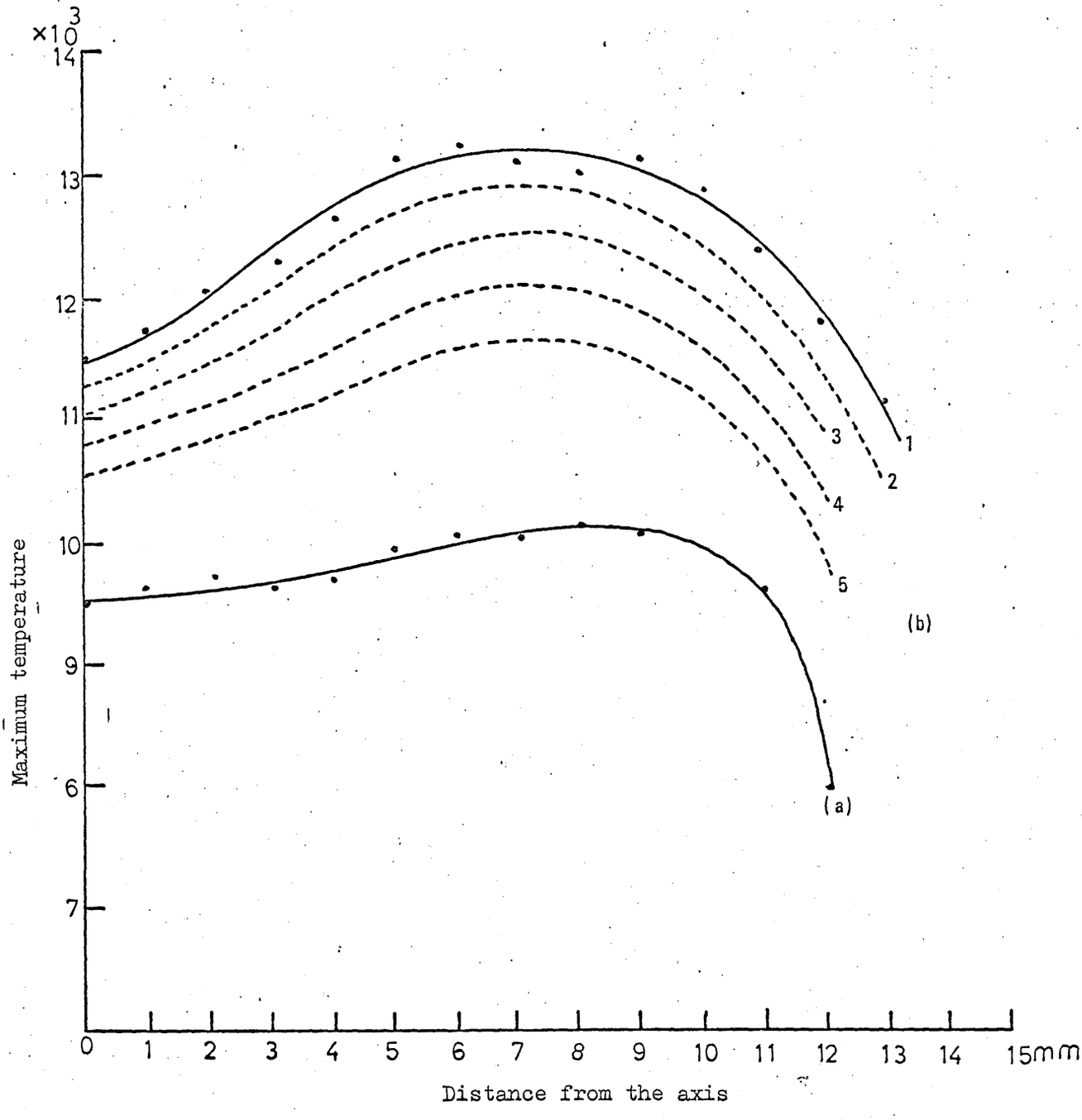

Fig.6.12 Steady and peak temperature distributions in the plasma at Z = 0.3 cm.
(a) No pulsed magnetic field. (b) When the pulsed magnetic field is at peak value 1) 1.25T, 2) 1.17 3) 1.08T, 4) 1.0T, 5) 0.92T.

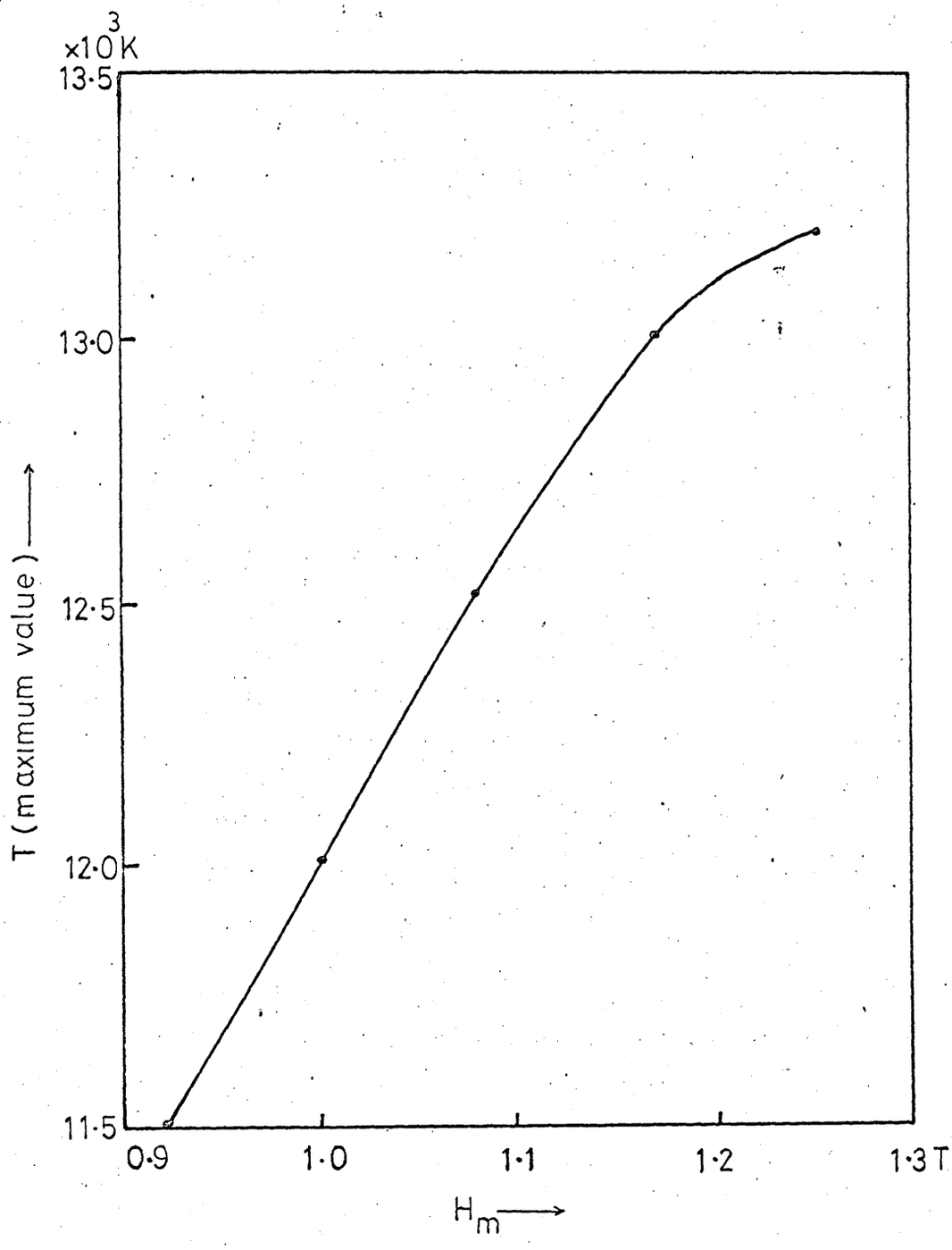

Fig 6.13 Variation of maximum plasma temperature with H_m.

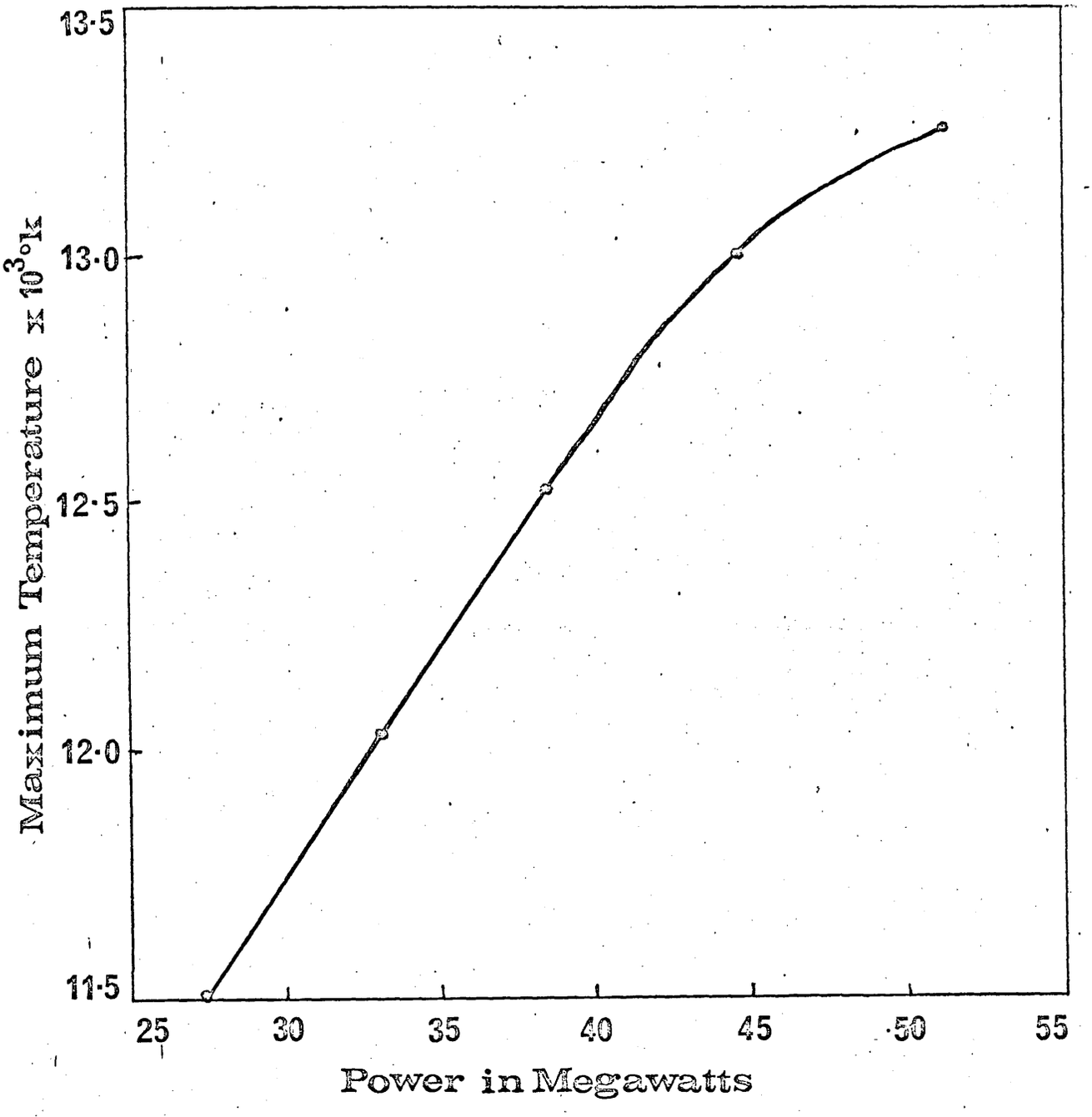

Fig.6.14 Dependence of maximum plasma temperature on the total power, consisting of pulsed and CW r.f. powers.

micro-second intervals at r = 0 and r = 0.7 cm. The values of T(m, r), at the above mentioned radial positions, were determined by the relative line intensity method. The radial intensity of the 425.9 nm spectral line at its peak value was normalised to T(m, r) at the appropriate radial positions (r = 0 d & = 0.7 cm). The decay of temperature was, then, determined by the decay in the intensity of the spectral line, using the Fowler-Milne method described in Section 5.4.5.2. The results of these measurements are presented in Fig. 6.15. The temperature decay is seen to be slower at r = 0.7 cm than at the axis after the magnetic pulse. Two factors may contribute to it (i) with the decreasing temperature the electrical conductivity of the plasma decreases and the skin depth for the r.f. field increases. This results in an improved r.f. power coupling, which slows down the plasma cooling (ii) heating of the plasma by instabilities which are excited by the pulsed field and mostly lie on the plasma surface, continues for some time after the magnetic pulse. At the axis, however, the plasma heating by instabilities is very small. The heating of plasma by instabilities will be further discussed in Section 6.4.5.1.1.

6.4.2.1.2.2. Effect of the pulsed field on a different part of the torch

To see the effect of the pulsed magnetic field on a different part of the torch, plasma temperature was measured at Z = 1.2 cm. The radial distribution of temperature was obtained only in the steady torch. This is presented in Fig. 6.16. With a pulsed field H_m = 1.25T an average temperature T(a) = 14,200 ^{o}K was obtained.

The plasma in the r.f. inductor is heated by the r.f. field and, therefore, it shows a marked skin effect as shown in Fig. 6.12 (a). But the part of the plasma away from the r.f. inductor would receive heat only from this hot region through thermal conduction. As heat is conducted along the axis it is continuously lost on the outer surface of the plasma to the cool atmosphere, producing a peak in the temperature distribution at the

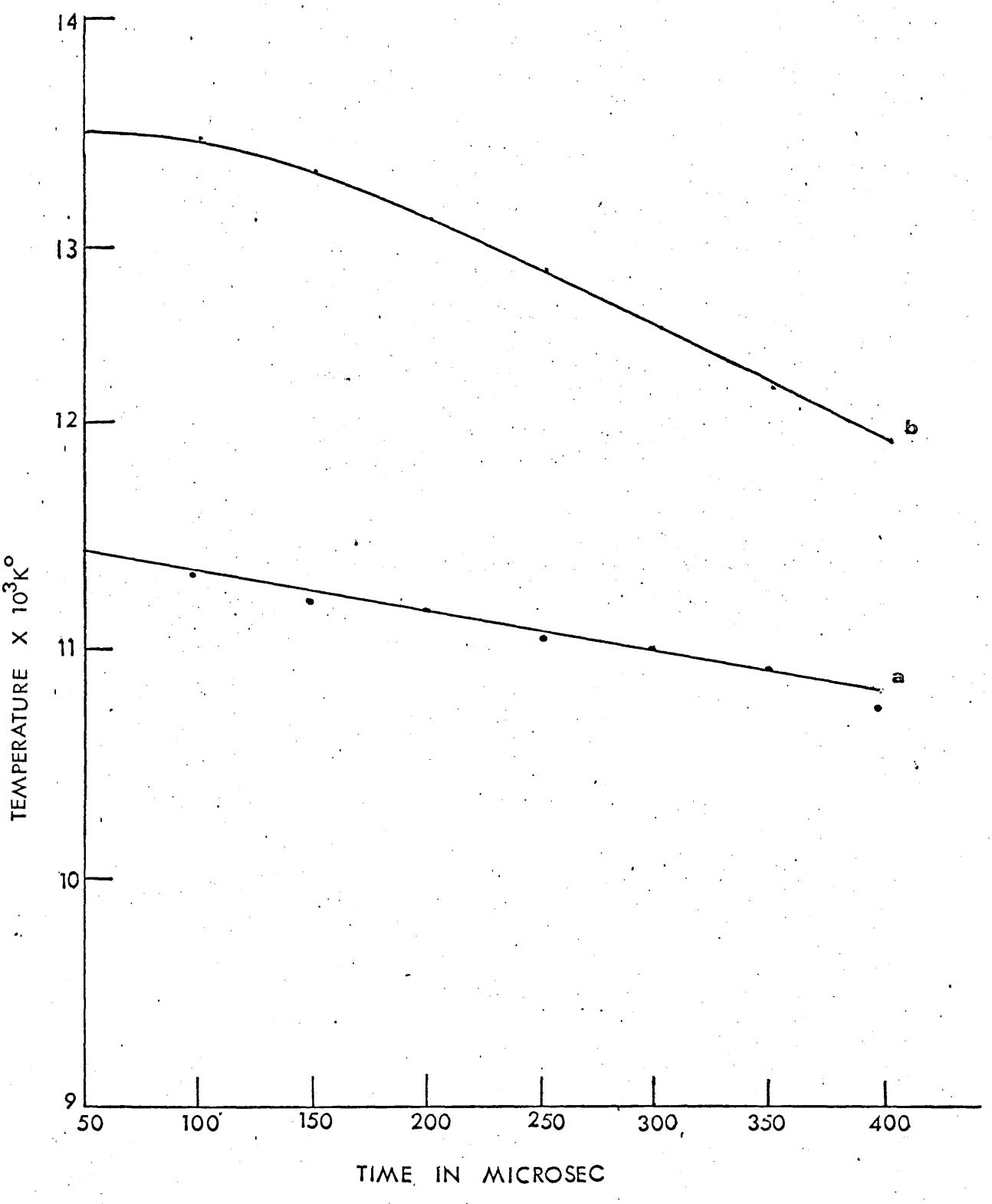

Fig.6.15 Variation of plasma temperature with time, after the application of a 1.25T pulsed magnetic field. The temperature was measured at 0.3 cm above the top of the r.f. hetix (a) at the discharge axis (b) 0.7 cm from the axis.

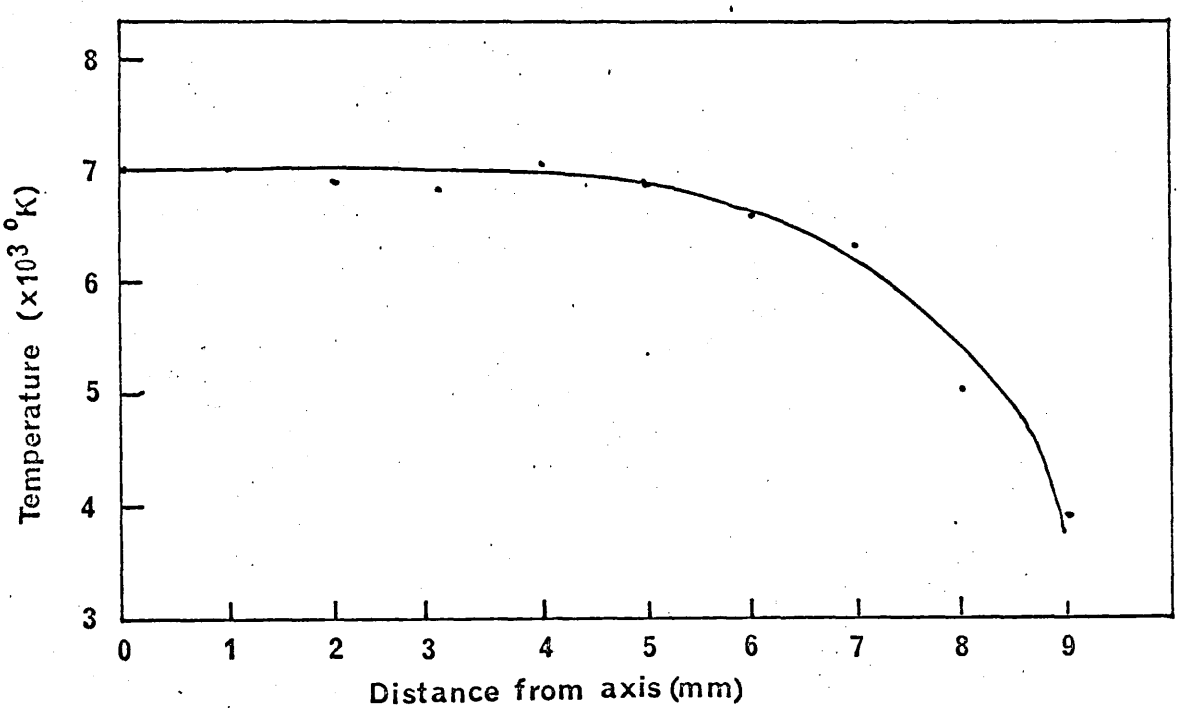

Fig. 6.16 Distribution of temperature in a steady 13.0 kW torch at 1.2 cm above the r.f. inductor.

axis. Such a distribution of temperature was actually observed by Hughes and Wooding [65]. Near the inductor the r.f. heating of the plasma, with its usual skin effect, also takes place. However, the r.f. heating decreases with the increasing distance from the inductor. At some distance the two effects just balance each other, producing a uniform temperature distribution which is further assisted by a deeper penetration of the r.f. field into the plasma at the lower temperature, existing at this position.

The temperature T(a) at Z = 1.2 cm in the pulsed field is higher than that at Z = 0.3 cm. The former position is nearer to the centre of the theta coil, where the pulsed field is higher, therefore, the plasma attains a higher temperature at that position.

6.4.2.2. Effect of the initial temperature of the steady torch

To see the effect of the initial low temperature on the final temperature attained by the plasma, a 2.0 kW torch, burning in the discharge tube DT-1 was chosen. The maximum temperature in a steady torch was found to be about 7000 ^{o}K, considerably lower than that in a 13.0 kW torch. The measured temperature distribution for H_m = 0 and H_m = 1.25T at Z=.3cm are compared in Fig. 6.17. As in a 13.0 kW torch, both distributions show off-axis peaks. The cold region suggested by the temperature distribution in the steady torch is also visible in the end on photograph of the torch shown in Fig. 6.18 where it is seen as a darker spot in the centre. The torch was quite small, in this case, as shown in Fig. 6.19.

The off-axis peak temperature (7000 ^{o}K) in the steady torch is significantly higher than the axial temperature of 4000 ^{o}K. The observed drop of the temperature cannot be explained on the usual assumption of radiation losses, often made in the theoretical [77,81] work on the induction plasma torches. The only possible mechanisms to remove heat from the axial region are (i) heat conduction along the axis which must be small because of the low thermal conductivity of Ar (ii) mass motion of the heated gas

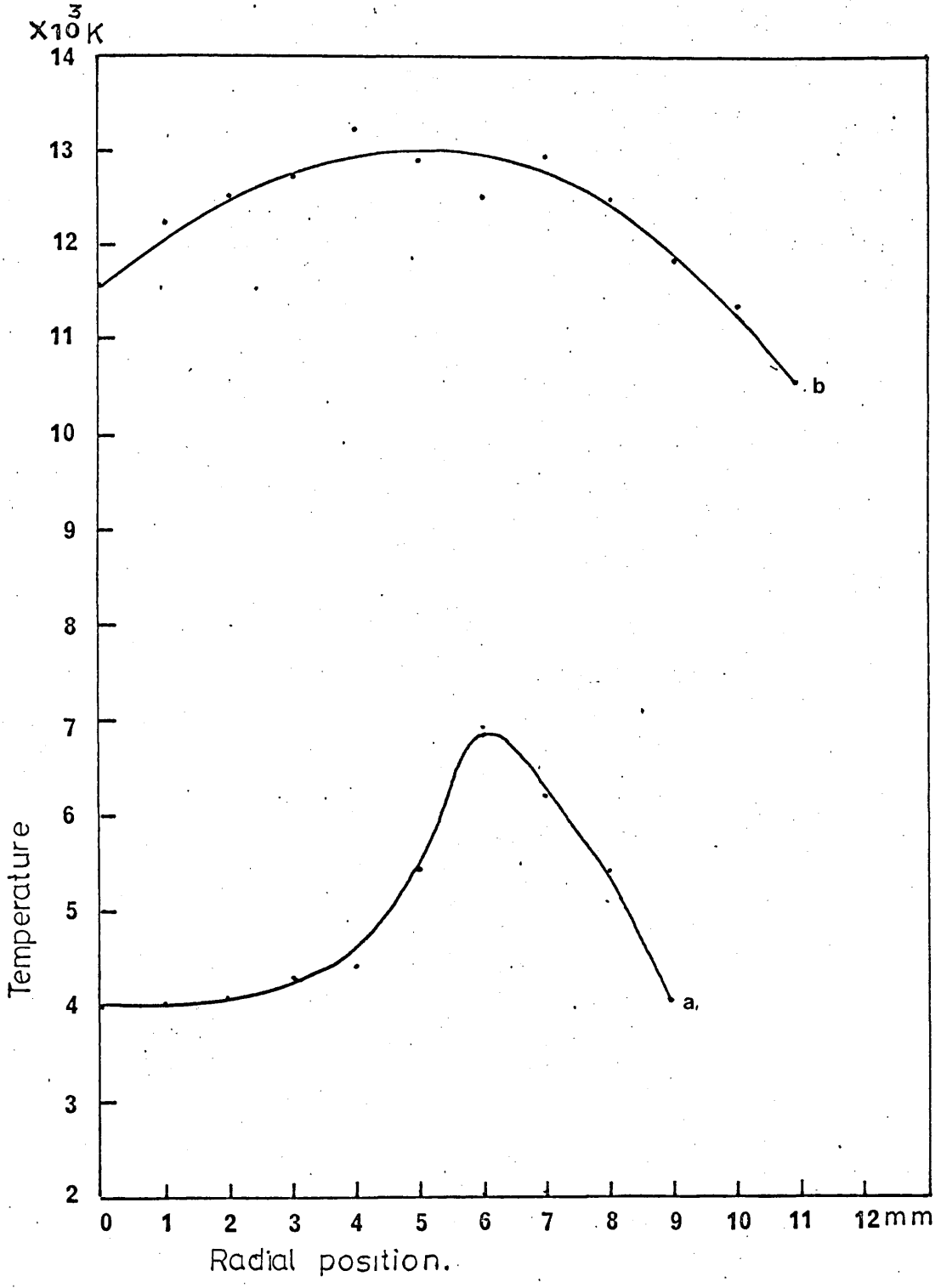

Fig. 6.17 Steady and peak temperature distributions in a 2.0 kW plasma torch at Z = 0.3 cm (a) No pulsed magnetic field (b) When the pulsed magnetic field is at maximum value of 1.25 T.

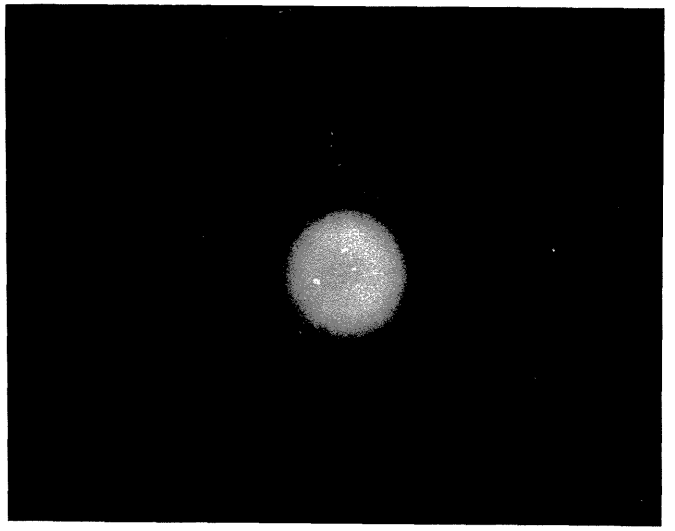

Fig.6.18 End-on photograph of a 2.0 KW torch showing a less luminous cold region in the middle.

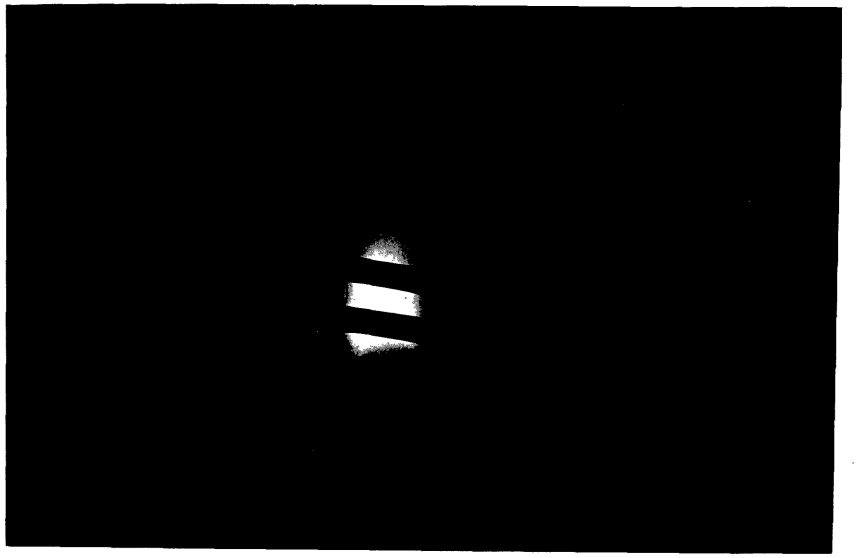

Fig.6.19 Side photograph of a 2.0 KW torch confined to the upper part of r.f inductor.

away from the central region of the plasma, which seems to be the dominant factor in heat removal from the axial region.

The maximum values of the off axis and the axial temperature after the application of a pulsed field H_m = 1.25T, are nearly equal to the corresponding values obtained with the 13.0 kW torch, described in Section 6.4.2.1.2.1. This shows that the maximum temperature is not much affected by the initial history of the plasma i.e. by its temperature and electron density etc. However, because of a smaller volume of the plasma under the present conditions, only a small amount of energy would go into it from the pulsed field. The off-axis peak in the temperature distribution is less pronounced in this case because of the greater penetration of the pulsed magnetic field into the plasma during the initial stages when the plasma temperature ($\simeq$ 7000 ^{o}K) and the electrical conductivity $\sigma \simeq 10^{3}$ (ohm-m)$^{-1}$ are still small. It is in this respect that the initial conditions of the plasma have influence on its heating. As regards the off-axis peaks in the temperature distributions, similar explanation applies here as given for a 13.0 kW torch in Section 6.4.2.1.2.1.

6.4.2.3. Effect of the plasma size

The effect of the low temperature of the steady torch and with it the effect of a small size of the plasma was investigated in the last article. In this article the affect of the large size and particularly the effect of the large diameter of the plasma on the maximum temperature reached by the plasma in a pulsed magnetic field will be studied. For this purpose a 11.6 kW torch, burning in the discharge tube DT-2, at an argon flow rate of 11.3 l/m was chosen.

As mentioned before in Section 5.2.6. the upper part of the discharge was unstable. Temperature measurements were, therefore, made between the lowest two turns of the r.f. inductor, where the plasma was stable. Only the average temperature T(a) along a plasma diameter was measured. A

temperature T(a) = 8500 ^{o}K was obtained for the steady torch.

Pulsed magnetic fields of intensities H_m = 1.08T and H_m = 1.25T were applied to the discharge and their effect on the plasma temperature investigated. In both cases the plasma collapsed and the torch was finally extinguished. Only 425.9, 426.6 and 425.9 nm lines of ArI were used to measure the temperature.

With H_m = 1.08T, a maximum temperature of 15600 ^{o}K was obtained. The variation of temperature is related to the variation of intensity of the spectral line 425.9 nm, which is presented in Fig. 6.20. The typical standard deviation in this case is 12 at the maximum intneisty of 65 a.u. The variations of temperature and spectral line-intensity will be further discussed in Section 6.4.5.2.

With H_m = 1.25T a maximum temperature of 19000 ^{o}K was obtained by the relative line intensity method. An estimate of the plasma temperature can also be made from the time-variation of 425.9 nm spectral line, which is shown in Fig. 6.21. The two peaks in the intensity versus time oscillogram may be associated with the normal temperature T_{norm} (= 15600 ^{o}K), the first being produced during the plasma heating when the increasing temperature passes through T_{norm} and the second being produced during the plasma cooling when the decreasing temperature passes again through T_{norm} The slight decrease in the second peak is probably due to the small change in the plasma diameter. Assuming the plasma diameter to change linearly with time between the two peaks, its effect on the first maximum and minimum has been taken into account in calibrating the maximum plasma temperature of 19,500 ^{o}K.

The high temperatures obtained in a 11.6 kW torch by the application of pulsed fields, may be attributed to the large instability heating of the plasma and the trapped magnetic field. These points will be further discussed in Section 6.4.5.2.

It is desirable at this stage to review the situation of equilibrium in the short intervals of time involved in the plasma heating. The time for establishment of kinetic equilibrium between electrons and heavy particles

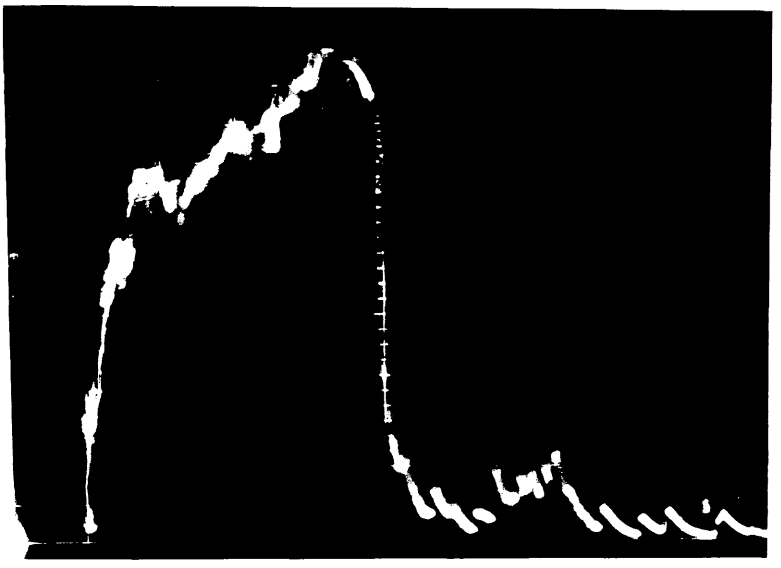

Fig.6.20 Variation of intensity of 425.9 n.m. spectral line on applying a pulsed magnetic field Hm = 1.08T to a 11.6 K.W torch

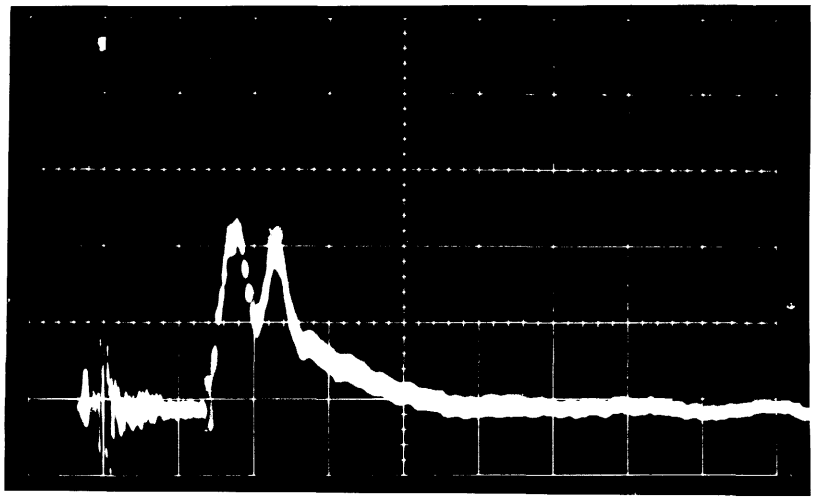

Fig.6.21 Variation of intensity of 425.9 n.m. spectral line on applying a pulsed magnetic field Hm = 1.25 to a 11.o K.W torch

calculated with the aid of Eq.(2.17) is found to be 0.4 micro-secs at 13000 K obtained with a field H_m = 1.25T applied to a 13.0 kW torch. The corresponding time at 19000 ^oK obtained with H_m = 1.25T applied to a 11.6 kW torch is 5.7 nano-sec. Other cases fall between these limits. The time 'τ_i' for distribution of energy over discrete terms of heavy particles has been calculated with the aid of Eq.(2.18) and found to be , respectively, 0.9 and 0.08 micro-secs for the two limiting cases described above. All these characteristic times are much shorter than the time of measurement of the plasma temperature, ( ) 5 micro-secs). The accuracy of temperature measurements, as regards equilibrium, is thus established.

6.4.3. The electron density and the electric conductivity of the plasma

Assuming the plasma to be in thermal equilibrium, electron density 'n_e' and the electrical conductivity σ of the plasma were computed by the methods described in Sections 2.6 and 2.10 respectively. In a 13.0 kW torch the radial distributions of electron density n_e for H_m = 0 and 1.25T, at Z = 0.3 cm, are presented in Fig. 6.22. The radial distributions of σ under the same conditions are presented in Fig. 6.23. These distributions of n_e and σ were obtained from the temperature distributions presented in Fig. 6.12. The distributions of n_e and σ in the steadily running torch at Z = 1.2 cm are shown in Fig. 6.24 for the temperature distribution shown in Fig. 6.16. Both n_e and σ rose to 1.54 x 10^{17} cm^{-3} and 71.4 $(ohm\text{-}cm)^{-1}$ respectively as the plasma temperature rose to 14200K on applying a pulsed field H_m = 1.25T.

Radial distributions of n_e and σ in a 2.0 kW torch for H_m = 0 and H_m = 1.25T at Z = 0.3 cm for the temperature distribution presented in Fig. 6.17 are shown in Figs. 6.25 and 6.26 respectively.

For the 11.6 kW torch, burning in the discharge tube DT-2, n_e equals 5-61 x 10^{17} cm^{-3}, at 15600 ^oK (i.e. H_m = 1.08T) and 6-72 x 10^{17} cm^{-3} at

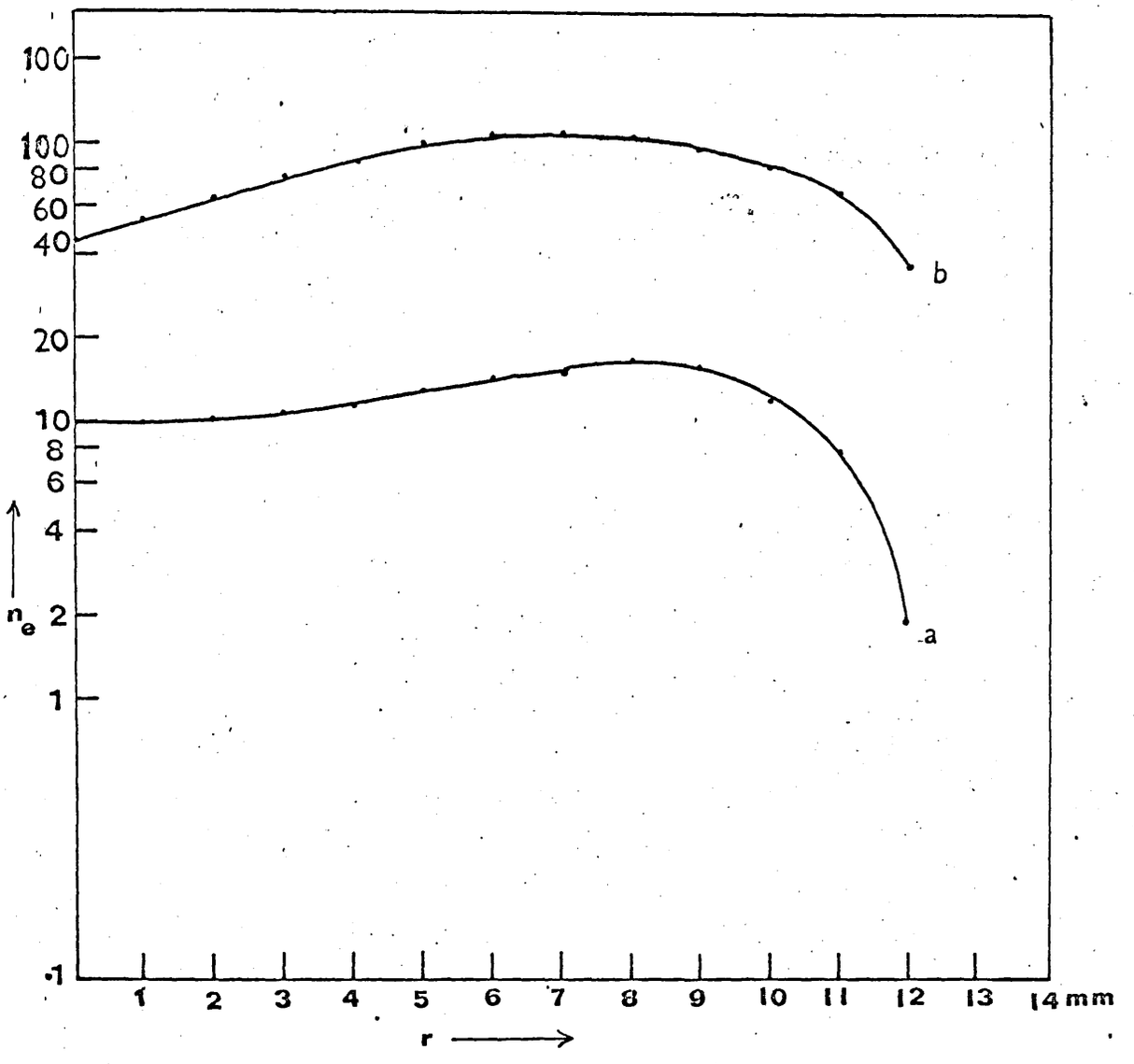

Fig.6.22 Steady and peak electron-density distribution in the plasma for a 13.0 K.W torch at Z = 0.3 cm. (a) No magnetic field. (b) When the pulsed magnetic field is at peak value 1.25T.

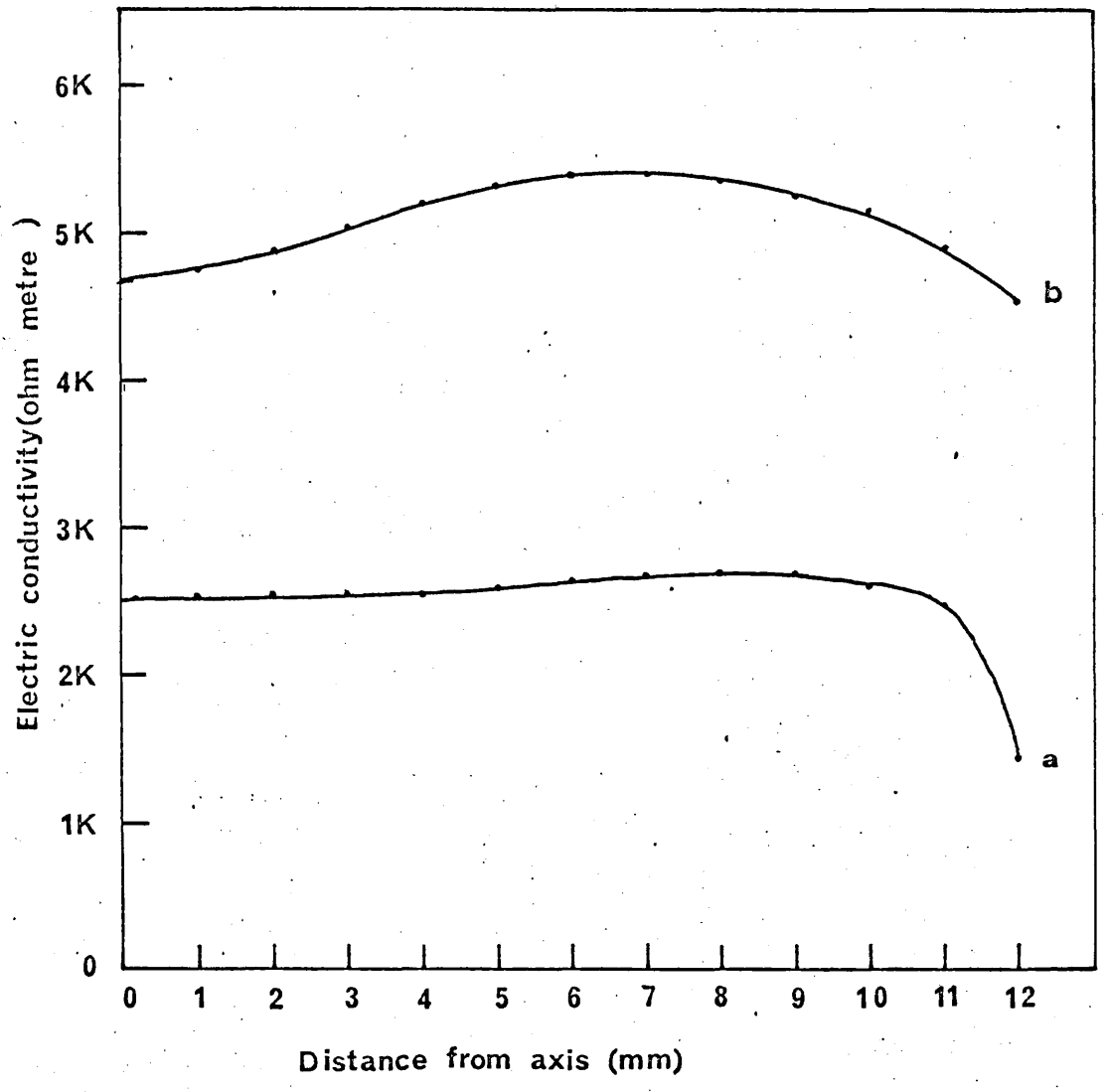

Fig. 6.23 Steady and peak electric conductivity distributions in the plasma at Z = 0.3 cm (a) No pulsed magnetic field (b) When the pulsed magnetic field is at the peak value of 1.25 T.

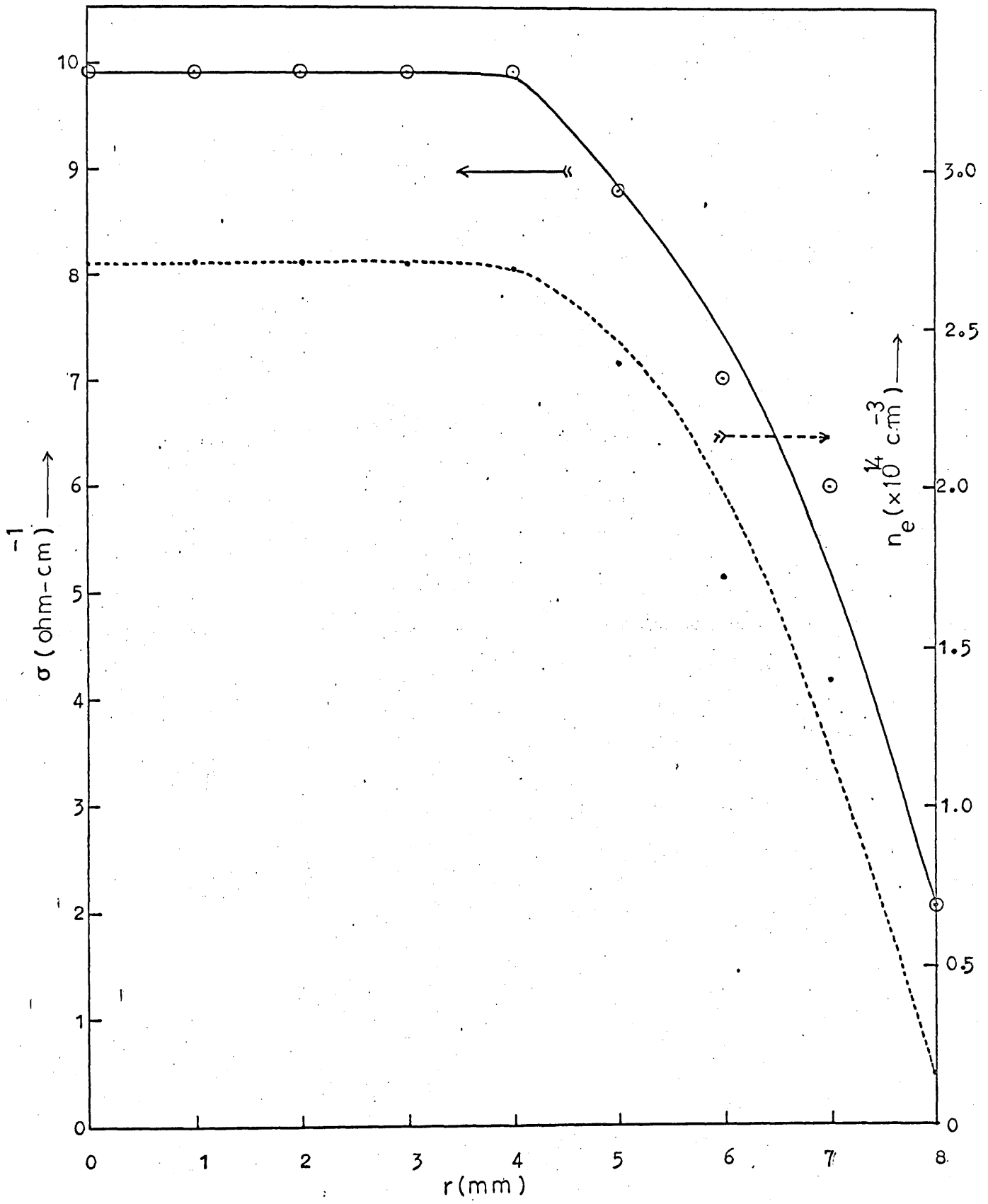

Fig.6.24 Radial distributions of n_e and σ at Z = 1.2 cm in a steadily running 13.0 KW torch.

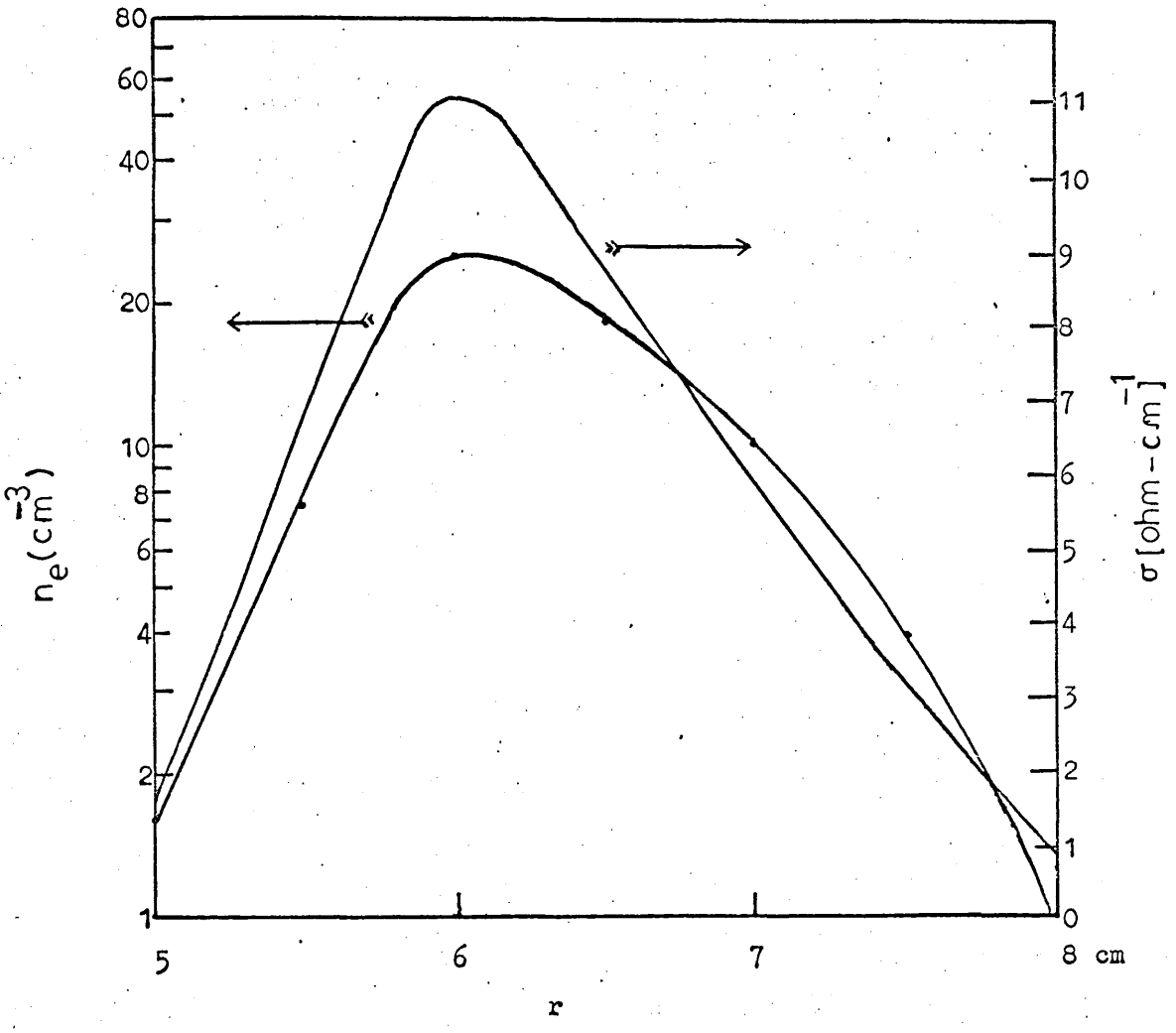

Fig. 6.25 Radial distributions of n_e and σ in a steadily burning 2.0 KW torch at Z=0.3 cm.

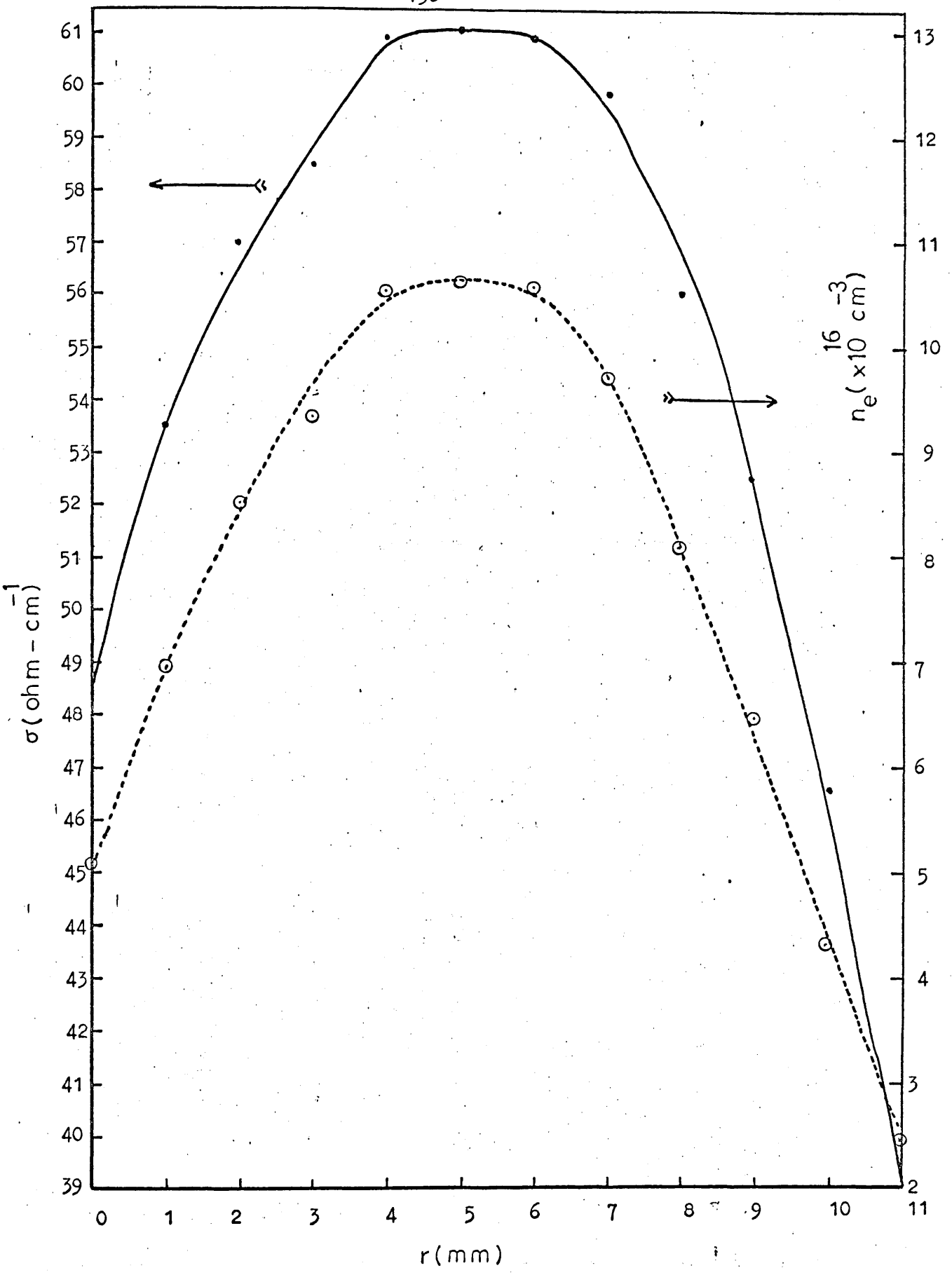

Fig. 6.26 Radial distributions of peak values of n_e and σ at Z = 0.3 cm in a 2.0 KW torch when a pulsed field H_m = 1.25 T is applied.

19500 ^{o}K (i.e. H_m = 1.25T). Corresponding values for σ are 81.5 and 96 40 (ohm-m)$^{-1}$. At a temperature of 8500 ^{o}K in the steady torch n_e and σ are equal to 3.36 x 10^{15} cm^{-3} and 20 20(ohm-m)$^{-1}$ respectively.

6.4.4 Plasma instabilities

Occasionally instabilities have been observed in a steadily running torch. These instabilities will be described in Section 7.2. However, the application of a pulsed field sometimes, excites them if they are not already present in the steady torch as shown in Fig. 6.27. On rarer occasions the magnetic pulse excites oscillations of a frequency which changes with time as shown in Fig. 6.28. In addition to these instabilities which persist even after the magnetic pulse, large amplitude oscillations of a higher frequency are always excited during the first 10 micro-seconds of the pulse as can be seen in the above mentioned figures.

Gross changes in plasma size and shape were also produced by a pulsed magnetic field in certain cases. However, no such change of any appreciable size was revealed by the high speed photographs taken with the image converter camera when a pulsed field H_m = 1.25T was applied to a 13.0 kW torch.

High speed photographs of a 11.6 kW torch in a pulsed field H_m = 1.08T were taken with the Fastex high speed cine camera. They are presented in Fig. 6.29. On applying the pulsed field, the plasma is seen to move upward through the theta coil with a decreasing density of the plasma blob below the r.f. inductor. Finally, the discharge is reduced to a filamentary structure which continues to move upward leaving a small portion behind. The faint filament grows larger and moves up. The whole cycle is repeated a few times before the filamentary structure completely disappears in about 65 milli-seconds.

High speed photographs of a 11.6 kW torch, on applying a pulsed field H_m = 1.25T, were obtained with the aid of an image converter camera and a

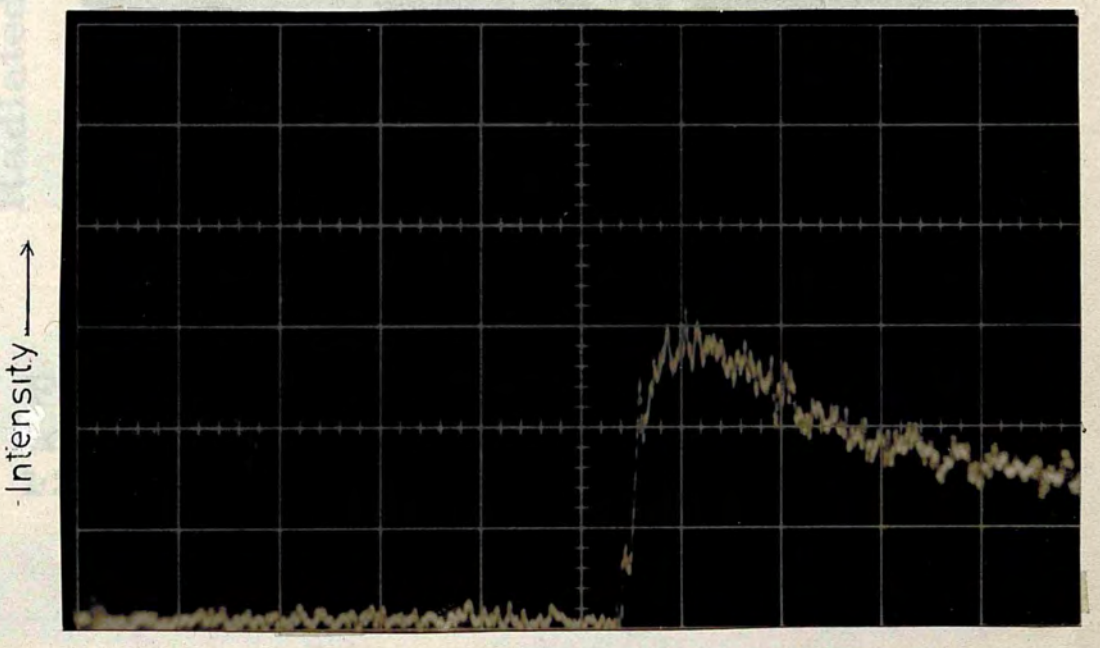

Time (1 cm = 20 micro seconds.)

Fig. 6.27 Excitation of oscillations in a 13.0 KW torch by a pulsed magnetic field (detected in radiation)

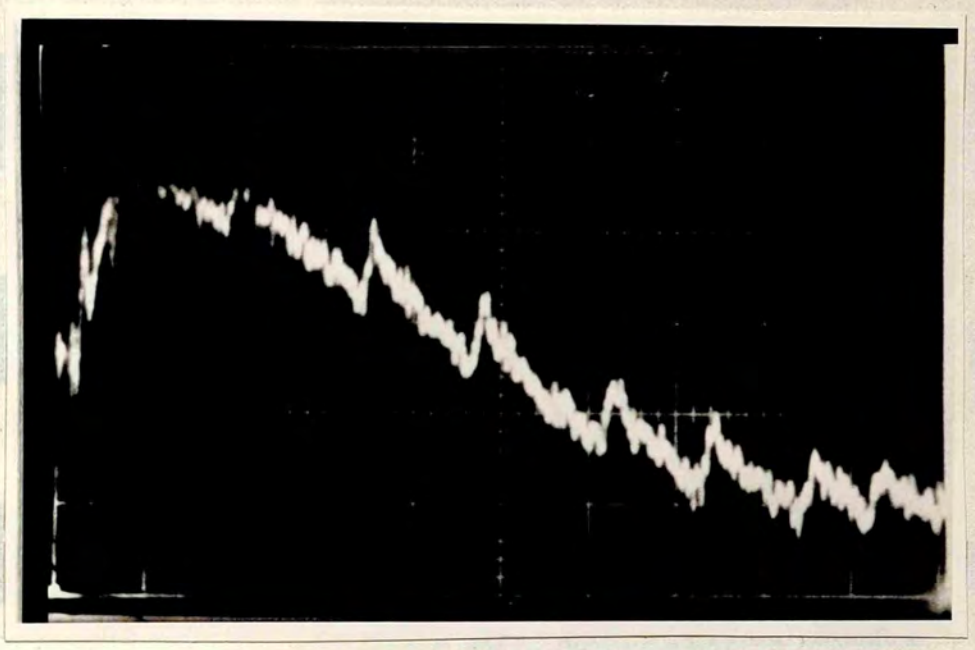

Fig6.28 Oscillogram showing the plasma instabilities after the application of a 1·25 T pulsed magnetic field.

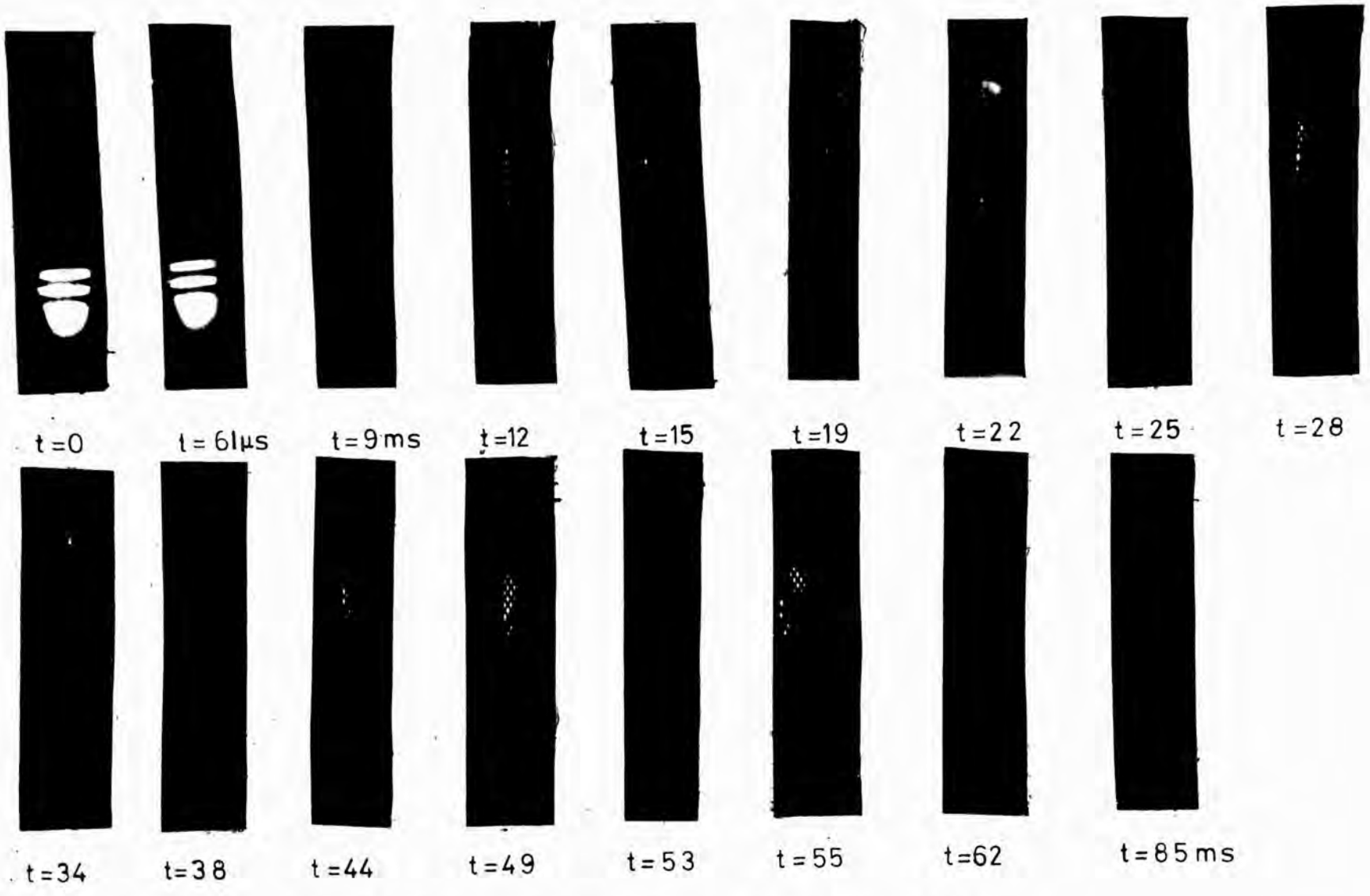

Fig 6.29 Collapse of a 11·6 KW torch in pulsed magnetic field H_m=1·08 T

high speed cine camera. Photographs in Fig. 6.30, tracing the development of the pinch during the first 10 micro-seconds after the theta coil was fired, were taken with the image converter camera with an exposure time of 100 nano-seconds. In these photographs the less luminous tail of the torch is not visible. The pulsed field is seen to have its maximum effect on the large plasma blob which is squashed in about 5.25 micro-seconds. This was followed by the breakdown of the discharge into a filamentary structure which underwent similar changes as described above.

6.4.5. Interpretation and discussion of the results

6.4.5.1. The 13.0 kW torch

Before examining other effects of a pulsed magnetic field on the plasma torch, it is desirable to examine, in some detail, the off axis peak temperature produced by the pulsed magnetic field, particularly in view of the low frequency (370 kHz) of the pulsed field. This is done in the next Section.

6.4.5.1.1. The off axis peak temperature

If the off axis peak temperature is produced due to the skin effect, the skin depth δ should be smaller than the plasma radius. δ, calculated with the aid of the usual formula

$$\delta = (\pi \mu \sigma \nu)^{-\frac{1}{2}} \qquad (6.1)$$

at T = 13000 ^{o}K i.e. $\sigma = 6.01 \times 10^{3}$ (ohm-m)$^{-1}$ for an oscillating magnetic field of time period 5.4 micro-seconds is 1.5 cm which is comparable with the maximum plasma radius R = 1.7 cm. In addition the plasma does not attain a temperature of 13000 ^{o}K right at the start of the magnetic pulse. In fact the rise time of the intensity of the spectral line 425.9 nm and

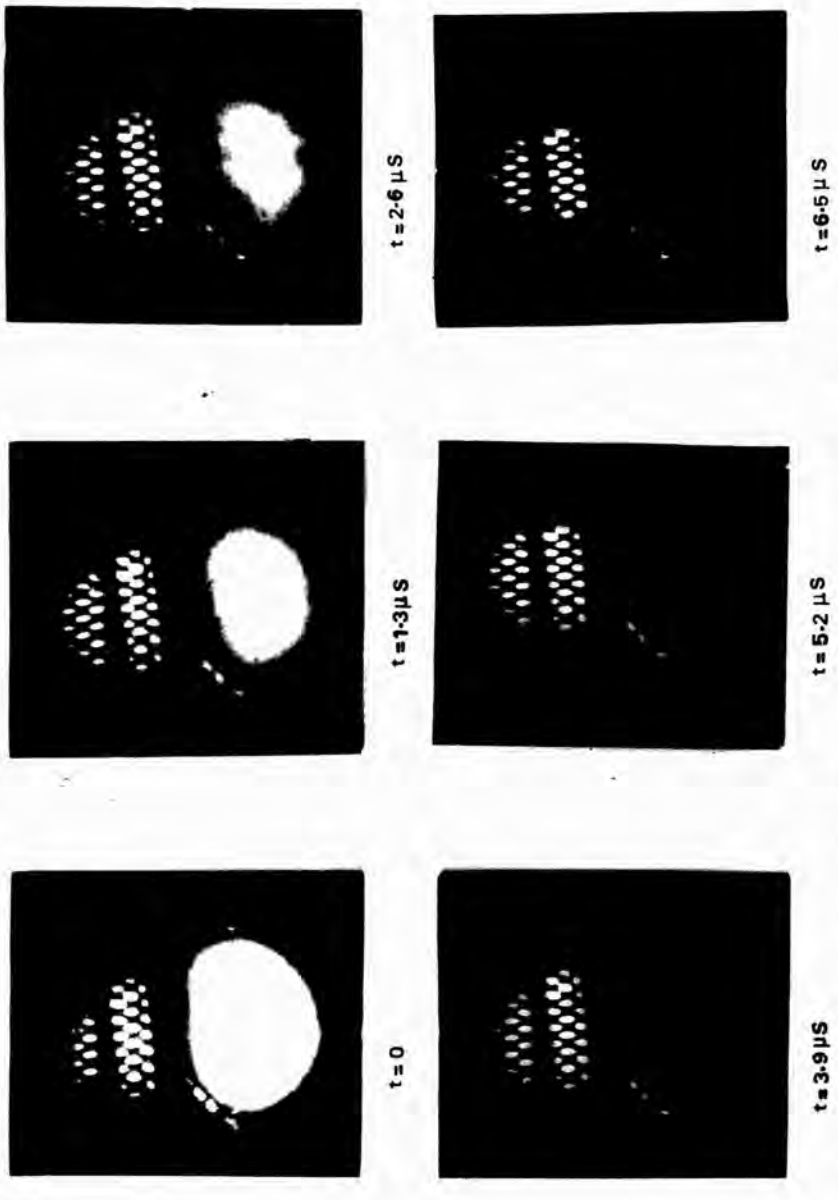

Fig 6.30 Collapse of an 11·6kW torch in a pulsed magnetic field $H_m = 1·25$ T

therefore the rise time of the temperature varies from shot to shot between 3 and 9 micro-seconds after the initiation of the magnetic pulse. On the basis of a large number of observations the average rise time has been found to be approximately 5.5 micro-seconds, almost the same as the time period of the oscillating magnetic field. Assuming the temperature to rise linearly during this period, the plasma is found to attain a temperature of 11,230 ^{o}K at the end of the first half cycle. Using the average value of σ (= 4,000 (ohm-m)$^{-1}$) in Eq. (6.1), one gets δ = 1.85 cm, which is greater than the plasma radius. This would result in a uniform heating of the plasma across its cross-section. However, Artizimovich [95] has shown that in a time 't', a rising magnetic field would penetrate into the plasma to a depth

$$\delta' = \sqrt{\frac{c^2 t}{4\pi\sigma}} \cdot \sqrt{\frac{kT\,(n_e + n_i)}{H_m^2/8\pi}} \quad \text{(cgs-units)} \qquad (6.2)$$

As the field becomes zero after every half cycle, the above formula should be applied to each half cycle separately to calculate field penetration. At the same time the change in 'n_e' due to a change in 'T' should also be taken into account. Reading the value of H_m from Fig. 6.4. at the centre of the r.f. inductor i.e. 4.0 cm below the centre of the theta coil and using the average value of H_m^2 over a half cycle in Eq. 6.2 one gets δ' = 0.44 cm.

This result is consistant with the negligibly small pulsed field measured at the discharge axis by the inductive probe as described in Section 6.3.

It will be shown in Section 6.4.5.1.3. that the major contribution to plasma heating is made by the first two half cycles due to their large amplitudes, when the skin depth is still small. Also, owing to the low thermal conductivity and short heating time, the axial region receives very little heat from the outer hotter regions. These two effects produce an

off axis peak in the radial temperature distribution of Fig. 6.12. However, the plasma at the axis is heated during the remaining half cycles when the skin depth becomes nearly equal to the plasma radius due to a drop in the magnetic pressure. The plasma is also heated by instabilities, produced by the pulsed field, which finally dissipate their energy as heat. As they mostly lie in the outer region of the *plasma they contribute to the formation of an off axis peak in the temperature distribution.

6.4.5.1.2. Determination of the radiative recombination coefficient

At the discharge axis $1/n_e$ is found to vary linearly with time, after the magnetic pulse, as shown in Fig. 6.31. This gives a value of 3.4×10^{-14} cm^{-3}/sec for the recombination coefficient at an average electron density 4.10^{16} cm^{-3} and an average temperature 11100 ^{o}K. For a high pressure plasma, Mitin and Pryadkin (74) deduced the theoretical formula:

$$\alpha = \frac{8.6 \times 10^{-23}}{e\, X_i \sqrt{T}} \quad cm^3/sec \qquad (6.3)$$

This formula, at the mean temperature of 11100 ^{o}K existing in the plasma, leads to a value of $\alpha_{Th} = 3.2 \times 10^{-14}$ cm^3/sec. They obtained an experimental value of 2.7×10^{-14} cm^3/sec for Ar at an atmospheric pressure, while Aleksandrov et al (96) obtained a value of 4×10^{-11} cm^3/sec at an electron density 2×10^{16} cm^{-3} and a temperature of 9000 ^{o}K. The agreement between the experimental value of this work and the theoretical value is good.

* This was revealed during the scanning of the discharge for spectroscopic measurements.

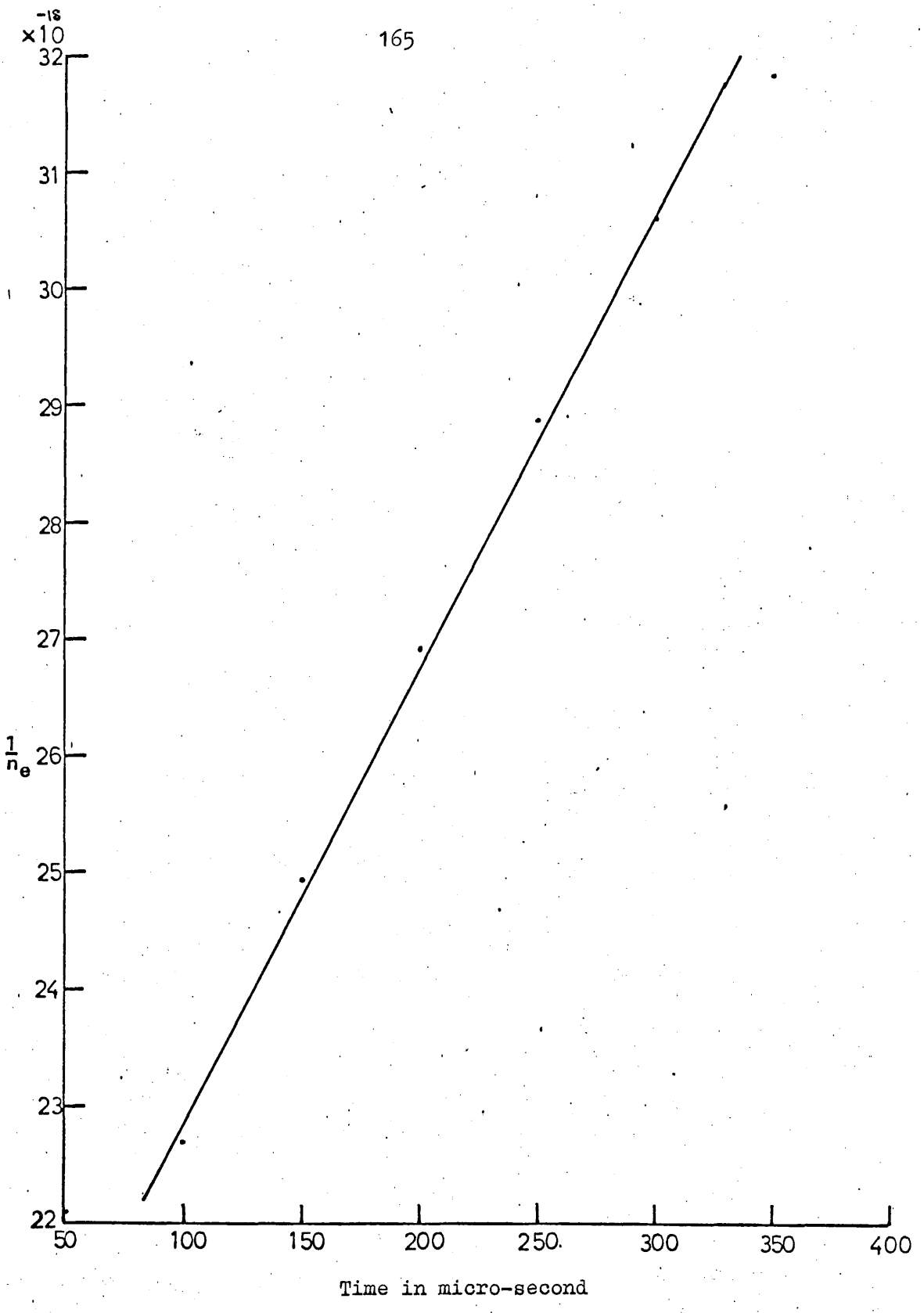

Fig.6.31 Variation of reciprocal of electron density with time, after the application of 12.5 K.G. pulsed magnetic field at Z = 0.3 cm and r = o.

6.4.5.1.3. Energy balance

In order to calculate the energy content and the heat dissipation the plasma may be approximated, as in Appendix II to a uniform cylinder of radius 1.23 cm and height 6.6 cm. If the energy of various excited states is neglected the energy content of the plasma at a temperature T ^{o}K is given by

$$\zeta_t = (1 + \alpha)\gamma RT + 1.6\times10^{-19} N_N \alpha X_i \qquad (6.4)$$

where R is in J mol^{-1} K^{-1} and X_i is in eV. During the short heating time (few micro-seconds) the plasma volume may be assumed to be constant and therefore γ may be taken equal to 3/2. The degree of ionisation α of the plasma is computed from Saha equation. The first term on the right hand side of Eq.(6.4) indicates the amount of heat ζ_h spent in increasing the plasma temperature and the second gives the energy ζ_i in producing ionisation. Variations of ζ_t, ζ_h and ζ_i with H_m and H_m^2 have been plotted in Figures 6.32 and 6.33. Energy content of the plasma at an average temperature 12500 ^{o}K (H_m = 1.25T) calculated with the aid of the above equation is 17.0 J. Out of this energy about 38 % is spent in increasing the plasma temperature, the rest of it is spent in ionising the gas.

The energy dissipated by an oscillating magnetic field in a plasma due to Joule heating, is given by (105)

$$\zeta = \frac{\hat{H}R\, i_2}{\sqrt{2}.4\pi\sigma\delta} \cdot \frac{\mathrm{ber}(\sqrt{2}R/\delta)\,\mathrm{ber}'(\sqrt{2}R/\delta) + \mathrm{bei}(\sqrt{2}R/\delta)\,\mathrm{bei}'(\sqrt{2}R/\delta)}{[\,\mathrm{ber}(\sqrt{2}R/\delta)\,]^2 + [\,\mathrm{bei}(\sqrt{2}R/\delta)\,]^2} \qquad (6.5)$$

As the pulsed field H_m varies along the discharge length, an average value of H_m^2 over the length of the plasma cylinder, for H_m = 1.25T, is used. Because the penetration depth of the magnetic field changes during the first few micro-seconds (see Section 6.4.5.1.1.) the energy dissipation is calculated for each half cycle separately and presented in table 6.3 along

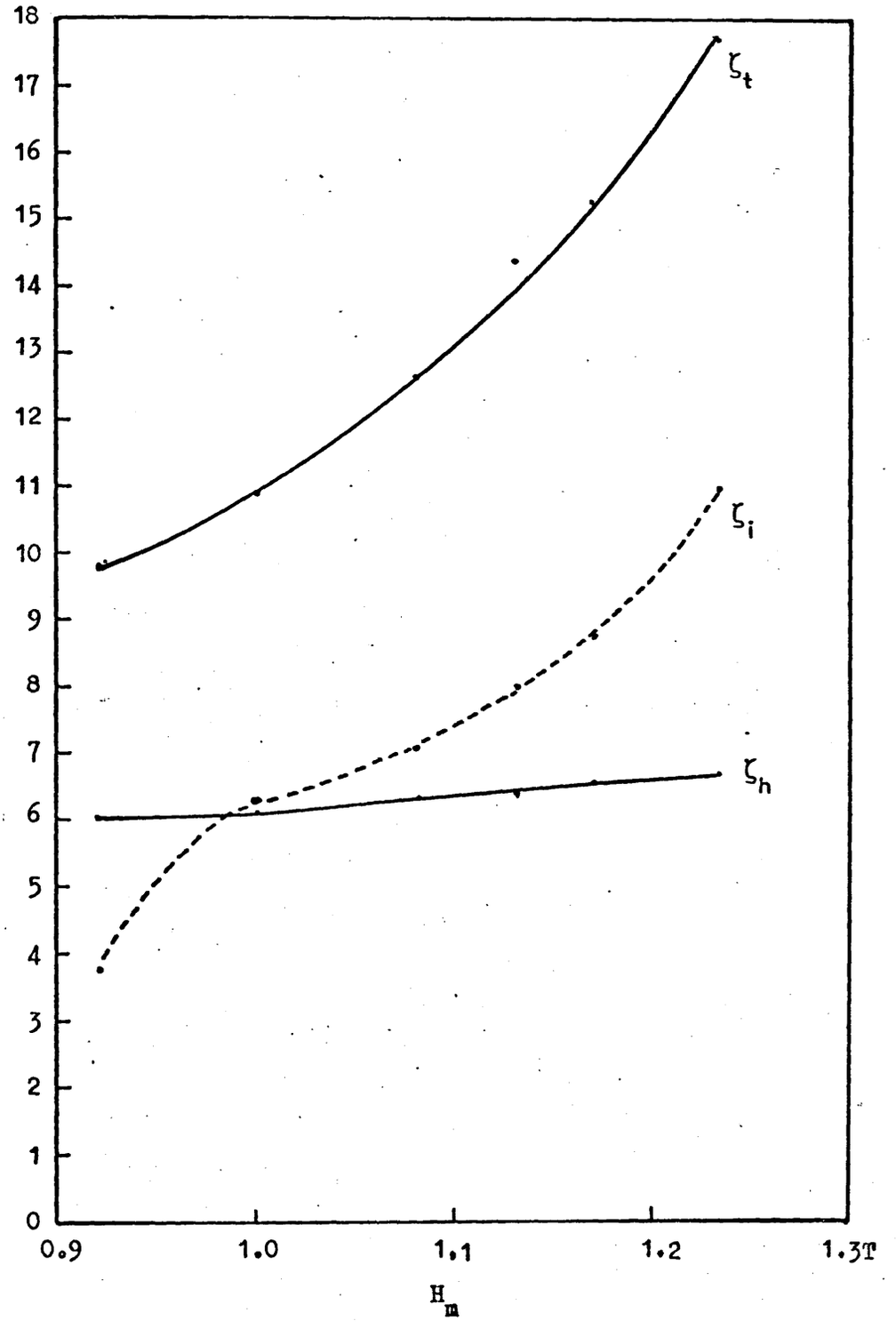

Fig. 6.32 Variation of ζ_h, ζ_i and ζ_t with H_m.

For $H_m = 0$ $\zeta_h = \zeta_{ho} = 5.38J$
$\zeta_i = \zeta_{io} = 1.34J$
$\zeta_{to} = \zeta_{to} = 6.72J$

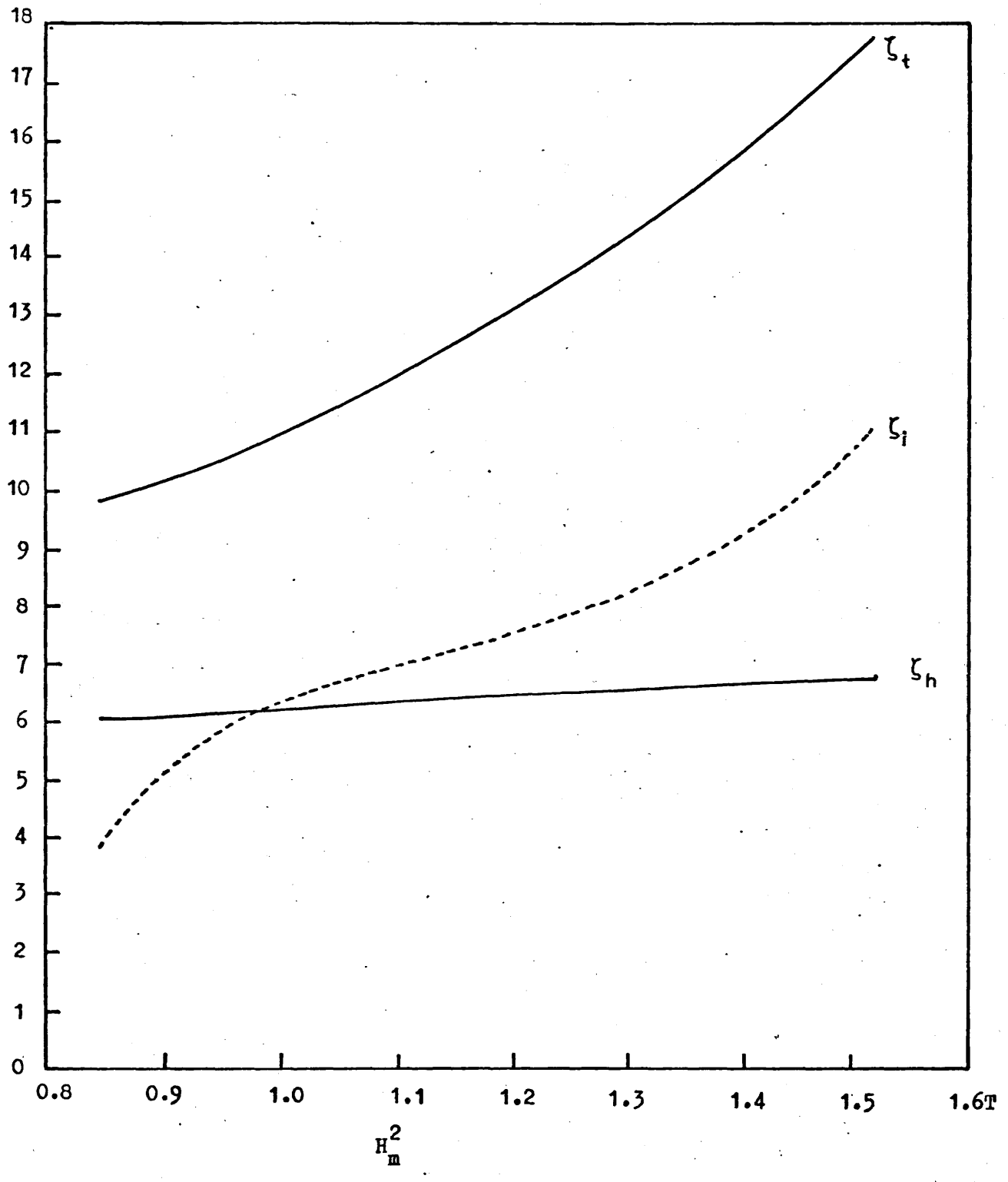

Fig. 6.33 Variation of ζ_h, ζ_i and ζ_t with H_m^2.

with δ and $\langle H^2 \rangle$ values. In all 9.03 J are dissipated. This figure is of the same order of magnitude as the maximum energy change ($\zeta_t - \zeta_{to}$) of 11·0J. In view of various approximations made in these calculations the agreement between the energy dissipated in and that received by the plasma is satisfactory.†

TABLE 6.3

Half cycle	$\langle H^2 \rangle$ tesla^2	δ'	ζ
1st	76.31×10^{-2}	0.0044 m	6·34 J
2nd	24.92×10^{-2}	0.00722 m	2·43 J
3rd	6.23×10^{-2}	0.0156 m	0·21 J
4th	1.56×10^{-2}	0.0156 m	0·05 J
			Total ζ_T = 9·03 J

6.4.5.1.4. Contributions of radiation and radial heat conduction to power loss

It is informative to examine the relative part played by the radiation and the radial heat conduction in the power loss from the plasma at various temperatures and various values of H_m. The radiative losses have already been computed in Section 6.4.1. In order to calculate the radial heat conduction loss the plasma boundary was fixed at r = 1.1 cm, a position beyond which the temperature had a rapid fall , (see Fig. 6.12), and the discharge tube was assumed at 500 ^{o}K so that the space in between scanned the temperature difference between the plasma and the discharge tube. The temperature at r = 1.1 cm was read from Fig. 6.12 and a mean value of the thermal conductivity was used to calculate the radial conduction loss. The radiation and the radial thermal conduction losses are plotted against

† The difference between ζ_{to} and ζ_T may be attributed to plasma-heating by instabilities.

'T' in Fig. 6.34 and against H_m in Fig. 6.35. In both cases the major contribution to the power loss is made by the radiation. However the radiation loss at $H_m = 1{\cdot}25T$ does not exceed 1·0J during the magnetic pulse.

6.4.5.2. Effect of the large plasma size on temperature and stability

The experimental results obtained on applying pulsed magnetic fields H_m = 1.08T and H_m = 1.25 on a 11.6 kW torch and described in Section 6.4.2.3. may now be discussed. At H_m = 1.08T the intensity of the 425.9 nm spectral line in Fig. 6.20. increases rapidly during the first 14 micro-secs i.e. during the magnetic pulse and then increases rather slowly to a maximum after which it falls rapidly to a very low value at t = 80 micro-sec, probably due to the movement of the plasma away from the position of observation. After the initial fall of intensity the plasma, which moves in and out of the observation position, shows strong but irregular oscillations. Assuming the discharge radius to remain constant and normalising the maximum intensity to the maximum temperature of 15,600 ^{o}K a temperature of 13900 ^{o}K i.e. 89% of the maximum temperature is obtained in t = 14 micro-sec. The later increase in the plasma temperature is due to the energy dissipation by instabilities.

With H_m = 1.25T the change in the 425.9 nm line intensity was rapid and the maximum temperature attained was considerably higher (19000 ^{o}K). It is interesting to observe in this case as shown by Fig. 6.21 that the time of maximum temperature (the minimum of intensity) coincides almost with the half period of the magnetic field i.e. the time when the induced electric field is maximum, a point that shows the significance of the Joule-heating in raising the plasma temperature.

The enhanced temperature produced in the 11.6 kW torch by a pulsed field H_m = 1.25T may be explained in the following way. Because of the low conductivity (= 20.2 mho/cm) of the discharge at an initial temperature T = 8500 k the pulsed magnetic field diffuses into the plasma where it is trapped due to increased conductivity accompanying the increasing plasma temperature. Fig. 6.6 shows strong trapping of the field in the plasma

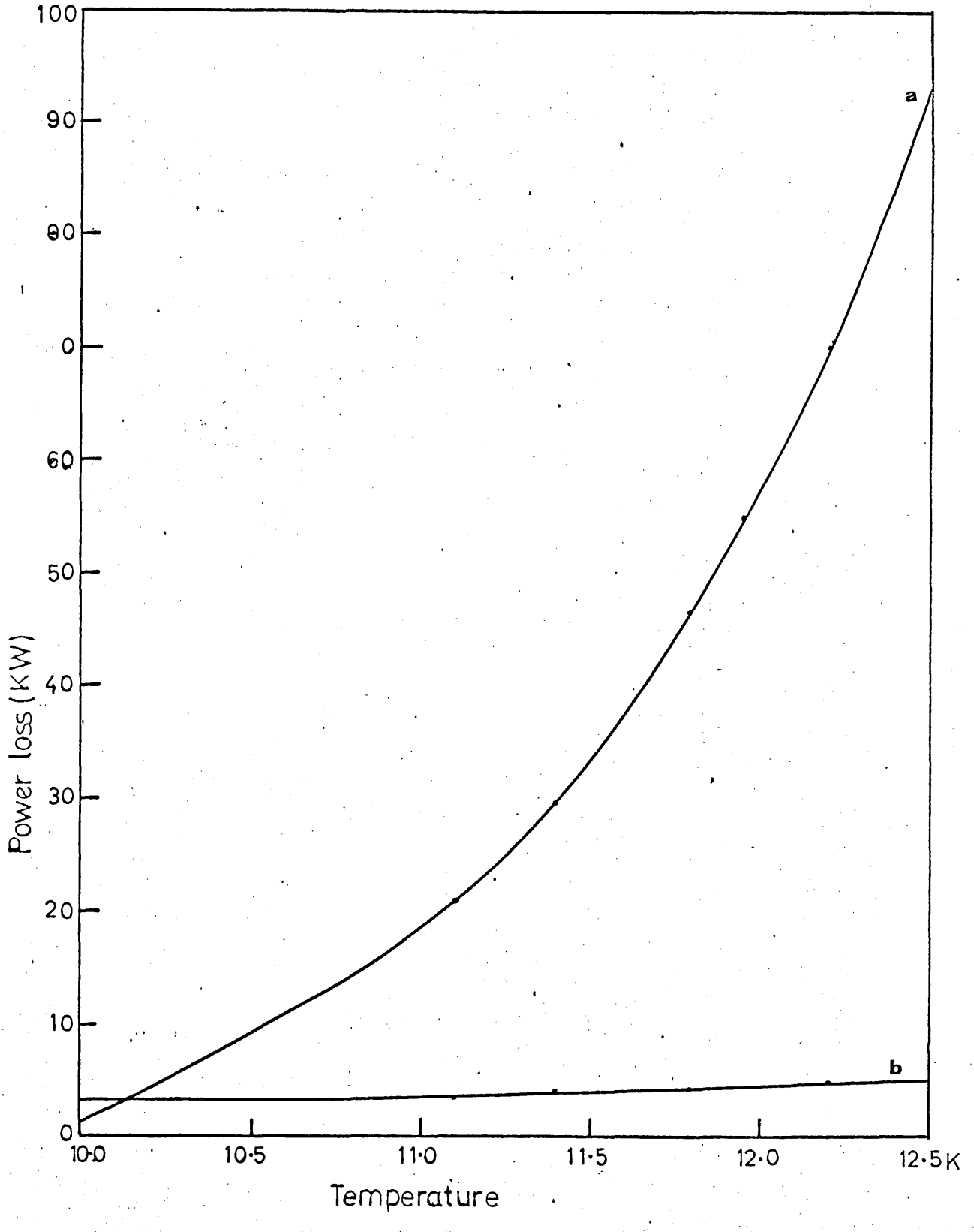

Fig 6.34 Power loss at various plasma temperatures due to (a) radiation (b) radial heat conduction

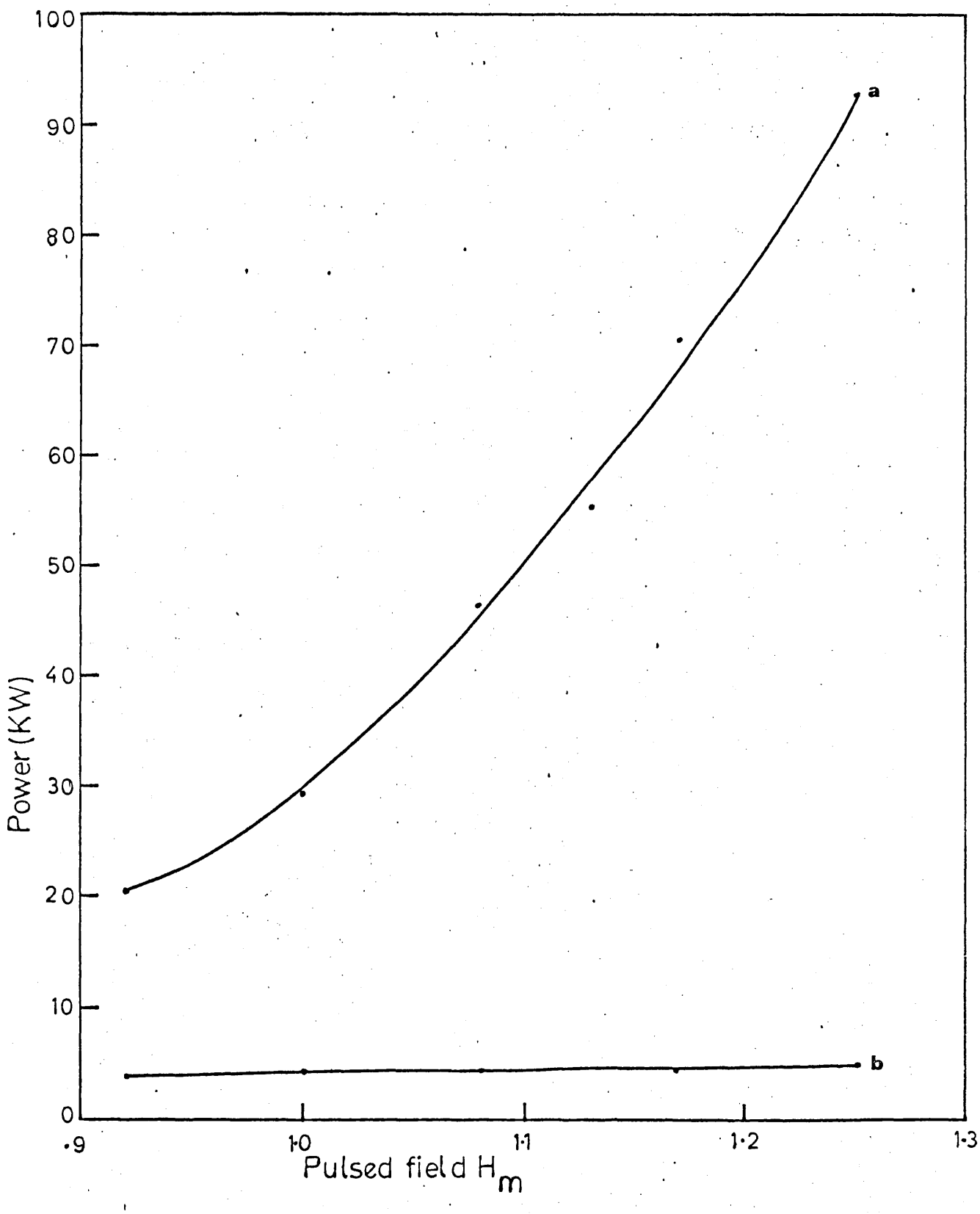

Fig. 6.35 Power loss at various values of Hm due to (a) radiation (b) radial heat conduction.

during the first half cycle. The second half magnetic cycle causes the internal field to form closed [97] loops threading the plasma cylinder, which deforms rapidly to a doughnut with surface currents to maintain the accompanying closed magnetic field. The configuation is equivalent to sausage or m = 0 mode instability. The rate of growth of this instability and the rate at which the ring current supporting the trapped field decreases determine the energy gained by the plasma particles. At a low pressure in a thetatron [97] the accelerated deutrons by this mechanism lead to the production of neutrons. But at a high pressure as in the present case, the directed energy of the particles is dissipated in heating the plasma to a high temperature.

The upward motion of the discharge into the region of higher magnetic fields may now be explained. A higher pressure r.f. induction plasma has been shown to be paramagnetic in the presence of a static magnetic field.[98,99] It was attributed to the partial rectification of the r.f. current circulating in the plasma. In the present case the pulsed magnetic field may be assumed quasi stationary compared to the r.f. field. This explains the paramagnetic behaviour of the 11.6 kW torch. The magnetic moment, which depends on the area enclosed by the rectified circulating current, would be much smaller in 13.0 and 2.0 kW torches because of their comparatively smaller radii. Therefore, these torches would exhibit little paramagnetism.

Alternatively the paramagnetic behaviour of the 11.6 kW torch may be explained thus. Because of the large size of the plasma and its location in a non uniform field region away from the theta coil, which is of short length, the pulsed field has a radial component in the plasma as shown in Fig. 6.36. The azimuthal current induced by the pulsed field interacts with the radial component of the field and produces a $\bar{J}\times\bar{B}$ force which pushes the plasma downward for an increasing field ($t < t_o/4$) and upward for a decreasing field ($t_o/4 < t < t_o/2$). Averaged over a half cycle these forces will cancel out for a constant azimuthal current. However, during the magnetic pulse the temperature of the plasma continuously increases leading to a higher

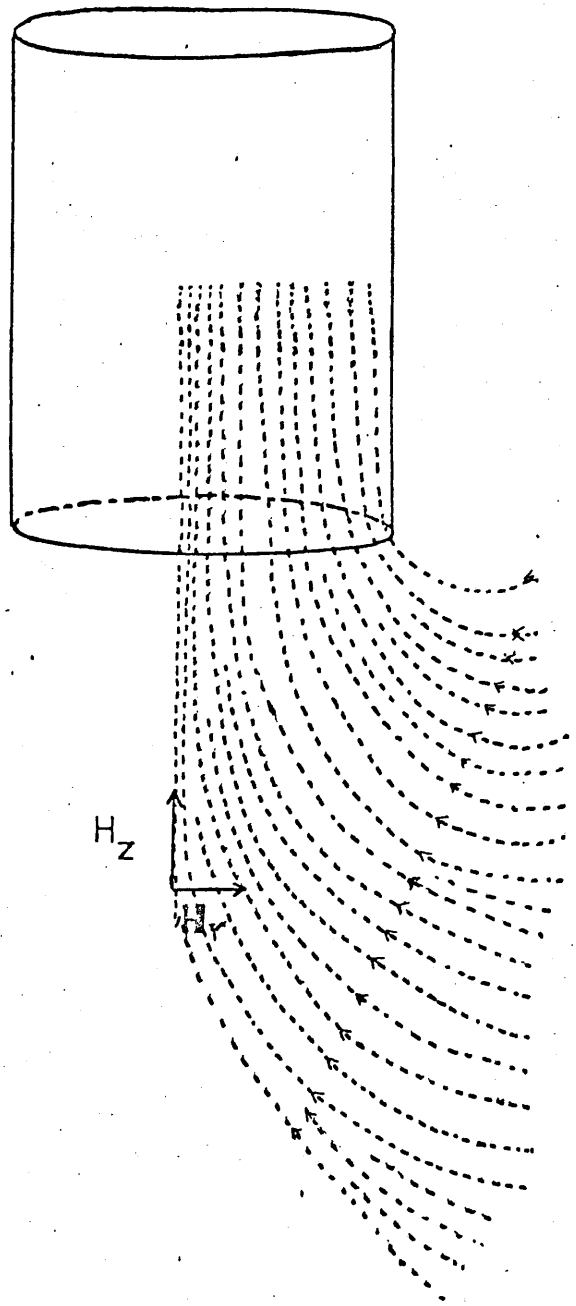

Fig.6.36 Divergent magnetic lines of force from theta coil, producing axial and radial components of the pulsed magnetic field(field partly shown)

conductivity and, therefore, to a higher azimuthal current during the second quarter cycle. A net upward force thus results. This reasoning equally applies to other half cycles. The effective force on the plasma is the sum of all the forces during each half cycle.

The upward motion of the plasma into the narrow funnel formed by the cold, dense surrounding gas decouples the discharge from the oscillator and finally extinguishes it.

Characteristics of an induction plasma torch in the absence of a pulsed magnetic field will be described in the next chapter.

Chapter 7

STUDY OF AN R.F INDUCTION PLASMA TORCH IN THE ABSENCE OF A PULSED MAGNETIC FIELD

CHAPTER 7

STUDY OF AN r.f. INDUCTION TORCH IN THE ABSENCE OF A PULSED MAGNETIC FIELD

7.1. Introduction

In this chapter a study of various properties and associated processes in an induction plasma torch, in the absence of a pulsed magnetic field , has been made. Plasma instabilities are described first. These are followed by an investigation of the torch with a magnetic probe. In the end the mechanism of gas break down at torch initiation is described.

7.2. Instabilities in an induction plasma torch

Various instabilities have been observed in the plasma of a steadily burning induction torch. Their spectrum extends from a few hundred hertz to hundreds of kilo-hertz. These instabilities have been studied in the light intensity and the acoustic noise.

Of particluar interest are the low frequency instabilities which produce the disagreeable acoustic noise. Their spectra, studied at various gas flows and oscillator powers, contain 300 Hz and harmonics, immediately suggesting a relation with the 300 Hz mains ripple in the high voltage supply of the oscillator. A careful filtering of the high voltage supply is thus suggested as a means of suppressing the acoustic noise.

Other instabilities, which were observed only in the light intensity, contained frequencies above 60 kHz.

Before studying the plasma instabilities it is desirable to examine various frequencies modulating the r.f. field. This is done in the next section.

7.2.1, Modulation of the r.f. field

Amplitudes of various frequencies, modulating the r.f. field were measured and the results are presented in Table 7.1. Only 300 Hz and harmonics are seen in the modulation spectrum. Rectification is suggested as a possible source of these harmonics, though some of them may already exist in the 3-phase a.c. supply.

TABLE 7.1. Values of m and α_n

Osc. power	Gas flow	m	α_2	α_3	α_4	α_5	α_6	α_7	α_8	α_9
13.0 kW	7.3l/m	.18	.440	.190	.075	.037	.019	.010	.006	.004
2.3 kW	4.5l/m	.26	.327	.211	.121	.066	.035	.021	.012	.108

Here m is the modulation factor and α_n the ratio of a harmonic to the fundamental.

7.2.2 Low frequency instabilities (300 Hz and harmonics)

The relative amplitudes of various harmonics in the light intensity are plotted on a semi logrithmic scale in Fig. 7.1 when the torch is run at an oscillator power of 13 kW and an argon of 10.5 l/m. The 300 Hz frequency has the highest amplitude of 1700 a.u. (arbitrary units). When the gas flow is decreased from 10.5 l/m to 1.9 l/m at the same oscillator power the amplitude at 300 Hz decreases from 1700 to 800 a.u. i.e. by about one half as shown in Fig. 7.2. Figs 7.3 and 7.4 show the results obtained at argon flows of 10.5 l/m and 1.9 l/m respectively in a 2.3 kW torch. In all the above cases the amplitude of a harmonic decreases with its order.

Frequency spectra of the acoustic noise of a 13.0 kW torch at gas flows of 10.5 l/m and 1.9 l/m are shown in Figs. 7.5 and 7.6 respectively and those of 2.3 kW torch at gas flows of 10.5 l/m and 1.9 l/m in Figs. 7.7

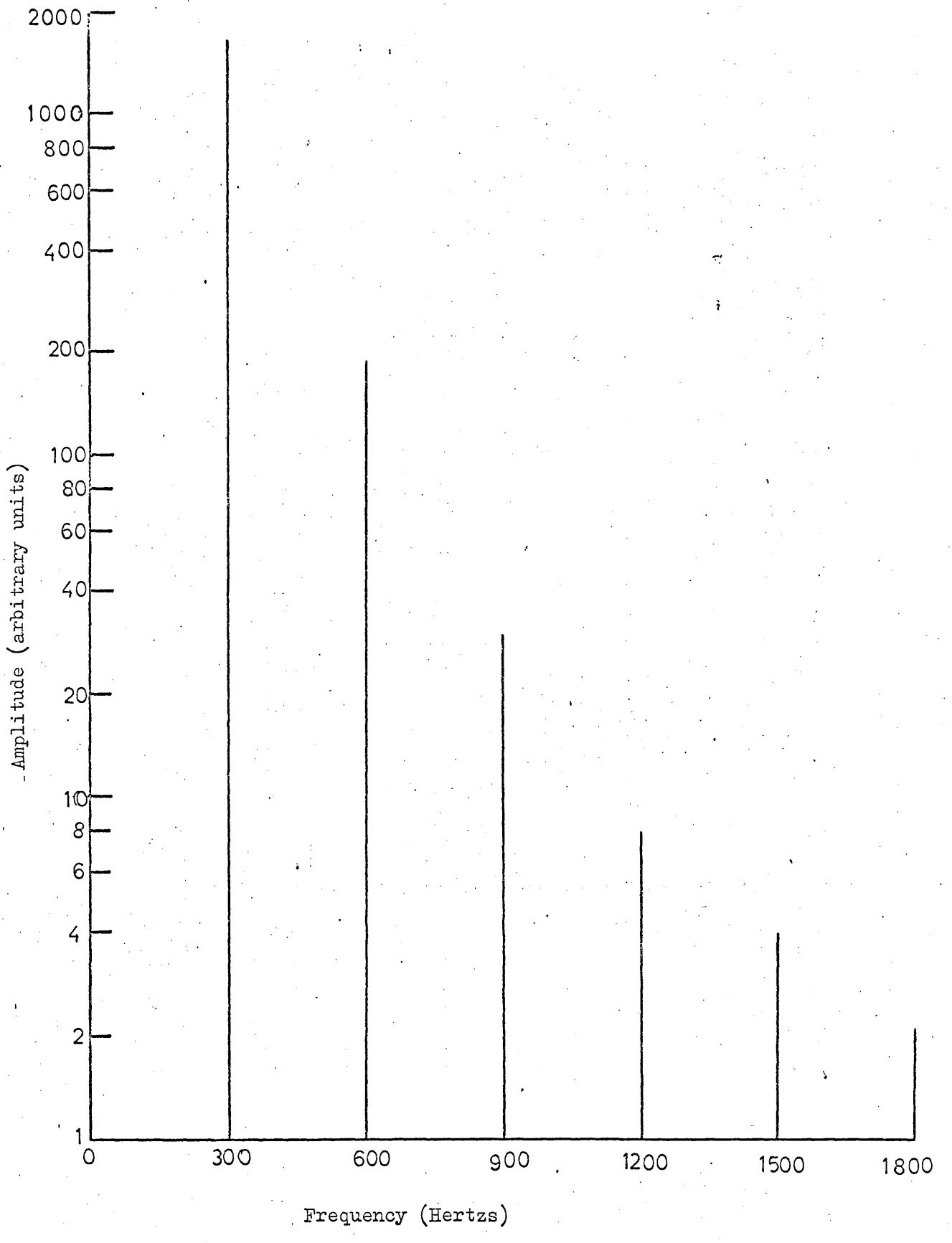

Fig.7.1 Frequency spectrum of light modulation of a 13.0 K.W. torch at an argon flow 10.5 l/m.

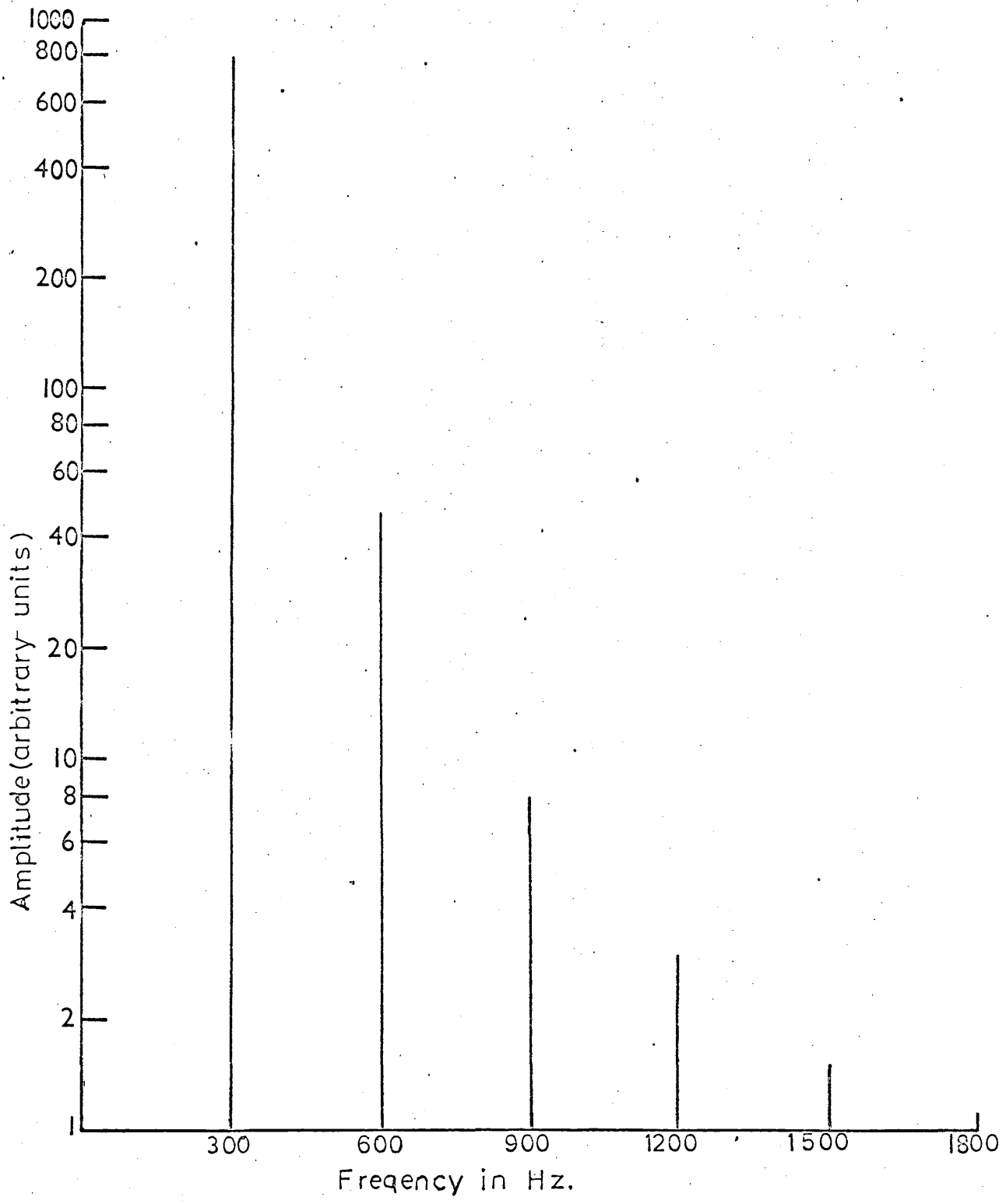

Fig. 7.2 Frequency-spectrum of light modulation of a 13·0KW torch at an argon flow 1.9 l/m.

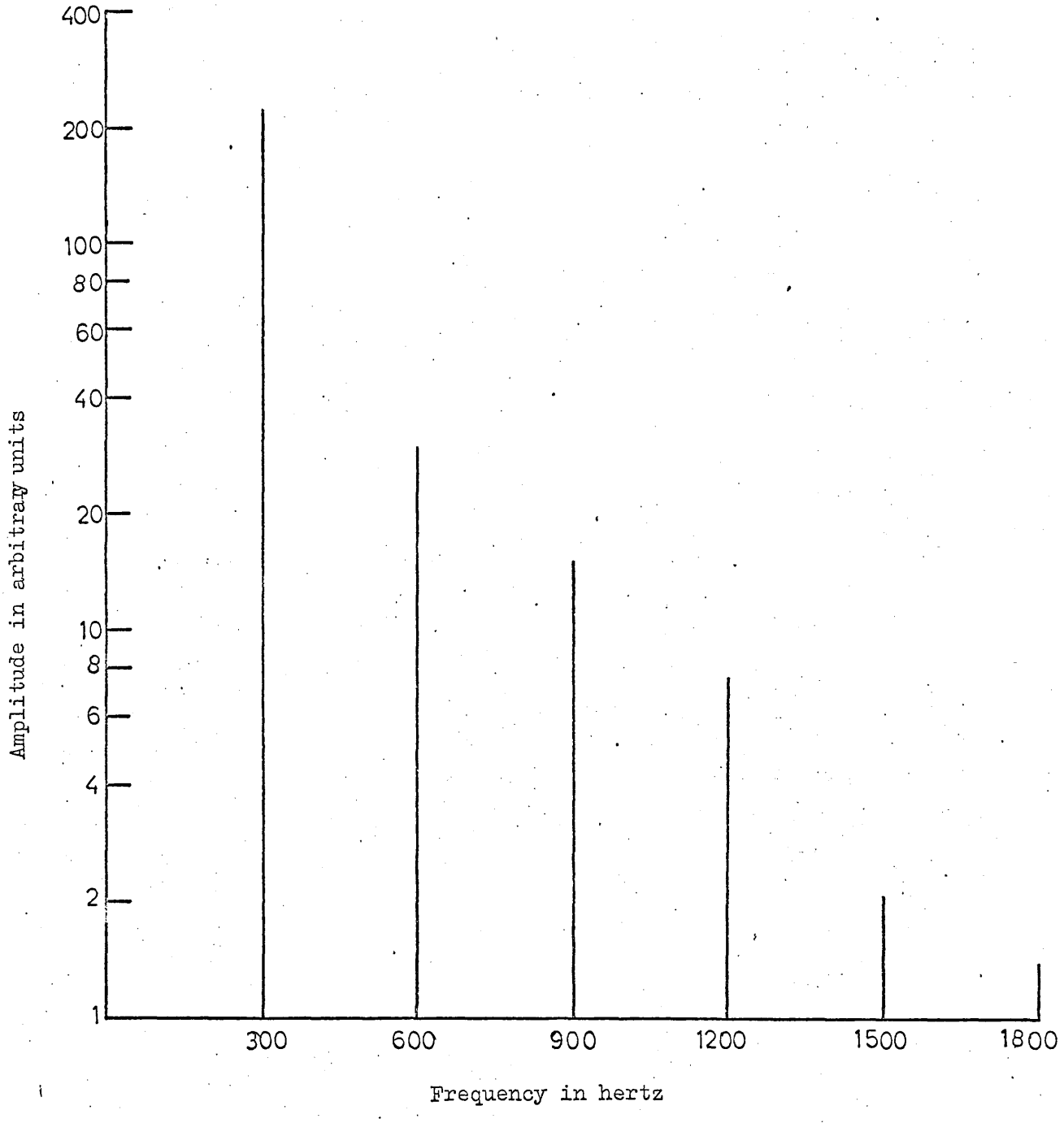

Fig.7.3 Frequency spectrum of light modulation of a 2.3 K.W. torch at an argon flow 10.5 l/m.

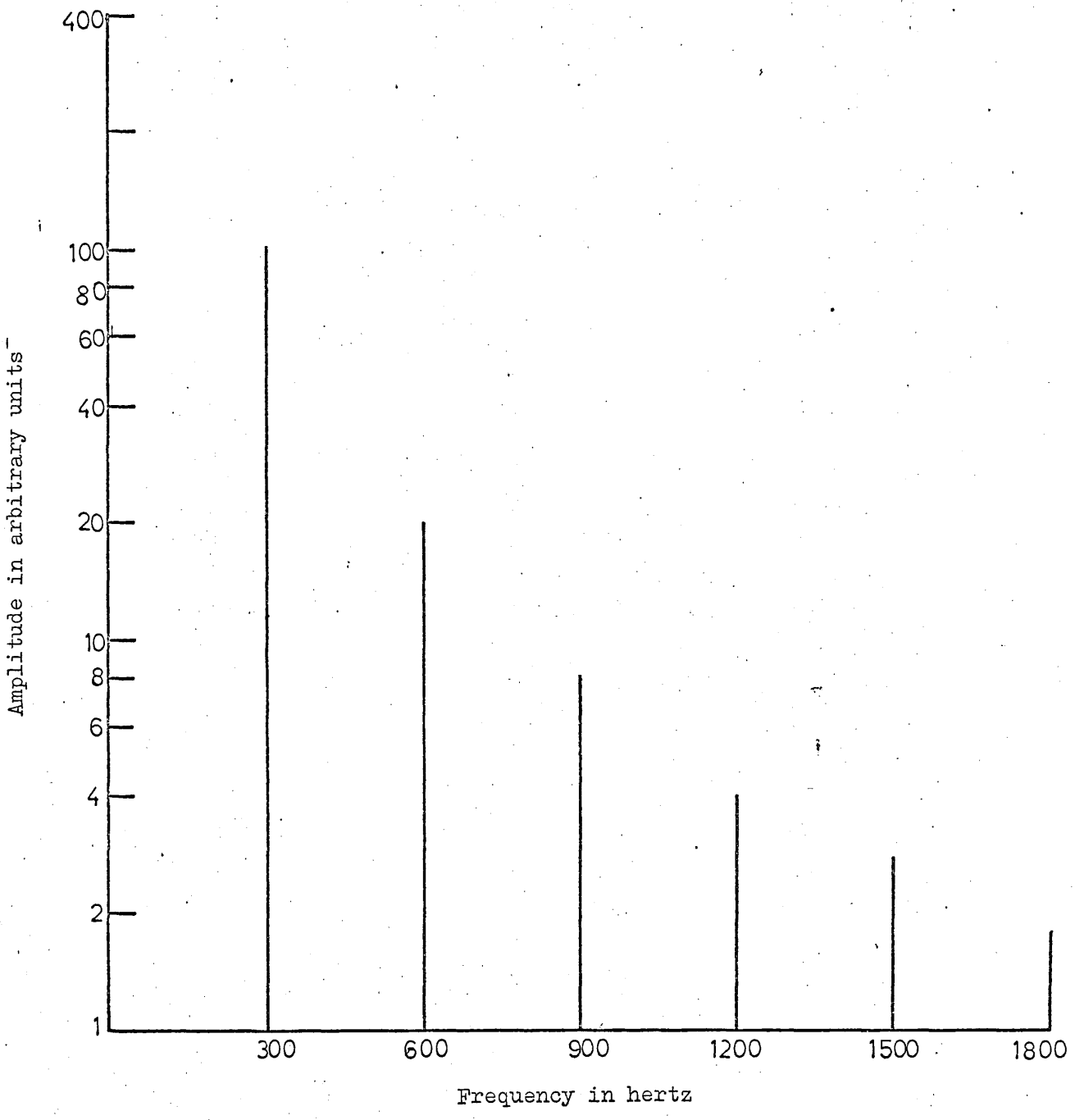

Fig.7.4 Frequency spectrum of light modulation of a 2.3 K.W. torch at an argon flow rate 1.9 l/m.

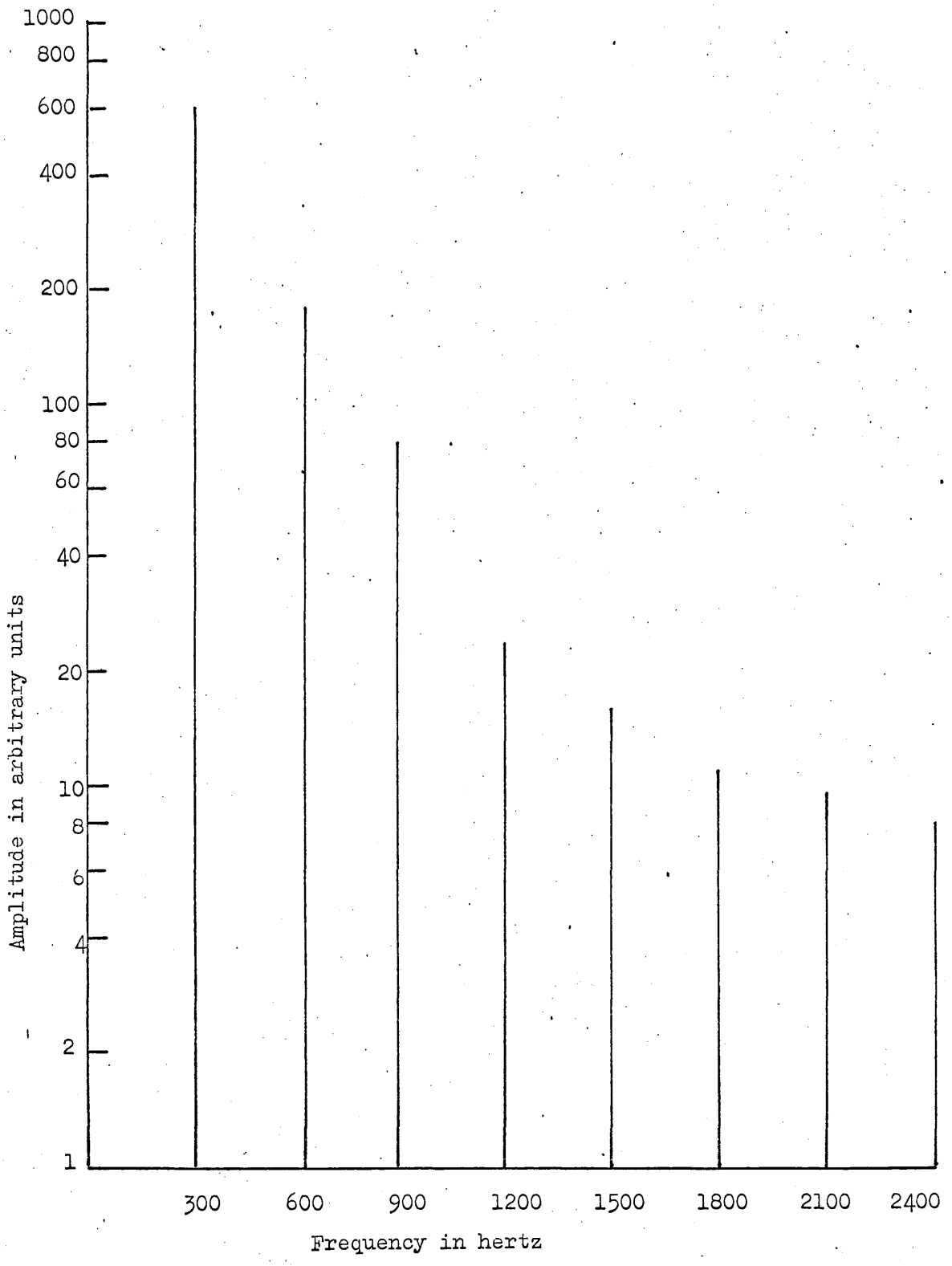

Fig.7.5 Frequency spectrum of the acoustic noise of a 13.0 K.W. torch at an argon flow rate 10.5l/m.

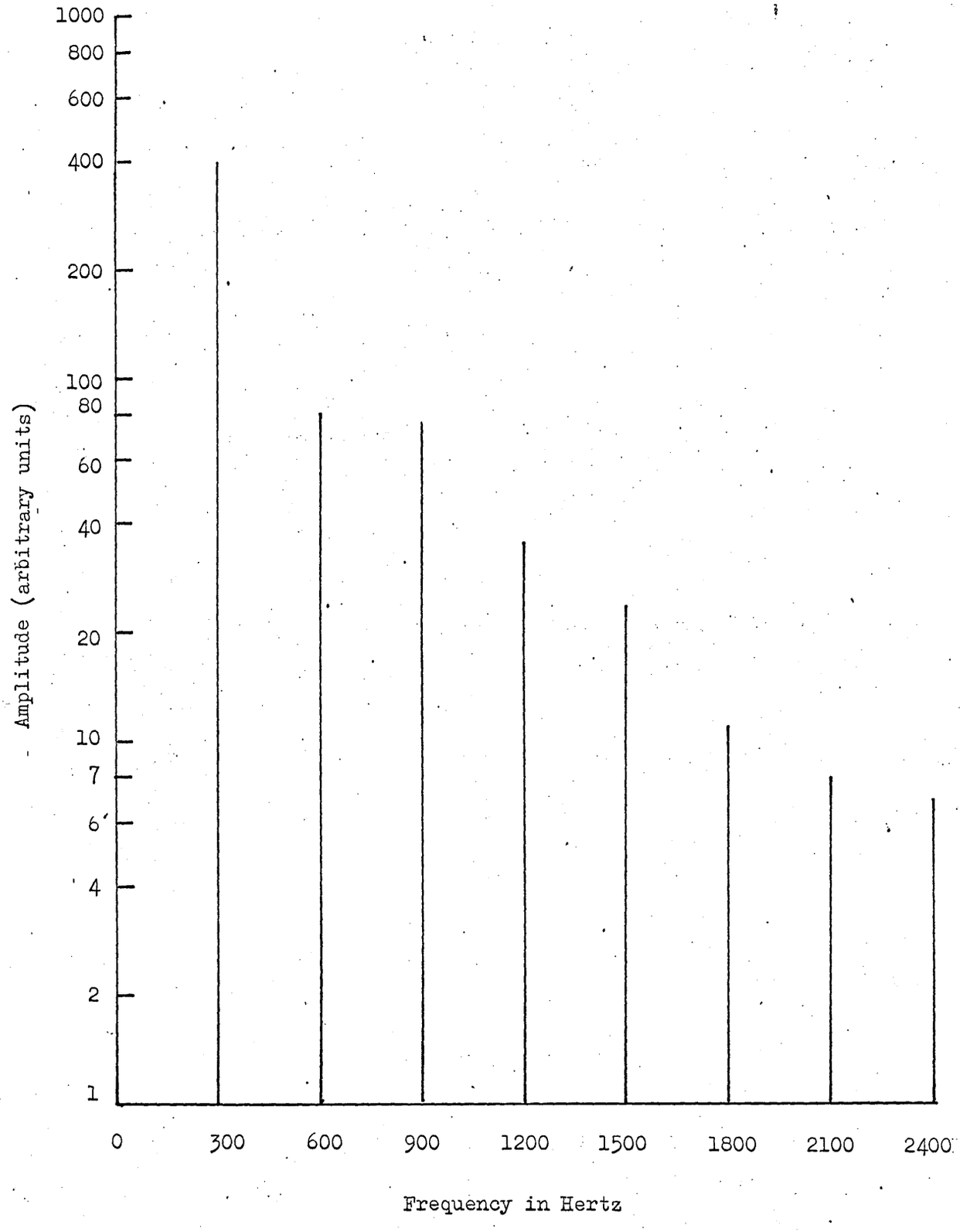

Fig.7.6 Frequency spectrum of the acoustic noise of a 13.0 K.W. torch at an argon flow rate 1.9 l/m.

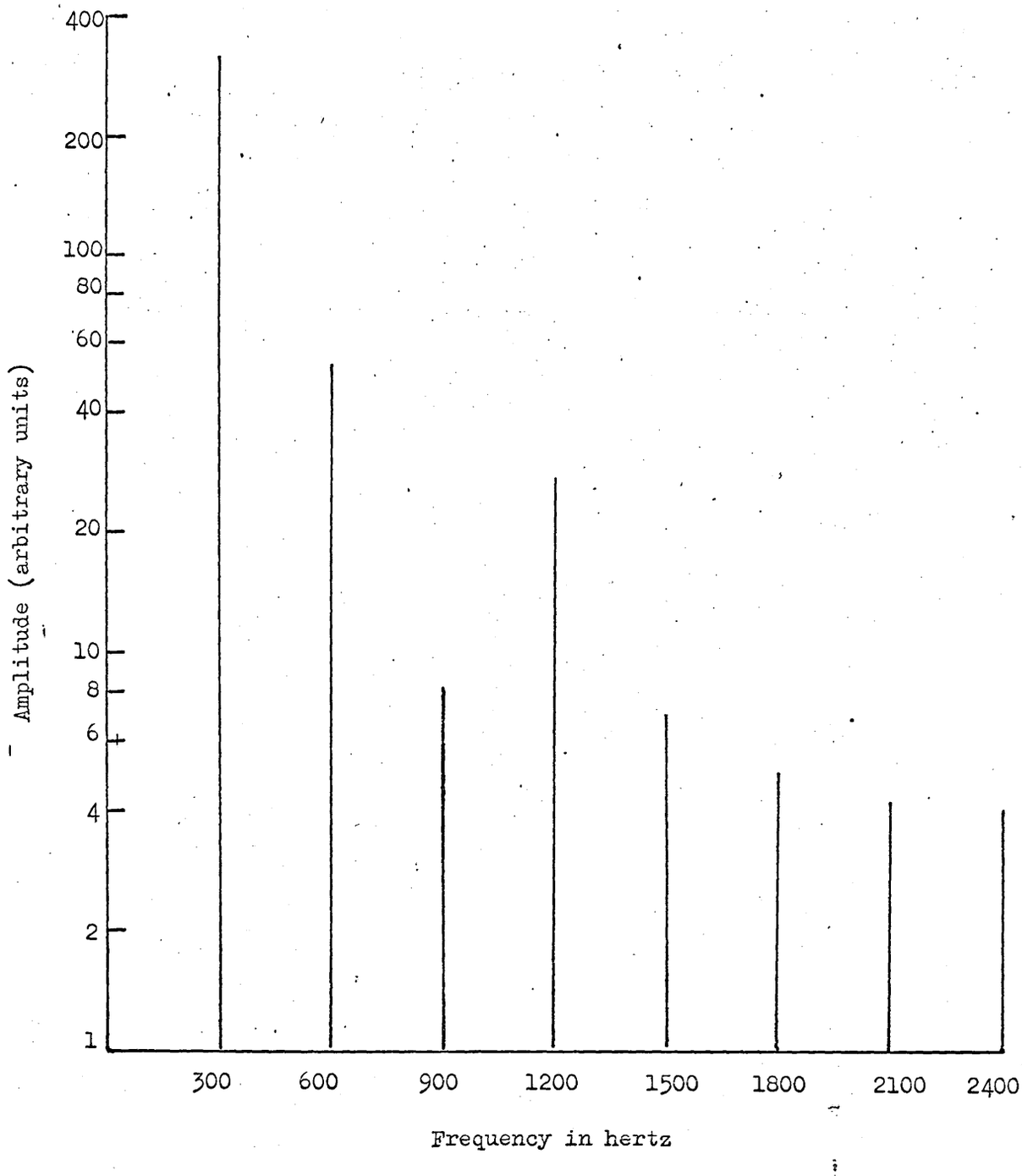

Fig.7.7 Frequency spectrum of the acoustic noise of a 2.3 K.W. torch at an argon flow rate 10.5 l/m.

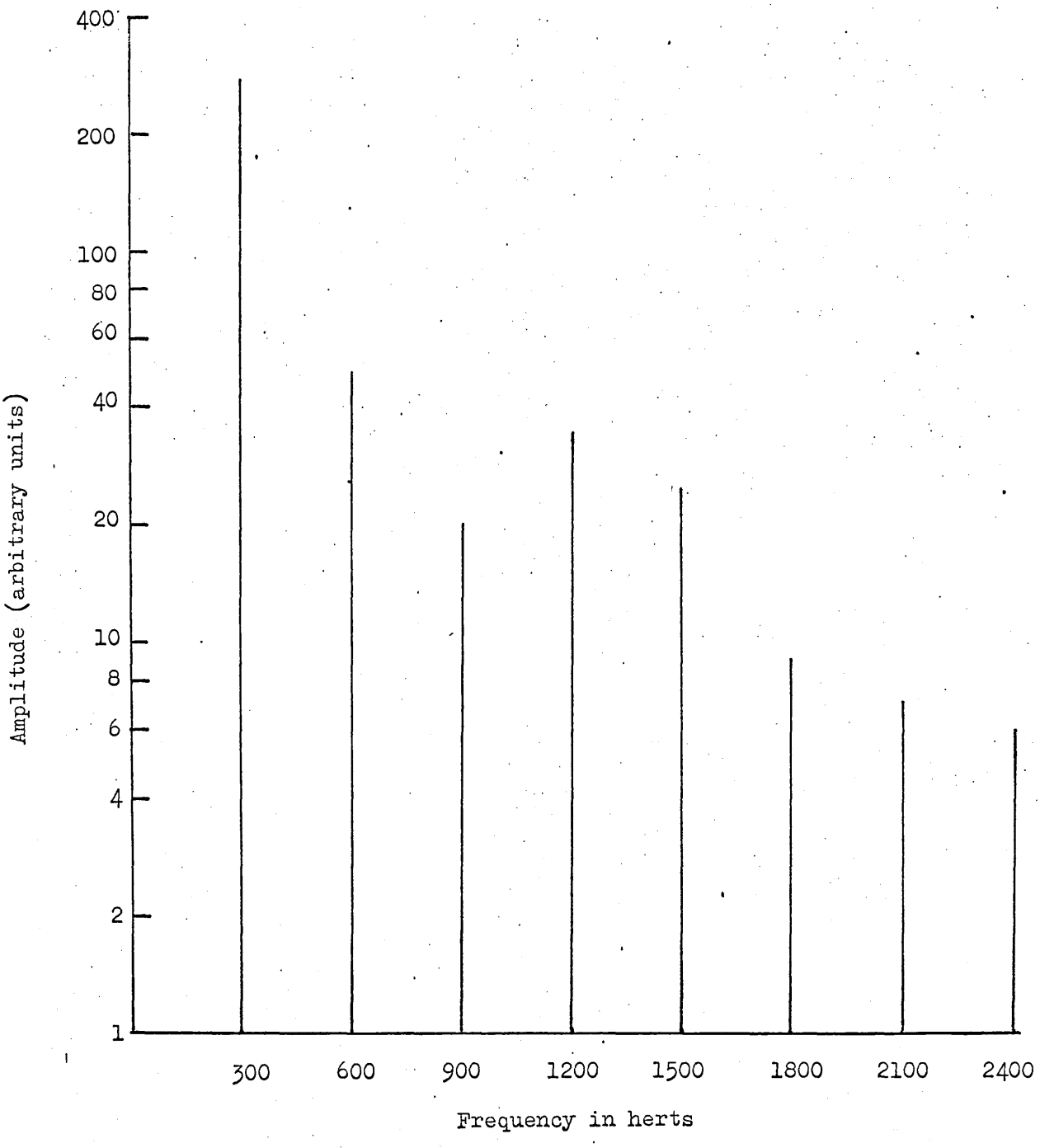

Fig.7.8 Frequency spectrum of the acoustic noise of a 2.3 K.W. torch at an argon flow rate 1.9 l/m.

and 7.8 respectively. In the 13.0 kW torch the decrease in the gas flow from 10.5 l/m to 1.9 l/m decreases the amplitude of the fundamental from 600 a.u. to 400 a.u. i.e. 0.67 times. In the 2.3 kW torch the corresponding decrease is from 320 a.u. to 280 a.u. i.e. 0.88 times. In the 13.0 kW torch the amplitude of a harmonic in the acoustic noise decreases with its order as in the light intensity but in the 2.3 kW torch the third harmonic shows a marked decrease at both gas flows, the decrease being greater at 10.5 l/m than at 1.9 l/m of argon. Other harmonics decrease in magnitude with their order.

It may be emphasized here that because two different devices, i.e. photomultiplier and microphone, were used to measure the light intensity modulation and the acoustic noise, their amplitudes cannot be inter-related.

7.2.3. Explanation and discussion of results

In order to see how the modulation of the r.f. electric field $E_o \cos \omega_o t$ induces instabilities in the induction plasma torch one may investigate the modulation of the power dissipated in the plasma. The electric field modulated by a periodic signal, which is proportional to $f(\omega,t)$, may be written as

$$E = (1 + m\, f(\omega,t))\; E_o \cos \omega_o t \qquad (7.1)$$

The power dissipated in the plasma is

$$W = \sigma E_{eff}^2 \left[1 + m\, f(\omega,t)\right]^2 \qquad (7.2)$$

where E_{eff} is the effective value of the r.f. electric field. Resolving $f(\omega,t)$ into its Fourier components

$$f(\omega,t) = \cos(\omega,t) + \sum_{n=2} \cos(n\omega t) \qquad (7.3)$$

where α_n is the ratio of the nth harmonic to the fundamental. In practice coefficients αs are less than unity so that during computation their products and squares may be neglected. Substituting for $f(\omega t)$ in Eq.(7.2)

$$W = \sigma E_{eff}^2 \left[\left(1 + \frac{m}{2}\right)^2 + (2m + m^2\alpha_2) \cos\omega t + \left(\frac{m^2}{2} + 2m\alpha_2 + m^2\alpha_3\right) \cos 2\omega t \right.$$

$$\left. + \sum_{n=3} (m^2\alpha_{n-1} + 2m\alpha_n + m^2\alpha_{n+1}) \cos n\omega t \right] \qquad (7.4)$$

To the first approximation the acoustic noise intensity and the amplitude of modulation of the radiation may be assumed to depend linearly on the oscillating component of the power i.e. on the terms, apart from the term $(1 + \frac{m^2}{2})$, on the right hand side of Eq. 7.4. In order to investigate which parts of the spectum agree with the above theory it is desirable to compare the ratios of consecutive harmonics computed and experimentally obtained. This is done in Table 7.2. where, with the decreasing order, the amplitude of a harmonic is seen to decrease more rapidly in the light intensity than in the acoustic noise. This is, most probably, due to the exponential dependence of light intensity on the temperature and, therefore, on the energy dissipated in the plasma. The agreement is quite satisfactory between the experimental and theoretical values for the higher harmonics, but not so good for the lower harmonics. The decrease in the amplitude of 300 Hz and harmonics at lower gas flows may be attributed to the formation of a smaller plasma by a low gas flow.

The above theory satisfactorily explains the effect of r.f. field modulation on the generation of acoustic noise and the modulation of light intensity. However, it says nothing about the effect of gas flow on the fundamental and various harmonics.

TABLE 7.2

Oscl-power	Gas flow	Accous / Rad	Theo / Expt	1st / Steady	Harmonic ratio						
					1st / 2nd	2nd / 3rd	3rd / 4th	4th / 5th	5th / 6th	6th / 7th	7th / 8th
13.0 kW	7.3 l/m	-	Theo	0.38	2.1	2.1	2.5	2.1	2.0	2.0	1.7
13.0 "	10.5 "	Rad	Expt		8.9	6.3	3.7	2.0	1.9		
13.0 "	1.9 "	"	"		16.3	6.1	2.7	2.0	1.4		
13.0 "	10.5 "	Acous	"		3.3	2.3	3.3	1.5	1.5	1.2	1.2
13.0 "	1.9 "	"	"		5	1.0	2.1	1.5	2.2	1.4	1.1
2.3 "	4.5 "	-	Theo	0.53	2.3	2.7	1.1	1.6	1.7	1.7	1.8
2.3 "	10.5 "	Rad	Expt		7.3	2.0	2.5	3.6	1.4		
2.3 "	1.9 "	"	"	0.33	5.0	2.5	2.5	2.0	1.6		
2.3 "	10.5 "	Acous	"		6.1	6.6	1.1	0.3	4.0	1.4	1.2
2.3 "	1.9 "	"	"		5.6	2.5	0.6	0.8	4.7	1.3	1.7

7.2.4. High frequency instabilities in light intensity (above 60 kHz)

Occasionally high frequency instabilities of 68.5, 125 and 250 kHz have been detected in radiation from a 13 kW torch. The reproducibility of these oscillations is poor. Fig. 7.9 shows an oscillogram of some of these oscillations. Sometimes they are excited by a pulsed magnetic field if they do not already exist in the steady plasma torch as mentioned before in Section 6.4.4. Referring back to Fig. 6.28 where large amplitude oscillations at about 330 kHz are observed during the 10 micro-secs after the application of the pulsed field, followed by oscillations of about 36 kHz which gradually change to 68.5 kHz in about 180 micro-secs, the following point may be observed. The change of frequency from 36 kHz to 68.5 kHz is not strictly associated with the magnetic pulse. Sometimes it is also observed in a steadily running torch as shown in Fig. 7.10.

7.2.5. Explanation and discussion of results

It is known that the cold gas enters the discharge from the side.[77] As it does so it is rapidly accelerated in a direction normal to the plasma surface due to sudden decrease in the gas density. This may generate a cylindrical wave in the plasma. The propagation velocity of an acoustic wave in argon at a temperature T is given by [100]

$$C_s = 319(T/273.16)^{\frac{1}{2}}$$

which, at T = 10,000 ^{o}K, equals 1930 $m\text{-}s^{-1}$ (7.5)

The fundamental frequency of the radial oscillations for an infinitely long cylindrical column of a gas is defined by the roots of equation [101]

$$J_n'(\xi R) = 0 \qquad (7.6)$$

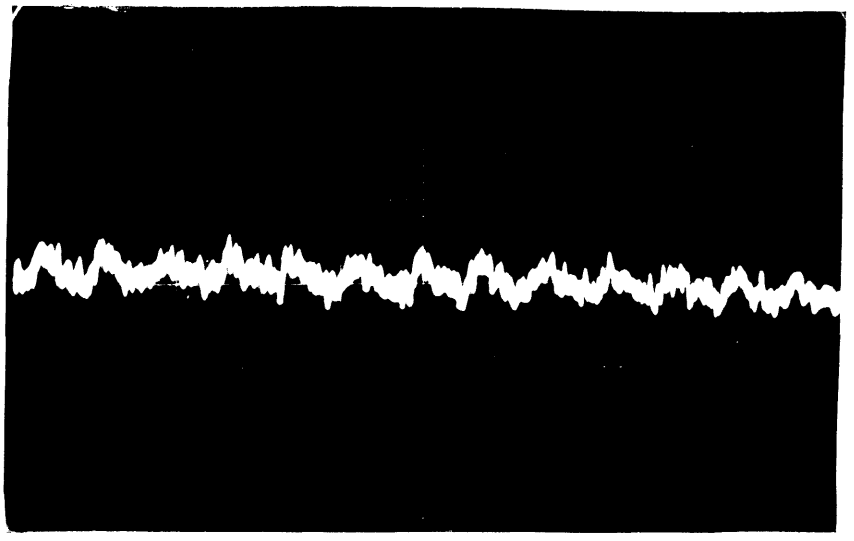

scale 1 cm = 20 μs

Fig.7.9 Light intensity modulation at 68.5 K.Hz in a 13.0 K.W. torch

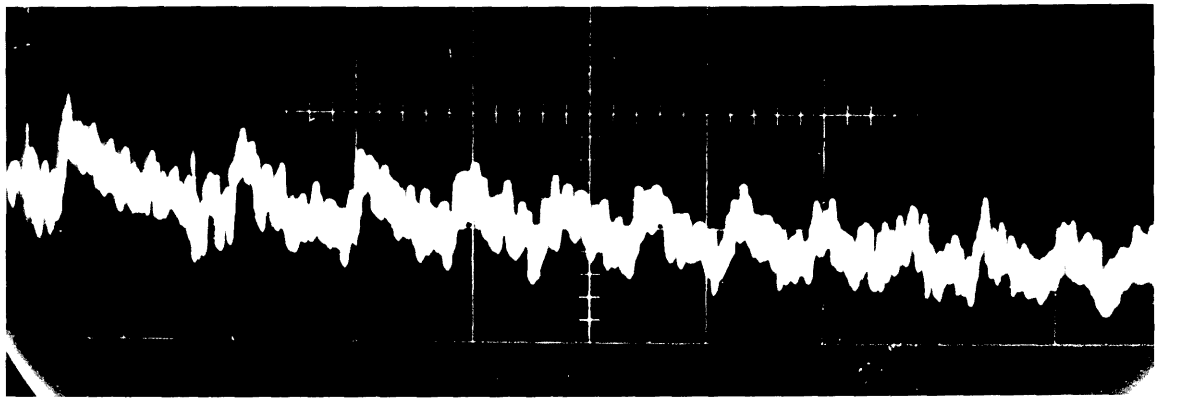

Scale 1 cm = 20 μs

Fig.7.10 Change in the frequency of oscillations, detected in the light radiated from a steady torch

where J_n' is the first derivative of the nth order Bessel function and $\acute{\varepsilon}$ is the wave number. The frequencies for these oscillations are given by

$$f = \frac{\acute{\varepsilon}\, v}{2\pi R} \qquad (7.7)$$

where $\acute{\varepsilon}$ is the mth root of Eq. (7.6). For $n = 0$, $\acute{\varepsilon}$ assumes values of 3.832, 7.015 [101] which gives $f = 69.2$, 126.5 kHz for $R = 1.7$ cm. The observed frequencies of 68.5 and 125 kHz agree well with these theoretical values. The radial oscillation mode determined by $n = 1$ when $\acute{\varepsilon}_{nm} = \acute{\varepsilon}_{10} = 1.841$ gives $f = 33.3$ kHz which is in fair agreement with the observed frequency $f = 36$ kHz, mentioned above. Other frequencies may be excited due to the generation of harmonics, other values of $\acute{\varepsilon}$ and also the variation in the plasma radius along its length.

7.3. Investigation of the torch with the aid of a magnetic probe

Efficient operation of an induction plasma torch depends on the operator having an adequate knowledge of the temperature, the circuit parameters and the overall efficiency. They are usually obtained by somewhat lengthy measurements using spectroscopy [25, 63, 66, 94] calorimetry [72] and electrical measurements. However, a considerable amount of information may be obtained by making comparatively simple measurements of r.f. magnetic field, frequency of excitation, and the inductor current. These measurements were made on a 13.0 kW and a 11.6 kW torch. Modulation of the r.f. field was minimised by filtering the high voltage supply of the oscillator.

Measurements were made to obtain the axial distributions of the axial component 'Hz" of the r.f. magnetic field in plasma and air, i.e. without plasma, and the results are presented in Fig.7.11 for a 13.0 kW torch and in Fig.7.12 for a 11.6 kW torch. In the 13.0 kW torch (Fig.7.11) the field in air (curve 'a') is almost a gaussian distribution about the

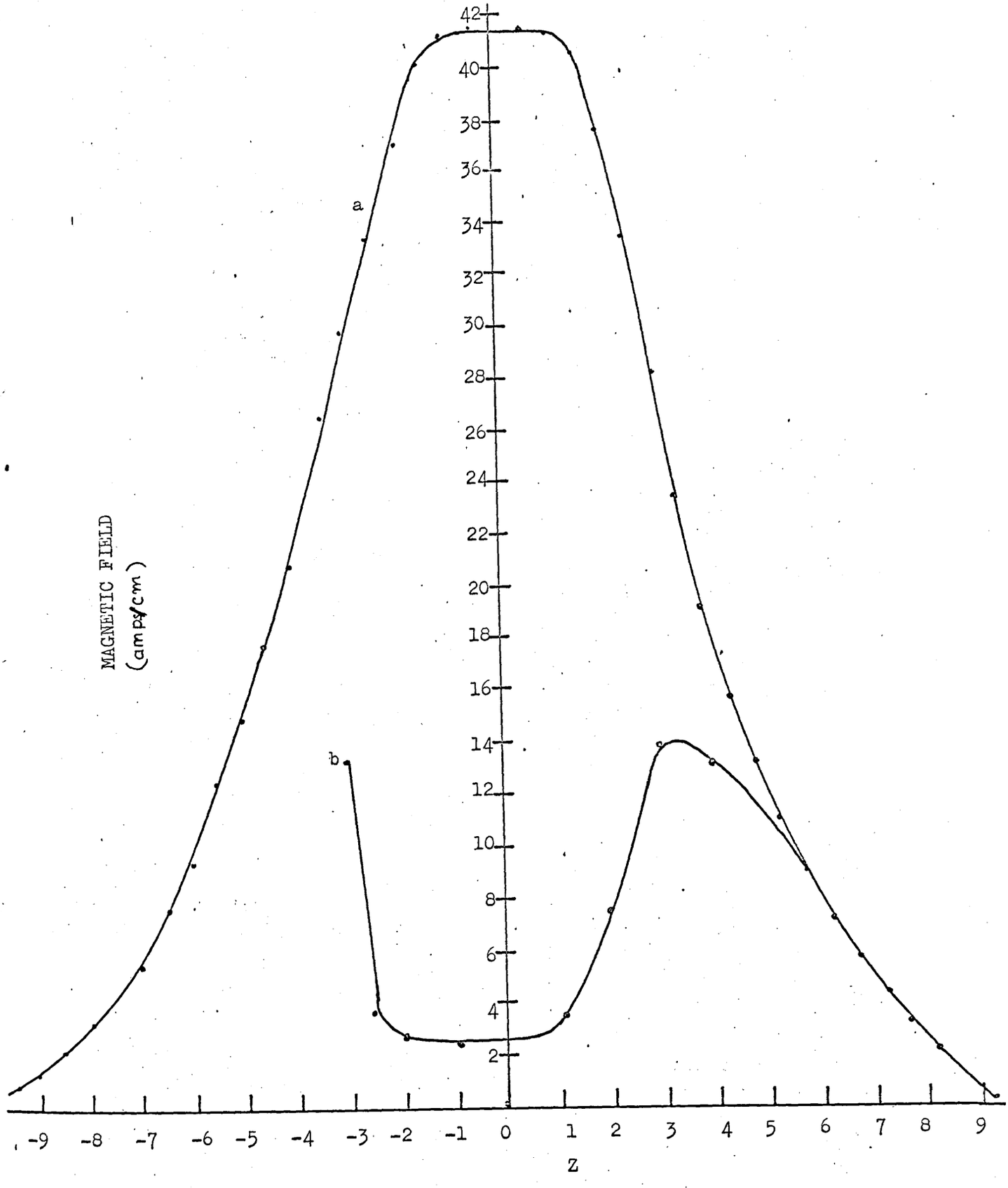

Fig.7.11 Axial magnetic field distribution in a 13.0 K.W. torch (a) in air (b) in plasma.

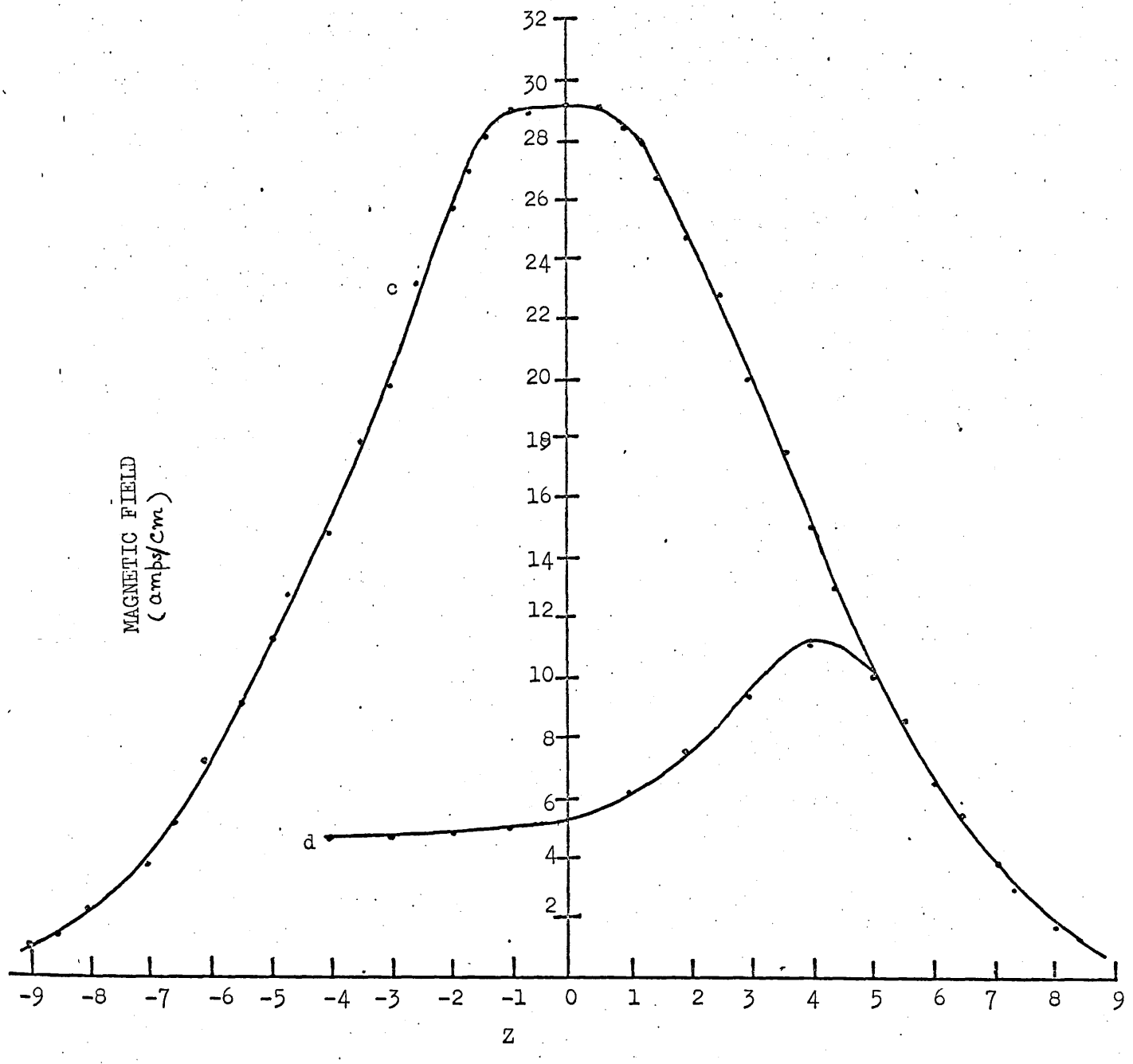

Fig.7.12 Axial magnetic field distribution in a 11.6 K.W. torch
(a) in air (b) in plasma

middle point of the coil. When the plasma is present (curve 'b') the field is almost uniform between 2.2 cm below the mid-point and 0.8 cm above, but rises rapidly on either side of this region to approach to the value of the field in air. The 11.6 kW torch displays a similar variation (Fig. 7.12) with less sharp transition regions. Radial distributions of Hz in air in the middle of the r.f. inductors of the two torches are compared in Fig. 7.13 at an inductor current of 70.0 amps. In either case the field is about 10% smaller at the centre than near an inductor turn.

For making estimates of plasma impedence, torch efficiency etc., which will be described in Section 7.3.2., values of Hz averaged over the inductor length are required. They have been computed from axial distribution of Hz in Figs.7.11 and 7.12 and presented in Table 7.3.

TABLE 7.3. Mean values of Hz

Torch	Torch ignited	Mean Hz
13.0 kW	Yes	4.4 A - cm^{-1}
" "	No	40.5 "
11.6 kW	Yes	5.7 "
" "	No	32.0 "

7.3.1. Inductor current and oscillator frequency

The inductor current and the oscillator frequency were measured in the presence and then in the absence of the plasma. The results are presented in Table 7.4. It is seen from the table that the presence of the plasma has a considerable effect on the inductor current which decreases by 13.8% in a 13 kW torch and by 20% in an 11.6 torch when the torch is ignited and, therfore, the load on the r.f. source changes. The changes in

oscillator frequency are comparatively much smaller.

TABLE 7.4. Inductor current and oscillator frequency

Torch	Torch ignited	Inductor current	Frequency
13.0 kW	Yes	70.0 A	6.20 MHz
" "	No	81.2 A	5.95 MHz
11.6 "	Yes	53.4 A	4.55 MHz
" "	No	66.8 A	4.43 MHz

7.3.2. Interpretation and discussion of results

The plasma in the torch may be approximated to a cylindrical column of length 'l' and radius 'r' as done previously in Section 6.4.5.1.3 As the magnetic field falls rapidly outside the r.f. inductor as shown in Fig. 7.11 and 7.12, the effective length of the plasma where energy is dissipated, is equated to the inductor length. The r.f. magnetic field penetrates the plasma to a depth of δ, the skin depth. Assuming the plasma to have a uniform conductivity across its cross-section, the ratio of the axial magnetic field in the plasma to that in the coil when no plasma is present, for the same inductor current as in the presence of the plasma, is

$$H_{za}/H_{zp} = \left((\mathrm{ber}(\sqrt{2}\, R/\delta))^2 + (\mathrm{bei}(\sqrt{2}\, R/\delta))^2 \right)^{\frac{1}{2}} \qquad (7.8)$$

The expression used for the skin depth is

$$\delta = (\pi f \mu \sigma)^{-\frac{1}{2}} \qquad (7.9)$$

By measuring the axial component Hz on the axis both with and without the plasma present and then inserting these values into Eq.(7.8), the value of the skin depth may be determined and hence from Eq.(7.9) the conductivity is estimated. The plasma temperature is determined with the aid of conductivity versus temperature graph of Fig.2.7. The results of these calculations are shown in Table 7.5.

TABLE 7.5. Plasma conductivity and temperature

Torch	Mean electrical conductivity	Mean temperature at the centre of inductor
13.0 kW	32.0 $(\text{ohm-cm})^{-1}$	9700 ^{o}K
11.6 "	16.0 "	7700 ^{o}K

In order to determine the circuit constants, the induction plasma torch may be represented by an inductively coupled circuit with the primary representing the inductor and the single turn short circuited secondary representing the plasma as shown in Fig.4.1 Current, resistance, inductance and impedence are represented respectively by i, R, L and Z. Suffixes 1 and 2 are used to designate these quantities in the primary and the secondary circuits respectively. The frequency shift, Δf, resulting from igniting the plasma in the coil is related to L_2, Z_2 and the mutual inductance 'M' between the primary and secondary circuits by

$$L_2/L_1 = \left(1 - \left(1 + \frac{\Delta f}{f}\right)^2\right) (Z_2/2\pi fM)^2 \qquad (7.10)$$

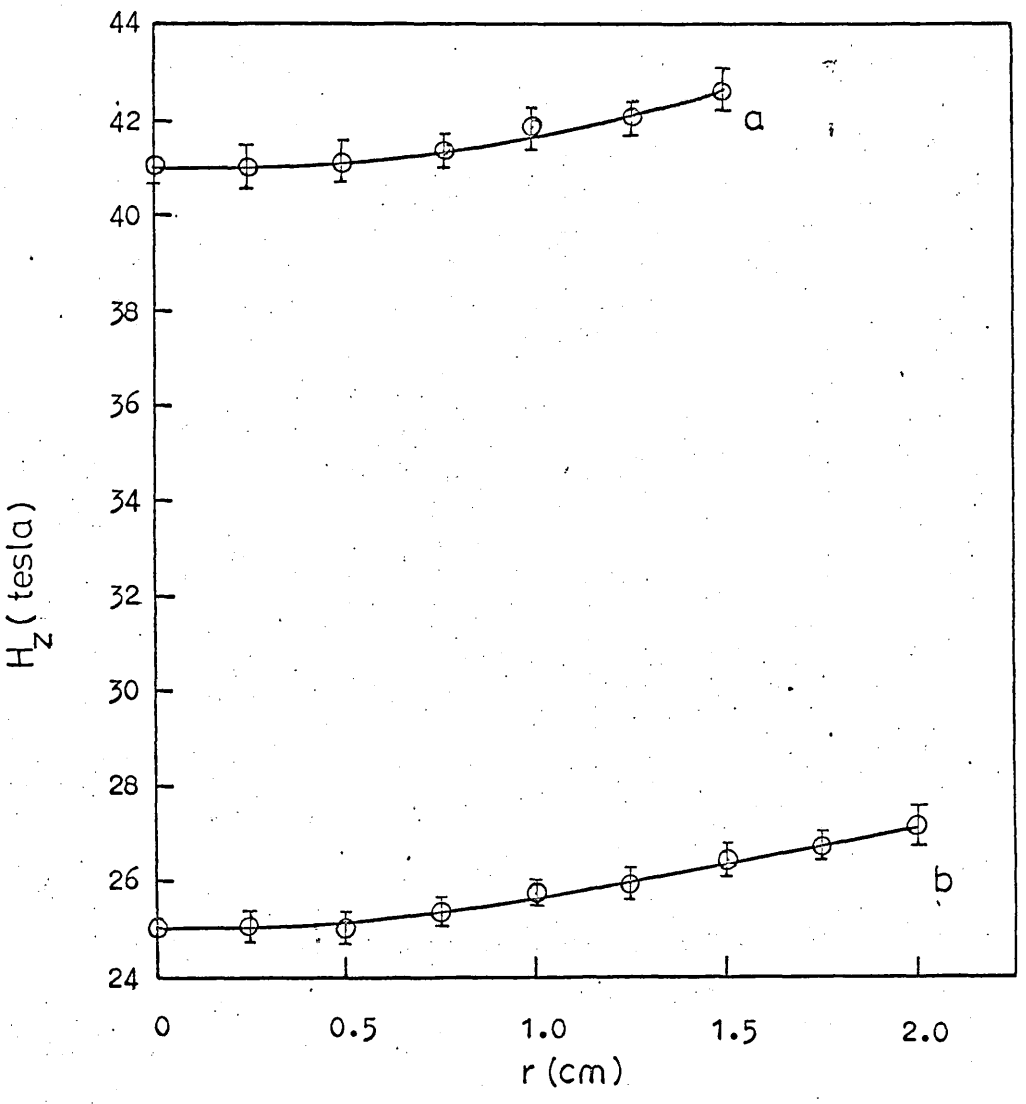

Fig.7.13 Radial distribution of H_z in air in the middle of rf inductor (a) type I (b) type II for an inductor current of 70 amps.

The ratio of currents in the primary and the secondary when the plasma is burning is

$$i_2/i_1 = 2\pi f M/Z_2 \qquad (7.11)$$

By putting the magnetic field H_{zp} in the plasma into units of $A\text{-}cm^{-1}$, the current in the plasma or secondary circuit is $i_2 = H_{zp}$ times the effective plasma length, l_2. The ratio of L_2 to L_1 may be determined for the known values of Δf, i_1 and i_2 with the aid of equations (7.10) and (7.11).

The inductance of the primary has been measured in Section 5.2.2. and hence the inductance of the secondary L_2 is now estimated.

The resistivity of the plasma may be expressed simply in terms of the skin depth, i.e. $R_2 = 4\pi r/\sigma l_2 \delta$. Furthermore, the impedence of the secondary consists simply of the resistive and the reactive components R_2 and $2\pi f L_2$, and hence may be determined from measurements made so far. From the equation

$$M = \gamma \sqrt{L_1 L_2} \qquad (7.12)$$

the coupling coefficient 'γ' may also be determined. Values determined for L_2, R_2, Z_2 and 'γ' are quoted in Table 7.6.

TABLE 7.6 Circuit constants

Torch	L_2	R_2	Z_2	
13.0 kW	25.5 nH	0.258 ohm	1.030 ohm	0.2957
11.6 "	28.0 "	0.447 "	0.917 "	0.2610

The overall efficiency of the torch may be determined with aid of the power $i_2^2 R_2$ dissipated in the plasma. Values of power and efficiency

in the two torches are quoted in Table 7.7.

TABLE 7.7.

Torch	$I_2^2 R_2$	Efficiency
13.0 kW	6.20 kW	48.2%
11.6 "	6.39 "	55.0%

The estimated values of 9700 ^{o}K and 7700 ^{o}K of the plasma temperature are in satisfactory agreement with the temperature values of 10,000 ^{o}K and 8500 ^{o}K respectively obtained spectroscopically in Section 6.4.2.1.2.1.

7.3.3. A Technique [102] of determining the temperature in an induction plasma torch with a water cooled inductive probe

Measurements of the r.f. magnetic field made with a water-cooled probe have already been used to estimate plasma temperature in 13 kW and 11.6 kW induction torches in Section 7.3.2. It is only necessary to extend the technique to different radii and excitation freqencies of an induction torch. From Eq.(7.8) and (7.9) a family of curves may be drawn to relate H_{zp}/H_{za} to the plasma [102]. conductivity. As the conductivity for an atmospheric-pressure argon plasma is a known function of temperature, Fig. 7.14 is produced which relates the plasma temperature to H_{zp}/H_{za}, the curves depending on the parameter $\alpha = R\sqrt{f}$. The temperature is estimated by calculating for the plasma torch operating condictions, measuring H_{zp}/H_{za} and reading the temperature from the appropriate curve in Fig. 7.14 . Values obtained from the probe measurements have already been compared with spectroscopic values in the previous section.

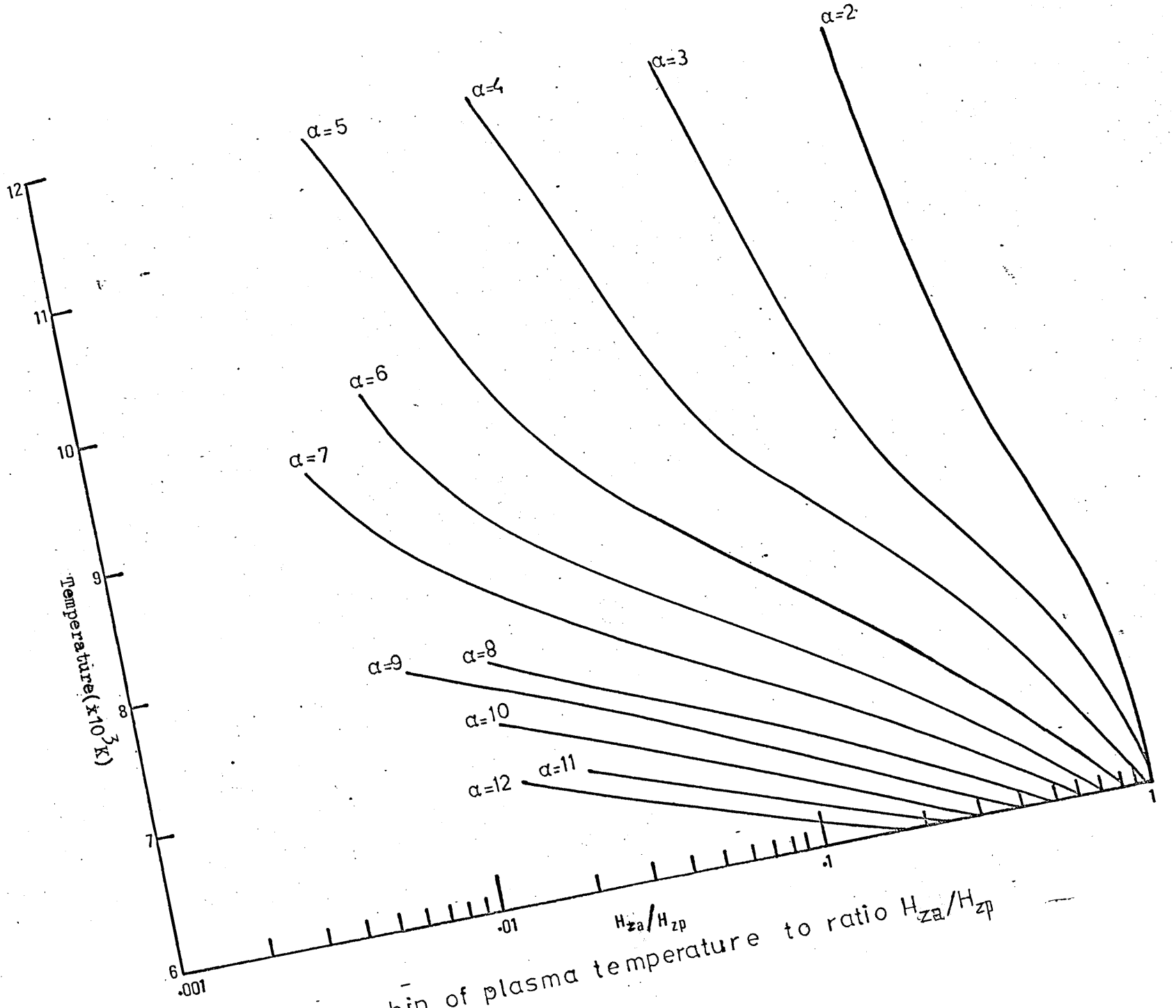

Fig7.14 Relationship of plasma temperature to ratio H_{za}/H_{zp}

7.4. Gas break down at torch initiation

The study of temperature changes during the early stages of the gas breakdown in an atmospheric pressure r.f. induction plasma torch provides information about the initiation mechanism of the torch. Using the particle diffusion model, Kustov and Arsenov[103] gave a criterion for the striking of the torch. Their experimental results were, however, confined to high speed photography of the initial stages of the gas break down. This work investigates the changes in the plasma temperature and the r.f. inductor current during these early stages. Other studies, which are relevent to this investigation, include various methods of striking the torch and the measurement of temperature of the filamentary structure which is formed in a large number of cases prior to the formation of the main plasma.

All these studies are made on a 13.0 kW torch burning in the discharge tube DT-1 at an argon flow of 10.5 l/m.

7.4.1. Striking the torch

The torch could be ignited either with a tesla coil, whose tip was held some distance away from the r.f. inductor against the discharge tube, or by introducing a 1.0 mm thick tungsten wire, after the oscillator had been switched on and the argon flow opened into the discharge tube. In either case, in the beginning, a filamentary structure, as shown in Fig. 6.15 was almost always formed. This filamentary structure was confined to the peripheral region of the tube and rotated with the gas in a vortex stabilisation. It disappeared completely when the main discharge was ignited either by repeated discharge of the tesla coil or by moving the tip of the tungsten wire a little up and down in the mid region of the r.f. helix. If used, the tungsten wire was immediately withdrawn on the formation of the main discharge.

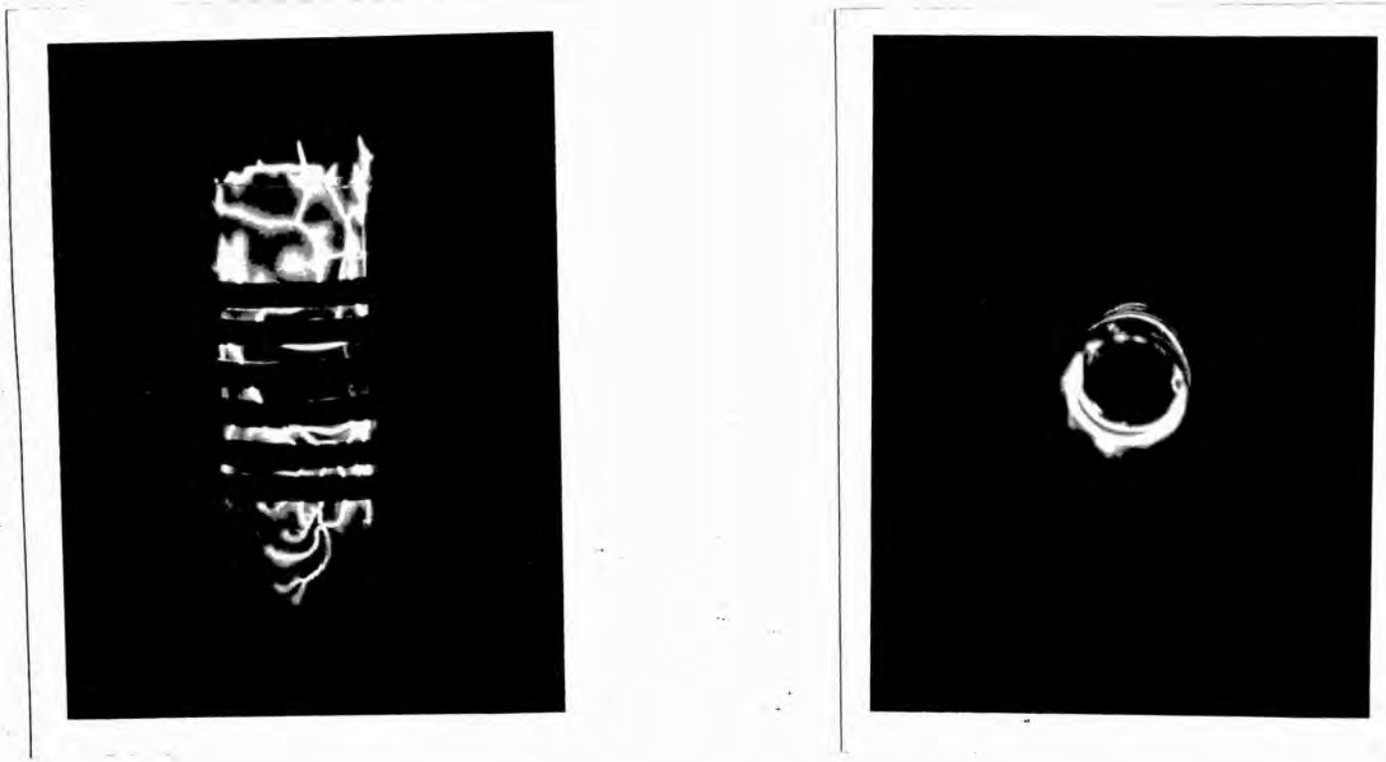

(a) (b)

Fig.7.15 Filamentary structure before the onset of the main discharge (a) side view (b) End-On view.

Once the filamentary structure was formed, the main discharge could also be struck by simply increasing the voltage across the r.f. inductor. This was achieved by increasing the d.c. plate voltage of the oscillator up to about 5.0 kV. Alternatively, the tungsten wire tip was held in the mid region of the r.f. helix, the gas flow was opened and then the oscillator was switched on. In a number of cases, the main discharge was formed without the formation of the filamentary structure. Occasionaly an intense discharge was formed, which put an excessive load on the oscillator and subsequently switched it off, by actuating the safety devices of the r.f. generator.

The 13.0 kW torch was found difficult to strike for the first time if it had not been used for some time (a few days) in the past. A large power setting of the oscillator was then found essential. But after the first few strikes, it could be struck easily even at the low oscillator power setting.

The 11.6 kW torch in the discharge tube DT-2 was found more difficult to ignite. However, ignition became a bit easier after a few runs. As with the 13.0 kW torch a filamentary structure, which was usually confined to the inductor region, was first formed. The torch was ignited only when the filamentary structure was extended fairly below the inductor region by lowering the tungsten wire. A large elongated plasma which tapered towards the tail, was formed in this case. The upper part of the plasma was a bit unsteady and wavered about the axis of the discharge tube. The d.c. power input recorded on the meters fluctuated by about 100 watts, showing a variable plasma load.

7.4.2. Temperature of the filament

The spectral region 200 to 400 nm was used to measure the filament temperature by the metnod described in Section 5.4.5.3. NO (0,1), OH(0,0) and N_2(0.2) bands were chosen to measure the temperature. However, except the

first, the other two bands showed considerable self absorption and, therefore, were not used for temperature determination. For NO (0,1) band densitometric plot is shown in Fig. 7.16 and the Maxwell-Boltzmann plot in Fig. 7.17. To show self absorption in NO_2(0,2) band, its Maxwell-Boltzmann plot is also presented in Fig. 7.18. The plot of Fig. 7.17 yields an average temperature of 3400 ^{o}K at an oscillator power of 4.1 kW.

As in a mono pole torch [104] the filamentary structure in this case also consisted of a bright central core surrounded by a less luminous aureola. Because of rotation of the filaments only the average temperature for the central core and the surrounding aureola was obtained as mentioned above. The actual temperature of the central core could be more than 3400 ^{o}K.

Grijorovici and Cristescu [50] quoted a temperature of 3850 ^{o}K in the filament core of a monopole high frequency torch, Cobine and Wilbur gave estimates of the mean temperature at about 4000 ^{o}K in a microwave torch [47].

7.4.3. Gas breakdown (Formation of the main discharge)

After a study of various methods of torch initiation and the formation of filamentary structure, the gas breakdown, leading to the formation of the main discharge, is now studied.

7.4.3.1. Temperature changes

Temperature measurements during the early stages of the main-discharge-formation were made by line-intensity-ratio-method, using 418.2, 425.9 and 427.2 nm lines of ArI, at two positions on the axis, Z = 1.2 and Z = 0.3 cm. Fig. 7.19 shows the intensity variation of 425.9 nm line of ArI with time at these positions. Temperature variations with time at these positions are presented in Fig. 7.20

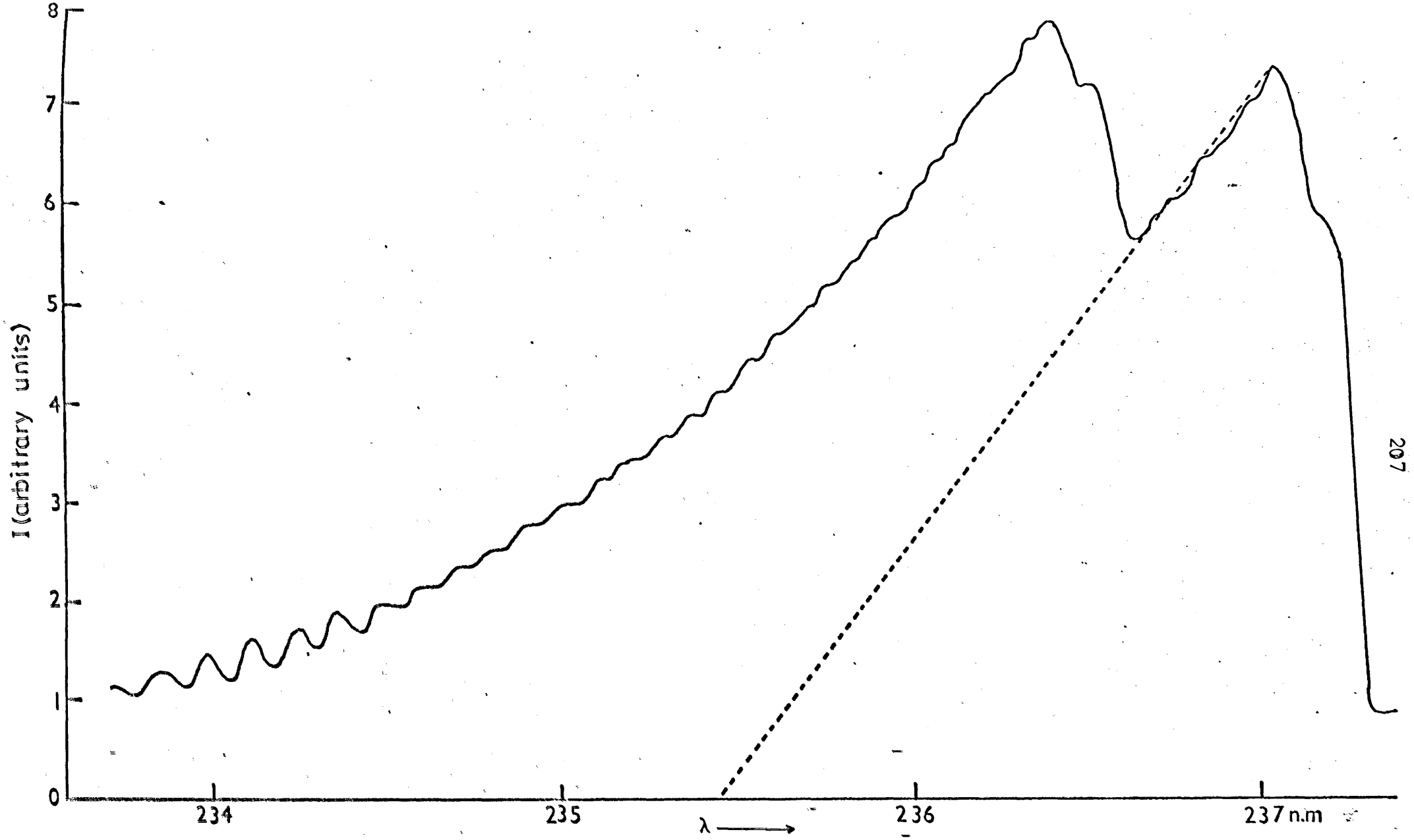

Fig 7.16 Densitometric plot of NOγ(0,1) band.

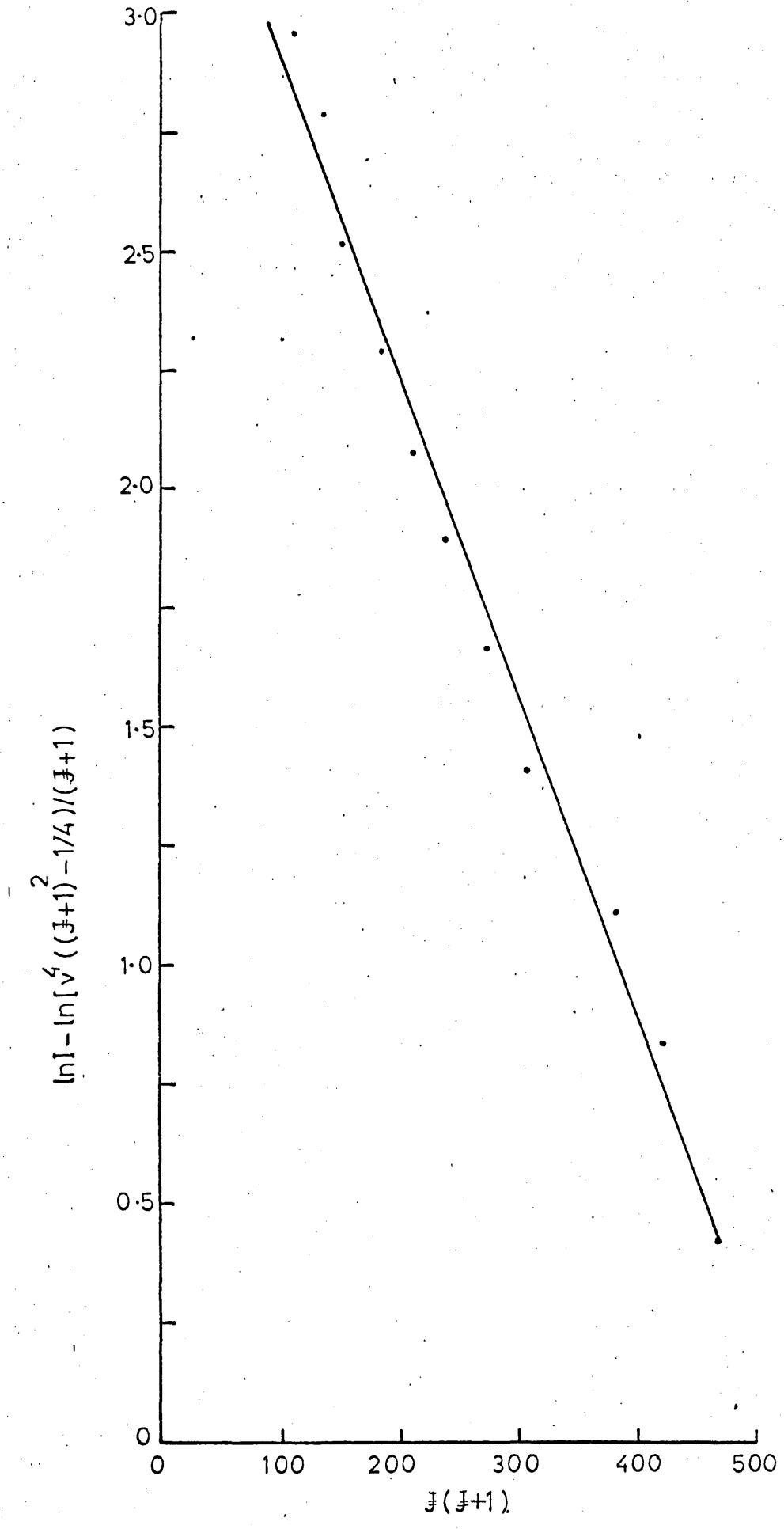

Fig 7.17 Maxwell Boltzmann plot of NO Y(0,1) band.

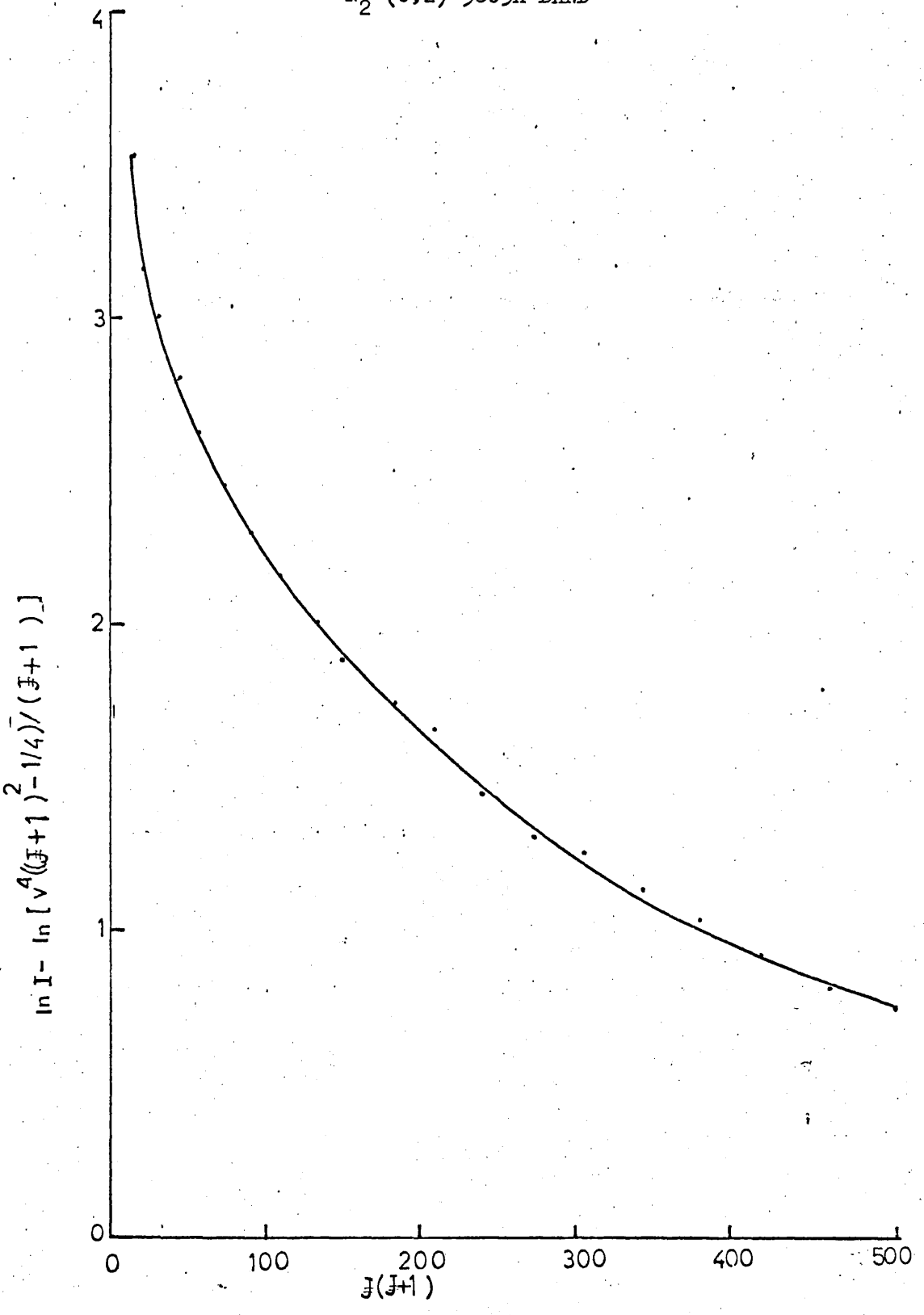

Fig.7.18 Maxwell-Boltzmannplot of $N_2(0,2)$ 380.5 nm band

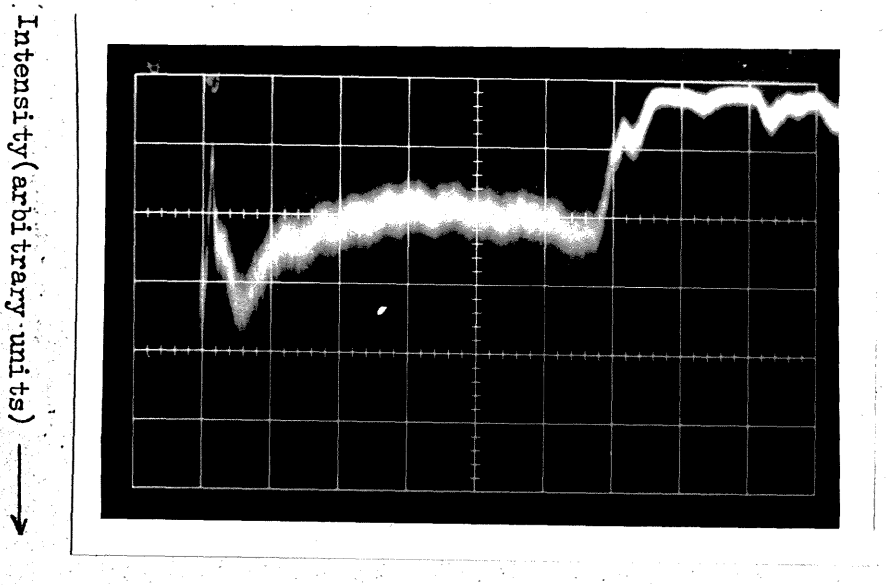

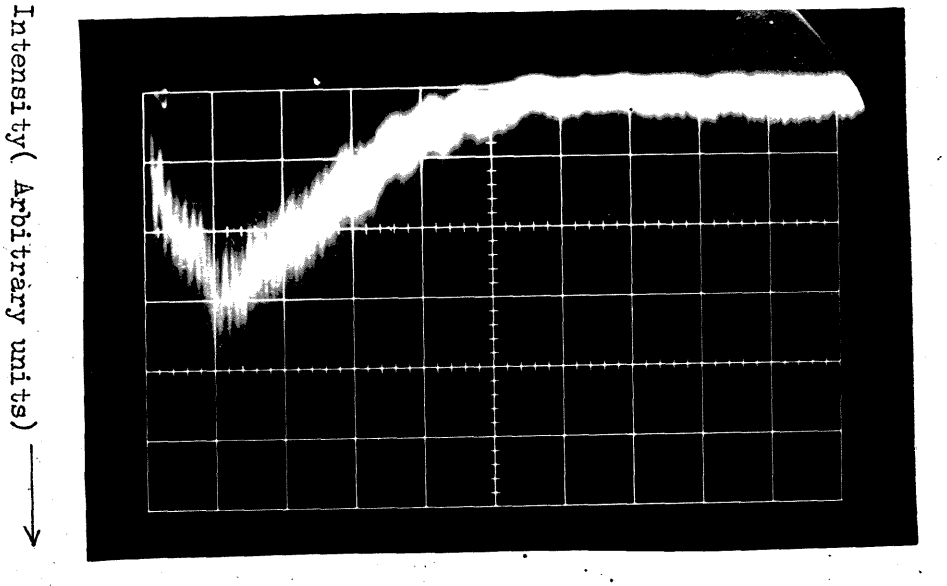

Fig.7.19 Intensity variation of 425.9 nm spectral line with time on striking a 13 K.W. torch at (a) Z = 0.3 cm, (b) Z = 1.2 cm.

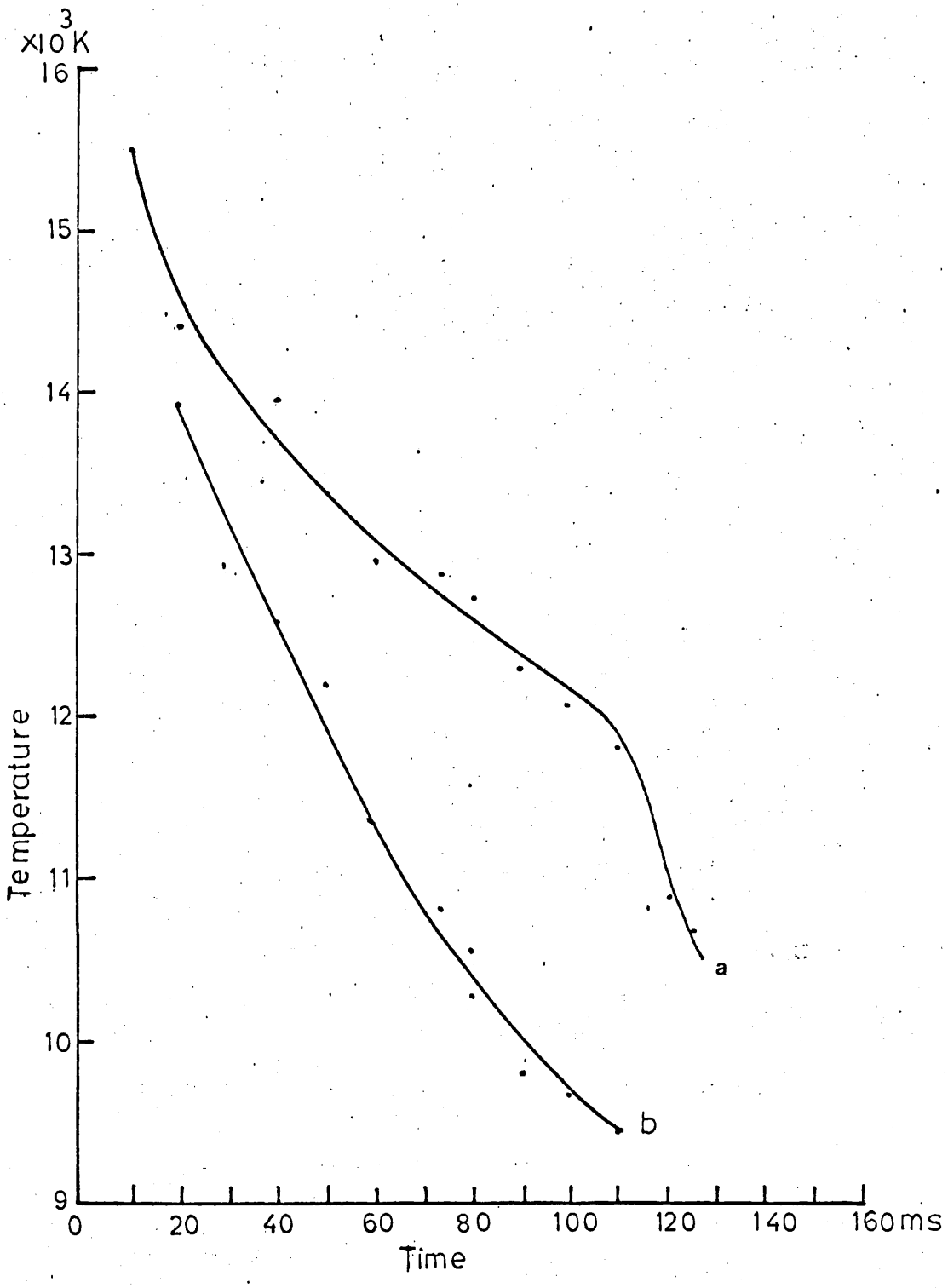

Fig.7.20 Temperature changes during the gas breakdown in a 13.0 k.W torch at (a) Z = 0.3 cm (b) Z = 1.2 cm.

Low frequency oscillations of about 83 Hz can be seen in the light intensities in Figs. 7.19 (a) and (b). Inside the discharge tube these are followed by large amplitude oscillations of about 5 Hz (Fig.7.19 (a)), soon after the steep intensity fall, occuring at 120 m-secs after the torch initiation. The plasma temperature rises to 15,500 K in 10 m secs., falling off later like an exponential variation (Fig.7.20 (a)) up to about 110 m secs when a knee occurs in the temperature variation. This is followed by a similar temperature decrease as before. At 1.2 Cm above the r.f. inductor the plasma temperature reaches a maximum value of 13900 K in about 20 m secs., i.e 10 m secs. later than inside the tube, falling off rapidly afterwards. The delay in the rise of temperature to its maximum value at Z = 1.2 Cm is caused by the delay in the plasma build up. This point will be taken up again in section 7.4.3.3.

7.4.3.2 Current-change in the r.f. inductor

During the gas break down, the current-change in the r.f. inductor was also measured. The results are presented in Fig.7.21. The current is seen to fall by about 19% as the discharge builds up and puts a load on the r.f. inductor.

7.4.3.3 High Speed photography

High speed photographs, tracing the development of the discharge, were taken with the image converter camera. They are presented in Fig.7.22. The discharge is seen to appear first in the mid region of the r.f. inductor. It then grows along the axis, causing a delay in the temperature rise at Z = 1.2 Cm, mentioned earlier in section 7.4.3.1. The plasma is also seen to flow out with the receding wire, which may serve as an aerial and

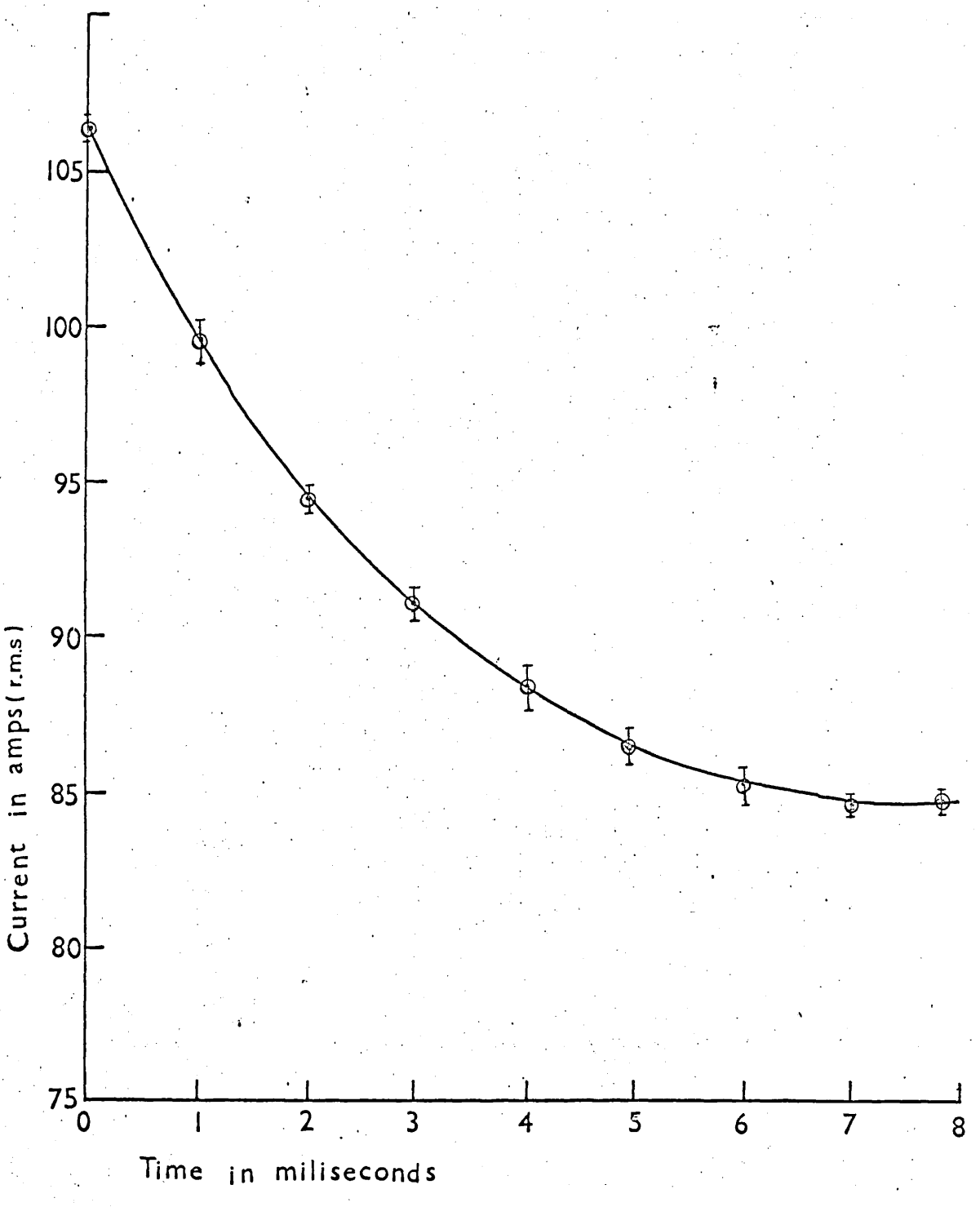

Fig.7.21 Current change in the r.f helix at the initiation of the plasma torch

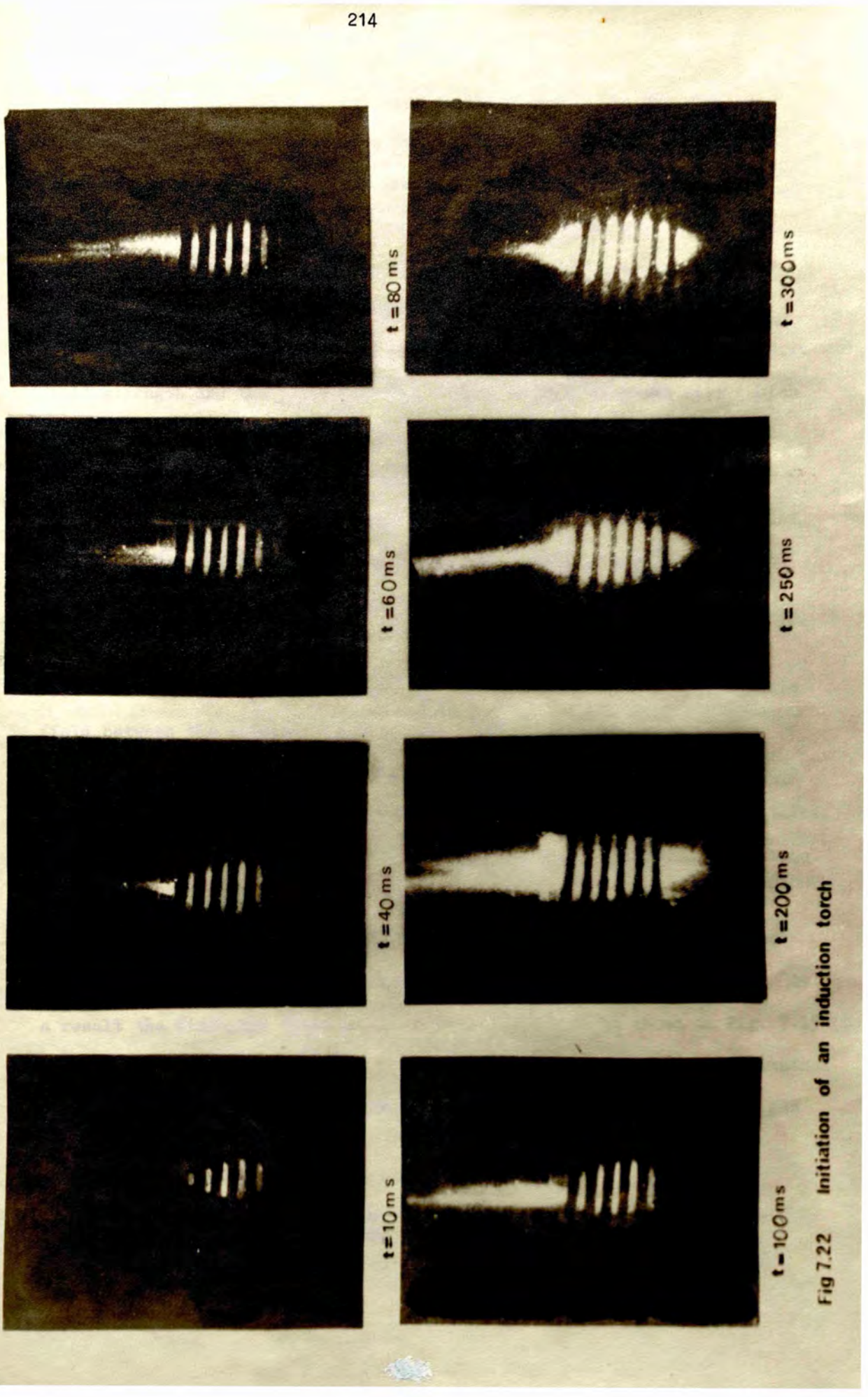

Fig 7.22 Initiation of an induction torch

couples energy from the r.f. inductor to the plasma. As the wire is also heated to a high temperature by the main discharge, some plasma regeneration may also take place around it due to thermionic emission from it.

7.4.3.4. Interpretation and discussion of results.

The onset and the intensity of the discharge depends on the electric field strength and the preionization. When using a tungsten wire (which was mostly used for torch ignition in this work) it is more likely that preionization is produced by virtue of an intense electric field at the pointed* tip of the wire rather than by gas-heating or thermionic emission from the wire. The wire was never found to acquire a high/ temperature in the r.f. field before the onset of the main discharge.

When formed the filamentary discharge is maintained by the electric field between the inductor turns. The conducting channels guide the r.f. field and absorb energy through ohmic heating as in a high frequency monopole torch. As the electric field is stronger near the inductor turns, the filamentary discharge tends to lie near the wall of the discharge tube. However, it is pushed away from the wall by the denser cold gas layers, flowing spirally upward. The gas layers expand on receiving heat from the discharge and push the discharge further away from the tube wall. As a result the discharge takes an intermediate position as shown in Fig. 7.15 (b). The filamentary discharge owes its peculiar shape to the axial and azimathal electric field components, and its rotation to the spiral flow of the gas in a vortex stabilisation.

* The tip of the tungston wire became pointed after a little use.
/ The wire became only dull-red hot in the r.f. field.

The onset of the main discharge is characterised by a transition from an E-Coupling to an H-Coupling. This requires a sufficiently conducting gas and hence a minimum temperature of 5000 K for argon. The irregular movement of the tungsten wire described in section 7.4.1 , may land its tip in a region of large ionization such as the point where many filaments meet. The additional ionization produced at the wire tip may make the gas sufficiently conducting and lead to its break-down.

For the gas breakdown it is informative to see how the average power density 'P_{cc}' of the discharge varies with time. This power density may be computed from:[105]

$$P_{cc} = 2.5 f H_o^2 \mu Q \, 10^8 \quad \text{watts/cc} \qquad (7.13)$$

where,
$$Q = \frac{\sqrt{2}\delta}{R} \; \frac{\text{ber}(\sqrt{2}R/\delta)\text{ber}(\sqrt{2}R/\delta) + \text{bei}(\sqrt{2}R/\delta)\text{bei}(\sqrt{2}R/\delta)}{\text{ber}(\sqrt{2}R/\delta) + \text{ber}(\sqrt{2}R/\delta)}$$

and H is the peak magnetic field. Q is plotted against $2R/\delta$ in Fig.7.23. It would appear from this figure that as soon as δ assumes a finite value i.e. the gas becomes conducting, Q also acquires a finite positive value, H-Coupling of the r.f. power into the plasma begins to operate. Assuming that the discharge starts from a small volume and that both the temperature and the plasma diameter increase linearly up to 15500 K and 0·86 cm respectively, during the first 10 m secs. i.e. the time during which the plasma attains a maximum temperature of 15500 K, P_{cc} has been computed as a function of time, and the results are presented in Fig. 7.24. Starting from a low volue at $t = o$, P_{cc} increases to a maximum value of 193 watts/cc in about 6 m secs., falling off to a value of 130 watts/cc at $t = 10$ m secs.

At temperatures above 11000 K radiation plays an increasingly dominant roll in energy loss from the plasma. Radiation has been computed

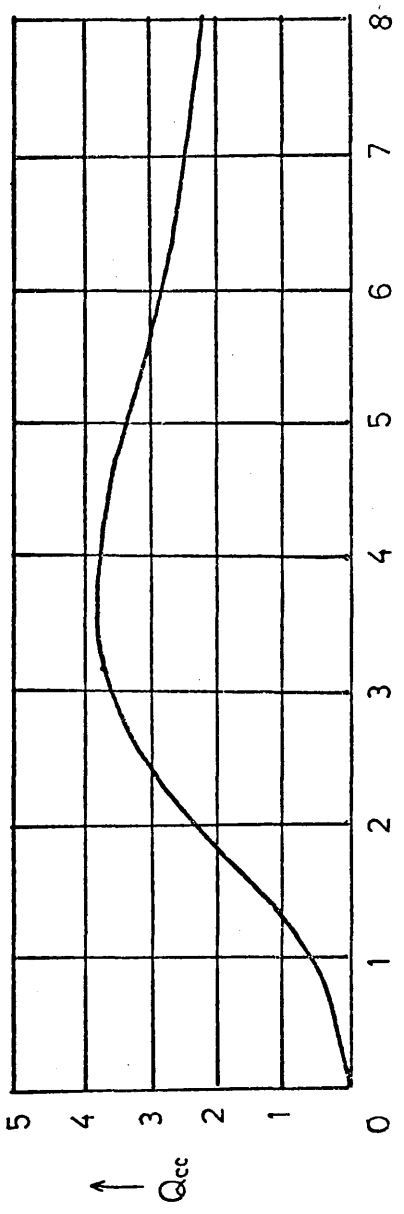

Fig. 7.23 Variation of 'Q_{cc}' with 'd/δ' (d = 2R)

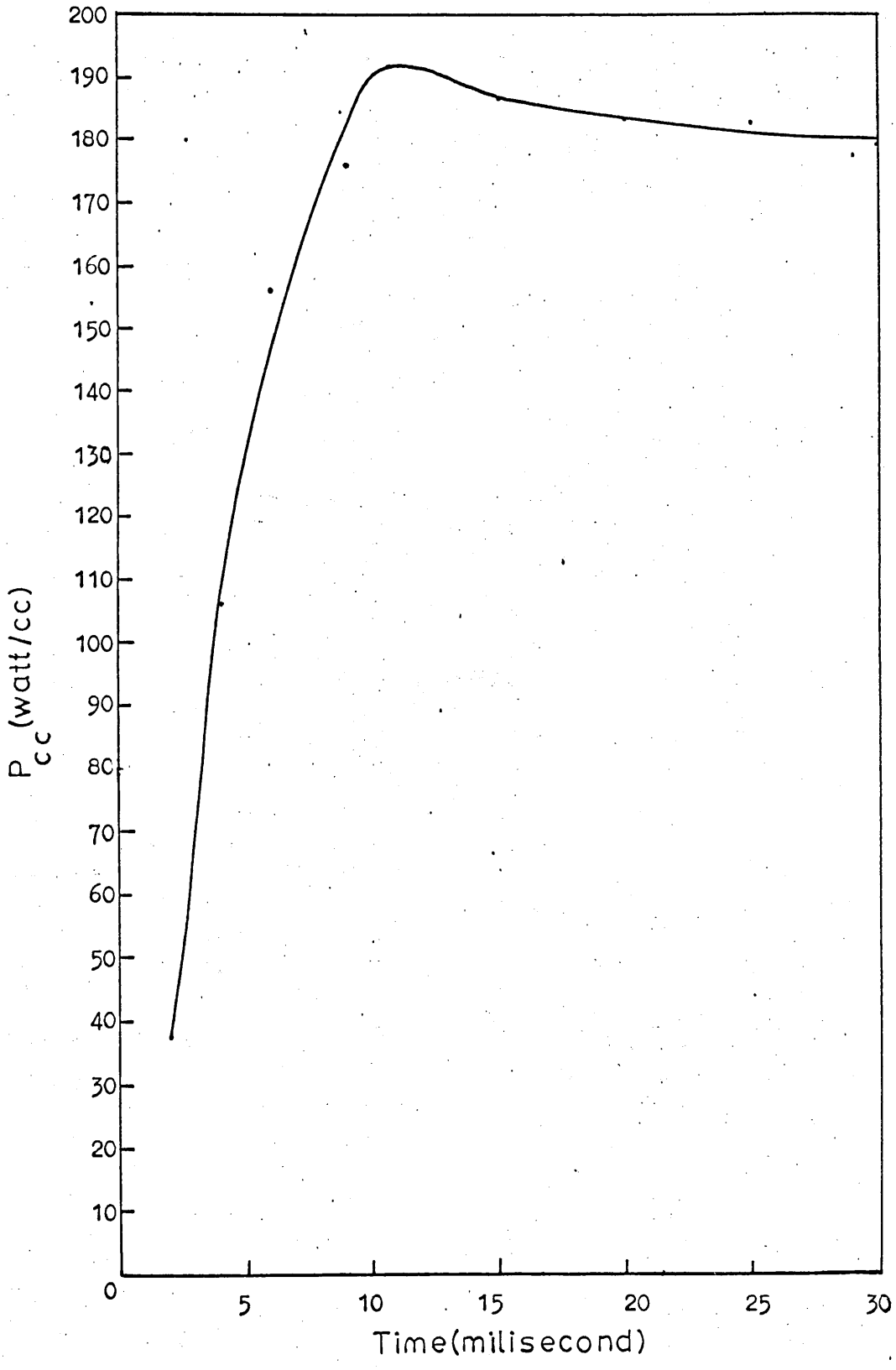

Fig.7.24 Variation of the power density P_{cc} with time during the formation of the main discharge.

at various temperatures by the methods described in sections. 2.11.4.1 and 2.11.4.2 and appendix II. The results are presented in Fig. 7.25. It would appear from Figs. 7.20 and 7.25 that the radiation loss/cc exceeds far more than the power density 'P_{cc}' produced by H-coupling. Also P_{cc} keeps increasing for $t \lesssim 10$ m-secs when the plasma temperature is still increasing. A diabatic compression of the plasma does help in raising the plasma temperature, but a detailed analysis shows that it cannot account for a 15500 K peak temperature. The only other mechanism of feeding energy into the plasma is through the electric field between r.f. inductor turns i.e. through E-coupling. With a peak potential difference of about 5 K.V existing across the r.f. inductor an electric field of the order of 500 V/Cm exists in the plasma region. With a mean free path of the order of 3.10^{-4} Cm, electrons can absorb sufficient energy from the field. Because of a high collision rate ($\sim 10^{11}$ sec^{-1}) between the electrons and the heavy particles this energy is soon randomised and converted to heat, raising the plasma to a high temperature (15500 K). It may, however, be pointed out that E-coupling is much smaller than H-coupling. It cannot feed large amounts of power to the plasma. It is effective only during the early stages of gas breakdown when the electron mobility is high and the plasma size is small, requiring less power to maintain it. As the plasma increases in size and its power requirement increases, E-coupling plays diminishing roll with the H-coupling completely taking over the energy transfer.

During the gas breakdown the plasma diameter increases continuously. When the discharge surface approaches the wall of the discharge tube, it compresses the cold unionized gas flowing spirally upward along the wall.

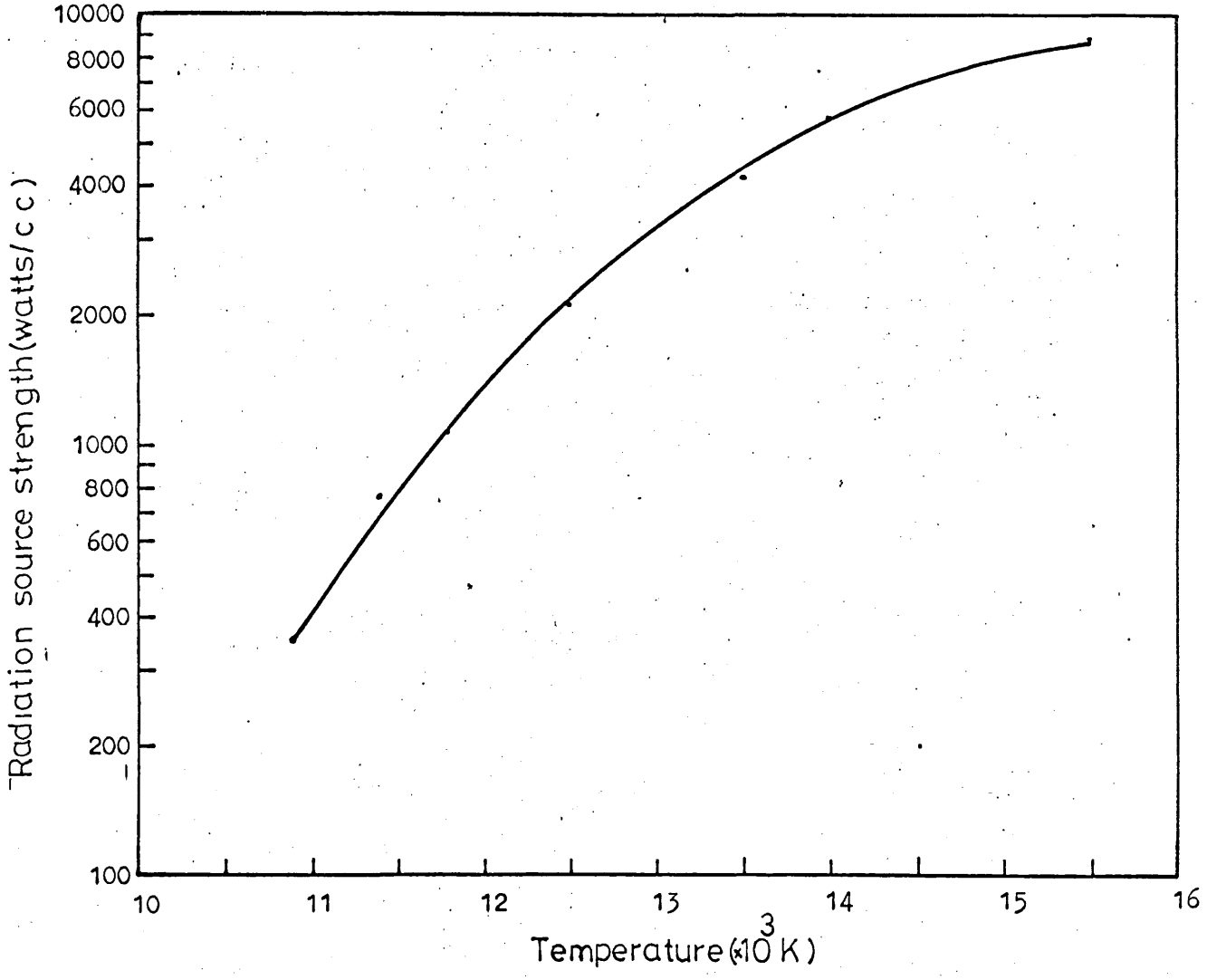

Fig. 7.25 Radiation source strength at various plasma temperatures.

Due to a rapid compression and heating the unionized gas may set into oscillations. These oscillations will be transmitted into the discharge, causing modulation of the light intensity as shown in Fig. 7.19. for $t > 120$ m-secs. At the same time plasma loses heat at a faster rate to the compressed cold flowing gas. The plasma temperature falls down rapidly producing a knee in the temperature variation at about 110 m sec (Fig. 7.20). Plasma cooling continues until the temperature gradient at the discharge surface acquires a value that ensures a balance between the energy dissipated by the r.f. field and the energy loss through thermal conduction, radiation loss at the steady plasma temperature (10000 K) being negligible.

During the first 10 m secs. of the gas breakdown, the plasma acquires a temperature which is about 50% higher than its steady value. Confinement of the plasma to a small volume and the large electric field existing in the plasma region due to a high potential drop across the r.f. inductor are thought to be mainly responsible for the high temperature.

8. Conclusion

It has been shown that the temperature of the plasma in a r.f. induction torch is not a simple function of the applied power since the power fed to the plasma is used in increasing the total number of ions which rises rapidly with the plasma temperature. However, a very short duration pulsed magnetic field is very effective in raising the temperature. In the course of this investigation techniques have been developed for measuring a recombination coefficient and for determining a range of plasma parameters and torch characteristics. The initiation stages of the torch have been examined. Also studies have been made of the stability and occurrence of fluctuations in the plasma.

An increase in the total input power resulted in a rapid increase in the plasma temperature, but with further increase in the power, the temperature-rise slowed down and showed a tendency towards saturation. The radiation losses were also found to increase rapidly with the input power and became about 30 times of their initial value in the absence of the pulsed magnetic field, for a total input power of 56 M.W. A large increase in the degree of ionization of the plasma was also produced by an increase in the power input.

A large increase in the plasma volume produced various instabilities and a higher plasma temperature (19000 K) for the same total input power.

It was found that in order to achieve an appreciable increase in the plasma temperature, a massive increase in the input power was required.

A technique was developed in this work to determine the recombination coefficient in a dense argon plasma (12) for which the values of the coefficient are rare, only two values being known in the literature. (96,106) This technique may be applied to any gas which can be used in an induction plasma torch.

Instabilities of low (300 Hz and harmonics) and high frequency (>60 K.Hz) were observed in an induction torch. The former were observed in both radiation and acoustic noise, the later being observed only in radiation. Large instabilities were also produced by a pulsed magnetic field.

Low frequency instabilities were found to be produced by the 300 Hz ripple in the high voltage supply of the oscillator. The inclusion of an inductive input filter, consisting of a 14 m.H. inductor and a 8.7 M.F.D. high voltage capacitor, reduced them to almost a negligible level.

A vast amount of information regarding the torch such as circuit parameters, plasma temperature, power efficiency etc. was obtained with the aid of a water cooled magnetic probe developed during the course of this work. A new technique of measuring the plasma temperature based on the measurements of the probe, was also developed.

At the torch initiation the temperature was found to increase about 50% higher than its steady value later on, in less than 10 m secs. A theoretical explanation based on partial adiabatic compression and the plasma heating through E-coupling when the plasma volume is still small, has been given for the initial high temperature.

Suggestions for future work

The technique used in this work to measure the radiative recombination coefficient in a dense argon plasma may be extended to other gases. In case of gases which are not available in sufficient quantities the flowing plasma used in this work may be replaced by a stationary discharge produced in a water cooled closed quartz vessel.

The theoretical model developed in this work to explain the acoustic noise predicts that a 100% modulation of the C.W. r.f. power would increase the power input by 50% and produce a more uniform temperature distribution and therefore a higher enthalply of the plasma. Experimental work in this direction i.e. effect of modulation on the plasma temperature, is suggested.

Appendix I

Fortran programme for Abels inversion for evaluating radial intensities.

```
      Program abel (input,output)
      Dimension Ex (30),Er (30),T(7)
      Read 10,NL,N,R
      Do 99 L= 1, NL
      Print 10 ,  NL, N, R
      Read 1, (T(I), I = 1,7)
      Read 2, (Ex(I), I =1,N)
      Call Inverse (N,Ex,Er,R)
      Print 3, (T(I), I =1,7)
      Do 100 I =1,N
  100 Print 4, I, Ex(I),Er(I)
   99 Continue
    2 Format (16F5.1/16F5.1)
    1 Format (7A10)
    3 Format (/////10X, 7A10///10X, 14HInput Intensity,6X,15Houtput Intensity 1)
    4 Format (T5, I3, T15, E12.4, T35, E12.4)
   10 Format (8,13,T18,13,T30, F5.2)
      Call Exit
      End
```

SUBROUTINE INVERSE

```
      Subroutine Inverse (N, Ex, Er,R)
      Dimension Ex(1),Er(1), A(30,30)
      IF (MM.EQ.33) Go to 1
      MM =33
      Do 10 K =1,30
      A3 =K*K
      Do 10 J =K,30
      A1 =J*J
      A2 = J+J+1
   10 A(J,K) =(SQRT (A1+A2-A3) - (A1-A3))/A2
    1 Continue
C
      M =N-1
      A4 =-2.*M/(R*3.1415926536)
   15 Do 2 K =1,M
      C =0.
      Do 3 J =K,M
    3 C =C+(Ex(J+1)-Ex(J)*A(J,K)
    2 Er(K) =C*A4
      Er(N) =0.0
      Return
      End
```

Appendix II

Calibration of photomultiplier 95923 for measuring total radiation from the torch.

The photomultiplier was calibrated with the aid of radiation from the torch. The plasma was approximated to a cylinder of radius 1.23 cm and length 6.6 cm as shown in Fig.I. Radiated power at measured plasma temperatures of 12,500; 12,200; 11,950; 11,600 and 11,000 K, mentioned earlier in sections 6.4.2.1.1, was computed by the methods described in sections 2.11.4.1; 2.11.4.2 and as described below.

In computing the power radiated per c.c from the plasma, the changes in ξ with wave length and temperature below 825 n.m. (Fig.2.4) were accounted for by dividing the appropriate spectral region into intervals each 50 n.m. wide, and calculating the contribution due to each. All these contributions were summed up to find the total radiation per c.c. In Fig.2.4 ξ has been plotted only for 8000 K and 16000 K. Values of ξ at other temperatures were extrapolated.

To compute the radiation power in spectral lines belonging to 4s-3p array half widths were taken from ref (14) and those for 4p-4s array from ref (107). Oscillator strengths for both arrays were taken from ref (108). Values of E_K, J_K and A_{ki} for optically thin lines, which correspond to transitions from 3d, 5s, 4d, 6s, 5d, 7s to 4p level, were taken from ref (108). Radiative recombination was found to make the major contribution to the radiated power (more than 85%) as suggested by Mitin and Pryadkin. The radiation source strength, which is obtained by dividing the total radiated power by the plasma volume/, is in agreement with the experimental results obtained by Emmons on a d.c. plasma torch as shown in table I.

/ Such an approach is not justified for absorbed lines but their contribution is very small.

The photomultiplier signal depends on (a) the fraction of light falling on the photocathode (b) the spectral response of the photomultiplier. It was easy to keep (a) constant. To account for (b) the wave length response curve of the photomultiplier was divided into a number of wavelength intervals each 50 n.m. wide. If η_i is the average efficiency* and δP_i the power falling in the i th interval at a given plasma temperature, then, the photomultiplier signal is given by

$$V_{pm}\ (\text{theo}) = \sum_{i=1} K' \eta_i \delta P_i$$

where K' is a constant and δP_i is calculated with the aid of Eqs (2.26) to (2.32). In table II V_{pm} (theo) is compared with the experimentally obtained photomultiplier signal V_{pm} (expt) at various plasma temperatures. It is seen that at any given temperature total energy radiated from the torch is proportional to both V_{pm} (theo) and V_{pm} (expt). An average conversion factor of 412.8 (watts/m.v) is obtained by which each value of V_{pm} (expt) must be multiplied to obtain the value of total radiation from the plasma.

* η_i is defined as the ratio of the photomultiplier signal to the amount of light energy which produces it and which lies in the i th interval.

Table I

Plasma temp	Radiation source strength 'Qr'	
	Present work	Emmon's results
12,500 K	25.9×10^8 W/m^3	20.2×10^8 W/m^3
12,200 "	19.7×10^8 "	15.1×10^8 "
11,950 "	14.6×10^8 "	11.3×10^8 "
11,800 "	12.4×10^8 "	9.83×10^8 "
11,400 "	7.8×10^8 "	6.13×10^8 "
11,100 "	5.5×10^8 "	4.22×10^8 "

Table II

Hm	Temp	V_{pm}(theo)	Total radiation p(theo)	$\frac{P(Theo).10^3}{V_{pm}(theo)}$	V_{pm}(expt)	$\frac{V_{pm}(expt)}{V_{pm}(theo)}$
1.25T	12500K	58.88W	93.1 K.W	1.58	210 mv	3.56
1.17"	12200"	43.60"	70.7 "	1.62	156 "	3.58
1.13"	11950"	34.03"	55.4 "	1.63	135 "	3.96
1.08"	11800"	28.89"	46.8 "	1.62	110 "	3.80
1.00"	11400"	18.29"	29.7 "	1.62	75 "	4.10
0.92"	11100"	14.87"	20.9 "	1.41	60 "	4.03

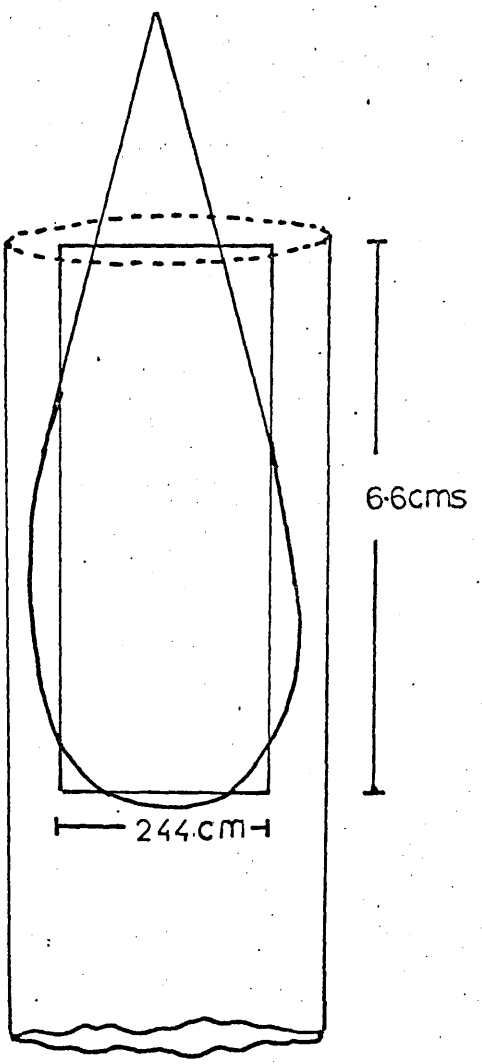

Fig.I. Approximation of a 13.0 K.W. torch (gas flow 10.5 l/m) to a uniform cylinder.

REFERENCES

Ref.No.	Details
1	G.W.Dickinson and Velmer A.Fassel; Anal.Chem. 41 1021 (1969)
2	R.H.Wendt and V.A.Fassel; Anal.Chem. 37 920 (1965)
3	" " " " " 38 337 (1966)
4	V.A.Fassel and G.W.Dickinson; Anal.Chem. 40 247 (1968)
5	S.Greenfield, I.L.Jones, and C.T.Berry; Analyst (London) 89 713 (1964)
6	S.Greenfield, I.L.Jones; C.T.Berry and L.G.Bunch; Proc.Soc. Anal.Chem. 2 111 (1965)
7	S.Greenfield; C.T.Berry and L.G.Bunch; "Spectroscopy with a High Frequency Plasma torch", Radyne International Inc. Des Plaines III; 1966
8	H.C.Hoare and R.A.Mostyn; Anal.Chem. 39 1153 (1967)
9	S.Greenfield; P.B.Smith; A.E.Breeze, and N.M.D.Chilton; Anal.Chim.Acta 41 385 (1968)
10	M.E.Britske; V.M.Borisov and Yu.S.Sukach; Ind.Lab. (U.S.S.R.) (English Trans) 33 301 (1967)
11	C.Veillon and M.Margoshes; Spectrochim.Acta 23B 503 (1968)
12	A.Shamin and E.R.Wooding; Phys.Lett. 34A 219 (1971)
13	Lyman Spitzer,Jr.; "Physics of Fully Ionized Gases", Interscience Publishers, 1962
14	H.R.Griem, Plasma Spectroscopy (M.C.Graw-Hill, New York, 1964)
15	H.J.Kusch and E.R.Mewes; Z.Naturforsch 22a 676 (1967)
16	S.C.Lin, E.L.Resler and A.R.Kantrowitz; J.Appl.Phys. 25 95 (1955)
17	S.Chapman and T.G.Cowling. The Mathematical Theory of Non-uniform Gases. Section 10.33. Cambridge University Press, London (1952)
18	L.Spitzer, and R.Harm, Phys.Rev. 89 977 (1953)
19	S.C.Brown; Basic Data of Plasma Physics. The M.I.T. Press (1966)
20	A.M.Howatson: An Introduction to Gas Discharges,Pergman Press (1965)
21	H.W.Drawin: Plasma Diagnostics Ch.14. North Holland Publishing Company, 1962
22	R.S.Devoto, Phys.Fluids 10 354 (1967)
23	H.W.Emmons, Phys.Fluids 10 1125 (1967)

Ref.No.	Details
24	T.R.Watson: "Tables of Thermodynamic and Transport Properties." Pergamon Press, 1960.
25	P.D.Johnston: Ph.D.Thesis, London University (1969)
26	A.Unsold: Ann.Phys.Lpz., 5.Folge 33, 607 (1938)
27	L.M.Biberman and G.E.Norman; J.Quant. Spectrosc.Radiat.Transfer 3 221 (1963)
28	P.D.Schluter; Astrophys.J. 61 7 (1965)
29	W.Lochte-Holtgreven, Plasma Diagnostics Ch.3 North-Holland Publishing Company (1968)
30	V.G.Sevastyanenko and I.T.Gakubov; Opt.Spectry 16 1 (1964)
31	L.M.Biberman, V.S.Vorobev and G.E.Norman; Opt.Spectry 14 176 (1963)
32	S.Katz, J.Edwin, and E.Raisen; Indust.Eng.Chem. 52 289 (1960)
33	H.Gerdien and A.Lotz; Wiss.Veroff Siemens-Werk 2 489 (1922)
34	J.H.McGinn: Proc. 5th Int.Conf. 'Ionization Phenomena in Gases' Munich 1 971 (1961)
35	H.N.Olsen; Phys.Fluids 2 614 (1959)
36	G.R.Jordan, Nature 210 84 (1966)
37	M.L.Thorpe; Research/Development II 1 (1960)
38	S.A.Rienzi and A.G.Gaydon; High Temp.High Pressure 1 231 (1969)
39	H.D.Watson; Canad.J.Phys. 41 1405 (1963)
40	G.R.Jordan and L.A.King; Brit.J.Appl.Phys. 16 431 (1965)
41	L.Rohde and H.Schwarz; Z.Phys. 85 161 (1933)
42	Y.Asami and T.Hori; Nature 144 981 (1939)
43	G.I.Babat; Proc.I.E.E. III 94 27 (1947)
44	Wulf B.Kunkel; 'Plasma Physics in Theory and Application', (Ch.10) McGraw-Hill Book Company, 1966
45	A.Mironer and F.Husfar; A.I.A.A. Electric Propulsion Conf., Colorado p.11 (1963)
46	J.S.Townsend and R.H.Donaldson; Phil.Mag. 5 178 (1928)

Ref.No. Details

47 J.D.Cobine and D.A.Wilbur; J.Appl.Phys. 22 835 (1951)

48 M.Mollwo; Ann.Phys.(Leipzig) 7 2 97 (1953)

49 R.Grigorovici and G.Cristescu; Rev.de Physique (Bucarest) 4 153 (1959)

50 R.Grigorovici and G.Cristescu; Opt.Spectry 6 85 (1959)

51 J.Swift; Eletronic Eng. 38 152 (1966)

52 A.Talsky; Czech.J.Phys. B14 594 (1964)

53 T.B.Reed; J.Appl.Phys. 32 821 (1961)

54 R.F.Baddoun and R.S.Timmins; Application of Plasma to Chemical Processing. Pergman Press (1967)

55 H.U.Eckert, F.L.Kelly and H.N.Olsen; J.Appl.Phys. 39 1846 (1968)

56 A.V.Donskoi, S.V.Dresvin and D.G.Ratnikov; High.Temp.3 858 (1965)

57 T.B.Reed; Proc.National Electronics Conf.Chicago, 19 654 (1963)

58 I.J.Floyd and R.K.Bayliss; Nature 211 841 (1966)

59 R.H.Fowler; Statistical Mechanics Second Edition Ch.XV Cambridge University Press

60 P.D.Johnston; Phys.Lett. 20 499 (1966)

61 Richard H.Tourin; 'Spectroscopic Gas Temperature Measurement', Elsevier Publishing Company, New York, 1966

62 H.Kleimann, R.Reynaud and A.Pelourson; High Temp-High Pressure 2 617 (1970)

63 V.M.Goldfarb, A.V.Donskoi, S.V.Dresvin and V.S.Klubnikin; High.Temp. 5 495 (1967)

64 A.D.Stokes; J.Phys.D.Appl.Phys. 4 916 (1971)

65 D.W.Hughes and E.R.Wooding; Phys.Lett 24A 70 (1967)

66 D.W.Hughes; Ph.D.Thesis, University of Wales, 1971.

67 R.E.Rovinskii, V.A.Gruzdev, and I.P.Shirkova; High.Temp. 4 35 (1966)

68 V.A.Gruzdev, R.E.Rovinskii and I.P.Shirokova; 5 994 (1967)

69 J.D.Chase; J.Appl.Phys. 40 318 (1969)

70 S.V.Dresvin, A.V.Donskoi and V.M.Goldfarb; Sov.Phys - Tech.Phys. 10 1270 (1966)

Ref.No.	Details
71	P.J.Vermeulen, W.Lee.Bodie, and F.A.Wierum; A.I.A.A.J. 5 1015 (1967)
72	T.B.Reed; J.Appl.Plys. 32 2534 (1961)
73	L.V.van Ruyven and J.D.Chase; J.Appl.Phys.Lett 12 214 (1968)
74	R.V.Mitin and K.K.Pryadkin; Sov.Phys-Tech.Phys. 13 1398 (1969)
75	R.V.Mitin and K.K.Pryadkin; Sov.Phys-Tech.Phys. 10 933 (1965)
76	R.V.Mitin and K.K.Pryadkin; Sov.Phys-Tech.Phys. 11 672 (1966)
77	Yu P.Raizer; Sov.Phys-Uspekhi 12 777 (1970)
78	M.P.Freeman and J.D.Chase; J.Appl.Phys. 39 181 (1967)
79	J.J.Thomson; Phil.Mag. 2 674 (1926)
80	H.U.Eckert; J.Appl.Phys. 41 1520 (1970)
81	H.U.Eckert; J.Appl.Phys. 41 1529 (1970)
82	Yu P.Raizer, Zhurnal prikladnoi mekhaniki i tekhnicheskoi fiziki 3 3 (1968) English translation
83	M.D.Gray, G.M.Kimber and J.T.Pennock; Chem.Eng. p.313 Nov. (1966)
84	D.G.Fearn and E.R.Wooding; J.Sci.Instrum, 44 571 (1967)
85	A.G.Gaydon; 'The Spectroscopy of Flames', Chapman and Hall (1957)
86	P.B.Coates and A.G.Gaydon; Proc.Roy.Soc. A293 452 (1966)
87	B.D.Adcock and W.E.G.Plumtree; J.Quant, Spectrosc.Rad.Transfer 4 29 (1964)
88	W.Lokhte-Holtgreven; Rev.Mod.Phys. 21 312 (1958)
89	K.Bockasten; J.Opt.Society of America, 51 943 (1961)
90	S.A.Rienzi and A.G.Gaydon; High.Temp-High.Pressure 1 231 (1969)
91	W.L.Bohn, M.U.Beth and G.Nedden; J.Quant, Spectrosc.Radiat.Transfer 7 661 (1967)
92	E.M.I.Photomultiplier Tubes. Brocher ref: 30M/6-67 (P.M.T.) Issue 1
93	W.Botticher; Plasma Diagnostics, Ch.10, North Holland Publishing Company (1968)
94	E.R.Rovinskii; V.A.Gruzdov; T.M.Gutenmakher and A.P.Sobolov; High.Temp. 5 557 (1967)

Ref.No. Details

95 L.A.Artsimovich; 'Controlled Thermonuclear Reactions', Oliver and Boyd, Edinburgh and London, 1964

96 V.Ya Aleksandrov; Opt.Spectry. 24 178 (1968)

97 V.Josephson; Phys.Rev.Lett. 5 416 (1960)

98 R.V.Mitin and K.K.Pryadkin; Sov.Phys-Tech.Phys. 11 672 (1966)

99 K.K.Pryadkin and R.V.Mitin; Sov.Phys-Tech.Phys. 13 618 (1968)

100 American Institute of Physics Handbook; McGraw-Hill Book Company 1964

101 Yu G.Kozlev and A.M.Shukhtin; Sov.Phys-Tech.Phys. 13 1197 (1969)

102 A.Shamin and E.R.Wooding; Proc.3rd.Int.Conf.Gas Discharges, London 639 (1974)

103 E.F.Kustov and P.A.Arsen'ev; Sov.Phys-Tech.Phys. 12 1594 (1968)

104 A.V.Kachanov, E.S.Trekhov, and E.P.Fetisov; Sov.Phys-Tech.Phys. 15 248 (1970)

105 P.G.Simpson; Induction Heating; Coil and system design Pub: McGraw-Hill Book Company, 1960

106 N.Van Trong; Comtes Rendus B264 217 (1967)

107 H.R.Griem; Phys.Rev. 128 515 (1962)

108 Atomic Transition Probabilities NSRDS-NBS 22 VolII. U S Department of Commerce. National Bureau of Standards.

LIST OF SYMBOLS

a_1	Cross-sectional area of r.f. inductor
a_2	" " " " plasma cylinder
A	Transition probability
b_o	Impact parameter
B	Magnetic induction
C	Velocity of light
C_s	Velocity of sound
d	Diameter of plasma cylinder
D_e	Electron diffusion coefficient
D_i	Ion " "
D_a	Ambipolar " "
e	Charge of electron
E	R.F. electric field
E_R	" " " on plasma surface
E_o	Amplitude of r.f. electric field
f	Frequency of r.f. generator
$f_{1,2}$	Oscillator strength
g_{fb}	Free-bound Gaunt factor
g_m	Statistical weight of m th energy level of atom
h	Plank's constant
H	R.F. Magnetic field
H_o	" " " outside the plasma
H_z	Axial component of r.f. magnetic field at the axis
H_{zp}	" " " " " " " " " in plasma
H_{za}	" " " " " " " " " in air
H_m	Maximum intensity of pulsed magnetic field

I	Intensity of light
I_m	Maximum intensity of light
i	Current
i_1, i_2	Primary and secondary currents
j	$\sqrt{-1}$
J	Current density
$\mathcal{J}$	Rotational quantum number
J_o	Bessel function of zero order
J_1	" " " order one
k	Boltzmann's constant
l_1	Length of primary coil
l_2	" " secondary coil
L_1	Inductance of primary coil
L_2	" " secondary coil
m	Modulation
m_e	Mass of electron
m_i	" " ion
M	Mutual inductance
$n, \tilde{n}$	Quantum number of energy levels of atom
n_e	Number density of electrons
n_i	" " " ions
n_o	" " " neutral particles
n_n	" " " particles in the excited state 'n'
N	Number of turns in primary coil
p	Pressure
p_e	Electron pressure
p_i	Ion pressure

P_2, P_3, P_4	Power radiated in spectral lines
$\bar{P}$	Poynting's vector
$\bar{P}_R, \bar{P}_o$	Poynting's vector on plasma surface
Q_H	Specific enthalpy of gas
Q_{oe}	Momentum transfer collision cross-section for electrons in argon
r	Radial position
R	Radius of plasma cylinder
R_o	" " discharge tube
R_y	Rydberg constant
R_2	Resistance of the plasma
S	Heat conduction potential
S_o	" " " at the axis
S_R	" " " on plasma surface
$\tilde{S}$	Area of curved surface of plasma cylinder
t_o	Time poriod of r.f. field
t	Time
T	Plasma temperature
T_m	Maximum plasma temperature
$T(m,r)$	Peak plasma temperature at a radial positio 'r'
$T(m)$	" " " at the axis
$T(a)$	" " " averaged over a plasma diameter
T_o	Temperature on plasma axis
T_i	Ionization temperature
T_e	Electron temperature
U_o	Internal partition function of atom
U_i	" " " " ion
V	Plasma volume
v	Velocity

v_{x1}, v_{x2}	Components of gas velocity normal to the discharge surface outside and inside the plasma
v_e	Electron velocity
v_i	Ion velocity
V_1, V_2	Primary and secondary voltages
V_e	Voltage drop at electrodes
V_g	" " across the arc
W_t	Total input power
W, W_g	Power dissipated in plasma
W_e	Power consumed at electrodes
x	x-co-ordinate
Z_2	Plasma impedance
z	Stage of ionization, z=1 being neutrals and z=2 singly ionized atoms
α	Radiative recombination coefficient
α_n	Ratio of n th harmonic to the fundamental
γ	Coupling coefficient
$\tilde{\gamma}$	A parameter which takes account of different statistical weight of the ground term of the parent ion as compared to that of hydrogen in recombination
δ	Skin depth
ε	Free-bound emission coefficient
$\dot{\varepsilon}$	Wave number
ζ_m	Energy associated with the m th energy level of atom
ζ_h	Energy stored in plasma due to temperature
ζ_i	" " " " " " ionization
ζ_t	Total energy in plasma
λ	Mean free path
μ	Permeability of plasma
μ_o	" " free space

μ_e	Electron mobility
μ_i	Ion "
ν	Frequency
ν_e	Electron collision frequency
ξ	A parameter which accounts for the penetration of the combining electron into the electron cloud surrounding the nucleus
ρ	Ratio r/R
ρ_e	Electron mass density
ρ_i	Ion " "
ρ_q	Charge density
ρ_o	Gas density outside the discharge
ρ'	" " inside the discharge
σ	Electrical conductivity
σ_R	" " on the discharge surface
σ_o	" " " " " axis
σ_c	Electrical conductivity due to close encounter
σ_d	" " " " distant encounter
τ_t	Time for establishment of kinetic equilibrium between electrons and heavy particles
$\tilde{\tau}$	Heat flux
ϕ_o	Magnetic flux
ϕ'_o	Time rate of change of magnetic flux
X_i	Ionization energy
X_H	Ionization energy of hydrogen
ω	Angular frequency
θ	Phase difference between electric and magnetic fields
θ_R	" " " " " " " on the plasma surface
k	Thermal conductivity
Θ	Moment of inertia of the molecule

a.u	Arbitrary units
$\acute{\alpha}$	Degree of ionization.
R_N	Avogadro's number.

PUBLICATIONS

Publication I	Phys.Lett. 34A 219(1971)
" II	Proc.Xth Int.Conf.'Phenomena in Ionized Gases' (Cotributed papers)26(1971)
" III	Proc.2nd Int.Conf.'Gas Discharges' London 161(1972)
" IV	Proc.3rd Int.Conf.'Gas Discharges' London 639(1974)

Volume 34A, number 4 PHYSICS LETTERS 8 March 1971

RECOMBINATION IN A DENSE ARGON PLASMA

A. SHAMIN * and E. R. WOODING
Physics Department, Royal Holloway College, Englefield Green, Surrey, UK

Received 8 February 1971

A recombination coefficient in an argon plasma at atmospheric pressure has been deduced from measurements of the temperature after the application of a pulsed magnetic field to an rf plasma.

If a dense plasma in an rf induction plasma torch is subjected to a pulsed magnetic field, the temperature rises by several thousand degrees and subsequently falls to the original steady value. Measurements of the accompanying changes in electron density n_e permit estimates to be made of the recombination coefficient.

The torch consists of a quartz tube 3.7 cm in diameter through which a steady stream of argon flows and rf power is inductively coupled into the plasma by means of a 6 turn water cooled coil 6.5 cm in diameter and 6.7 cm long. The coil is in the tank circuit of an rf generator operated at 6 MHz at a power of 13 kW. The plasma is stabilized by vorticity of the flowing gas and is allowed to exhaust to the atmosphere.

When the torch is running steadily, a pulsed magnetic field is applied by means of a theta coil coaxial with the rf coil but placed so that it contains the emergent plasma. The theta coil is 10.7 cm in diameter and 8.0 cm long. A 5 microfarad capacitor discharges 0.5 kjoule through the theta coil and produces a magnetic field, having a peak value of 1.25 T with a half period of 2.7 microsecond.

Radial temperature distributions were obtained spectroscopically [1] by viewing the plasma through a narrow slit in the theta coil. The intensities of the Ar I lines at 415.9, 418.2, 425.9, 426.6 and 427.2 nm were measured. A straight line plot of log (I_λ/Ag) against the upper excitation energy level for each line indicates the existence of a Maxwell Boltzmann distribution of electron energies.

In fig. 1 the maximum-temperature distribution is compared with that of the steady rf discharge. The generator was subject to 300 Hz

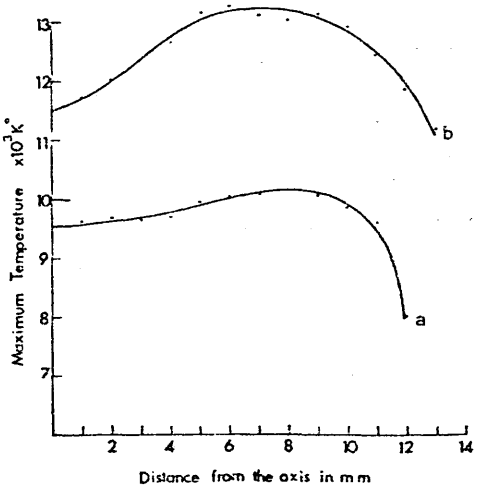

Fig. 1. Temperature distribution in the plasma 0.3 cm above the top of the rf coil. a. No magnetic field: b. When magnetic field is at peak value 1.25 T.

ripple due to the absence of smoothing filter in the high voltage supply of the oscillator, but consistent values of the plasma temperature were obtained by firing the theta coil at the same phase position in the ripple in each experiment.

In fig. 2 the fall of temperature at a fixed point on the torch axis is shown. Because of the high collision frequency, ($\nu \simeq 10^{11}$) the plasma is in thermal equilibrium and the electron density may be calculated by means of the Saha equation. A plot of $1/n_e$ against time is linear giving a recombination coefficient:

$$\alpha = 3.4 \times 10^{-14}\ \mathrm{cm^3/sec}$$

at an average electron density 4.10^{16} cm^{-3} and average temperature 11 100°K.

For a high pressure plasma, Mitin and

* On leave of absence from Physics Department, Government College, Lahore, West Pakistan.

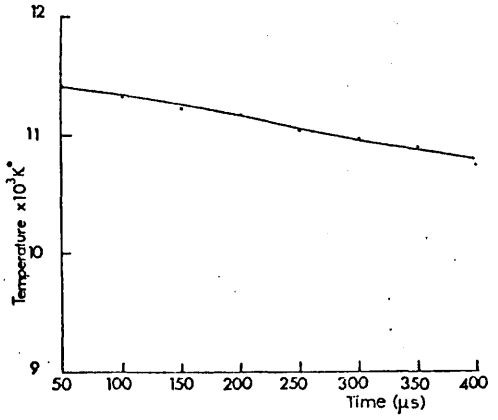

Fig. 2. Variation of plasma temperature with time after the application of a pulsed magnetic field. The temperature was measured 0.3 cm above the top of the rf coil.

and Pryadkin [2] deduced a theoretical formula for the recombination coefficient which, at the mean temperature of 11 100°K existing in the present plasma, leads to a value:

$$\alpha_T = 3.2 \times 10^{-14}\ \mathrm{cm^3/sec}.$$

They obtained an experimental value of 2.7×10^{-14} $\mathrm{cm^3/sec}$ for α at atmospheric pressure, while Aleksandrov et al. [3] obtained a value of 4×10^{-11} $\mathrm{cm^3/sec}$ at an electron density 2×10^{16} $\mathrm{cm^{-3}}$ and a temperature of 9000°K. The agreement between experimental and theoretical values is good. This preliminary result indicates a useful technique for studying decay processes in dense plasma.

One of us, A. Shamin, is grateful to the Government of Pakistan for granting study leave. The authors express their gratitude to Messrs. J. Henley, W. Howell and J. Taylor for assistance in constructing apparatus.

References

[1] D. W. Hughes and E. R. Wooding. Phys. Letters 24A (1967) 70.
[2] R. V. Mitin and K. K. Pryadkin. Sov. Phys. Techn. Phys. 13 (1969) 1398.
[3] V. Ya. Aleksandrov, D. B. Gurevich and I. V. Podmoshenskii. Opt. and Spectrosc. 24 (1968) 178.

* * * * *

1.1.3.14

DIFFUSION AND RECOMBINATION IN A DENSE ARGON PLASMA

D.W.Hughes*, A.Shamim** and E.R.Wooding

Royal Holloway College,(University of London) Englefield Green, Surrey

*Present address: Electrical Engineering Department, University of Surrey, Guildford, Surrey

** On leave of absence from Physics Department, Government College, Lahore, West Pakistan

1. Introduction

An r.f. induction argon plasma at atmospheric pressure has a high collision frequency and so is close to local thermodynamic equilibrium. Hence measurement of the temperature at a point in the plasma allows the electron density at that point to be calculated from Saha's equation. When measurements are made as a function of time in a decaying plasma or as a function of position in a steady plasma, changes in the electron density can be used to estimate the recombination and diffusion rates in the plasma.

2. Procedure

The r.f. torch consists of a quartz tube 3.7 cm in diameter through which a steady stream of argon flows, r.f. power being inductively-coupled into the gas by means of a 6-turn water-cooled coil 6.5 cm in diameter and 6.7 cm long. The coil is in the tank circuit of an 18 kW generator operated at 5 - 6 MHz. The plasma is stabilized by vorticity of the flowing gas and is allowed to exhaust to atmosphere. A pulsed magnetic field can be applied by means of a theta coil coaxial with the r.f. coil but placed so that it contains the emergent plasma. The theta coil is 10.7 cm in diameter and 8.0 cm long. A 5 microfarad capacitor discharges 0.5 kjoule through the theta coil, producing a magnetic field having a peak value of 1.25 tesla with a half-period of 2.7 microsecond.

Radial and axial temperature distributions have been obtained spectroscopically from measurements of the intensity of Ar I lines between 390 and 430 nm [1]. A straight line plot of log ($I\lambda$/Ag) against the upper excitation energy level for each line indicates the existence of a Maxwell-Boltzmann distribution of electron energies and, for a high pressure discharge [2], allows electron densities to be calculated from the temperatures using Saha's equation. The axial electron density in the steady plasma is plotted in Fig.1.

Now, assuming the mean gas velocity, v, in the plasma (approximately 20 m s^{-1} [3]) to be constant, the rate of change of electron density in a decaying plasma, dN_e/dt, will be given by vdN_e/dz, where dN_e/dz is the axial density gradient in the steady plasma. When recombination is the rate controlling process in a singly ionized gas, a graph of $(N_e)^{-1}$ against t is linear with a slope of α, where α is the recombination coefficient. Similarly, when diffusion dominates

$$N_e \propto \exp(-D_a t/\Lambda^2)$$

where D_a is the ambipolar diffusion coefficient, and Λ the characteristic diffusion length. In this case a graph of log N_e against t is linear.

3. Results for the Steady Plasma

Graphs of $(N_e)^{-1}$ against z and log N_e against z show linear regions for $z < 4$ cm and $z > 4$ cm respectively, where $z = 0$ is taken as the end of the r.f. coil where the plasma emerges. Then recombination dominates in the high density plasma near the coil, but diffusion is more important in the lower density of the plasma tail. It has been shown experimentally [3] that the radial electron density distribution in the tail has a Bessel J_0 profile, which is consistent with the controlling process being diffusion.

From the results, we obtain $\alpha \sim 5 \times 10^{-13}$ cm^3 s^{-1} at an average electron density of 2×10^{15} cm^{-3}, and $D_a \approx 400$ cm^2 s^{-1}. Including residual recombination [4] , the effective value of D_a at $z = 4$ cm is approximately 500 cm^2 s^{-1}. The mean temperature of the plasma was 6500°K.

4. The Pulsed Plasma

A more precise value for the recombination coefficient was obtained from time-resolved measurements of the temperature after applying a pulsed magnetic field. The temperature was measured spectroscopically at 50 microsecond intervals at $z = 0.3$ cm on the axis of the plasma. The r.f. generator was subject to 300 Hz ripple due to the absence of a smoothing filter in the high voltage supply of the oscillator, but consistent temperatures were obtained by firing the theta coil at the same phase in the ripple in each experiment.

The time-varying temperature is plotted in Fig.2. A plot of $(N_e)^{-1}$ against time is linear, giving a recombination coefficient

$$\alpha = 3.4 \times 10^{-14} \text{ cm}^3 \text{ s}^{-1}$$

at an average electron density of 4×10^{16} cm^{-3} and a mean temperature of 11 100°K. This compares well with the theory and experiment of Mitin and Pryadkin [5] , but is 3 orders of magnitude smaller than other experimental values obtained under similar conditions [6], [7].

5. Conclusions

Recombination has been shown to be important in the high density plasma near the induction coil of a high pressure r.f. argon plasma torch, and the recombination coefficient has been calculated to be about 3×10^{-14} cm^3 s^{-1} when the electron density is between 10^{15} and 10^{16} cm^{-3}. Ambipolar diffusion has been shown to be the governing process at the lower densities in the plasma tail, the diffusion coefficient being about 400 cm^2 s^{-1}.

Acknowledgement

The authors acknowledge the support of the Science Research Council.

References

[1] D.W.HUGHES and E.R.WOODING, Phys.Letts. 24A, 70-71(1967)
[2] H.R.GRIEM, Plasma Spectroscopy, ch.6, McGraw-Hill(1964)
[3] D.W.HUGHES, Ph.D. Thesis, University of Wales (1971)
[4] S.C.BROWN, Basic Data of Plasma Physics, ch.8, Wiley (1959)
[5] R.V.MITIN and K.K.PRYADKIN, Sov.Phys.Tech.Phys. 13 1398-1400 (1969)
[6] V.Ya ALEKSANDROV et al, Opt. and Spectroscop. 24, 178-181 (1968)
[7] N. VAN TRONG, Comptes Rendus B264, 217-219 (1967)

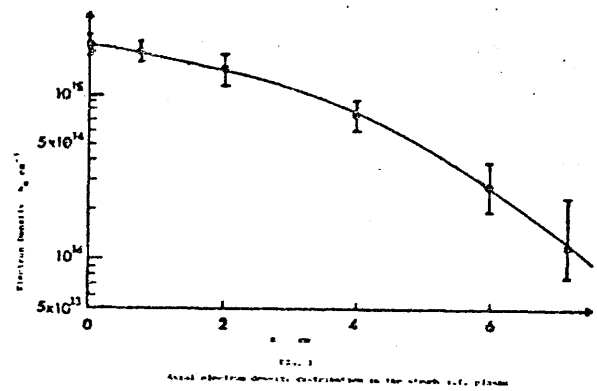

Fig. 1

Axial electron density distribution in the steady r.f. plasma

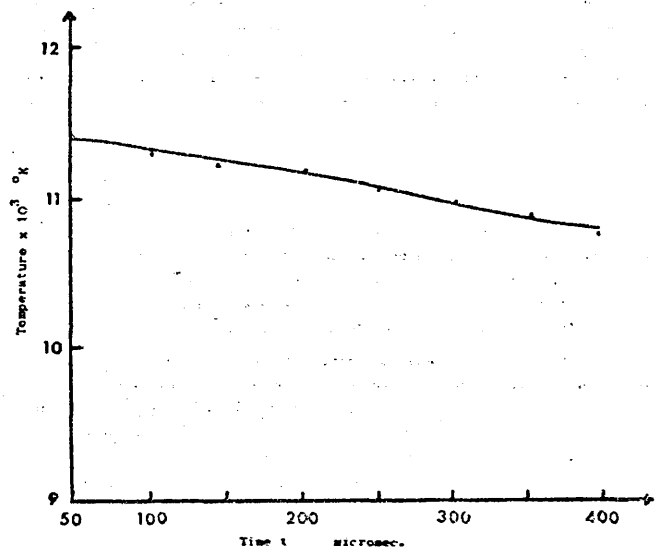

FIG. 2

Variation of temperature with time at $z = 0.3$ cm after application of a pulsed magnetic field

EFFECT OF A PULSED MAGNETIC FIELD ON A PLASMA IN AN R F TORCH

A Shamim* and E R Wooding
Royal Holloway College, University of London, Englefield Green, Surrey.

*on leave of absence from Physics Department, Government College, Lahore, West Pakistan.

An r f induction plasma torch is a convenient source for the production of high temperatures, and the study of ionic processes in a dense plasma. The temperature of such a torch supplied with argon remains around 10 000°K for a wide range of gas flow rates and r.f. powers of 5 to 15 kW although the size of the plasma varies. The application of a pulsed magnetic field, however, has been shown to increase the plasma temperature by several thousand degrees Kelvin.

The torch consists of a quartz tube 3.7 cm in diameter through which a steady stream of argon flows upward and r.f. power is coupled to the plasma by means of a 6-turn water-cooled copper tube, 6.5 cm in diameter and 6.7 cm long, connected in the tank circuit of a C.W. 15 kW, 4 to 7 MHz r.f. generator. In this work the generator is operated at 6 MHz at a power of 13.0 kW. The torch is vorticity stabilized and the hot gas is allowed to exhaust to the atmosphere.

A pulsed magnetic field is applied to the steadily running torch by discharging a 5 microfarad capacitor through a theta coil coaxial with the r.f. helix and so placed as to contain the emergent plasma. The theta coil is 10.7 cm in diameter and 8.0 cm long and produces a damped oscillatory magnetic field with a half period of 2.7 microsec.

Radial temperature distributions were obtained spectroscopically [1] by viewing the plasma through a narrow slit in the theta coil. The intensities of 415.9, 428.2, 425.9, 426.6 and 427.2 nm lines of ArI were measured with a calibrated photomultiplier. The intensity of a spectral line rose to maximum in about 10 microsec. and had a decay constant about 10 times this figure. A linear plot of $\log(I\lambda/Ag)$ against the upper excitation energy level for each line indicated the existence of a Maxwell-Boltzmann distribution of electron energies. Due to large amplitude intensity oscillations, difficulties were experienced in temperature measurement during the first 10 microsec. However, the maximum of the radial temperature distribution was found at 8 microsec. to be higher than that at the peak of the spectral line intensity. The temperature distribution at the peak spectral line intensity, after the application of a pulsed magnetic field of maximum intensity 1.25 T, is compared with that of the steady torch in Fig.1.

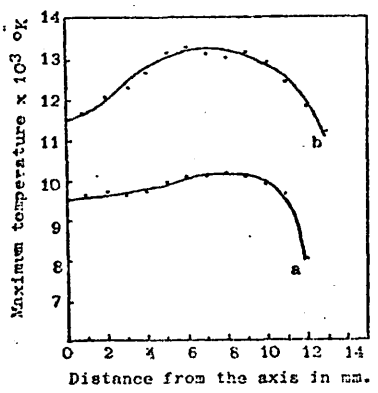

Fig.1. Temperature distribution at the peak of the spectral line intensity in the plasma 0.3 cm above the top of the r.f. coil a) No magnetic field; b) When magnetic field attains a peak value of 1.25 T.

Temperature distributions attain maximum values at 6 to 8 mm from the axis due to a skin-effect, and those of the steady torch are in agreement with previous values [4].

It would appear that the skin depth of the discharge at temperatures below 13000°K is nearly equal to the discharge radius. An attempt was therefore made to measure the pulsed magnetic field at the discharge centre with a water cooled inductive probe, but the field was too small to be measured. This suggests a skin depth appreciably less than 1.4 cm and a plasma conductivity greater than 6.2 K (ohm-metre)$^{-1}$, corresponding to a plasma temperature 14300°K, if thermal equilibrium may be assumed.

During the scanning of the plasma for spectroscopic measurement of temperature, after the application of the magnetic pulse, large amplitude plasma oscillations were found which were mainly confined to the boundary-layers of the plasma. These oscillations eventually dissipated their energy to the boundary region and thus contributed to an off-axis peak temperature distribution of the plasma.

The plasma temperature, at the peak spectral intensity was measured as a function of (a) the maximum intensity of the pulsed magnetic field, (b) the total power, which is the sum of the pulsed and r.f. powers; at a radius of r = 0.7 cm and are shown in Figs 2 and 3.

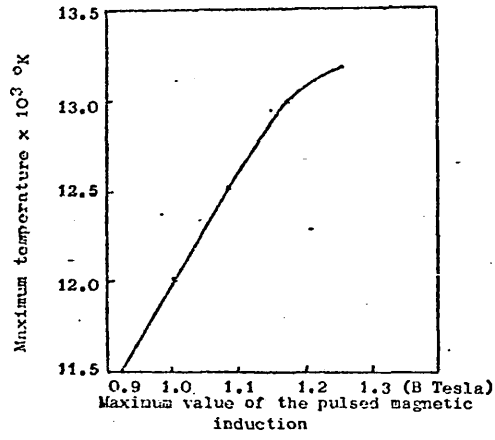

Fig.2. Dependence of maximum plasma temperature on the pulsed magnetic field.

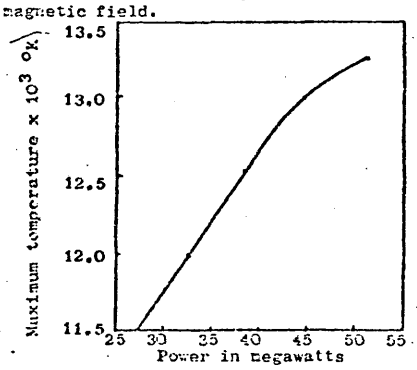

Fig.3. Dependence of maximum plasma temperature on the total power, consisting of pulsed and CW r.f. powers.

The gradients of these curves are seen to decrease with the increasing plasma temperature, an effect attributed to the increased radiation losses for the plasma at higher temperatures. Horn [3] devised a theoretical method of determining the radiation losses from a plasma including both continuum and line emission. Applying his method to the present plasma, the radiation losses are seen to increase from 60 Watts cm^{-3} at 10 000°K, to 2.35×10^3 Watts cm^{-3} at 13 000°K.

The variation of the plasma temperature with time at r = 0 and r = 0.7 cm is shown in Fig.4. At r = 0.7 cm the temperature is found to decrease rather slowly at 50 microsec, because the plasma losses are partly compensated for by the increased r.f. power input, caused by an increase in the electrical conductivity at higher temperature.

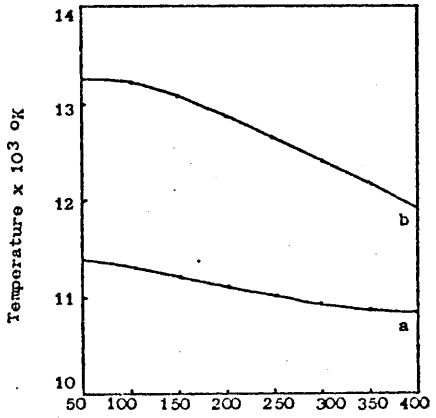

Fig.4. Variation of plasma temperature with time, after the application of a 1.25 T pulsed magnetic field. The temperature was measured 0.3 cm above the top of the r.f. helix (a) at the discharge axis, (b) 0.7 cm from the axis.

High speed photography of the plasma does not show any appreciable change in the plasma size except near its tail where a small axial compression of the plasma is observed. This suggests a heating mechanism consisting mainly of joule-heating of the plasma.

In an atmospheric pressure plasma, the particles have a high collision frequency ($\nu_{ei} \sim 10^{11} sec^{-1}$) so that the plasma is near to thermal equilibrium. This enables the electron density, n_e, to be calculated by means of the Saha equation. With n_e known, the electrical conductivity of the plasma may be calculated, following the method used by Olsen [4]. At the temperature distribution of Fig.1 at r = 0, $n_e = 4.8 \times 10^{16}$ cm^{-3} with $\sigma = 5.5$ K ohm^{-1} $metre^{-1}$, while at r = 0.7 cm and $n_e = 11.35 \times 10^{16}$ cm^{-3} with $\sigma = 4.97$ K ohm^{-1} $metre^{-1}$.

Oscillations at a frequency of 300 Hz with harmonics up to the seventh order have been detected both in the radiated light intensity and the acoustic noise of the C.W. torch; the intensity of the harmonics rapidly decreasing after the third order. These oscillations originate from the residual 300 Hz ripple and its harmonics in the high voltage supply of the oscillator. Occasionally a number of other frequencies have been detected in the light intensity of the torch, the most prominent being 50, 100 and 250 kHz. The reproducibility of these oscillations is poor.

When a pulsed magnetic field is applied, large amplitude oscillations of about 330 kHz are observed in the light intensity as shown in Fig.5. These oscillations subside at the end of the first 10 microsec. and afterwards, in some cases, the plasma oscillates at a frequency of about 36 kHz, gradually increasing to

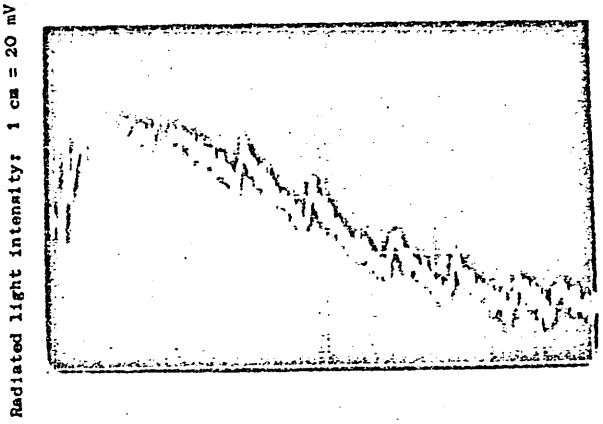

Fig.5. Oscillogram showing the plasma instabilities after the application of a 1.25 T pulsed magnetic field.

50 kHz in about 180 microsec. Sometimes the pulsed magnetic field excites 50 kHz directly, if it does not already exist in the steady plasma. The origin of these oscillations is under continuing investigation.

A plot of $1/n_e$ against time, obtained on the axis of the discharge, after the application of a pulsed magnetic field of maximum intensity 1.25 T, is found to be linear after 50 microsec, giving a recombination coefficient of 3.4×10^{-14} $cm^3 sec^{-1}$ at an average electron density $4 \times 10^{16} cm^{-3}$ and an average temperature 11 000°K [5,6].

The application of a pulsed magnetic field to a steady induction plasma torch is found to increase its temperature by an amount determined by the intensity of the pulsed field. With increasing temperature the radiation losses increase, decreasing the power coupling efficiency. The technique is useful for studying decay processes in a dense plasma.

Acknowledgement

One of us, A Shamim, is grateful to the Government of Pakistan for leave of absence. The authors thank Professor K Hirano for several discussions, and Mr J Henley and Mr W Howell for technical assistance.

References

1 D W Hughes and E R Wooding. Phys.Letters 24A (1967) 70.
2 V M Gol'dfarb, A V Donskoi, S V Dresvin and V S Klubnikin. Fizika Vysokikh Temp. 5 (1967) 549.
3 K P Horn, H Wong and D Bershader. J.Plasma Phys.20 (1966) 157.
4 H N Olsen. Phys.Fluids 2 (1959) 614.
5 A Shamim and E R Wooding. Phys.Letters 34A (1971) 219.
6 A Shamim and E R Wooding. Proc. of Xth International Conference on the Phenomena in Ionized Gases (contributed papers) p.26.

MEASUREMENTS OF AN R.F. PLASMA TORCH

A.Shamim[+] - E.R.Wooding*

The magnetic field distribution in a radio frequency plasma has been determined with the aid of a probe which was water-cooled to prevent damage. Estimates of the plasma temperature were made from the magnetic field and are compared with spectroscopic values.

The plasma torch, described elsewhere,[(1)] consists of a quartz tube open at the upper end with argon flowing through at atmospheric pressure. Power from an r.f. generator is coupled into the plasma through a watercooled copper coil wound round the quartz tube. The operating conditions are given in Table 1.

TABLE 1.

Inductor turns.	Inductor length.	Inductor diameter.	Quartz tube diameter.	Generator Power.	Generator Frequency.
5.75.	5.1 cm	5.6 cm	3.7 cm	13 kW	6.0 MHz.
5.75	5.1	6.6	3.7	13	6.0
5.75	6.0	7.8	5.4	11.6.	4.6
5.75	6.0	7.8	5.4	11.6	4.6

The quartz tube is 25 cms long.

In the 11.6 kW torch it was found that the major portion of the plasma resided below the coil on account of the gas circulation. This plasma was stable and almost filled the tube cross section but that plasma higher in the tube tended to move from side to side. The inductor current was determined with the aid of a current probe Tektronix type CT5.

A 300Hz ripple component in the d.c. supply to the r.f. generator was filtered out to avoid modulating the plasma density.

The magnetic probe is shown diagrammatically in figure 1. Six turns of 0.025 mm diameter enamelled copper wire were wound over one end of a Pyrex capillary tube through which water flowed. The turns were insulated with epoxy resin and coated with colloidal silver paint to provide an electrostatic screen. Four slots parallel to the coil axis were made in this screen to permit penetration of the magnetic field. A balanced differential arrangement of coils further reduced capacitive coupling, the centre turn being grounded through the silver coating. The Pyrex capillary tube was enclosed in a quartz jacket closed at one end and sealed to the mounting at the other. The

+ on leave of absence from Government College, Lahore, Pakistan.
* Royal Holloway College, University of London.

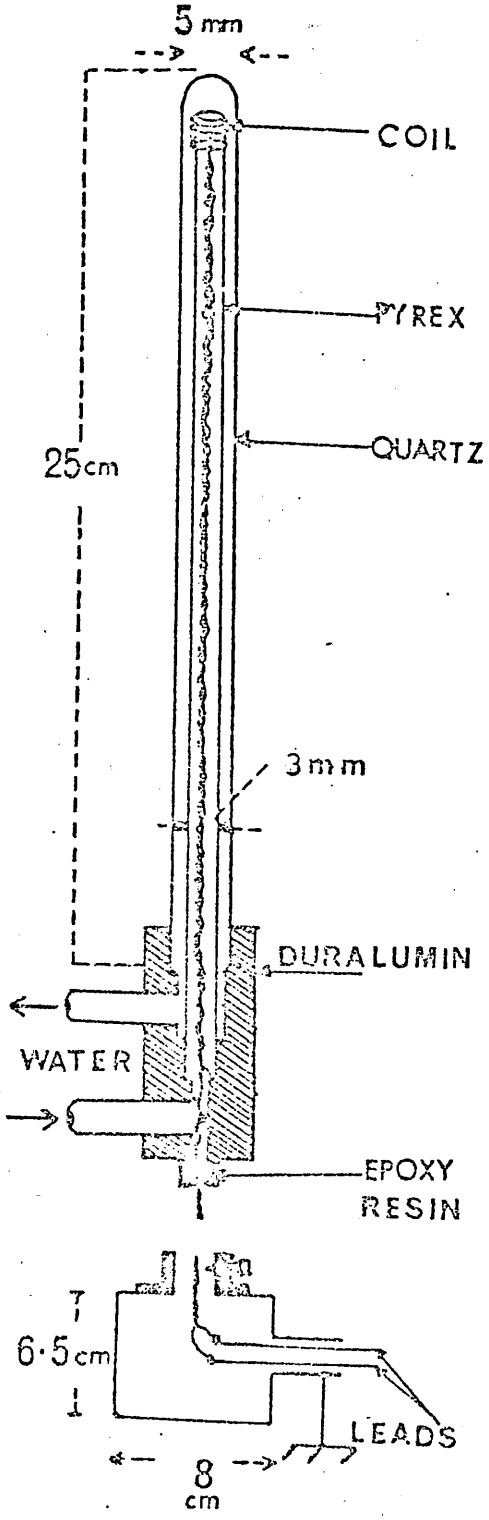

Fig. 1. Magnetic Probe.

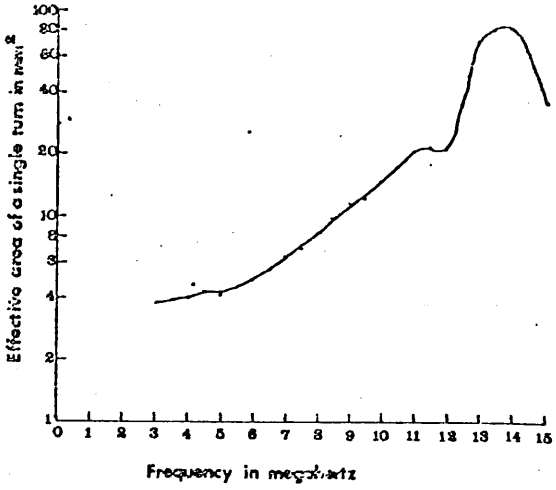

Fig. 2. Frequency response of magnetic probe.

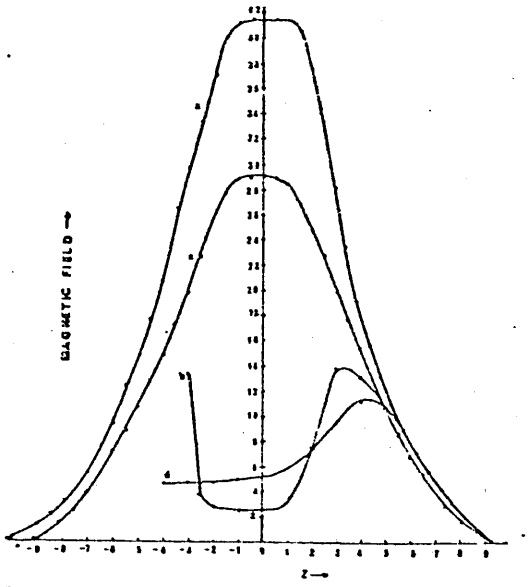

Fig. 3. Axial Magnetic Field distribution.

leads from the coil were twisted and led into a pair of 50 ohm Coaxial cables with the outer screen and appropriate terminations. The torch was operated within an expanded metal screen with the oscilloscope placed outside.

The probe was calibrated with the aid of a pair of Helmholtz coils in parallel with a tuning capacitor and a signal generator. The

geometrical cross section of the coil was 5.0 mm^2 but the effective cross section of the coil determined over a range of frequencies is plotted in figure 2 for a constant signal power.

Since the probe diameter was of the same order as the plasma skin depth, only the axial magnetic field (H_z) could be measured with adequate resolution. However, it was found that this field varied by about 10% in the radial direction in the absence of plasma.

The variation in the axial magnetic field is shown in figure 3. With the 13.0 kW torch the field in air (a) is almost a gaussian distribution about the mid point of the coil. When plasma is present (b) the field is almost uniform between 2.2cm below the mid-point and 0.8 cm above but rises rapidly on either side of this region to approach the value of the field in air. The 11.6 kW torch (c) displays a similar variarion with less sharp transition regions (d).

The plasma temperature was estimated from the magnetic field assuming that the plasma had a constant conductivity over its cross section. The ratio of the field H_o with plasma present to the field H in the absence of plasma is

$$H_o/H = \left((\text{ber}\sqrt{2}\rho)^2 + (\text{bei}\sqrt{2}\rho)^2\right)^{1/2} \qquad (1)$$

where ρ is the ratio of plasma radius a to skin depth or:-

$$\rho = 10^3 a/(\pi\mu f\sigma)^{\frac{1}{2}} \qquad (2)$$

where f is the generator frequency in megahertz H and Hoare normalised to the same inductor current. The variation in the generator frequency caused by the presence of the plasma is negligible. The plasma permeability differs by a negligible amount from the free space value.

The values of conductivity at various[2] temperatures may be used to estimate the plasma temperature. From equations 1 and 2 a family of curves may be drawn to relate the ratio H_o/H to the conductivity. Hence figure 4 is produced which relates the plasma temperature to H_o/H, the curves depending on the parameter $a\sqrt{f}$. The temperature is then estimated by calculating α for the plasma torch operating conditions, measuring H_o/H and reading the temperature from the appropriate curve in figure 4. Values obtained from the probe measurement are compared with spectroscopic values (1) in table 2.

Torch type.	a	f	α	H_o/H.	Temperature (Probe)	Temperature (Spectroscopic)
13.0kW	1.6 cm	6.00MHz	3.92	.058	9700°k	10,000°k
11.6 "	2.4	4.55	5.00	.172	7700	8500.

Temperatures obtained by the two techniques differ by about 10%.

The watercooled probe has been shown to provide a satisfactory method of measuring the magnetic field in a continuously running r.f. torch which produces a dense, high temperature plasma.

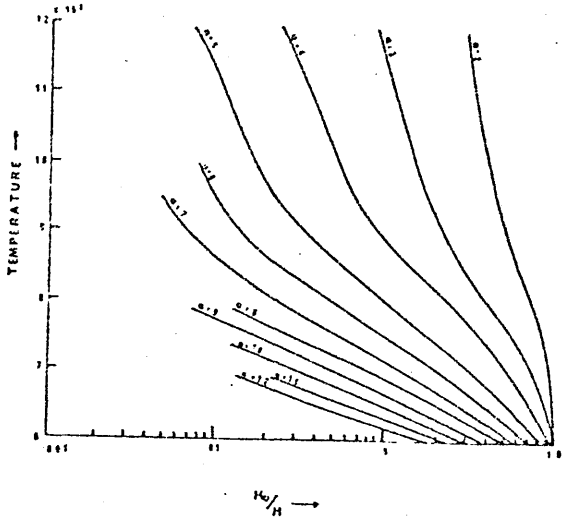

Figure 4. Relationship of plasma temperature to ratio H_O/H.

References.

1. Shamim A. and Wooding E.R.
Phys Rev Lett 34A 219 1971.

2. Raizer Yu P. Sov Phys - USPEKHI 12 777 (1970).

3. Eckert H.U. J. Appl. Phys 42 3108 (1971)

N.C.
Library